Quantifying the generation of T cell immunity using a systems biology approach

by

Chang Gong

A dissertation submitted in partial fulfillment
of the requirements for the degree of
Doctor of Philosophy
(Bioinformatics)
in The University of Michigan
2015

Doctoral Committee:

Professor Denise E. Kirschner, Co-chair
Professor Jennifer J. Linderman, Co-chair
Associate Professor Victoria Booth
Assistant Professor Irina L. Grigorova
Associate Professor Patrick D. Schloss
Associate Professor Santiago D. Schnell

To my family

ACKNOWLEDGEMENTS

I would first like to thank my advisors Professor Denise Kirschner and Professor Jennifer Linderman for their guidance during my graduate studies. When I started with little experience in this field, they took me on the trip with great patience. As I become familiar with the tools, they granted me the freedom to try out my own ideas and develop them into research projects. They are the best mentors I could ever have, and showed me examples of what it takes to be excellent scientists. I would also like to thank my committee members: Santiago Schnell, Victoria Booth, Patrick Schloss and Irina Grigrova. Their discussion and feedback have been invaluable for my thesis research.

I would like to Thank current and former members of Kirschner-Linderman lab for their help. Thanks to Simeone Marino for helpful guidance about principles in model construction and statistical analysis. Thanks to Paul Wolberg and Cory Perry for giving me great tips in programming. Thanks to Elsje Pienaar, Cordelia Ziraldo, Hayley Warsinske, Mohammad Fallahi-Sichani, Nick Cilfone and Laura Chang for their great input in collaboration and general discussion. Thanks to Joseph Waliga for keeping the lab systems always up and running. I would also like to thank my friends here in University of Michigan. Thanks to them for making my years here in Ann Arbor such a fulfilling experience.

Finally I would like to thank my family. Thanks to my parents for being supportive of me exploring the world in ways I want. They always encourage me to take on adventures, but also ease my mind and let me know there is always a place to fall back on. To Wenting, thank you for been there for me all the time. Without you, my world would never have been as colorful and fun.

TABLE OF CONTENTS

LIST OF FIGURES

Figure

LIST OF TABLES

Table

LIST OF APPENDICES

Appendix

ABSTRACT

The immune system is our defense against pathogens. Quantitatively predicting its response to foreign stimulation is key toward developing tools to interfere with or prevent infection (e.g. vaccines and immunotherapies). I use a systems biology approach and develop computational models describing dynamics occurring within lymph nodes, sites where activated immune cells are generated. These effector cells circulate out into blood and to sites of infection participating in immunity. I both quantitatively and qualitatively study dynamics of immune cells during a generalized infection as well as during infection with *Mycobacterium tuberculosis* (Mtb). The models predict that their 3-dimensional configuration enables the lymph nodes to support rare antigen-specific T cells to efficiently search for antigen-bearing dendritic cells, and this efficiency is not reduced when the precursor frequency increases in a wide range. The models also predict strategies to manipulate the differentiation of immune cells to maximize specific subtypes of T cells populations, depending on different immunomodulation goals. When coupled with Mtb infection models, our models are able to assist vaccine design by finding correlations between immune cell subsets and protection against Mtb, and also help identify mechanisms controlling different disease outcomes at host level.

CHAPTER I

Introduction

1.1 Motivation

The adaptive immune response is a highly sophisticated system developed to defend invasion of potentially dangerous foreign materials. This system involves pre-deployed lymphocytes circulating the entire body with random foreign patterns (antigens) that each can recognize. Due to the almost infinite patterns that could be encountered, the numbers of cells that can react to each possible pattern are in very low numbers in steady state (Casrouge et al., 2000; Blattman et al., 2002; Jenkins and Moon, 2012), but can be induced to expand several orders of magnitude upon recognition of the specific antigens. After an immune response, memory cells remains, preparing to generate a stronger and faster respond in future against the same antigen (Zinkernagel et al., 1996; Ahmed and Gray, 1996).

When this system occasionally fails to exert its full functionality, pathogens have an edge. This is when infectious illness occurs. Tuberculosis (TB) is an infectious disease caused by infection with the bacterium *Mycobacterium tuberculosis* (Mtb), a highly successful pathogen that infects one-third of the world population (WHO, 2014). There currently is no effective vaccine to prevent Mtb infection in adults; traditional diagnostics are slow and are even unavailable in some epidemic regions; and lengthy treatment regimens often lead to non-compliance, giving rise to emergence of drug resistance. These factors contribute to the global epidemic of TB, which is exacerbated

by increasing number of multi-drug resistant TB cases. Successful management of the global TB epidemic calls for a better understanding of mechanisms it uses to evade natural immunity and for improved clinical interventions.

The study of the human immune system has been greatly advanced in the past a few decades based on the development of molecular biology, but a lot of promising new findings are not exploited to their full potential in translational research (Sung et al., 2003). A systems level perspective can provide comprehensive insights into the behavior of the immune system and its interaction with invading pathogens, allowing more quantitative and clinically relevant predictions. For example, how the adaptive immune system identifies antigen specific precursor lymphocytes of extremely low frequency in a timely manner, and expand them to a sizable population? Why does the response fail to provide sufficient protection in cases like Mtb infection? In what ways can we apply our knowledge of immune system machinery to advance our arsenal against infectious diseases, e.g. theory-driven vaccine design? In this dissertation, I utilize computational systems biology approaches to investigate key aspects of these issues.

1.2 Overview of the human Immune System

Any living organisms, including humans, are open thermodynamic systems under constant material exchange with the environment in order to sustain an active metabolism, which allows their maintenance and reproduction. As a result, we are inevitably exposed to environmental pathogenic materials during this process. Our immune system has developed to fend off potentially harmful agents. The human immune system consists of a complex network of organs and involves coordinated activities of an array of subtypes of leukocytes (or white blood cells, WBC). Together, these components perform the fundamental duty of the immune system: identify non-self substances from self, and eliminate them to prevent damage.

The immune system can be further classified into two subsystems: the innate immune system

and the adaptive immune system. The innate immune system includes all the non-specific mechanisms to antagonize pathogen invasion. When encountered with foreign materials, the first line of defense is held by physical and chemical surface barriers such as skin, mucous membranes in our respiratory and gastrointestinal track, along with enzymes they secrete. Once pathogens make their way into the interior of the body, various leukocytes are deployed to counter the invasion. These cells originate from hematopoietic stem cells in bone marrow. Prior to infection, they either continue to circulate in the blood stream or enter peripheral tissues. Upon infection, the tissue-resident cells can engulf pathogens via phagocytosis (neutrophils, macrophages, dendritic cells), secrete mediators to defend against pathogen (basophils, eosinophils), or kill compromised host cells (natural killer cells) (Murphy, 2011). In addition to the cell-mediated mechanisms, there are also humoral components in innate immunity: the complement system. Produced by the liver, these pro-proteins circulate in the blood as inactive precursors, but can mount a cascade of reactions to kill microorganisms after triggered by activation signals. As an evolutionarily early form of the immune system, innate immune responses do not have antigen specificity and cannot generate immunological memory. Innate immune cells identify pathogens via various pattern-recognition receptors (PRRs), which respond to pathogen-associated molecular patterns (PAMPs), such as lipopolysaccharide (LPS) from Gram-negative bacteria and double-stranded RNA (dsRNA) from viruses (Akira et al., 2006). Nevertheless, innate immunity is initiated immediately after exposure and reaches its maximal potential in a short period of time.

The adaptive immune system generates immune responses that are specific to pathogens upon infection. Adaptive immunity also has two components: cell-mediated adaptive immunity involving killer cells eliminating host cells infected by intracellular microbe, and humoral immunity mediated by antibodies and to clear extracellular infection. The main actors in this system are lymphocytes. Lymphocytes are leukocytes that can be divided into two subsets: T lymphocytes (T cells) involved in cell-mediated adaptive immunity, and B lymphocytes (B cells) involved in

humoral immunity. Lymphocytes are developed in central/primary lymphoid organs. In particular, B cells enter blood directly from bone marrow, while T cells mature in thymus. During maturation, lymphocytes are genetically modified to recognize specific molecular structures. These naive cells circulate between blood and secondary/peripheral lymphoid organs in search of the patterns they can respond to. When such (cognate, antigen specific) matches are found, and in the presence of inflammation and danger signals induced costimulation, the specific lymphocytes are activated and undergo clonal expansion, which produce a large population of effector cells specific to the pathogen (thus "adaptive"). B cells differentiate into plasma cells and release antibodies to neutralize pathogens, while T cells differentiate into cytotoxic T lymphocytes (CTL) that kill infected host cells, or T helper cells that modulate function of other immune cells. After clearing the infection, the majority of the lymphocyte population generated during the immune response will die; however, a small proportion (usually 5-10%) of these cells remain as long lasting memory cells, resulting in immunological memory. When the host is faced with the same pathogen in the future, these memory cells will allow a faster and stronger immune response, leading to more successful resolution of infection.

Compared with innate immune responses, adaptive immune responses lags after exposure to pathogen, and their magnitudes reaches maximal level weeks after infection begins. Because adaptive immunity appears only after an encounter with specific antigens, it is also called acquired immunity. The adaptive immune system is not independent of the innate immune system; instead, the two systems collaborate at different stages to achieve their full potentials (Hoebe et al., 2004). The phagocytic process of dendritic cells (DCs) is necessary to obtain exogenous antigens, which precedes activation of antigen specific T cells; effector T cells can secret cytokines that modulate activities of cell-mediated innate immune functions; antibodies can provide signals that initiate antibody-dependent cell-mediated cytotoxicity (ADCC), complement cascades and phagocytosis etc.(Carroll, 2004; Nimmerjahn and Ravetch, 2008).

1.3 Lymph node structure and function

Adaptive immune responses are initiated in secondary lymphoid organs, including the spleen, lymph nodes (LNs), and mucosa-associated lymphoid tissue (MALT) such as tonsils and Peyer's patches. The structure of a LN is representative of these organs. There are 600-700 lymph nodes distributed throughout a human body. LNs are bean-shaped organs, with multiple afferent lymphatic (AL) vessels connected to the convex side and efferent lymphatic (EL) vessels connected to the concave side. The outer layer of each LN is a capsule composed of connective tissue and muscle fibers. The interior of the LN can be divided into cortex and medulla. Cortex consists of B cell follicles (outer cortex) and T cell zone (deeper cortex, or paracortex). Supporting reticular networks are constructed with stromal cells, including follicular dendritic cells (FDCs) in follicles and fibroblastic reticular cells (FRCs) in the T cell zone. The capsule extends into the LN towards the medulla and form membranous structures called trabeculae, which divide the LN into incomplete sub-compartments.

The structural characteristics of a LN are closely linked with its function as the venue of lymphocyte activation. Lymph circulates from peripheral tissue to the LN via AL, bringing professional antigen-presenting cells (APCs), especially DCs, along with free-floating antigens. AL drains into subcapsular sinus (SCS), from which DCs enter the cortex region to scan for lymphocytes specific to the antigen they are presenting on their surfaces. Meanwhile, lymphocytes are recruited from specialized blood vessels called high endothelial venues (HEVs) into the LN cortex and migrate towards T zone (T cells) or follicles (B cells) (Girard and Springer, 1995), where they spend time meandering in search of APCs presenting antigens they can specifically recognize. In T cell zone, some studies find the FRC network gives T cells directional guidance towards DCs (Bajénoff et al., 2006), while others claim that the search is a random walk and FRC network only provides attaching surfaces for cells during the search (Miller et al., 2002). The FRC network is

also found to form a conduit system, where smaller antigens along are transported into the paracortex and picked up by DCs and presented to T cells. When cognate matches are found, T cells and B cells are activated and a clonal expansion begins. In the presence of cognate T cell help, activated B cells can give rise to germinal center (GC) B cells that seed GCs within the folliciles, where they further mature and produce high affinity antibodies. Exiting lymphocytes (naive or activated) drain into cortical sinuses (CS), then medullary sinuses and eventually leave the LN via EL (Grigorova et al., 2010).

1.4 Biology of dendritic cells

Traditionally, an antigen (Ag) was defined as a foreign or self-biological polymer that can bind specifically to its corresponding antibodies; however, the current concept of antigen has expanded to any molecules that can be recognized by specific receptors expressed by lymphocyte surface including T cell receptors (TCR), B cell receptors (BCR) or antibodies (secreted form of BCR). In order to elicit a successful adaptive immune response, an antigen needs to be processed by professional antigen-presenting cells (APCs), such as DCs, and then presented to naive T lymphocytes.

1.4.1 Subtypes of DCs and their migration patterns

Dendritic cells include several subsets of cells with different properties. The two major categories of DCs are CD11c- plasmacytoid DC (pDC, BDCA-2+BDCA-4+ in humans) and CD11c+ conventional DC (cDC). In mouse, cDC can be further divided into subsets such as CD8α+CD11b- DCs and CD8α-CD11b+ (lymphoid) DCs. In humans, cDCs can be BDCA-1+ (CD1c+) DC or BDCA-3+ (CD141+) DCs, and the latter represent the counterpart of mouse CD8α+ DC. In addition, DCs can also derive from monocyte circulating in the blood stream. The developmental lineage of these subsets of DCs is reviewed in Wu and Liu (2007).

At steady state, precursors of cDC seed peripheral tissues from blood and differentiate locally. From peripheral tissues, some of these cells continuously migrate to draining LN via afferent

lymphatics, and are identified as migratory DCs, e.g. CD8α- DCs, dermal DCs and Langerhans cells (Randolph et al., 2005). Other cells, including CD8α+ DCs, are thought to only enter the LNs directly from blood by traversing HEV, and thus often referred to as LN-resident DCs (Kamath et al., 2002). In contrast with cDCs, pDCs are differentiated in bone marrows before they enter the blood (D'Amico and Wu, 2003). They can access peripheral tissues at a low level in steady state. During inflammatory conditions, circulating pDCs build up in peripheral tissues, and also acquire access to LNs due to the increased expression of adhesion molecules and chemokines allowing them to transmigrate across HEV (Diacovo et al., 2005). However, research found that pDCs are not able to migrate to draining LNs from peripheral tissues (Nakano, 2001).

1.4.2 Antigen presentation on DCs

Antigen presentation is the process in which antigenic materials are degraded into small fragments and mounted onto specialized molecules called major histocompatibility complexes (MHC). In conjunction, each peptide-MHC (pMHC) is displayed on cell surface so that they can be specifically recognized by structurally matching TCRs expressed on surface of a T cell. In humans, MHC is instead called human leukocyte antigen (HLA).

Two distinct pathways exist for antigen presentation, each associated with one MHC class. Endogenous antigens are presented by MHC class I (MHC-I) molecules, which is expressed ubiquitously in all nucleated cells and can be recognized by CD8+ T cells. Cytosolic proteins, including viral peptides, are digested by proteasome system and added to MHC class I molecules in a peptide-loading complex (PLC) in the endoplasmic reticulum (ER) (Hansen and Bouvier, 2009). In contrast, MHC class II (MHC-II) molecules are only expressed by professional APCs, including DC, macrophages, and B cells and present antigen to CD4+ T cells. Exogenous antigens, such as bacterial and parasitic proteins, are transported through endocytic pathway, degraded by lysosomal proteases, and loaded to MHC-II in specialized MHC-II containing (MIIC) compartments (van den

Hoorn et al., 2011).

Initially, these two antigen-presenting pathways were thought to be relatively independent; however, new evidence indicates the boundary is blurred by cross-presentation (Heath et al., 2004; Zhou and Blum, 2004). Through autophagy pathways (mainly macro-autophagy and chaperone-mediated autophagy, CMA), endogenous antigen can be routed to lysosome for proteolysis, then transport to MIIC and presented on MHC-II (Schmid et al., 2007; Zhou et al., 2005). Exogenous antigens can be presented on MHC-I via two main pathways: cytosolic pathway, and vacuolar pathway, as reviewed in Joffre et al. (2012). In the cytosolic pathway, exogenous antigens in endosomal compartments are translocated to the cytosol and digested by proteasome before added to PLC. In the vacuolar pathway, exogenous proteins are degraded in phagosomes, and loaded to MHC-I. The efficiency of cross-presentation varies among DC subsets. CD8+ DCs in mouse and BDCA3+ DCs in humans are found to specialize in cross-presentation (den Haan et al., 2000; Jongbloed et al., 2010). Cross-presentation is essential in that it allows antigens from either exogenous or endogenous to activate both CD4+ and CD8+ T cells and mount an orchestrated immune response.

MHC genes are highly polymorphic. To this date, 10,532 HLA alleles are identified in humans (`http://www.allelefrequencies.net/`). The variation mostly occurs in the peptide binding groove of MHC proteins and determines the specificity of peptide an allele that it can present. The diversity of MHC proteins ensures that a wide range of antigen peptides are "presentable" at a population level. In each individual, there are three MHC-I genes (HLA-A, B and C) and three MHC-II genes (HLA-DP, DQ and DR), and two copies of each gene are inherited from parents. The haplotype of MHC genes of a person is associated with susceptibility of many diseases Chapman and Hill (2012). Mismatch of MHC type is the molecular basis for immunological rejection during organ and bone marrow transplantation.

1.4.3 DC maturation and licensing

DCs are responsible for presenting foreign antigens using these aforementioned mechanisms to initiate an adaptive immune response during an infection. In steady state, both tissue and lymphoid resident DCs are mostly immature DC (IDC) and express low levels of MHC and costimulatory molecules on cell surface (Wilson et al., 2003). Microbial compounds and environmental stimuli can induce DC maturation (Rescigno et al., 1999; Joffre et al., 2009), a process by which DCs down-regulate their endocytic activity and up-regulate surface level of MHC and costimulatory molecules (CD80, CD86), which are necessary for fully activating T cells (Trombetta and Mellman, 2005). For migratory DCs, the constitutive trafficking to draining LN is further induced, due to increased expression of CCR7 upon maturation (Förster et al., 1999). In LN, resident IDCs can pick up free antigens brought in by lymph (Sixt et al., 2005), or acquire pMHC from other mature DC (MDC) via exosomes and become MDC from inflammatory factors (Théry et al., 2002; Segura et al., 2005).

MDCs can be further activated by CD4+ T cells via CD40/CD40L interaction. This process is referred to as DC "licensing" (Smith et al., 2004). When immunized with noninflammatory antigens such as ovalbumin (OVA), licensed DCs (LDC) are required to elicit a primary CD8+ T cell immune response (Bennett et al., 1997; 1998; Ridge et al., 1998). This requirement differs in the context of infection, depending on the capability of pathogen to directly activate DCs via pattern recognition receptors (PRR) (Bachmann et al., 1998). However, in some cases where CD4+ T cell help and LDC are not necessary for primary immune response, such as lymphocytic choriomeningitis virus (LCMV) and Listeria monocytogenes infection, they are still critical for the generation of functional memory CD8+ T cells and provide long-term protection (Sun and Bevan, 2003; Shedlock and Shen, 2003).

1.5 Biology of T lymphocytes

T cells are lymphocytes that express T cell receptor (TCR) on cell surfaces. These cells play a major role in cell-mediated adaptive immune responses. When activated, CD8+ cytotoxic T cells (CTL) directly kill host cells that are infected or dysfunctional, while CD4+ helper T cells modulate the functions of other immune cells in stimulatory or regulatory manners (Swain, 1983). The activation of T cells requires specific antigen stimulation from professional APCs, especially DCs. Other types of T cells include natural killer T (NKT) cells and $\gamma\delta$T cells, which recognize non-conventional MHCs and are able to produce effector cytokines immediately after activation in an innate fashion (Taniguchi et al., 2003; Bonneville et al., 2010).

1.5.1 Antigen specificity of T cells

T cells recognize antigens using TCRs. TCRs are heterodimers consisting of α and β chain. Each chain has two extracellular domains, a variable domain containing hypervariable or complementarity determining regions (CDRs), and a constant domain connected to the transmembrane region. Together, the CDRs of α and β chains form the antigen-binding site, which accounts for the antigen specificity of TCRs. Via its antigen-binding cite, TCR selectively bind to pMHC expressed on an APC with complement spatial structure (Garboczi et al., 1996). A co-receptor is employed to control the MHC class specificity of a T cell. Mature T cells express one of two co-receptors, CD4 or CD8. CD4 molecules can bind with MHC-II at a region distinct from TCR interacting site, and CD8 molecules can bind with MHC-I. The co-receptors are involved in signal transduction and amplify TCR stimulation (Veillette et al., 1988; Janeway, 1992).

T cells derive from thymocytes, which are hematopoietic progenitor cells in the thymus. To develop into mature T cells, thymocytes need to go through positive and negative selection (Surh and Sprent, 1994). During the positive selection phase, genes of α and β chains undergo somatic DNA recombination, which results in the diversity of CDR specificity (Greenberg et al., 1995).

Humans are diploid organisms and contain two copies of TCR genes. Through a process called allelic exclusion, only one of them is expressed after positive selection (Malissen et al., 1992). MHC class restriction is also determined at this stage. Positive selection is followed by negative selection, where thymocytes expressing TCR with high affinity to self pMHC are eliminated to avoid autoimmunity. As a result, mature T cells are generated from the thymus as CD4 or CD8 single positive cells, with a single type of TCR capable of recognizing self-MHC, but do not bind to them with high affinity. When released to blood, these naive T cells circulate between blood and lymphoid organs to search for antigen they are specific to. Due to the extremely high diversity of TCR, the frequency of T cells that are specific to each antigen (referred to as precursor frequency) is as low as $10^{-}5$ to $10^{-}6$ (Casrouge et al., 2000; Blattman et al., 2002; Jenkins and Moon, 2012).

1.5.2 T cell priming and differentiation

Naive T cells circulate between blood and lymphoid system, in search of professional APCs presenting antigens they are specific to. Upon cognate encounter, naive T cell bind with APCs for an extended period of time to accumulate activation signals, before they can proliferate and differentiate into effector cells. This process is called T cell priming. T cell priming consists of several distinct phases (Miller et al., 2004). When traveling through the T zone of LNs, T cells constantly make exploratory contacts with DC dendrites. When cognate antigens are identified by TCR, T cells first bind to DC in a series of brief and dynamic intermittent interactions, before establishing relatively stable contact via an organized interface structure called immunological synapse (IS) (Grakoui, 1999). The interface area is termed supra-molecular activation complex (SMAC). The center region of the SMAC (cSMAC) is TCR enriched, where TCR and CD4/CD8 co-receptor bind to pMHC on DC. CD28 also localize in this region, interacting with CD80/CD86 on the DC side. The peripheral ring around cSMAC (pSMAC) mainly contains adhesion integrin leukocyte function associated antigen 1 (LFA1), which stabilizes the interaction. The structure of

IS is reviewedin Huppa and Davis (2003).

T cells receive three types of signals during priming: TCR signal, co-stimulation, and cytokines. TCR and co-stimulatory (most importantly, CD28) signal synergize to promote T cell activation by inducing IL-2 production (Jenkins et al., 1991). TCR signal also induces expression of high affinity IL-2 receptor on activated T cells (Smith, 1988). Such autocrine signaling drives T cells to a committed series of division, which generate a population of T cells with the same TCR specificity but are orders of magnitudes higher in amount than their naive precursors. This process is called clonal expansion. During this period, early activation signal CD69 is expressed, resulting in internalization of S1P receptor ($S1P_1$). S1P mediate the exit of T cells from the LN, thus CD69 expression prevents the activated T cells from leaving the LN before they successfully expands (Shiow et al., 2006). The third signal – cytokine signal – directs functional differentiation of activated T cells, especially CD4+ T cells. This polarization is pathogen-type driven, and controlled by APCs in contact with the T cells. For example, intracellular bacteria infection promote DCs to produce IL-12, which direct CD4+ T cells to differentiate to Th1 type, produce interferon gamma (IFN-γ) and induce cellular immunity; whereas parasitic infection can promote DCs to produce IL-4, which induce Th2 differentiation and humoral immunity (Kapsenberg, 2003). Other identified T helper cell subtypes include Th9, Th17 and T follicular helper (Tfh) cells, each playing different roles in an immune response The environmental cues for CD4+ T cell differentiation is reviewedin Zhou et al. (2009). After differentiation, cytotoxic CD8+ T cells, Th1 and Th17 enter blood circulation, while Th2 and Tfh remains in the LN and facilitate B cell response.

When T cells mature in the thymus, negative selection precludes most potentially self-reactive T cells from entering blood circulation. However, some T cells specific to self-antigens that are not presented in thymus might escape (Walker and Abbas, 2002). Also, immune responses need to diminish when infection resolves to avoid excessive inflammation. To prevent self-reactivity in the peripheral at steady state and maintain homeostasis after infection, multiple mechanisms

are employed. If strong TCR signal is received in the absence of co-stimulation of CD28, T cells enter a prolonged hypo-responsive state, referred to as anergy (Jenkins et al., 1987; Harding et al., 1992). Activated T cells die from apoptosis, which is also antagonized by CD28 during normal priming phase in the presence of professional APCs (Lenschow et al., 1996). Regulatory T cells (Treg) are major players in cell-mediated negative regulation of T cell response. Developed in thymus (naturally occurring Treg, nTreg) or periphery (inducible Treg, iTreg), these CD4+Foxp3+ cells can be activated via TCR and expand in the presence of paracrine sources of IL-2 (Sakaguchi et al., 2008; Curotto de Lafaille and Lafaille, 2009) . Once activated, they mediate contact-based, "bystander" suppression of immune cells including CD4+, CD8+ T cells as well as professional APCs.

1.5.3 T cell memory

After infection resolves, the effector T cell population generated during the immune response undergo drastic contraction, leaving only a small fraction as long-lived memory cells. Upon future infection of the same pathogen, memory cells can mount a faster and more potent secondary immune response (Zinkernagel et al., 1996; Ahmed and Gray, 1996), due to epigenetic modifications and reorganization of cell surface receptors during the primary response (Sallusto et al., 2004; Kersh et al., 2003). The mechanism by which memory cells are generated is not clear, and different models are proposed to explain experimental observations, as reviewed in Kaech and Cui (2012). It has been confirmed that a single precursor cell can give rise to both effector and memory progenies (Stemberger et al., 2007; Gerlach et al., 2013). In general, inflammatory stimuli such as IL-2 and IL-12 are found to drive activated T cells towards terminal effector differentiation, in which situation they divide to expand extensively but gradually lose potential fori longevity and self-renewal (Pearce and Shen, 2007; Pipkin et al., 2010). T cells may commit to effector or memory subtypes early after priming (Kaech et al., 2003), but there is still some level of plasticity in these cells and

their fate can be influenced by environmental signals later on (Arens and Schoenberger, 2010).

Two major subsets of memory cells are produced after an immune response: effector memory (T_{EM}) cells and central memory (T_{CM}) cells (Sallusto et al., 1999). T_{EM} cells are thought to derive from effector cells. Lacking CCR7 and CD62L, they are unable to access lymphoid organs, but recirculate between blood and peripheral tissues to serve as surveillance mechanism after infection clearance (Reinhardt et al., 2001). Upon secondary infection, they are readily available to proliferate and exert effector function and rapidly contain pathogens; however, they do not survive as long as T_{CM} cells. T_{CM} cells are similar to naive T cells in that both subsets express CCR7 and CD62L and recirculate between lymphoid tissue and blood. These cells can last through the entire lifetime, and when cognate antigens are present again, they expand and generate a new wave of effector cells. The maintenance of T_{CM} differs from that of naive cells. Naive T cells rely on TCR signal via nonspecific interaction with self-pMHC as well as IL-7 for survival and homeostatic proliferation, while T_CM homeostasis is MHC-independent and requires both IL-15 and IL-7 (Sprent et al., 2008).

1.6 Tuberculosis

Tuberculosis (TB) is an infectious disease caused by Mycobacterium tuberculosis, a highly successful pathogen that currently infects one-third of the world population. The majority of infected individuals have what is known as a latent TB infection (LTBI), where bacteria reside inside granulomas that control their growth. Granulomas are spherical collections of cells formed by various types of immune cells including lymphocytes surrounding infected macrophages (Flynn and Chan, 2001). During their lifetime, 5% - 10% of latently infected people develop active and contagious TB. Little is known about the causes of these different infection outcomes. In addition, the lack of appropriate biomarkers to identify patients with latent infection is holding back efforts to control worldwide prevalence of this disease.

1.6.1 Granuloma development

Granuloma formation is the hallmark of TB, and is now understood to play a central role in disease dynamics. Non-human primate studies showed that granuloma development can start with a single bacterium after it enters pulmonary alveoli Lin et al. (2014). Ideally, resident macrophages in the lungs are responsible for taking up inhaled pathogens via phagocytosis and keeping the lung clear of infection. However, Mtb successfully evolved different mechanisms to evade the protective mechanisms of host immunity. When internalized, Mtb manages to grow inside macrophages, avoid lysosomal digestion, and utilize that intracellular environment to achieve optimal growth (Rengarajan et al., 2005). Bacteria released through cytolysis infect more surrounding macrophages, but also trigger innate immunity and attract an influx of phagocytes, including neutrophils, macrophages and DCs. Activated macrophages surround an infected center to contain the situation, while DCs migrate to draining LNs and induce a wave of adaptive immune response. Effector T cells and B cells generated within LNs then recirculate to the site of infection and form a cuff of lymphocytes in the outer layer of a granuloma. These events are reviewed in O'Garra et al. (2013).

From the host's point of view, granuloma serves as a protective structure that immunologically restrains and physically contains bacteria, preventing further disease progression. However, from the bacterial standpoint, they utilize this structure to avoid clearance and facilitate growth (Ramakrishnan, 2012). Instead of being a stationary structure, each granuloma is a highly dynamic structure reflecting an on-going battle between host and microbe. If the immune response is initiated timely, the granuloma may resolve; if the protection is insufficient, Mtb may as well enter uncontrolled growth and eventually disseminate to form new granulomas. At the host level, during both latent and active Mtb infection, multiple granulomas form at sites of infection, which could include lungs and also LNs (Chackerian et al., 2002; Lin et al., 2009). It is observed that these granulomas take a heterogeneous course of development over time (Lin et al., 2014). Despite their asynchronous

development, all granulomas within one host stimulate the same host immune system to promote adaptive immune responses, which produces effector T cells that migrate via blood circulation and thus indirectly influence each other. All granulomas in one host are speculated to collectively shape the course of disease among the spectrum of latency (Barry et al., 2009). However, little is known about factors controlling the differential outcome of Mtb infection in each patient.

1.6.2 TB treatment and vaccination

Treatment for TB requires 6 months or more of a combination of 4 different antibiotics (Dartois, 2014). This empirically tested unusual regimen reflects difficulties in treatment posed by TB infection dynamics. First, the dense and complicated structure of a granuloma and its limited vascularization render poor drug penetration (Dartois and Barry, 2013; Pienaar et al., 2014). Further more, some extracellular bacteria enter caseous niches in granulomas and act as drug tolerant "persisters" (Lenaerts et al., 2007). As a result, these prolonged regimens leads to patient non-compliance, treatment withdrawal, and can even give rise to drug resistant bacteria strains. Thus, new treatment regimens with shorter time frame and new drugs targeting bacterial or host mechanisms are imminently needed to relieve global TB epidemics.

The ultimate weapon against TB would be a vaccine that prevents new infections. Currently, there is no efficacious TB vaccine available for adults. Bacille Calmette-Guérin (BCG) is a vaccine prepared from attenuated bovine tuberculosis bacillus. Recommended for newborns in countries with high TB burden, this vaccine prevents severe forms of tuberculosis disease, but does not ward off infection of TB after childhood (World Health Organization, 2004). It is postulated that different combinations of immune agents need to be generated against multiple Mtb antigens at various stage of infection (Andersen and Woodworth, 2014), but so far no biomarker of protection has been confirmed. Many vaccine trials have fail to date, with more still on-going at various phases (Weiner and Kaufmann, 2014).

1.7 Computational models of immune responses and TB infection

Traditional reductionist approaches have proven to be powerful in finding fundamental principles of how "parts" of a subject operate in isolation or simple groups. These findings can usually make predictions for a controlled environment. However, the body of a multicellular organism such as human is a complex system. Biological processes occur on multiple spatial and temporal scales, involving crosstalk between scales and interplay of agents from different organ systems. It is difficult to extrapolate findings concerning isolated entities at lower scale to long-term whole-body effects without quantitatively taking into account of the complex network of control bridging the two scales. The over-simplification can result in loss of predicting power, which is reflected in poor translation of basic research findings into clinical applications (Glasgow et al., 2003). Computational and mathematical models are promising tools to bridge the gap. Instead of operating on one or a few simple hypotheses, these models can serve as a way to integrate large amounts of data and hypotheses into multi-scale, temporal-spatial explicit networks, which possess the power to make more generalizable predictions.

Agent-based models (ABM) originate from cellular automaton (CA) (Wolfram, 1984). In this type of model, autonomous discrete agents are assigned to an explicitly represented grid space, where they can move around and interact among each other or with the environment based on a pre-defined set of rules. The rules are usually local, and agents can only sense and influence other agents within their neighborhood. However, collective behaviors can appear globally as "emergent properties". ABMs are especially relevant in studying biological systems at a tissue scale, as they imitates the autonomous and localized decision making process of cells. ABMs are also highly flexible. As computer simulations, with properly designed interfaces, they can be connected with other model systems running as sub-models or in parallel. Utilizing this property, we can construct multi-compartment and multi-scale hybrid models, in which dynamics in other physiological

compartments or at molecular levels are represented with deterministic systems such as ordinary differential equations (ODEs). One drawback of ABMs is that they are computationally expensive compared with other types of models. To tackle this issue, we formulated the idea of tuneable resolution: a multi-scale model should be able to adapt to both internal systemic status and interest of a specific study (Kirschner et al., 2014). It should be capable of automatically (preferably in real-time) choose between adopting abstract forms of representation to save computational resources (coarse-grain) and engaging with detailed mechanisms to preserve fidelity (fine-grain).

1.7.1 Models of lymph node T cell dynamics

T cells play pivotal roles in an adaptive immune response. Subsets of T cells can kill infected host cells (CTL), mediate humoral immunity (Th2 and Tfh), and negatively regulate immune activity (Treg). Understanding T cell priming and differentiation in the LN provides key information towards immune profile manipulation. Many modeling efforts have been made to this end. Early models of T cell dynamics are largely ODE-based. These simple deterministic models are useful in estimating population kinetics (De Boer and Noest, 1998), predicting dynamics of immune responses during infection (Bajaria et al., 2002; Marino et al., 2004), and can help discriminating between contradicting hypotheses (Antia et al., 2005). However, due to the lack of spatial information and stochasticity, this type of model cannot capture events such as T-DC searching in a mechanism-driven manner. Nevertheless, ODE models of T cell activation can be used as sub-compartments in hybrid models if they can give a phenomenological approximation that is compatible with desired resolution (Marino et al., 2011).

In order to correctly incorporate the influence of spatial components and randomness, traditional ABMs and cellular Potts models (CPMs, a special class of ABM where cells are modeled as deformable objects operating on energy principles) are employed to study various aspects of T cell dynamics in the LN. These models are reviewed in Mirsky et al. (2011). Benefitting from progress

made in intravital two-photon microscopy (2PM), T cell short-range migration is statistically analyzed in LNs of live animals (Miller et al., 2002). These data guided development of 3D models with more specific motility rules. Models attempting to replicate the 2PM and found short-term persistence is necessary in addition to random walks (Beltman et al., 2007; Bogle and Dunbar, 2008), but the role of FRC constraint is still unclear. Based on these short-range motility patterns, T cell-DC search is studied, with the role of chemotactic attraction to DC examined. However, different models reached contradictory results: DC chemotaxis is found to interfere with scanning efficiency by Riggs et al. (2008), but is also found to promote rare Ag detection by Vroomans et al. (2012). Furthermore, models of T cell priming in LN are developed to study efficiency of LN to help expand T cell population in an immune response (Linderman et al., 2010). With newly available imaging results containing comprehensive details in a LN environment, it is now possible to more accurately estimate T cell density and map entry/exit locations of T cells in the LN. The natural next step is to study how such a LN environment facilitates efficient DC-T cell searching, and what mechanisms are governing the outcome of subsequent priming and differentiation.

1.7.2 Models of granuloma development

Granuloma is key to course of TB progression. Mechanisms that control granuloma outcome are potential targets of TB intervention. ODE models are developed to describe TB at different scales. To understand the in-host dynamics of immune cells and bacteria interactions during TB infection, these models are used to describe total populations of Mtb in lungs over time (Wigginton and Kirschner, 2001; Marino and Kirschner, 2004). At populations scale, numerous models that track the dynamics of TB epidemics under various scenarios have also been built (Kirschner, 1999; Murphy et al., 2002; 2003; Singer and Kirschner, 2004; Young et al., 2008; Feng et al., 2000; Castillo-Chavez and Feng, 1997; Guzzetta et al., 2011; Castillo-Chávez and Aparicio, 2009; Blower et al., 1995; Dye et al., 1998; Milner et al., 2002). However, concerning the infection

outcome of a single individual, granulomas are believed to be the focal point of study. Taking into account the distinctive spatial organization of this emergent structure, it is optimal to study this structure using multi-scale models with an ABM representation of cell level dynamics that manifests at a tissue level as emergent behavior.

Our group have been developing ABMs to capture spatio-temporal dynamics of individual granuloma formation and function for over a decade (Segovia-Juarez et al., 2004; Fallahi-Sichani et al., 2010; Marino et al., 2011; 2010; Fallahi-Sichani et al., 2012a;b; Cilfone et al., 2013). Current versions of this model capture events at multiple scales. Cellular and tissue scale dynamics are implemented with an ABM, with rules governing movement, interaction and state changes of various subtypes of T cells and macrophages. At the molecular level, receptor/ligand dynamics and intracellular signaling are modeled with ODE embedded in each cell agent, while free-floating molecules are tracked by numerically solving the partial differential equations (PDEs). Using this model, in silico experiments are performed to study the correlation between different factors and granuloma stability. The recruitment of T cells to the grid (lung) is dependent on an ODE LN sub-model (Marino et al., 2011). As an improvement over earlier versions, the immune response is adaptive to dynamics in granulomas, thus the model should be able to better resemble course of granuloma development; however, when TB antigen is scarce, the intermitted random burst of priming events may not be well reproduced by a deterministic ODE model. This notion may be particularly relevant if a granuloma is well contained and DCs have little chance of accessing bacteria, that exit from the granuloma and enter draining lymphatic vessels.

1.7.3 Uncertainty and sensitivity analysis

Uncertainty analysis measures the variability in model output generated from parameter variability overall, while sensitivity analysis attributes this overall variability to each input source and evaluates the responsiveness qualitatively or quantitatively (Saltelli et al., 2000). When model-

ing complex biological systems, ABMs usually incorporate large amount of different interactions among multiple agent types, thus sometimes enticing critics of having the potential to be over-parameterized. In an ideal situation most of the rules should be based on elementary and established facts with only a small fraction as working hypotheses under investigation. Nonetheless, in reality, knowledge could be partial, ambiguous or even lacking. In these situations, uncertainty and sensitivity analysis techniques need to be employed to account for the variability induced on model outputs by missing information. This analysis also provides another important piece of information: because some parameter values correspond to biological mechanisms, high sensitivity of target output to particular parameters indicate those mechanisms may play important roles in determining the outcomes of interest.

Due to the discrete and stochastic nature of ABMs, and the large amount of computational resource required to run the simulations, it is usually impossible to obtain local parameter sensitivity analytically. Instead, global sensitivity analysis tools can be applied with these models. Two of specific methods are often used: partial rank correlation coefficient (PRCC) and extended Fourier amplitude sensitivity test (eFAST). In both methods, a selected group of parameters are chosen to vary in an arbitrarily chosen but biologically realistic range, and the rest are fixed. In PRCC, the process starts with using Latin Hypercube Sampling (LHS) to sample the high dimensional parameter space efficiently and generate a list of parameter combinations. Each set of parameter combinations is considered as an input, simulations run, and statistics recorded as output. By calculating the PRCCs, non-linear monotonic relationships can be detected. eFAST is a variance decomposition method. Parameter values are varied at different frequencies, and variability of output is transformed into frequency space with Fourier analysis to compute contributions of input frequency. Therefore, the fraction of the variance explained by each input parameter is an indication of model sensitivity to a specific parameter. These methods are discussed with more details in Marino et al. (2008).

1.8 Dissertation Overview

The goal of my thesis is to study the generation of adaptive immunity, and apply it in a disease-specific context (TB). In particular, my thesis work is designed to identify mechanisms driving the generation and maintenance of different T cell populations, and how they interact dynamically in space and time with mycobacterial infection. I am most interested in the dynamics of immune cells in three different physiological compartments (Figure 1.1): lymph nodes, blood stream, and the lung. Draining lymph nodes are responsible for hosting antigen presentation events occurring between dendritic cells (DCs) and T cells, which initiates an adaptive immune response. This leads to production of large populations of T cells of various subpopulations to combat infection. The blood stream is the conduit that carries effector T cells to sites of infection, such as lungs, and also harbors memory T cells that recirculate to help prevent reinfection. Lungs are the sites where mycobacteria initially enter and invade the host. Granulomas form predominantly in the lung as a result of immune cells' attempt to contain TB infection.

In my thesis, I use a computational systems biology approach and develop models of the aforementioned multi-compartment system to study its properties and make predictions regarding mechanisms that drive different outputs of an immune response, which in turn influence infection outcomes. This will then provide key foci for further studies regarding treatment and vaccination strategies. I conduct my research with the following aims:

Aim 1: Investigate T cell priming in the LN. I develop and test a 3 dimensional (3D) ABM of the lymph node to study T cell priming and differentiation in generalized infection scenarios and perform global uncertainty and sensitivity analysis (U/SA) using Latin Hypercube Sampling (LHS) technique to explore the parameter space and Partial Rank Correlation Coefficient (PRCC) to assess the relationship between parameter input and model output. This model helps determine how LN effector cell output and LN "efficiency" change with system properties. I also investigate

how model dimensionality (i.e. 2D vs. 3D model formulation) affects model predictions, and test whether Fibroblastic reticular cell (FRC) network guidance and/or chemotactic signals facilitate T cell searching by DC or if random walks are sufficient. Model development and analyses are discussed in Chapter II and III.

Aim 2: Explore how T cell effector and memory differentiation is controlled. I develop a hybrid 2-compartmental model with an ODE blood compartment added to the lymph node model of Aim 1 to explore trafficking between the two physiological compartments. As in Aim 1, I use uncertainty and sensitivity analyses to investigate how memory and effector T cell differentiation and the extent of recall responses are affected by DC stimulation. I predict vaccination strategies to maximize memory cell production. The implementation of this model and its analyses are discussed in Chapter IV.

Aim 3: Connect immune responses with dynamics at the site of infection. I develop multi-compartment models by adding an existing agent-based lung model (previously developed in the lab) to study dynamics of cells in TB infection within all three physiological compartments involved. The model incorporates the idea of tunable resolution. I use this model to explore ideas of vaccine design and immune protection. Development of these model and proof-of-concept results are discussed in Chapter V.

Aim 4: Build a population model of TB granuloma dynamics at host level. I use this model to explore how single granuloma outcomes can be scaled to host scale, and identify potential tissue scale mechanisms that correlate with differential disease outcomes of individuals. Model formulation and results are discussed in Chapter VI.

Figures

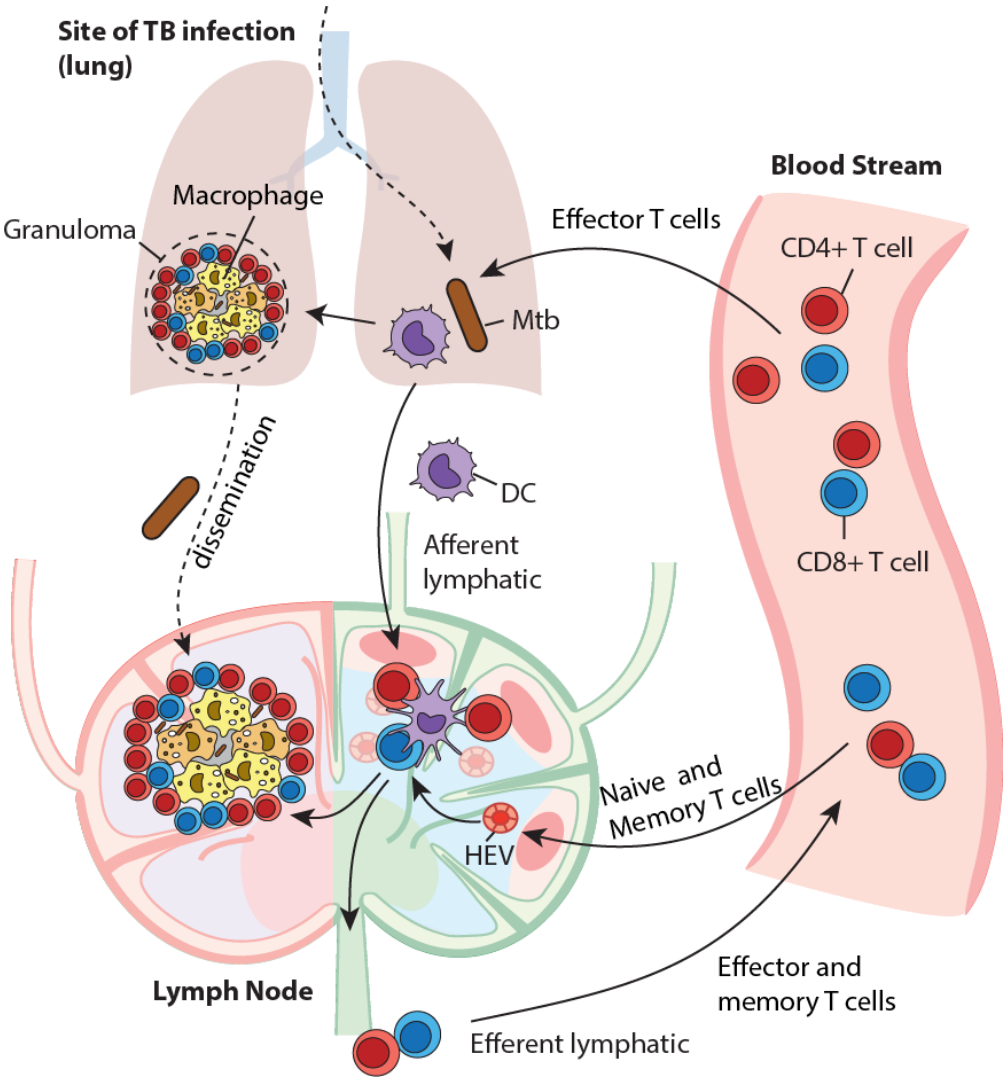

Figure 1.1: Physiological compartment involved in an adaptive immune response. Three physiological compartments are involved: the lungs, which are the sites of infection; LNs, where the adaptive immune response occurs, and blood circulation where immune cell are transported. Upon *Mtb* infection, bacteria enter the lung and infect mostly resident macrophages, but some of them are picked up by DCs and brought to the LN. In the LN, T cells are recruited from blood vessels and primed by Ag-bearing DCs. After priming, they proliferate and differentiate into effector and memory cells, and enter the blood circulation again via efferent lymphatics. Effector cells then enter the site of infection, where they join with activated and infected macrophages to form a granuloma. Granuloma immunologically restrains and physically contains bacteria. The structure of a granuloma is relatively stable if contained, but bacteria may disseminate to other parts of the lung, and even to LNs.

Bibliography

Ahmed, R. and Gray, D. Immunological memory and protective immunity: understanding their relation. *Science*, 272(5258):54–60, 1996.

Akira, S., Uematsu, S. and Takeuchi, O. Pathogen recognition and innate immunity. *Cell*, 124(4):783–801, 2006.

Andersen, P. and Woodworth, J. S. Tuberculosis vaccines–rethinking the current paradigm. *Trends in immunology*, 35(8):387–95, 2014.

Antia, R., Ganusov, V. V. and Ahmed, R. The role of models in understanding CD8+ T-cell memory. *Nature reviews. Immunology*, 5(2):101–111, 2005.

Arens, R. and Schoenberger, S. P. Plasticity in programming of effector and memory CD8 T-cell formation. *Immunological reviews*, 235(1):190–205, 2010.

Bachmann, M. F., Zinkernagel, R. M. and Oxenius, A. Immune responses in the absence of costimulation: viruses know the trick. *Journal of immunology (Baltimore, Md. : 1950)*, 161(11):5791–4, 1998.

Bajaria, S. H., Webb, G., Cloyd, M. and Kirschner, D. Dynamics of naive and memory CD4+ T lymphocytes in HIV-1 disease progression. *Journal of acquired immune deficiency syndromes*, 30(1):41–58, 2002.

Bajénoff, M., Egen, J. G., Koo, L. Y., Laugier, J. P., Brau, F., Glaichenhaus, N. and Germain, R. N. Stromal cell networks regulate lymphocyte entry, migration, and territoriality in lymph nodes. *Immunity*, 25(6):989–1001, 2006.

Barry, C. E., Boshoff, H. I., Dartois, V., Dick, T., Ehrt, S., Flynn, J., Schnappinger, D., Wilkinson,

R. J. and Young, D. The spectrum of latent tuberculosis: rethinking the biology and intervention strategies. *Nature reviews. Microbiology*, 7(12):845–55, 2009.

Beltman, J. B., Maree, A. F., Lynch, J. N., Miller, M. J. and de Boer, R. J. Lymph node topology dictates T cell migration behavior. *Journal of Experimental Medicine*, 204(4):771–780, 2007.

Bennett, S. R., Carbone, F. R., Karamalis, F., Flavell, R. A., Miller, J. F. and Heath, W. R. Help for cytotoxic-T-cell responses is mediated by CD40 signalling. *Nature*, 393(6684):478–80, 1998.

Bennett, S. R., Carbone, F. R., Karamalis, F., Miller, J. F. and Heath, W. R. Induction of a CD8+ cytotoxic T lymphocyte response by cross-priming requires cognate CD4+ T cell help. *The Journal of experimental medicine*, 186(1):65–70, 1997.

Blattman, J. N., Antia, R., Sourdive, D. J. D., Wang, X., Kaech, S. M., Murali-Krishna, K., Altman, J. D. and Ahmed, R. Estimating the precursor frequency of naive antigen-specific CD8 T cells. *The Journal of experimental medicine*, 195(5):657–664, 2002.

Blower, S. M., McLean, A. R., Porco, T. C., Small, P. M., Hopewell, P. C., Sanchez, M. A. and Moss, A. R. The intrinsic transmission dynamics of tuberculosis epidemics. *Nature Medicine*, 1(8):815–821, 1995.

Bogle, G. and Dunbar, P. R. Simulating T-cell motility in the lymph node paracortex with a packed lattice geometry. *Immunology and cell biology*, 86(8):676–687, 2008.

Bonneville, M., O'Brien, R. L. and Born, W. K. Gammadelta T cell effector functions: a blend of innate programming and acquired plasticity. *Nature reviews. Immunology*, 10(7):467–78, 2010.

Carroll, M. C. The complement system in regulation of adaptive immunity. *Nature immunology*, 5(10):981–6, 2004.

Casrouge, A., Beaudoing, E., Dalle, S., Pannetier, C., Kanellopoulos, J. and Kourilsky, P. Size estimate of the alpha beta TCR repertoire of naive mouse splenocytes. *Journal of immunology (Baltimore, Md. : 1950)*, 164(11):5782–5787, 2000.

Castillo-Chávez, C. and Aparicio, J. Mathematical modelling of tuberculosis epidemics. *Mathematical Biosciences and Engineering*, 6(2):209–237, 2009.

Castillo-Chavez, C. and Feng, Z. To treat or not to treat: the case of tuberculosis. *Journal of mathematical biology*, 35(6):629–656, 1997.

Chackerian, A. A., Alt, J. M., Perera, T. V., Dascher, C. C. and Behar, S. M. Dissemination of Mycobacterium tuberculosis Is Influenced by Host Factors and Precedes the Initiation of T-Cell Immunity. *Infection and Immunity*, 70(8):4501–4509, 2002.

Chapman, S. J. and Hill, A. V. S. Human genetic susceptibility to infectious disease. *Nature reviews. Genetics*, 13(3):175–88, 2012.

Cilfone, N. A., Perry, C. R., Kirschner, D. E. and Linderman, J. J. Multi-scale modeling predicts a balance of tumor necrosis factor-α and interleukin-10 controls the granuloma environment during Mycobacterium tuberculosis infection. *PloS one*, 8(7):e68680, 2013.

Curotto de Lafaille, M. A. and Lafaille, J. J. Natural and adaptive foxp3+ regulatory T cells: more of the same or a division of labor? *Immunity*, 30(5):626–35, 2009.

D'Amico, A. and Wu, L. The early progenitors of mouse dendritic cells and plasmacytoid predendritic cells are within the bone marrow hemopoietic precursors expressing Flt3. *The Journal of experimental medicine*, 198(2):293–303, 2003.

Dartois, V. The path of anti-tuberculosis drugs: from blood to lesions to mycobacterial cells. *Nature reviews. Microbiology*, 12(3):159–67, 2014.

Dartois, V. and Barry, C. E. A medicinal chemists' guide to the unique difficulties of lead optimization for tuberculosis. *Bioorganic & medicinal chemistry letters*, 23(17):4741–50, 2013.

De Boer, R. J. and Noest, A. J. T cell renewal rates, telomerase, and telomere length shortening. *Journal of immunology (Baltimore, Md. : 1950)*, 160(12):5832–7, 1998.

den Haan, J. M., Lehar, S. M. and Bevan, M. J. CD8(+) but not CD8(-) dendritic cells cross-prime cytotoxic T cells in vivo. *The Journal of experimental medicine*, 192(12):1685–96, 2000.

Diacovo, T. G., Blasius, A. L., Mak, T. W., Cella, M. and Colonna, M. Adhesive mechanisms governing interferon-producing cell recruitment into lymph nodes. *The Journal of experimental medicine*, 202(5):687–96, 2005.

Dye, C., Garnett, G. P., Sleeman, K. and Williams, B. G. Prospects for worldwide tuberculosis control under the WHO DOTS strategy. *The Lancet*, 352(9144):1886–1891, 1998.

Fallahi-Sichani, M., Flynn, J. L., Linderman, J. J. and Kirschner, D. E. Differential risk of tuberculosis reactivation among anti-TNF therapies is due to drug binding kinetics and permeability. *Journal of immunology (Baltimore, Md. : 1950)*, 188(7):3169–78, 2012a.

Fallahi-Sichani, M., Kirschner, D. E. and Linderman, J. J. NF-κB Signaling Dynamics Play a Key Role in Infection Control in Tuberculosis. *Frontiers in physiology*, 3:170, 2012b.

Fallahi-Sichani, M., Schaller, M. A., Kirschner, D. E., Kunkel, S. L. and Linderman, J. J. Identification of key processes that control tumor necrosis factor availability in a tuberculosis granuloma. *PLoS computational biology*, 6(5):e1000778, 2010.

Feng, Z., Castillo-Chavez, C. and Capurro, A. F. A model for tuberculosis with exogenous reinfection. *Theoretical population biology*, 57(3):235–247, 2000.

Flynn, J. L. and Chan, J. Immunology of tuberculosis. *Annual review of immunology*, 19:93–129, 2001.

Förster, R., Schubel, A., Breitfeld, D., Kremmer, E., Renner-Müller, I., Wolf, E. and Lipp, M. CCR7 Coordinates the Primary Immune Response by Establishing Functional Microenvironments in Secondary Lymphoid Organs. *Cell*, 99(1):23–33, 1999.

Garboczi, D. N., Ghosh, P., Utz, U., Fan, Q. R., Biddison, W. E. and Wiley, D. C. Structure of the complex between human T-cell receptor, viral peptide and HLA-A2. *Nature*, 384(6605):134–41, 1996.

Gerlach, C., Rohr, J. C., Perié, L., van Rooij, N., van Heijst, J. W. J., Velds, A., Urbanus, J., Naik, S. H., Jacobs, H., Beltman, J. B., de Boer, R. J. and Schumacher, T. N. M. Heterogeneous differentiation patterns of individual CD8+ T cells. *Science*, 340(6132):635–639, 2013.

Girard, J. P. and Springer, T. A. High endothelial venules (HEVs): specialized endothelium for lymphocyte migration. *Immunology today*, 16(9):449–57, 1995.

Glasgow, R. E., Lichtenstein, E. and Marcus, A. C. Why don't we see more translation of health promotion research to practice? Rethinking the efficacy-to-effectiveness transition. *American journal of public health*, 93(8):1261–7, 2003.

Grakoui, A. The Immunological Synapse: A Molecular Machine Controlling T Cell Activation. *Science*, 285(5425):221–227, 1999.

Greenberg, A. S., Avila, D., Hughes, M., Hughes, A., McKinney, E. C. and Flajnik, M. F. A new antigen receptor gene family that undergoes rearrangement and extensive somatic diversification in sharks. *Nature*, 374(6518):168–73, 1995.

Grigorova, I. L., Panteleev, M. and Cyster, J. G. Lymph node cortical sinus organization and relationship to lymphocyte egress dynamics and antigen exposure. *Proceedings of the National Academy of Sciences of the United States of America*, 107(47):20447–20452, 2010.

Guzzetta, G., Ajelli, M., Yang, Z., Merler, S., Furlanello, C. and Kirschner, D. Modeling socio-demography to capture tuberculosis transmission dynamics in a low burden setting. *Journal of theoretical biology*, 289:197–205, 2011.

Hansen, T. H. and Bouvier, M. MHC class I antigen presentation: learning from viral evasion strategies. *Nature Reviews Immunology*, 9(7):503–513, 2009.

Harding, F. A., McArthur, J. G., Gross, J. A., Raulet, D. H. and Allison, J. P. CD28-mediated signalling co-stimulates murine T cells and prevents induction of anergy in T-cell clones. *Nature*, 356(6370):607–9, 1992.

Heath, W. R., Belz, G. T., Behrens, G. M. N., Smith, C. M., Forehan, S. P., Parish, I. A., Davey, G. M., Wilson, N. S., Carbone, F. R. and Villadangos, J. A. Cross-presentation, dendritic cell subsets, and the generation of immunity to cellular antigens. *Immunological reviews*, 199:9–26, 2004.

Hoebe, K., Janssen, E. and Beutler, B. The interface between innate and adaptive immunity. *Nature immunology*, 5(10):971–4, 2004.

Huppa, J. B. and Davis, M. M. T-cell-antigen recognition and the immunological synapse. *Nature reviews. Immunology*, 3(12):973–83, 2003.

Janeway, C. A. The T cell receptor as a multicomponent signalling machine: CD4/CD8 coreceptors and CD45 in T cell activation. *Annual review of immunology*, 10:645–74, 1992.

Jenkins, M. K. and Moon, J. J. The role of naive T cell precursor frequency and recruitment in dictating immune response magnitude. *Journal of immunology (Baltimore, Md. : 1950)*, 188(9):4135–4140, 2012.

Jenkins, M. K., Pardoll, D. M., Mizuguchi, J., Chused, T. M. and Schwartz, R. H. Molecular events in the induction of a nonresponsive state in interleukin 2-producing helper T-lymphocyte clones. *Proceedings of the National Academy of Sciences of the United States of America*, 84(15):5409–13, 1987.

Jenkins, M. K., Taylor, P. S., Norton, S. D. and Urdahl, K. B. CD28 delivers a costimulatory signal involved in antigen-specific IL-2 production by human T cells. *Journal of immunology (Baltimore, Md. : 1950)*, 147(8):2461–6, 1991.

Joffre, O., Nolte, M. A., Spörri, R. and Reis e Sousa, C. Inflammatory signals in dendritic cell activation and the induction of adaptive immunity. *Immunological reviews*, 227(1):234–47, 2009.

Joffre, O. P., Segura, E., Savina, A. and Amigorena, S. Cross-presentation by dendritic cells. *Nature reviews. Immunology*, 12(8):557–69, 2012.

Jongbloed, S. L., Kassianos, A. J., McDonald, K. J., Clark, G. J., Ju, X., Angel, C. E., Chen, C.-J. J., Dunbar, P. R., Wadley, R. B., Jeet, V., Vulink, A. J. E., Hart, D. N. J. and Radford, K. J. Human CD141+ (BDCA-3)+ dendritic cells (DCs) represent a unique myeloid DC subset that cross-presents necrotic cell antigens. *The Journal of experimental medicine*, 207(6):1247–60, 2010.

Kaech, S. M. and Cui, W. Transcriptional control of effector and memory CD8+ T cell differentiation. *Nature reviews. Immunology*, 12(11):749–761, 2012.

Kaech, S. M., Tan, J. T., Wherry, E. J., Konieczny, B. T., Surh, C. D. and Ahmed, R. Selective

expression of the interleukin 7 receptor identifies effector CD8 T cells that give rise to long-lived memory cells. *Nature immunology*, 4(12):1191–8, 2003.

Kamath, A. T., Henri, S., Battye, F., Tough, D. F. and Shortman, K. Developmental kinetics and lifespan of dendritic cells in mouse lymphoid organs. *Blood*, 100(5):1734–1741, 2002.

Kapsenberg, M. L. Dendritic-cell control of pathogen-driven T-cell polarization. *Nature reviews. Immunology*, 3(12):984–93, 2003.

Kersh, E. N., Kaech, S. M., Onami, T. M., Moran, M., Wherry, E. J., Miceli, M. C. and Ahmed, R. TCR Signal Transduction in Antigen-Specific Memory CD8 T Cells. *The Journal of Immunology*, 170(11):5455–5463, 2003.

Kirschner, D. Dynamics of co-infection with M. Tuberculosis and HIV-1. *Theoretical population biology*, 55(1):94–109, 1999.

Kirschner, D. E., Hunt, C. A., Marino, S., Fallahi-Sichani, M. and Linderman, J. J. Tuneable resolution as a systems biology approach for multi-scale, multi-compartment computational models. *Wiley Interdisciplinary Reviews: Systems Biology and Medicine*, 6(4):289–309, 2014.

Lenaerts, A. J., Hoff, D., Aly, S., Ehlers, S., Andries, K., Cantarero, L., Orme, I. M. and Basaraba, R. J. Location of persisting mycobacteria in a Guinea pig model of tuberculosis revealed by r207910. *Antimicrobial agents and chemotherapy*, 51(9):3338–45, 2007.

Lenschow, D. J., Walunas, T. L. and Bluestone, J. A. CD28/B7 system of T cell costimulation. *Annual review of immunology*, 14:233–58, 1996.

Lin, P. L., Ford, C. B., Coleman, M. T., Myers, A. J., Gawande, R., Ioerger, T., Sacchettini, J., Fortune, S. M. and Flynn, J. L. Sterilization of granulomas is common in active and latent

tuberculosis despite within-host variability in bacterial killing. *Nature medicine*, 20(1):75–79, 2014.

Lin, P. L., Rodgers, M., Smith, L., Bigbee, M., Myers, A., Bigbee, C., Chiosea, I., Capuano, S. V., Fuhrman, C., Klein, E. and Flynn, J. L. Quantitative comparison of active and latent tuberculosis in the cynomolgus macaque model. *Infection and immunity*, 77(10):4631–4642, 2009.

Linderman, J. J., Riggs, T., Pande, M., Miller, M., Marino, S. and Kirschner, D. E. Characterizing the dynamics of CD4+ T cell priming within a lymph node. *Journal of immunology (Baltimore, Md. : 1950)*, 184(6):2873–2885, 2010.

Malissen, M., Trucy, J., Jouvin-Marche, E., Cazenave, P. A., Scollay, R. and Malissen, B. Regulation of TCR alpha and beta gene allelic exclusion during T-cell development. *Immunology today*, 13(8):315–22, 1992.

Marino, S., El-Kebir, M. and Kirschner, D. A hybrid multi-compartment model of granuloma formation and T cell priming in tuberculosis. *Journal of theoretical biology*, 280(1):50–62, 2011.

Marino, S., Hogue, I. B., Ray, C. J. and Kirschner, D. E. A methodology for performing global uncertainty and sensitivity analysis in systems biology. *Journal of theoretical biology*, 254(1):178–196, 2008.

Marino, S. and Kirschner, D. E. The human immune response to Mycobacterium tuberculosis in lung and lymph node. *Journal of theoretical biology*, 227(4):463–486, 2004.

Marino, S., Linderman, J. J. and Kirschner, D. E. A multifaceted approach to modeling the immune response in tuberculosis. *Wiley interdisciplinary reviews. Systems biology and medicine*, 3(4):479–89, 2010.

Marino, S., Pawar, S., Fuller, C. L., Reinhart, T. A., Flynn, J. L. and Kirschner, D. E. Dendritic cell trafficking and antigen presentation in the human immune response to Mycobacterium tuberculosis. *Journal of immunology (Baltimore, Md. : 1950)*, 173(1):494–506, 2004.

Miller, M. J., Safrina, O., Parker, I. and Cahalan, M. D. Imaging the single cell dynamics of CD4+ T cell activation by dendritic cells in lymph nodes. *The Journal of experimental medicine*, 200(7):847–856, 2004.

Miller, M. J., Wei, S. H., Parker, I. and Cahalan, M. D. Two-photon imaging of lymphocyte motility and antigen response in intact lymph node. *Science*, 296(5574):1869–1873, 2002.

Milner, F. A., Iannelli, M. and Feng, Z. A Two-Strain Tuberculosis Model with Age of Infection. *SIAM Journal on Applied Mathematics*, 62(5):1634–1656, 2002.

Mirsky, H. P., Miller, M. J., Linderman, J. J. and Kirschner, D. E. Systems biology approaches for understanding cellular mechanisms of immunity in lymph nodes during infection. *Journal of theoretical biology*, 287:160–70, 2011.

Murphy, B. M., Singer, B. H., Anderson, S. and Kirschner, D. Comparing epidemic tuberculosis in demographically distinct heterogeneous populations. *Mathematical Biosciences*, 180(1-2):161–185, 2002.

Murphy, B. M., Singer, B. H. and Kirschner, D. On treatment of tuberculosis in heterogeneous populations. *Journal of Theoretical Biology*, 223(4):391–404, 2003.

Murphy, K. M. *Janeway's immunobiology*. Garland Science, 2011.

Nakano, H. CD11c+B220+Gr-1+ Cells in Mouse Lymph Nodes and Spleen Display Characteristics of Plasmacytoid Dendritic Cells. *Journal of Experimental Medicine*, 194(8):1171–1178, 2001.

Nimmerjahn, F. and Ravetch, J. V. Fcgamma receptors as regulators of immune responses. *Nature reviews. Immunology*, 8(1):34–47, 2008.

O'Garra, A., Redford, P. S., McNab, F. W., Bloom, C. I., Wilkinson, R. J. and Berry, M. P. R. The immune response in tuberculosis. *Annual review of immunology*, 31:475–527, 2013.

Pearce, E. L. and Shen, H. Generation of CD8 T Cell Memory Is Regulated by IL-12. *The Journal of Immunology*, 179(4):2074–2081, 2007.

Pienaar, E., Cilfone, N. A., Lin, P. L., Dartois, V., Mattila, J. T., Butler, J. R., Flynn, J. L., Kirschner, D. E. and Linderman, J. J. A computational tool integrating host immunity with antibiotic dynamics to study tuberculosis treatment. *Journal of theoretical biology*, 367:166–179, 2014.

Pipkin, M. E., Sacks, J. A., Cruz-Guilloty, F., Lichtenheld, M. G., Bevan, M. J. and Rao, A. Interleukin-2 and inflammation induce distinct transcriptional programs that promote the differentiation of effector cytolytic T cells. *Immunity*, 32(1):79–90, 2010.

Ramakrishnan, L. Revisiting the role of the granuloma in tuberculosis. *Nature reviews. Immunology*, 12(5):352–366, 2012.

Randolph, G. J., Angeli, V. and Swartz, M. A. Dendritic-cell trafficking to lymph nodes through lymphatic vessels. *Nature reviews. Immunology*, 5(8):617–28, 2005.

Reinhardt, R. L., Khoruts, A., Merica, R., Zell, T. and Jenkins, M. K. Visualizing the generation of memory CD4 T cells in the whole body. *Nature*, 410(6824):101–5, 2001.

Rengarajan, J., Bloom, B. R. and Rubin, E. J. Genome-wide requirements for Mycobacterium tuberculosis adaptation and survival in macrophages. *Proceedings of the National Academy of Sciences of the United States of America*, 102(23):8327–8332, 2005.

Rescigno, M., Granucci, F., Citterio, S., Foti, M. and Ricciardi-Castagnoli, P. Coordinated events during bacteria-induced DC maturation. *Immunology Today*, 20(5):200–203, 1999.

Ridge, J. P., Di Rosa, F. and Matzinger, P. A conditioned dendritic cell can be a temporal bridge between a CD4+ T-helper and a T-killer cell. *Nature*, 393(6684):474–8, 1998.

Riggs, T., Walts, A., Perry, N., Bickle, L., Lynch, J. N., Myers, A., Flynn, J., Linderman, J. J., Miller, M. J. and Kirschner, D. E. A comparison of random vs. chemotaxis-driven contacts of T cells with dendritic cells during repertoire scanning. *Journal of theoretical biology*, 250(4):732–51, 2008.

Sakaguchi, S., Yamaguchi, T., Nomura, T. and Ono, M. Regulatory T cells and immune tolerance. *Cell*, 133(5):775–87, 2008.

Sallusto, F., Geginat, J. and Lanzavecchia, A. Central memory and effector memory T cell subsets: function, generation, and maintenance. *Annual review of immunology*, 22:745–63, 2004.

Sallusto, F., Lenig, D., Forster, R., Lipp, M. and Lanzavecchia, A. Two subsets of memory T lymphocytes with distinct homing potentials and effector functions. *Nature*, 402:34—-38, 1999.

Saltelli, A., Chan, K., Scott, E. M. and Others. *Sensitivity analysis*, volume 1. Wiley New York, 2000.

Schmid, D., Pypaert, M. and Münz, C. Antigen-loading compartments for major histocompatibility complex class II molecules continuously receive input from autophagosomes. *Immunity*, 26(1):79–92, 2007.

Segovia-Juarez, J. L., Ganguli, S. and Kirschner, D. Identifying control mechanisms of granuloma formation during M. tuberculosis infection using an agent-based model. *Journal of theoretical biology*, 231(3):357–76, 2004.

Segura, E., Amigorena, S. and Théry, C. Mature dendritic cells secrete exosomes with strong ability to induce antigen-specific effector immune responses. *Blood cells, molecules & diseases*, 35(2):89–93, 2005.

Shedlock, D. J. and Shen, H. Requirement for CD4 T cell help in generating functional CD8 T cell memory. *Science (New York, N.Y.)*, 300(5617):337–9, 2003.

Shiow, L. R., Rosen, D. B., Brdicková, N., Xu, Y., An, J., Lanier, L. L., Cyster, J. G. and Matloubian, M. CD69 acts downstream of interferon-alpha/beta to inhibit S1P1 and lymphocyte egress from lymphoid organs. *Nature*, 440(7083):540–544, 2006.

Singer, B. H. and Kirschner, D. E. Influence of backward bifurcation on interpretation of r(0) in a model of epidemic tuberculosis with reinfection. *Mathematical biosciences and engineering : MBE*, 1(1):81–93, 2004.

Sixt, M., Kanazawa, N., Selg, M., Samson, T., Roos, G., Reinhardt, D. P., Pabst, R., Lutz, M. B. and Sorokin, L. The conduit system transports soluble antigens from the afferent lymph to resident dendritic cells in the T cell area of the lymph node. *Immunity*, 22(1):19–29, 2005.

Smith, C. M., Wilson, N. S., Waithman, J., Villadangos, J. A., Carbone, F. R., Heath, W. R. and Belz, G. T. Cognate CD4(+) T cell licensing of dendritic cells in CD8(+) T cell immunity. *Nature immunology*, 5(11):1143–1148, 2004.

Smith, K. Interleukin-2: inception, impact, and implications. *Science*, 240(4856):1169–1176, 1988.

Sprent, J., Cho, J.-H., Boyman, O. and Surh, C. D. T cell homeostasis. *Immunology and cell biology*, 86(4):312–9, 2008.

Stemberger, C., Huster, K. M., Koffler, M., Anderl, F., Schiemann, M., Wagner, H. and Busch, D. H. A single naive CD8+ T cell precursor can develop into diverse effector and memory subsets. *Immunity*, 27(6):985–997, 2007.

Sun, J. C. and Bevan, M. J. Defective CD8 T cell memory following acute infection without CD4 T cell help. *Science (New York, N.Y.)*, 300(5617):339–42, 2003.

Sung, N. S., Crowley, W. F., Genel, M., Salber, P., Sandy, L., Sherwood, L. M., Johnson, S. B., Catanese, V., Tilson, H., Getz, K., Larson, E. L., Scheinberg, D., Reece, E. A., Slavkin, H., Dobs, A., Grebb, J., Martinez, R. A., Korn, A. and Rimoin, D. Central challenges facing the national clinical research enterprise. *JAMA : the journal of the American Medical Association*, 289(10):1278–1287, 2003.

Surh, C. D. and Sprent, J. T-cell apoptosis detected in situ during positive and negative selection in the thymus. *Nature*, 372(6501):100–3, 1994.

Swain, S. L. T cell subsets and the recognition of MHC class. *Immunological reviews*, 74:129–42, 1983.

Taniguchi, M., Harada, M., Kojo, S., Nakayama, T. and Wakao, H. The regulatory role of Valpha14 NKT cells in innate and acquired immune response. *Annual review of immunology*, 21:483–513, 2003.

Théry, C., Duban, L., Segura, E., Véron, P., Lantz, O. and Amigorena, S. Indirect activation of naïve CD4+ T cells by dendritic cell-derived exosomes. *Nature immunology*, 3(12):1156–62, 2002.

Trombetta, E. S. and Mellman, I. Cell biology of antigen processing in vitro and in vivo. *Annual review of immunology*, 23:975–1028, 2005.

van den Hoorn, T., Paul, P., Jongsma, M. L. M. and Neefjes, J. Routes to manipulate MHC class II antigen presentation. *Current opinion in immunology*, 23(1):88–95, 2011.

Veillette, A., Bookman, M. A., Horak, E. M. and Bolen, J. B. The CD4 and CD8 T cell surface antigens are associated with the internal membrane tyrosine-protein kinase p56lck. *Cell*, 55(2):301–308, 1988.

Vroomans, R. M. A., Marée, A. F. M., de Boer, R. J. and Beltman, J. B. Chemotactic migration of T cells towards dendritic cells promotes the detection of rare antigens. *PLoS computational biology*, 8(11):e1002763, 2012.

Walker, L. S. K. and Abbas, A. K. The enemy within: keeping self-reactive T cells at bay in the periphery. *Nature reviews. Immunology*, 2(1):11–9, 2002.

Weiner, J. and Kaufmann, S. H. E. Recent advances towards tuberculosis control: vaccines and biomarkers. *Journal of internal medicine*, 275(5):467–80, 2014.

WHO. *Global Tuberculosis Report 2014*. World Health Organization, 2014.

Wigginton, J. E. and Kirschner, D. A Model to Predict Cell-Mediated Immune Regulatory Mechanisms During Human Infection with Mycobacterium tuberculosis. *The Journal of Immunology*, 166(3):1951–1967, 2001.

Wilson, N. S., El-Sukkari, D., Belz, G. T., Smith, C. M., Steptoe, R. J., Heath, W. R., Shortman, K. and Villadangos, J. A. Most lymphoid organ dendritic cell types are phenotypically and functionally immature. *Blood*, 102(6):2187–94, 2003.

Wolfram, S. Cellular automata as models of complexity. *Nature*, 311(5985):419–424, 1984.

World Health Organization. BCG vaccine. WHO position paper. *Wkly Epidemiol Rec*, 79(4):27, 2004.

Wu, L. and Liu, Y.-J. Development of dendritic-cell lineages. *Immunity*, 26(6):741–50, 2007.

Young, D., Stark, J. and Kirschner, D. Systems biology of persistent infection: tuberculosis as a case study. *Nature reviews. Microbiology*, 6(7):520–528, 2008.

Zhou, D. and Blum, J. S. Presentation of cytosolic antigens via MHC class II molecules. *Immunologic research*, 30(3):279–90, 2004.

Zhou, D., Li, P., Lin, Y., Lott, J. M., Hislop, A. D., Canaday, D. H., Brutkiewicz, R. R. and Blum, J. S. Lamp-2a facilitates MHC class II presentation of cytoplasmic antigens. *Immunity*, 22(5):571–81, 2005.

Zhou, L., Chong, M. M. W. and Littman, D. R. Plasticity of CD4+ T cell lineage differentiation. *Immunity*, 30(5):646–55, 2009.

Zinkernagel, R. M., Bachmann, M. F., Kündig, T. M., Oehen, S., Pirchet, H. and Hengartner, H. On immunological memory. *Annual review of immunology*, 14:333–67, 1996.

CHAPTER II

Predicting lymph node output efficiency through systems biology

2.1 Introduction

Adaptive immunity develops in response to pathogens that cannot be cleared by first line defenses. It relies on the selective recognition of foreign antigens (Ags) to direct the immune response and can lead to long-lived immunological memory. Secondary lymphoid tissues such as the Peyer's patches, lymph nodes (LNs) and spleen are the canonical sites where adaptive immune responses are initiated. Here, naive lymphocytes (both CD4+ and CD8+ T cells) encounter antigen-presenting cells (APCs), such as dendritic cells (DCs), bearing foreign Ag. Each naive T cell clone expresses a T cell receptor (TCR) with unique specificity for antigenic peptides bound to major histocompatibility (MHC) molecules on the surface of an APC. The clonal frequency of T cells for any given Ag varies, but is typically low, with about one in a million T cells specific for each unique Ag epitope (referred to as *cognate frequency*).

Two-photon microscopy (2PM) allows single-cell lymphocyte dynamics to be analyzed deep within intact lymphoid tissues and in living mice (Miller et al., 2002; Germain and Jenkins, 2004; Miller et al., 2004a). However, a comprehensive understanding of immune cell interactions during

The work in Chapter II is pubished as Gong, Chang, Joshua T. Mattila, Mark Miller, JoAnne L. Flynn, Jennifer J. Linderman, and D. Kirschner. 2013. *"Predicting Lymph Node Output Efficiency Using Systems Biology."* Journal of Theoretical Biology 335 (October): 169184. doi:10.1016/j.jtbi.2013.06.016.

infection is still lacking, and, in particular, the fate of individual cells over longer timeframes is difficult to track *in vivo*. Systems biology approaches can be used to integrate knowledge into a discrete and stochastic representation of LNs and simulate cellular dynamics occurring within a LN(Mirsky et al., 2011). Agent-based models (ABM) are widely used to study emergent properties of complex systems with interacting heterogeneous components, making them ideal for studying immune cell dynamics and lymphoid tissue function.

ABMs have been used to examine important aspects of LN dynamics, including naive T cell motility and behavior in the LN (Bogle and Dunbar, 2008; Riggs et al., 2008), the physical interaction between DCs and T cells (Beltman et al., 2007; Zheng et al., 2008) and the role of chemotaxis is facilitating cognate T cell-DC interactions (Castellino et al., 2006; Riggs et al., 2008). In particular, we (Linderman et al., 2010) used an ABM to study factors influencing CD4+ T cell priming and proliferation; our two dimensional (2D) model predicted a LN efficiency, the ratio of the number of effector T cells leaving the LN to the number of naive cognate T cells entering the LN. Our model indicated that the primed CD4+ T cell output is linearly correlated with cognate frequency, but not with the number of Ag-bearing DCs. Bogle et al (Bogle and Dunbar, 2010a) developed a 3D ABM to simulate T cell activation in the LN during an immune response, and a recent extension of this model (Bogle and Dunbar, 2012) incorporated detailed mechanisms regarding T trafficking. However, infection dynamics and the capacity of LN to produce effector T cells has yet to be analyzed in the context of realistic LN structure and T cell density.

New data presented here regarding LN anatomy allow us to update our previous model framework (Riggs et al., 2008; Linderman et al., 2010). As new experimental data increase our understanding of lymphoid tissue structure and function, this information provides an opportunity to refine, expand and validate our models and simulations. In addition, we are interested in using a 3D ABM model to test how LN output (defined by the generation of primed T cells) responds to changes in numbers of APCs and cognate T cells during different infection scenarios. Fur-

thermore, we address a debate within the modeling community: do 2D computational models of LN have predictive value for understanding 3D cell dynamics and LN function *in vivo* or are 3D models required?

In this study, we present a novel 3D ABM that captures T cell and DC dynamics, can accommodate low (physiological) cognate T cell frequencies, and includes T cell activation and expansion kinetics. We built and validated this model by comparing our model simulations to data generated by in situ imaging approaches. We use this model to address questions that are currently intractable with *in vivo* imaging, due to the limits of tracking individual cells over long time scales. Our model allows us to test quantitative predictions for how perturbations to LNs affect not only single-cell dynamics, but more importantly T cell activation and expansion kinetics, which has direct relevance for vaccine design and guiding therapeutic interventions for infection.

2.2 Methods

2.2.1 Model geometry and cell density

Our 3D model represents a trabecular region of a generalized LN. Figure 2.1 shows an idealized LN structure. Afferent lymphatic vessels deliver lymph fluid and DCs into the subcapsular sinus, where they enter into LN parenchyma. LN parenchyma is organized into B cell follicles and T cell zones. Trabeculae further divide the parenchyma into incompletely separate compartments. T cells are recruited from high endothelial venules (HEV). Within the T cell zone, our region of focus, DCs and T cells interact. T cells drain into the medullary sinuses and exit the LN via efferent lymphatic vessels. In order to determine the size and structure of a LN (and the T cell zone in particular), we used immunofluorescence images of LN sections from non-human primates (NHPs). As shown in Figure 2.2, the deeper cortex of an LN mainly consists of T cells (blue). In this LN section, the area is bean-shaped with a diameter of 2.6 mm. The T cell zone is a shell about 800 μm thick surrounding the medulla. PNAd is a marker for High Endothelial Venules (HEVs), the sites

where CD4+ and CD8+ T cells enter the LN. From the image we can see that HEVs are distributed through out the T cell zone. LYVE-1 is a marker of medullary and cortical sinuses, from which T cells are collected into efferent lymphatics and exit a LN. Medullary sinuses are distributed at the bottom of T cell zones. Cortical sinuses can be found near the structures that divide T cell zones laterally, and are typically in vicinity of HEV. This distribution pattern of cortical sinuses is also observed in mouse studies(Grigorova et al., 2010).

We also analyzed the T cell zones of these images and calculated the T cell density. We measured the cell density from the NHP LN images using the software CellProfiler (Carpenter et al., 2006). We sampled five 200 x 200 μm regions of the T cell zone. The depth of the sections is 5 μm, which is approximately the diameter of a T cell. We calculated the density of CD3+ cells (both CD4+ and CD8+ T cells) to be $4.0 \pm 0.4 \times 10^6 mm^{-3}$.

Based on these first time data from primate LNs (Figure 2.2) and other studies (Grigorova et al., 2010), we designed the grid structure of our 3D LN ABM (Figure 2.3). We abstracted the shape of the T zone in the LN to be part of a spherical shell, with thickness of 800 μm. Accounting for symmetry within T zones (Figure 2.1, 2.2), we chose a section of the LN to model by defining a computational grid in the shape of a cone-plug similar to a trabecular section (Figure 2.3). This volume represents roughly 0.5% of a LN and balances biological relevance and computational performance. Volumes up to 2% of a LN were tested in simulations to confirm that model behavior is preserved. We define our grid compartments as cubes of edge length 5 μm. The entire LN grid has 344148 grid compartments, and the total volume is 0.043 μL. The number of T cells on the grid in steady state is about 7×10^5.

We also generated a fibroblastic reticular cell (FRC) network, which occupies 17% of the entire LN grid (Beltman et al., 2007). This network has a wide range of functions in LNs, but in our current model it serves to blocks movement of cells. We explore the role of the FRC further in other work.

2.2.2 Model agents and interactions

Within the T cell zone, DCs display peptide-MHC (pMHC) on their surfaces and move randomly. T cells migrate through the T cell zone until they encounter a DC bearing cognate Ag. T cells recognizing pMHC are activated over several hours while bound to DCs (Celli et al., 2007). After detaching from the DC, T cells are primed and undergo several rounds of division before exiting the LN.

Our model is based on a stochastic cellular automaton, in which different types of cells (T cells and DCs) are represented as agents on a 3D grid. In discrete time steps, the agents move on the grid. Agents interact with their environment as well as other agents following a defined set of rules with stochastic components. These rules are based on current understanding of immunology, or in the case where experimental evidence is insufficient, assumptions were made. For a complete list of agent rules see the on-line Supplement. Figure 2.4 depicts the model and below we give more details regarding how data were used to build and validate the model, with data from both mice and NHP studies (Figure 2.2). The emergent behavior of our virtual LN is quantitatively analyzed in real-time simulations.

The LN ABM includes three sets of cells: CD4+ T cells, CD8+ T cells and DCs, each with different activation states: CD4+ and CD8+ T cells can be resting, bound or proliferating. When cells have undergone a sufficient number of divisions, they can exit the LN and we refer to them as effector T cells, even though they need continual cytokine or Ag stimulation to remain full activated. DCs can be immature, Ag-bearing (Ag-DC), or licensed (LDC). We briefly summarize the rules for the cell agent here, but a full list of rules is given in the on-line supplement.

CD4+ T cells

CD4+ T cells are 5 x 5 x 5 μm in size, which is equal to the size of one grid compartment. These cells are recruited via HEVs with probability specified in the parameter file (see Appendix A). At each time step, free CD4+ T cells move one grid compartment in a randomly selected

direction. We define preferred and non-preferred movement directions relative to the previous movement direction (based on the idea of random walk with persistence (Riggs et al., 2008)), and assign probabilities to the possible 26 different direction options in 3D. Movement of CD4+ T cells are periodic or toroidal at boundaries, so if a cell steps off the grid, the same type of cell emerges on the opposite side of the grid.

Cognate CD4+ T cells can be primed by Ag-DCs and LDCs. When a T cell enters the LN grid, it will be either a cognate or non-cognate cell based on the cognate frequency specified (ranging from 1.6×10^{-5} to 1×10^{-2} in our simulations). At each time step, we check whether there are Ag-DCs or LDCs in the binding radius of a cognate CD4+ T cell. If there are DCs available for binding, one is chosen randomly and attempts binding with a probability based on a logistic function that accounts for pMHC-II levels (see Supplement). Before unbinding from the DC (Miller et al., 2004b), the amount of accumulated stimulation is calculated, and a T cell will either be primed and become activated, or remain in the resting naive state. Activated T cells proceed through a series of cell divisions. Daughter cells are identical to mother cells in most attributes. After 4 divisions (as estimated in a previous study (Linderman et al., 2010)), the CD4+ T cells are classified as effector cells and can leave the LN.

CD4+ T cells can die anytime during these dynamics when they exhaust their life span. They can also leave the grid by draining through medullary sinuses and exiting via efferent lymphatics (ELs) in both resting and effector states. The rate of T cells exiting the grid is controlled by the parameter specifying the number of the EL elements generated the grid (See appendix). Actively dividing cells are excluded from exiting because of down regulated $S1P_1$ on the surface of T cells needed for their egress (Shiow et al., 2006).

CD8+ T cells

The rules and dynamics of CD8+ T cells are similar to those outlined above for CD4+ T cells. However, only LDCs can prime CD8+ T cells. This rule represents a requirement for CD4+ T cell

help for CD8+ T cell expansion (Smith et al., 2004), and the binding and priming are based on pMHC-I molecule level on the surfaces of these LDCs. The model is flexible to account for testing other CD8+/CD4+ dependencies for activation.

Dendritic cells

DCs are larger in size than T cells; they occupy 8 compartments (2 x 2 x 2) on our grid (see Figure 2.4). DCs are recruited from the top of the grid (representing afferent lymphatics, Figure 2.1). The region of entry is controlled by two parameters, specifying top and bottom grid slices (See Appendix A). Unlike T cells, DCs are not allowed to leave the LN. This assumption is based on experimental data showing that DCs are not typically found in the medullary sinuses. When recruited, DCs can be immature (IDC) or Ag-DCs. At each time step, one DC is recruited with a given probability. DCs can move in any of 26 directions (defined as the Moore neighborhood) with the same probability. To capture DC movement around other cells, we assume that if there are T cells in the destination grid space that a DC is moving into, the T cells will be relocated to neighboring compartments. We also assume that DCs exhibit some plasticity, and can bend around the FRC structure. We assume reflecting boundary conditions for DCs (i.e. DCs cannot cross the LN boundary). This assumption is appropriate because DCs rarely reach the boundaries as their movement is slow compared to T cells and then accumulate around HEVs (Miller et al., 2004a;b; Girard et al., 2012). It also simplifies computations, as DCs simultaneously occupy 8 model compartments.

At the time of entry into the LN, each DC is assigned a number of both surface pMHC-I and pMHC-II molecules from a given range of values. The number of pMHCs decrease over time according to a value for the pMHC-I and pMHC-II half-life decay values (Zehn et al., 2004). IDCs can be activated if they come into contact (the Moore neighborhood- the 26 surrounding compartments) with an Ag-DC or LDC. Primed CD4+ T cells in contact with an Ag-DC can license that Ag-DC to become an LDC with a given probability. The numbers of pMHC I and II

on the surface of a DC increase after activation or licensing (Brophy et al., 2007). DCs die when their ages exceed the limit drawn from a distribution.

2.2.3 Model Parameter Estimation

There are a total of 74 parameters in our 3D LN model, governing the behavior of CD4+ T cells, CD8+ T cells, DCs and the environment of the LN. We grouped parameters into different functional sets such as anatomical structure or based on mechanisms they are involved in, for example: motility, population size, priming related, etc. Values of parameters were taken from experimental studies when available, or adopted from previous models. For those parameters for which we are unable to find an experimental value, we estimate a range based on biological knowledge. These values and ranges are shown in Appendix A. , All parameters were studied using uncertainty analysis to assess how changes in their values affect simulation outputs and to help fine tune their values based on validation with data. Values of parameters related with physiological structure and cell movement are estimated with an uncertainty analysis. A baseline situation ("no infection/no antigen") in which no Ag-DCs are recruited to the LN is established with these parameter values.

2.2.4 Definition of Model Outputs

We define a several outputs that we use to explore model behavior in detail:

Transit time: average time for a T cell to travel through a LN (Linderman et al., 2010). A non-cognate T cell requires about 24 h to travel through the entire lymph system and exit into the blood, based on data from cannulated thoracic ducts (Sprent and Tough, 2001). Since there are 700 LNs distributed throughout the body, we estimate that it should take on average less than 24 hours but more than 1 hour for a T cell to traverse a LN. For each T cell, we record when it enters the grid from HEV and when it exits through an EL.

Search time: average time for a T cell to find the first matching Ag-DC or LDC.

Match percentage: percentage of cognate T cells that detected Ag-DC or LDC before exiting

the LN.

Scanning rate: average number of T cells contacted by a DC per unit time. Mature or licensed DCs constantly probe their surroundings for cognate T cells. A scanning rate is calculated by dividing the increment of a scanning event during unit time by the average Ag-DC/LDC ratio. In mice the T cell scanning rate has been reported to be between 500 and 4000, depending on the experimental system (Bousso and Robey, 2003; Miller et al., 2004a). We keep a record of both the total number of scanning **apparent scanning rate**, as well as the number of T cells that have not been previously scanned by the same DC **unique scanning rate**.

Displacement: distance traveled by a cell. For both T cells and DCs, we record the number of steps taken by cells (maintained within vectors). By vector addition, we get the displacement of the cell over any given time interval; and by summing the length of these vectors we calculate the distance that the cell travels in a time interval.

Motility coefficient: Assuming a random walk, the motility coefficient M (Miller et al., 2004b) is calculated from $M = x^2/6t$ where x is the displacement of a T cell and t is time. We also calculated the velocity of these cells by obtaining the regression coefficient of distance versus time. We used the same algorithm to calculate motility coefficient and velocity for both 2PM data from mouse experiments and model simulations.

Free path: The average length of a cell traveling without changing its direction is a description of T cell movement in a LN (Miller et al., 2003). In our model, we implemented explicit criteria for a free path called **current trajectory free path**, which compares the direction of each single step in a current free path to the direction of the vector from the initial point to current location of cell. If a step is longer than 5μm and the angle is larger than 45 degrees, we assume the current free path ends and a new free path starts. This algorithm was developed to enable the comparison between simulated results and 2PM data (see supplemental rules for more information).

LN priming efficiency: the ratio of the number of effector T cells leaving the LN to the number

of naive cognate T cells entering the LN (Linderman et al., 2010). We use this measurement as an indicator of the capacity of LN to expand the cognate T cell population during an immune response. As a primary model output, we record the number of effector T cells exiting the LN and the numbers of incoming naive cognate T cells during a period of time and calculate their ratio. We apply this method to chronic infection scenarios where different cell populations are in steady-state, so that the start/end time points of the simulation will not introduce bias.

2.2.5 Simulated acute and chronic infection scenarios

We introduce Ag-DCs to the system in two ways to simulate 2 different types of generalized infection scenarios: acute infection (brief Ag input and then waning after a specified number of days) and chronic infection (constant Ag input). We first simulate cellular dynamics within a LN in the absence of Ag-DC until a steady state is reached. Then, Ag-DCs are recruited to the system. To mimic an acute infection dynamic, we chose a DC recruitment period of 5 days to model a generalized host response. To mimic chronic infection, Ag-DCs are introduced into the system at a constant rate until the end of the simulation.

2.2.6 Uncertainty and sensitivity analysis

A complete list of all model parameters and their values are listed in Table 2.1 of the Appendix A. We use uncertainty analysis to study how parameter variability induces variability of model outputs. Latin Hypercube Sampling (LHS) is employed in order to sample the high dimensional parameter space efficiently (Marino et al., 2008). In cases where a distribution for a parameter is unknown, we assume a uniform distribution within a physiologically plausible, but large, range. For each parameter value combination, simulations are performed with multiple replications (to account for stochastic uncertainty, i.e. aleatory uncertainty) and statistics are recorded. Partial Rank Correlation Coefficients (PRCCs) are calculated to evaluate global parameter sensitivity (Marino et al., 2008). The variability of each recorded output statistic is apportioned to the variability of in-

put parameter values, and non-linear monotonic relationships are detected. We use this correlation coefficient as an indicator of sensitivity of a specific model output to different model mechanisms and inputs. This allows us to predict factors in the model that are key to driving system dynamics.

After defining a baseline simulation, we use sensitivity analysis to focus on a specific set of parameters involved in T cell priming events to study how they affect model output. This allows us to make predictions for how LN output will change if we modify corresponding mechanisms *in vivo*. 500 experiments are performed, and each experiment is simulated with 5 replications. After the simulation, the model outputs of each experiment were averaged, and the PRCC of average model output of interest (e.g. scanning rate, match percentage and output of effector cells) was calculated against the parameters that were varied. Then, PRCCs were tested for significance with significance level of α = 0.001.

To complement the uncertainty and sensitivity performed above, we also apply, for the first time in the setting of an ABM, an additional tool known as the extended Fourier amplitude sensitivity test (eFAST) (Cukier, 1973; Collins and Avissar, 1994; Saltelli and Bolado, 1998; Saltelli et al., 2012; 2004; Marino et al., 2008). This method is more general than PRCC (i.e. it applies to non-linear non-monotonic relationship between input and output variability) and will help confirm the sensitivity of parameters as determined using the LHS/PRCC method. eFAST is a variance decomposition method: parameter values are varied at different frequencies, and variability of output is quantified and partitioned by Fourier analysis. Therefore, the fraction of the variance explained by each input parameter is an indication of the model's sensitivity to this parameter. We picked parameters related to priming and simulated the chronic infection with 65 sampling, 2 re-sampling and 4 replications focusing on each of these parameters. We use the first order effect (S_i) and total effect (S_{Ti}, sum of first order and higher order effects) of eFAST protocol to evaluate sensitivity. Details of the implementation can be found in an earlier publication(Marino et al., 2008).

To understand the robustness of the model, we examined the source of uncertainty by comparing results from replications and results from different parameter sets. As discussed in previous studies (Marino et al., 2008), in ABMs, it is not possible to entirely separate the aleatory uncertainty that is generated from stochastic components of simulations from epistemic uncertainty that is generated from variations in parameter values. Although for some of the outcomes the two effects can be distinguished (Figure 2.5A), for others, aleatory uncertainty could partially mask epistemic uncertainty (Figure 2.5). We address this by using the mean of multiple simulations as the input into the PRCC program (Marino et al., 2008).

2.2.7 Computational simulations and implementation

Our ABM is written in C++ and runs on Linux/Mac/Windows. Pseudo code for the agent rules is available in the online Supplement (`http://malthus.micro.med.umich.edu/lab/movies/3dLN/`). Simulations require about 6-10 hours depending on the total number of time steps and the size of LN grid. Each simulation is repeated 5 to 10 times in the sensitivity analysis.

2.3 Results

The key goals of this work are predictions about the efficiency of LNs in priming T cells and determination of how the model simulation environment dimension (i.e., 2D vs 3D) affects those predictions. We built, calibrated and validated an ABM model based on available data and data generated herein as described in Methods. A sample snap shot simulation is shown in Figure 2.3C.

2.3.1 T cell motility validation

Figures 2.6A,B show T cell track data measured by 2PM. We generated 2 sets of data describing T cell tracks from 3D live tissue, with imaging intervals of 11 and 27 seconds respectively, and calculated the mean free path of the recorded T cell tracks (Figure 2.5A,B). We then calculated the motility coefficient and velocity of these data (Table 2.1). Any discrepancy between velocities

calculated from these two datasets arises as a consequence of a more detailed track from a finer imaging interval in the 2PM.

We used these data to calibrate our model before introduction of Ag-DCs. Our simulations agree with these data as well as with data from other modeling studies regarding duration of T cells travelling through a LN and the rate of T cells exiting the LN (700-1400 per minute per 10^6 cells) (Bogle and Dunbar, 2010b) (Table 2.1).

We also create time-lapse simulations of cell movement in our 3D LN model. Simulations in the absence of Ag-DCs are available at `http://malthus.micro.med.umich.edu/lab/movies/3dLN/` (On-line Supplement Movie 1).

2.3.2 Simulating acute infection dynamics

The temporal dynamics of an acute infection scenario are shown in Figure 2.7 and spatiotemporal dynamics are shown in a time-lapse simulation (Supplement Movie 3,`http://malthus.micro.med.umich.edu/lab/movies/3dLN/`). The number of Ag-DCs begins to increase from day 0. CD4+ T cells are activated after binding with Ag-DCs, and then further differentiate into fully primed T cells. Ag-DCs are gradually activated to LDC phenotypes after about 2 days, in the presence of these newly primed CD4+ T cells. Licensed DCs are able to prime CD8+ T cells. The priming of CD8+ T cells and the initiation of proliferation and generation of activated cells exhibit a delay of about 2.5 days compared to CD4+ T cells (Figure 2.7B and C.) After DC recruitment ceases, primed T cell counts drop while Ag-DCs and LDCs die out (they have a very short half-life), and the system gradually returns to a baseline uninfected scenario. When Ag-DCs and LDCs are present, we observed almost a constant rate of CD4+ and CD8+ primed T cell output from the LN, where primed CD8+ T cells appear a few days later, and more of them are produced during the process (Figure 2.7D). The dynamics generated in this case is representative of what happens in an acute infection where an adaptive immune response to a generalized pathogen clears

infection (reduces Ag to zero) within a couple of weeks.

2.3.3 Simulating Chronic infection dynamics

In a chronic scenario, the initial pattern of cellular dynamics follows closely what is observed during our acute infection simulations (compare Figure 2.7 with Figure 2.8 for early points by day 8). However, after about day 8, numbers of different subpopulations of DCs (Figure 2.8A) and T cells (Figure 2.8B,C) reach a new steady state, resulting in a constant rate of output of fully primed (effector-like) CD4+ and CD8+ T cells (Figure 2.8D). The dynamics generated above reflect the response of an immune system when faced with a chronic infection, constantly challenging host defense mechanisms.

2.3.4 Baseline LN statistics and LN priming efficiency scales with grid size

We compare simulations using a LN model of original size (Figure 2.3) to those run on a larger grid to test whether cell dynamics are independent of grid size. The larger grid has the same height, but twice the length and width to yield a grid representing four times the volume of our standard simulated LN region. The number of HEVs, ELs and the DC recruitment rate are increased proportionally on the larger grid. For each grid, 10 simulations were performed and the results are shown in Table 2.2. T cell density, motility and transit time are preserved over the two LN grid sizes. Furthermore, the priming process and related results were not sensitive to LN grid size, as scanning rate, LN priming efficiency and search time all remain unchanged. Thus, the section of the LN T zone we model (Figure 2.3) is sufficient to capture larger scale LN dynamics. These results also suggest that using reflecting boundary conditions (as opposed to toroidal boundary conditions) for DCs does not affect model output.

2.3.5 LNs maintain a high priming efficiency when cognate frequency increases

In our previous studies, we found that LN efficiency related to priming of CD4+ T cells is unaffected by cognate frequency in a 2D ABM model of a LN but increased and then plateaued with the number of Ag-DCs (Riggs et al., 2008; Linderman et al., 2010). To test whether this also holds true in our 3D model, we uncoupled cognate frequency of CD4+ and CD8+ T cells to study how priming of each cell type is affected. For each set of simulations, we varied the maximum number of Ag-DCs in the simulation from 50 to 550 (total or per time point), together with the DC recruitment rate (Figure 2.9A, B). This allows us to test how varying levels of APC affects priming. In addition, we simultaneously varied cognate frequency of CD8+ T cells from 1.6×10^{-5} (in the range of true physiological condition) to 0.01 (a boosted high frequency, similar to that used in 2PM studies). Simulations are carried out with low and high CD4+ cognate frequencies. Under both conditions, CD8+ T cell priming efficiency increases as DC recruitment is increased, until LN efficiency plateaus near 350 Ag-DCs. Additional Ag-DCs do not lead to additional T cell priming, indicating that saturating the LN with Ag-DCs would not be effective. For each given Ag-DC level, the increase of cognate frequency only resulted in slight reduction of LN efficiency, indicating the effector output is almost linear to the precursor cognate frequencies. We also tested how CD4+ T cell cognate frequency affects LN efficiency for priming of CD4+ T cells. Our results show that across different DC numbers, LN efficiency of CD4+ T cells is also only altered in a relatively small range when CD4+ cognate frequency increases in orders of magnitudes, from 1.6×10^{-5} to 0.01 (Figure 2.9C). These results agree with our previous study (Linderman et al., 2010) ; LNs have a high theoretical T cell priming capacity over a wide range of cognate frequencies. In other words, LNs potentially maintain T cell priming efficiency for cognate frequencies that range from high physiological values to over 3 orders of magnitude larger.

We also calculated the CD8+ T cell priming efficiency when CD4+ T cell cognate frequencies vary between low and high ranges, and observed that CD8+ T cell LN efficiency is higher when

more cognate CD4+ T cells are present, as expected. , In the case of high CD4+ cognate frequency, the differences in efficiency across various CD8+ cognate inputs are even smaller (Figure 2.9A vs. B), and the plateau is reached earlier. These simulations suggest that if the LN system is augmented by introducing more cognate CD8+ T cells to the system (e.g. by vaccination), LN efficiency will remain almost unaffected. In addition, LN efficiency can be enhanced by adding exogenous Ag-DCs and/or cognate CD4+ T cells.

2.3.6 LN scanning is more efficient in 3D than 2D

In our previous 2D study, we calculated a LN efficiency for CD4+ T cells of about 4-5 (Linderman et al., 2010). Using our 3D ABM of a LN T zone, we now find LN efficiencies for CD4+ T cells of up to 15. We also assessed the match percentage and search time, and results are shown in Table 2.3. The match percentage in our 3D model is about 90%, higher than the 40-60% measured in our 2D model (Linderman et al., 2010). The average 3D search time is only 10 min, less than the 2-5 hours measured in our 2D model.

We next "flattened" our 3D LN grid to mimic a 2D model (which preserves dimensions in the previous 2D simulations as well). Using the same set of parameters, simulations yield a match percentage of 50% and a search time of 150 min (Table 2.3), similar to those obtained in our previous 2D model (Linderman et al., 2010). Thus, match percentage and search time are highly dependent on model dimensionality.

Why is it easier for cognate T cells to find their matched Ag-DC in 3D compared to 2D? To understand this, we calculated the average distance to the nearest neighbor among DCs in 2D and 3D (Clark, 1954; Clark and Evans, 1979) using:

$$\mu(r) = \frac{[\Gamma(k/2+1)]^{1/k}\Gamma(1/k+1)}{\rho^{1/k}\pi^{1/2}}, \tag{2.1}$$

where $\mu(r)$ is the expected mean distance between individuals when a population is randomly

distributed; k is the dimension and ρ is the population mean density. For the DC density used in our model, the average nearest neighbor distance between DCs calculated by Equation 2.1 is 29.5 μm in 3D, and 82.5 μm in 2D. Thus a large part of the increase in the T cell search efficiency in 3D is due to shorter neighbor distances between DCs.

The frequency of T cells visiting the same DC was less in 3D than 2D. We tested this by tracking how many T cells a DC can scan on average per hour. As shown in Table 2.3, the apparent scanning rate is about 2.5 times the unique scanning rate for both CD4+ and CD8+ T cells in 3D, but about 4.5 in 2D. Compared to 2D, DCs in 3D are more likely to encounter T cells that they have not previously contacted. This explains the different predictions between 2D and 3D models.

2.3.7 Sensitivity analysis detects mechanisms that correlate with higher effector T cell output

Cognate frequency and Ag-DC recruitment correlate with the production of primed T cells leaving a LN (Figure 2.9). However, other parameters may significantly influence LN output as well. In order to identify such correlations, we used sensitivity analyses.

We examine 16 parameters that are likely to either directly or indirectly influence T cell priming (See Appendix A). The parameters that show significant correlation are shown in Table 2.4 and 2.5, for acute and chronic scenarios, respectively.

For the acute scenario, we chose day 4 (when the total DC count is maximum, and priming is ongoing) to examine the influence of various mechanisms on outcomes such as scanning rate and match percentage, as well as effector T cell output on day 14 (after the immune response is dampened). The result shows that in an acute scenario, both CD4+ and CD8+ T cells scanning rates were correlated positively with Ag-DC licensing probability, and correlated negatively with CD4+ T cell binding time and the pMHC level needed for 50% priming probability (Table 2.4). The match percentage is correlated negatively with Ag-DC licensing probability, and correlated positively with T cell binding time and pMHC stimulation requirements (Table 2.4). These results indicate

that faster DC licensing and a more sensitive priming system induces high levels of scanning, but that they negatively affect the percentage of T cells that have been scanned by DCs before they exit. This effect is likely due to a reduced average lifespan of the DCs, since both Ag-DC (with an average lifespan of 60 hrs) and LDC (with an average lifespan of 36 hrs) can prime CD4+ T cells. The production of primed cells also has a significant negative correlation with the Ag-DC licensing probability, as well as the average binding of T cells to DCs. Because a higher Ag-DC licensing probability leads to reduced DC lifespan, it also reduces effector T cell output. However, a shorter CD4+ T cell binding time, as long as it is productive, permits more T cell binding opportunities and therefore results in more primed T cells.

We tested whether these same mechanisms were at work during a simulated chronic infection. We chose day 14 for our analysis since cell dynamics approach a steady-state. In these simulations, we found that higher licensing probability by Ag-DCs still increases scanning rates and reduces match percentages of T cells, but it has a less significant role on the production of primed CD4+ and CD8+ T cells (Table 2.5). This could be explained by the continuous influx of Ag-DCs in the chronic infection scenario. Even though the average number of Ag-DCs and LDCs will be lower when licensing probabilities are high, the impact is still much smaller considering the high LN efficiency achieved when DC density is low, as discussed in previous sections.

As shown by the PRCC results, the parameters that most strongly affect our 3D model outputs are different from those in the 2D model (Linderman et al., 2010). To test whether this is due to dimensionality, we performed the same PRCC analysis using the 2D version of the 3D model. The results for the chronic scenario (Table 2.6) are consistent with the previous 2D results. CD4+ T cell output is sensitive to the priming threshold and binding threshold. This discrepancy might be explained by the more efficient searching in 3D. Because Ag-DCs are comparatively easier for cognate T cells to find, T cells have a higher chance of being primed, so the threshold for binding or priming is no longer a bottleneck for the production of effector cells.

We used eFAST to confirm our sensitivity analysis results. We varied the values for a focused list of parameters, including binding threshold and maximum binding time for CD4+ T cells, maximum binding time for CD8+ T cells, and Ag-DC licensing probability. Results are shown in Table 2.7. These results are consistent with the PRCC analysis performed earlier (see Table 2.5). Using this method, CD4+ and CD8+ T cell outputs are most sensitive to binding time, and sensitivity is induced mainly by first order effects (i.e. explained by this parameter alone and in a linear manner). In addition, scanning rates of both CD4+ and CD8+ T cells are sensitive to binding time of CD4+ T cells, while match percentage of CD4+ T cell is sensitive to the licensing probability of Ag-DCs. In summary, using two distinct analysis tools (PRCC and eFAST), we confirmed that the mechanisms stated above strongly influence the LN functionality.

2.4 Discussion

In this work, we created a 3D ABM model of a LN T zone that embodies the physiological structure of non-human primate LNs and is calibrated with cell motility data obtained with 2PM. We used the model to learn how LN output efficiency is affected by the number of entering cognate T cells and DCs and by model dimensionality (2D vs. 3D). We performed computational simulations of T cell repertoire scanning followed by clonal expansion in the LN under various conditions. We found that a high LN efficiency can be induced by small numbers of DCs and is almost unaffected by increased cognate frequency, as was found in an earlier 2D model (Linderman et al., 2010). However, the efficiency of cognate T cell searching is highly dependent on model dimensionality, with the 3D model being more efficient.

We varied the cognate T cell frequency over three orders of magnitude in our simulations and found that LN efficiency (effector T cell output/naive cognate T cell input) remains fairly constant at any given DC number. A proportional relationship between endogenous naive cognate frequency and expanded primed T cell populations has been shown in recent studies (Moon et al.,

2007; Obar et al., 2008). Our model results not only agree with this, but also predict that this correlation is maintained when the initial cognate frequency is further increased. This theoretical excess capacity in the system has important implications for vaccine design: large increases in cognate T cell numbers in the LN are still expected to yield an almost linear increase in effector T cell output. This result evinces both promise and caution. In many infectious disease studies, extremely high levels of transgenic T cells (up to 10^7), all of which are naive but specific for a single epitope, are transferred to animals, and the priming and effector functions of these T cells are analyzed. Our results suggest that increasing the number of cognate T cells in a system may lead to an increase in priming compared to an un-manipulated system, and therefore could be misleading when comparing to non-manipulated scenarios. Compared with CD4+ T cells, LN efficiency of CD8+ T cells is less straightforward. LN efficiency of CD8+ T cell priming drops when CD4+ cognate frequency or DC recruitment is low, since in our model LDCs are necessary for CD8+ T cell priming and effector cell survival as observed *in vivo* (Smith et al., 2004). This result provides another explanation regarding the disconnect between naive and expanded T primed T cell population as observed in some studies examining CD8+ T cell expansion (La Gruta et al., 2010; Ruckwardt et al., 2011). This is in addition to a threshold effect and differentially sustained proliferation as suggested by Jenkins et al (Jenkins and Moon, 2012). Therefore, when cognate CD8+ T cells are abundant, such as after a viral infection, immunotherapy that increases an influx of antigen presenting DCs and CD4+ T cells into LNs may be helpful for taking full advantage of the excess priming capacity and increasing CD8+ T cell output.

By comparing results from our 3D model to the 2D model by Linderman et al.(Linderman et al., 2010) and also a 2D version of our 3D model performed herein, we found that a T cell search for Ag-DCs is more efficient in 3D. We tested several possible explanations for this, and showed that the average minimum distance between DCs is shorter in 3D, and also that T cells are less likely to revisit the same DCs and therefore the proportion of unique T cell DC interactions increases.

Both of these factors are likely to contribute to a more efficient repertoire scanning in an actual 3D LN. This result suggests that 2D LN models underestimate LN efficiency and may not properly reflect the nature of LN function *in vivo*. T cell search times in 3D are significantly shorter, but this assumes random T cell migration. In ongoing work, we are investigating the effects of chemotaxis on T cell repertoire scanning. Since steric inhibition of T cell-DCs contact is less of a barrier in 3D than on 2D grids, it will be interesting to test whether chemotaxis can enhance T cell search times and unique DC contacts in our 3D model.

The intention of this model is to build a generic NHP LN that allows computational simulation and analysis of the core functions in T cell priming. For this reason, we did not fit the model to infection specific data, but instead we assumed that all the dynamics are based on a generalized antigen, like ovalbumin, as is used in the 2PM studies; all calibrations we made to our model based on cell movement used data from 2PM studies (Miller et al., 2004b). We used our LN ABM to produce dynamics that qualitatively match immune responses, and to study how dynamics are affected when the dimensionality of the environment changes. We are now ready to use the model to test specific infection scenarios that will require the LN be connected with compartments such as blood, lymph and peripheral tissues. Furthermore, LNs can be seeded with pathogens and become a site of infection (Golden and Vikram, 2005).

Figures

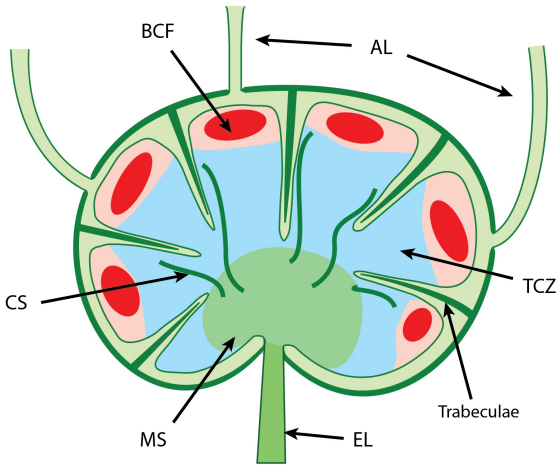

Figure 2.1: Structure of a human lymph node. Afferent lymphatics (AL) bring lymph to the lymph node. Parenchyma is organized into B cell follicles (BCF) and T cell zone (TCZ). Trabeculae further divide the parenchyma into incompletely separated compartments. Lymphocytes drain through cortical sinuses (CS) to medullary sinuses (MS), and eventually exit the lymph node via efferent lymphatics (EL).

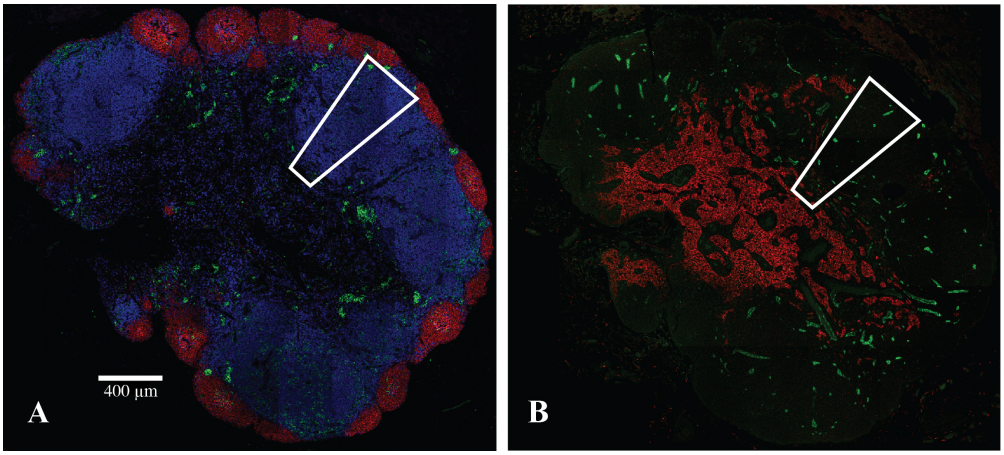

Figure 2.2: *Cynomolgus macaques* LN cross-section. A: Stained for CD3 (blue; T cells), CD11c (green; DCs) and CD20 (red; B cells). White bar in lower left corner indicates the length 200 μm. B: Stained for PNAd (green; HEV) and LYVE1 (red; medullary and cortical sinuses). White box indicates size of the modeled region. These mages are produced by JoAnne Flynn group from the University of Pittsburgh. See Gong et al. (2013) for details.

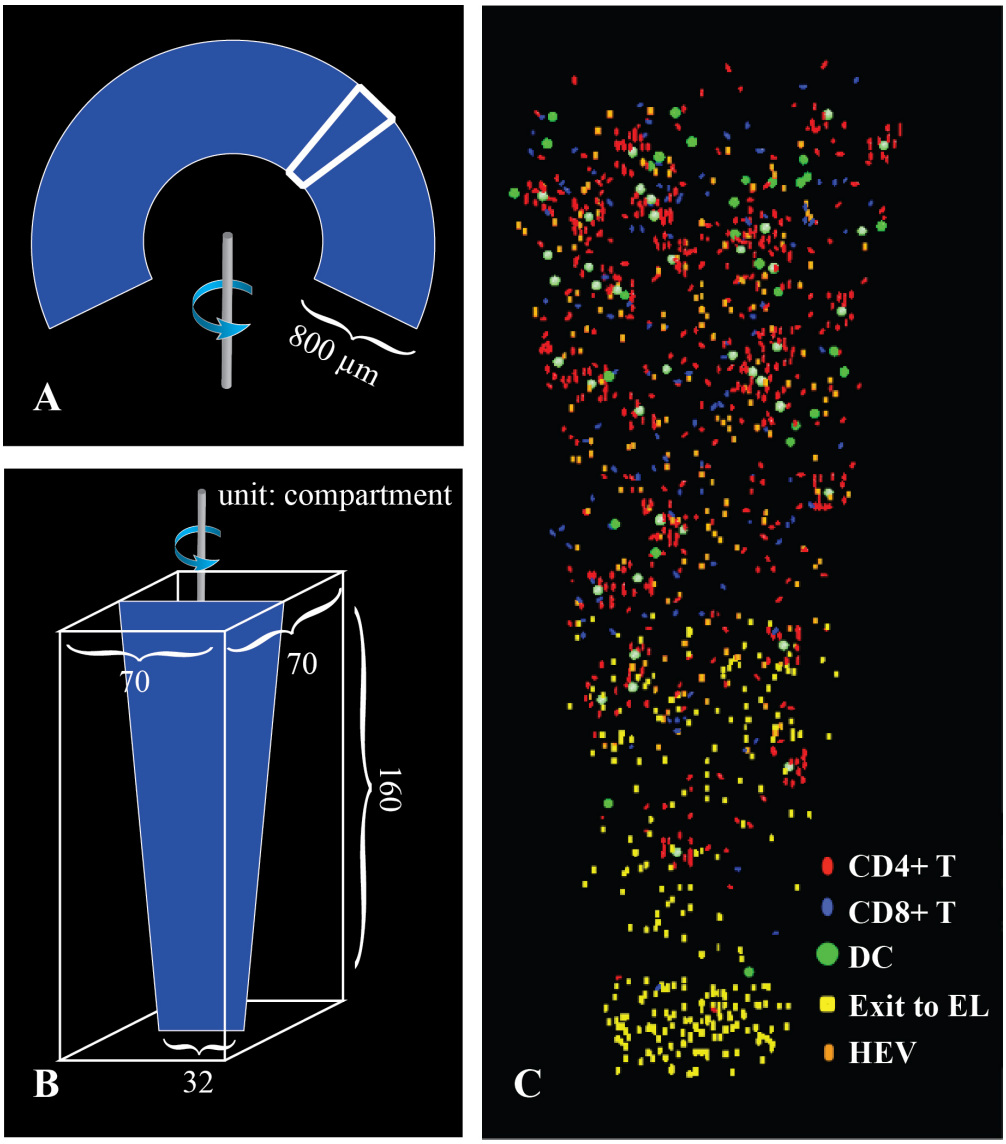

Figure 2.3: Structure of computational model *LymphSim*. A: Abstracted shape of the T cell zone (blue) and modeled portion (white outline). The T cell zone is a spherical shell with thickness 800 μm. B: Approximately 1/200 of the T cell zone volume is modeled, shaped as a cone plug. Dimensions (in μm) are as indicated. The modeled section of a LN has 344148 compartments, each a cube of edge length 5 μm (roughly the size of a T cell), and total volume of 0.043 μL. C: Simulation image showing LN populated with cells. As in 2PM studies, for clarity, not all cells are displayed.

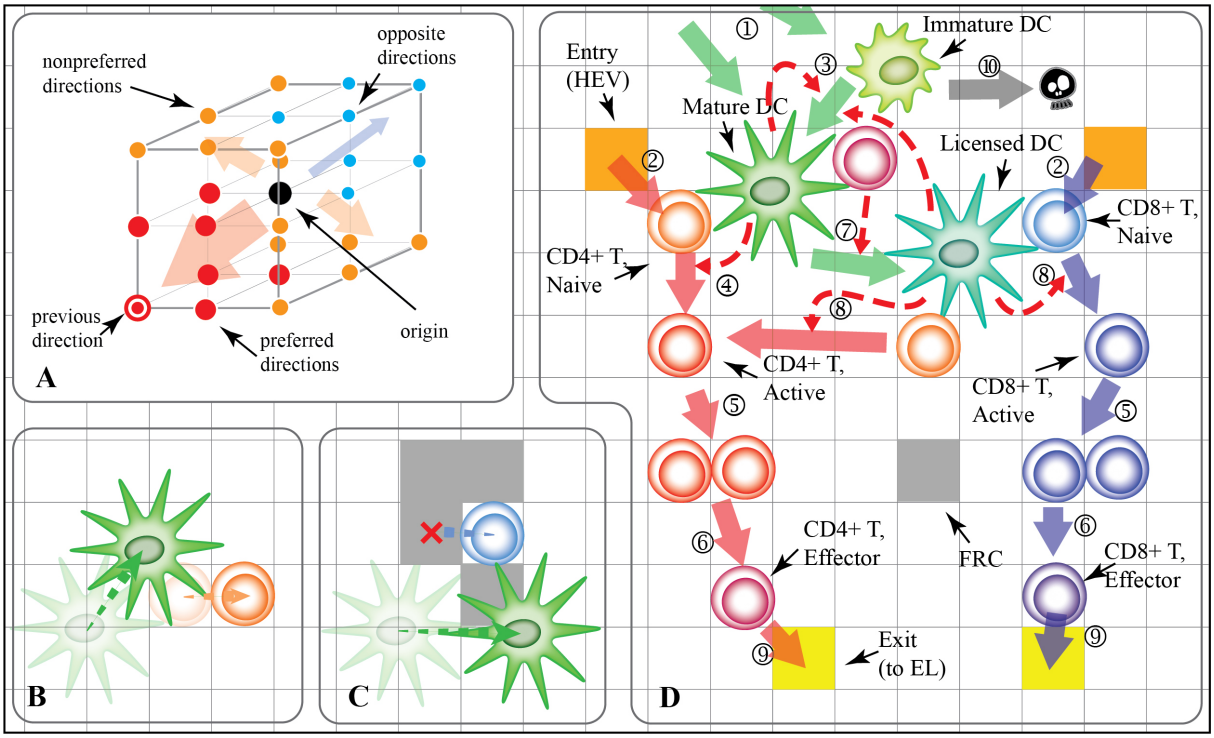

Figure 2.4: *LymphSim* model schematics and rules. A: Cells undergo a biased random walk; probabilities of movement in different directions are unequal and depend on previous movement. B: T cells (orange) occupy one grid compartment (5 x 5 x 5 μm). DCs (green) occupy 8 grid compartments (i.e., a cube of edge length 2). A DC can push a T cell away to make room for its movement. C: When encountering the FRC network (grey), DCs are allowed to overlap, but T cells move around the FRC. D: Cell rules are labeled with numbers on the diagram. 1. DCs are recruited from top of grid (via ALs). 2. Naive CD4 and CD8 T cells are recruited from HEVs. 3. Ag-DCs and LDCs can induce IDC maturation. 4. Ag-DCs prime CD4 T cells. 5. Primed CD4/CD8 T cells proliferate. 6. After a given number of divisions, both kinds of T cell become effector cells. 7. Effector CD4 T cells license Ag-DCs, turning them into LDCs. 8. LDCs prime CD8 and CD4 T cells. 9. Effector CD4/CD8 T cells exit LNs from ELs. 10. Cells may die. The distribution of life spans is cell-type specific. See text and online supplement for more detail.

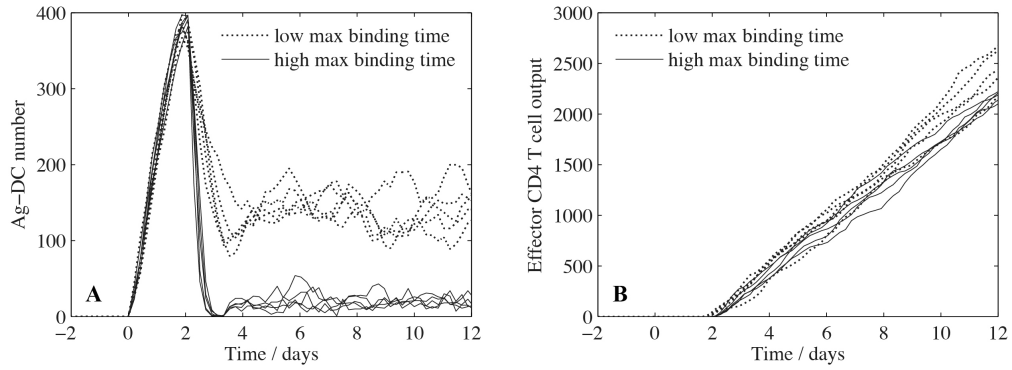

Figure 2.5: Aleatory and epistemic uncertainties of the model. Two parameter sets from one LHS analysis are selected, with low or high maximum binding times for CD4 T cells. The number of Ab-DCs (A) and effector CD4 T cells output(B) are chosen as model read-outs. A: Aleatory uncertainty is small compared to epistemic uncertainty. B: The two sources of uncertainty are partially convoluted.

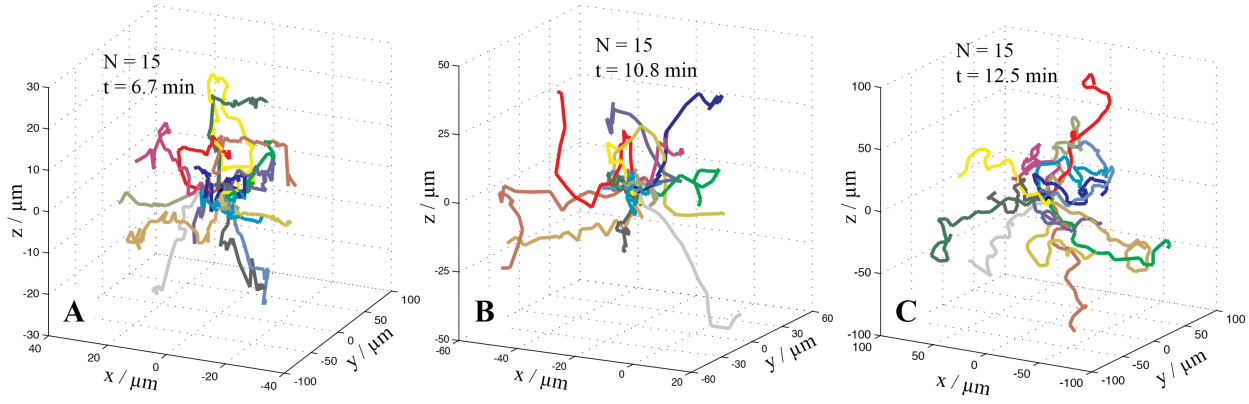

Figure 2.6: Cell tracks for comparison of experiments and simulations. A: Cell tracks from 2PM experiment with an imaging interval of 11 seconds. 15 tracks were obtained over a period of 6.7 min and are plotted. B: Cell tracks from 2PM experiment with an imaging interval of 27 seconds. 15 tracks were obtained over a period of 10.8 min and are plotted. C: Simulated cell tracks with 3D LN ABM. 15 tracks were obtained over a simulated period of 12.5 min and are plotted. The 2-Photon Microscopy data are generated by Mark Miller group from the Washington University in St. Louis. See Gong et al. (2013) for details.

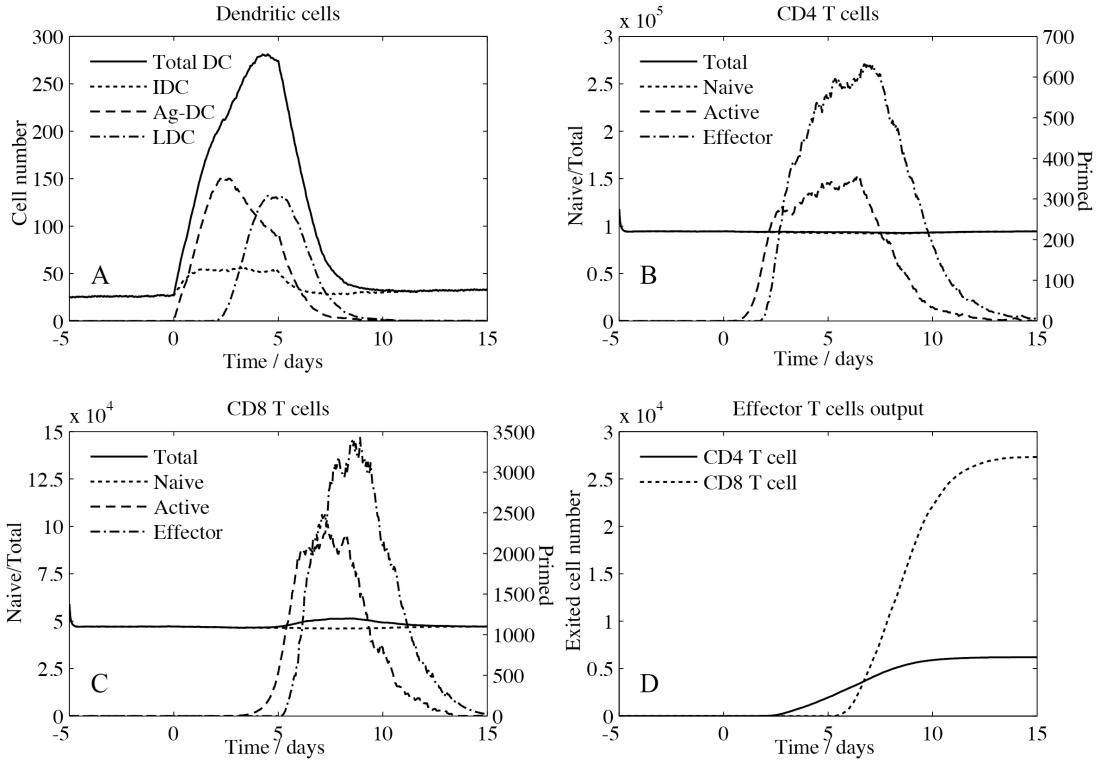

Figure 2.7: Simulation of an acute infection scenario. The introduction of Ag-bearing DCs stops on day 5. A. Simulated numbers of DCs on the LN grid. B. Simulated numbers of CD4 T cells (nave, primed, effector) on the LN grid. C. Simulated numbers of CD8 T cells in different states on the LN grid. D. Simulated output of effector CD4 and CD8 T cells exiting from the LN.

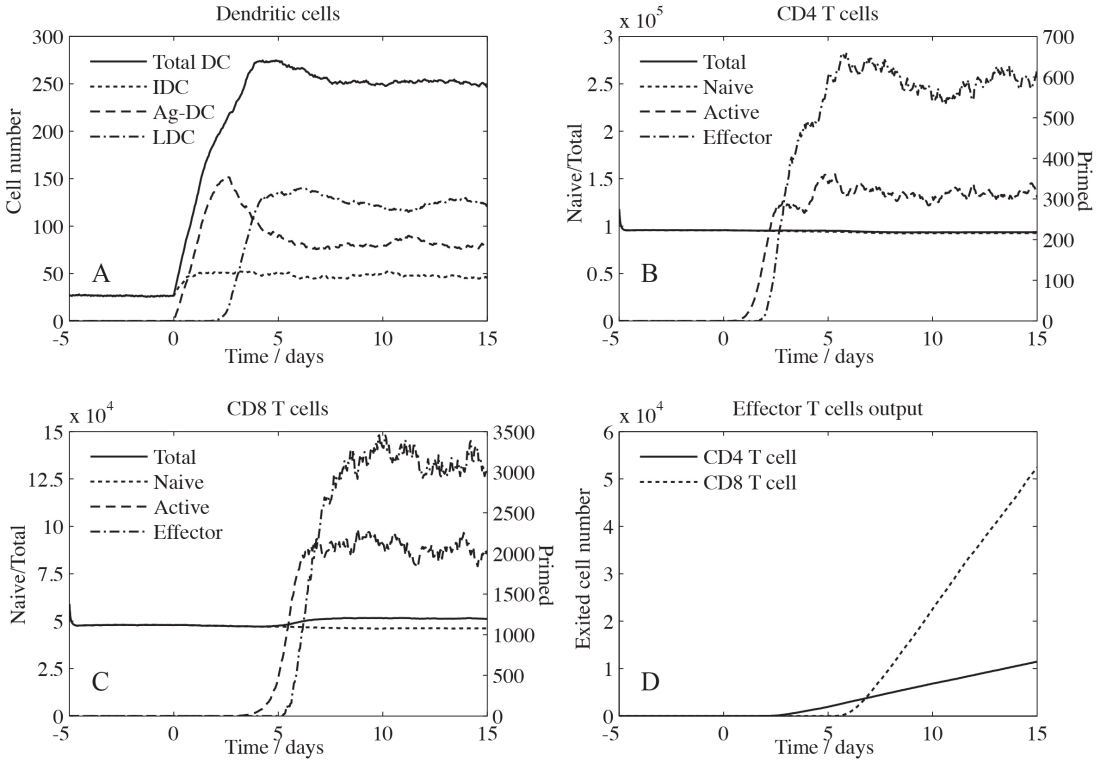

Figure 2.8: Simulation of a chronic infection scenario. The introduction of Ag-bearing DCs does not stop after day 5. A. Simulated numbers of DCs on the LN grid. B. Simulated numbers of CD4 T cells in different states on the LN grid. C. Simulated numbers of CD8 T cells in different state on the LN grid. D. Simulated output of effector CD4 and CD8 T cells exiting from the LN.

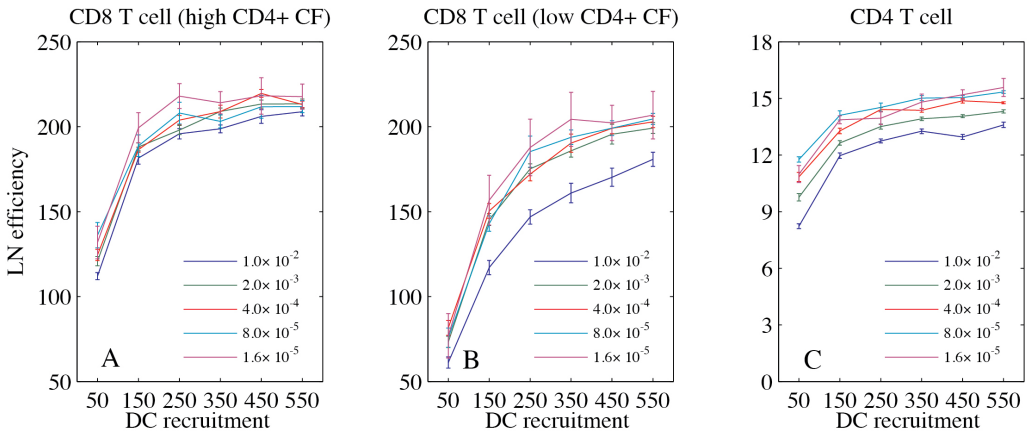

Figure 2.9: Lymph node efficiency. Simulations of lymph node efficiency in generating primed T cells by Ag-DCs in a LN. Different colors represent different cognate frequencies (CF). A. CD8 T cell LN efficiency in the context of high CD4 T cell cognate frequency. B. CD8 T cell LN efficiency in the context of low CD4 T cell cognate frequency. C. CD4 T cell LN efficiency for different cognate frequencies and different levels of Ag-bearing DCs on the grid.

Tables

Table 2.1: *LymphSim* model calibration.

Source	Mean free path μm	Motility coefficient $\mu m^2 min^{-1}$	Velocity $\mu m \cdot min^{-1}$	Transit time $hour$	Exit rate $min^{-1}(10^6 cells)^{-1}$
Simulation	15.96	45.87	13	18	915
2PM, 11 s	17.48	47.18	14.6	-	-
2PM, 27 s	15.6	42.86	9.8	-	-
Literature	20	-	12	12-24	700-1400

Table 2.2: Simulation outputs when model size is scaled from 0.5% to 2% of an entire LN.

	$1\times$ Grid	$4\times$ Grid
Size (μL)	0.043	0.172
Density ($10^6 cell/\mu L$)	4.20 ± 0.08	4.16 ± 0.05
Mean free path (μm)	15.88 ± 0.07	15.93 ± 0.05
Transit time (hr)	18.0 ± 0.6	17.7 ± 0.3
CD4+ scan rate (hr^{-1})	$2.93 \pm 0.03 \times 10^3$	$2.89 \pm 0.02 \times 10^3$
CD8+ scan rate (hr^{-1})	$1.46 \pm 0.01 \times 10^3$	$1.43 \pm 0.01 \times 10^3$
CD4+ priming efficiency	13.5 ± 0.1	13.7 ± 0.1
CD8+ priming efficiency	$2.10 \pm 0.02 \times 10^2$	$2.14 \pm 0.01 \times 10^2$
Search time (hr)	0.316 ± 0.006	0.311 ± 0.003

Table 2.3: Comparing search times, match percentages and scanning rates from 2D and 3D simulations.

	2D		3D	
	CD4+	CD8+	CD4+	CD8+
Match %	55.77 ± 0.73	49.75 ± 1.34	92.64 ± 0.87	86.41 ± 1.19
Search time (min)	140.2 ± 4.2		10.64 ± 0.26	
Scan rate (cell/hr):				
Apparent	562 ± 6	277 ± 3	2977 ± 26	1479 ± 13
Unique	125 ± 2	64 ± 1	1189 ± 9	592 ± 5
Ratio	4.488 ± 0.018	4.335 ± 0.018	2.504 ± 0.003	2.498 ± 0.003

Table 2.4: Sensitivity analysis for parameters involved in priming performed during an acute infection scenario.

	CD4+		CD8+	
Output	Mechanism	PRCC	Mechanism	PRCC
Scanning rate:				
	CD4+ T cell binding time	-0.57	CD4+ T cell binding time	-0.61
	Priming threshold for pMHC-II	-0.49	Priming threshold for pMHC-II	-0.48
	Ag-DC licensing probability	0.73	Ag-DC licensing probability	0.8
Match %:				
	Ag-DC licensing probability	-0.76	Ag-DC licensing probability	-0.62
	CD4+ T cell binding time	0.4	CD4+ T cell binding time	0.38
	Priming threshold for pMHC-II	0.42	Priming threshold for pMHC-II	0.39
Effector output:				
	CD4+ T cell binding time	-0.71	CD8+ T cell binding time	-0.66
	Ag-DC licensing probability	-0.44	CD4+ T cell binding time	-0.22
			Priming threshold for pMHC-II	-0.17

Table 2.5: Sensitivity analysis for parameters involved in priming performed during a chronic infection scenario.

	CD4 +		CD8+	
Output	Mechanism	PRCC	Mechanism	PRCC
Scanning rate:				
	Ag-DC licensing probability	0.66	Ag-DC licensing probability	0.69
Match %:				
	Ag-DC licensing probability	-0.48	-	-
Effector output:				
	CD4+ T cell binding time	-0.68	CD8+ T cell binding time	-0.64
	Ag-DC licensing probability	-0.23	CD4+ T cell binding time	-0.21

Table 2.6: Sensitivity analysis of parameters involved in priming during a chronic infection scenario. 2D case.

	CD4+		CD8	
Output	Mechanism	PRCC	Mechanism	PRCC
Scanning rate:				
	Ag-DC licensing probability	0.2	Ag-DC licensing probability	0.34
Match %:				
	Ag-DC licensing probability	-0.19	Ag-DC licensing probability	0.61
	IDC Activation Probability	0.36	IDC Activation Probability	0.28
Effector output:				
	CD4+T cell binding time	-0.44	CD8+T cell binding time	-0.52
	Priming threshold for pMHC-II	-0.31	Ag-DC licensing probability	0.49
	Binding threshold for pMHC-II	-0.15	IDC Activation Probability	0.19
	IDC Activation Probability	0.28		

Table 2.7: Significant (p-value ¡ 0.05) eFAST results for parameters during a chronic infection scenario.

	CD4+			CD8+		
Output	Mechanism	S_i	S_{ti}	Mechanism	S_i	S_{ti}
Scanning rate:						
	CD4+ T cell binding time	0.44	0.89	CD4+ T cell binding time	0.44	0.86
Match %:						
	Ag-DC licensing probability	0.19	0.88			
Effector output:						
	CD4+ T cell binding time	0.76	0.91	CD8 T cell binding time	0.61	0.89

Bibliography

Beltman, J. B., Maree, A. F., Lynch, J. N., Miller, M. J. and de Boer, R. J. Lymph node topology dictates T cell migration behavior. *Journal of Experimental Medicine*, 204(4):771–780, 2007.

Bogle, G. and Dunbar, P. R. Simulating T-cell motility in the lymph node paracortex with a packed lattice geometry. *Immunology and cell biology*, 86(8):676–687, 2008.

Bogle, G. and Dunbar, P. R. Agent-based simulation of T-cell activation and proliferation within a lymph node. *Immunology and cell biology*, 88(2):172–9, 2010a.

Bogle, G. and Dunbar, P. R. T cell responses in lymph nodes. *Wiley interdisciplinary reviews. Systems biology and medicine*, 2(1):107–116, 2010b.

Bogle, G. and Dunbar, P. R. On-lattice simulation of T cell motility, chemotaxis, and trafficking in the lymph node paracortex. *PloS one*, 7(9):e45258, 2012.

Bousso, P. and Robey, E. Dynamics of CD8+ T cell priming by dendritic cells in intact lymph nodes. *Nature immunology*, 4(6):579–585, 2003.

Brophy, S. E., Jones, L. L., Holler, P. D. and Kranz, D. M. Cellular uptake followed by class I MHC presentation of some exogenous peptides contributes to T cell stimulatory capacity. *Molecular immunology*, 44(9):2184–2194, 2007.

Carpenter, A. E., Jones, T. R., Lamprecht, M. R., Clarke, C., Kang, I. H., Friman, O., Guertin, D. A., Chang, J. H., Lindquist, R. A., Moffat, J., Golland, P. and Sabatini, D. M. CellProfiler: image analysis software for identifying and quantifying cell phenotypes. *Genome biology*, 7(10):R100, 2006.

Castellino, F., Huang, A. Y., Altan-Bonnet, G., Stoll, S., Scheinecker, C. and Germain, R. N.

Chemokines enhance immunity by guiding naive CD8+ T cells to sites of CD4+ T cell-dendritic cell interaction. *Nature*, 440(7086):890–5, 2006.

Celli, S., Lemaître, F. and Bousso, P. Real-time manipulation of T cell-dendritic cell interactions in vivo reveals the importance of prolonged contacts for CD4+ T cell activation. *Immunity*, 27(4):625–634, 2007.

Clark, P. J. F.C. Evans, Distance to nearest neighbor as a measure of spatial relationships in populations. *Ecology*, 1954.

Clark, P. J. and Evans, F. C. Generalization of a Nearest Neighbor Measure of Dispersion for Use in K Dimensions. *Ecology*, 60(2):316, 1979.

Collins, D. C. and Avissar, R. An Evaluation with the Fourier Amplitude Sensitivity Test (FAST) of Which Land-Surface Parameters Are of Greatest Importance in Atmospheric Modeling. *Journal of Climate*, 7(5):681–703, 1994.

Cukier, R. I. Study of Sensitivity of Coupled Reaction Systems to Uncertainties in Rate Coefficients. 1 Theory. *Journal of Chemical Physics p*, 59(8):3873–3878, 1973.

Germain, R. N. and Jenkins, M. K. In vivo antigen presentation. *Current opinion in immunology*, 16(1):120–125, 2004.

Girard, J.-P., Moussion, C. and Förster, R. HEVs, lymphatics and homeostatic immune cell trafficking in lymph nodes. *Nature reviews. Immunology*, 12(11):762–73, 2012.

Golden, M. P. and Vikram, H. R. Extrapulmonary tuberculosis: an overview. *American family physician*, 72(9):1761–1768, 2005.

Gong, C., Mattila, J. T., Miller, M., Flynn, J. L., Linderman, J. J. and Kirschner, D. Predicting

lymph node output efficiency using systems biology. *Journal of theoretical biology*, 335:169–184, 2013.

Grigorova, I. L., Panteleev, M. and Cyster, J. G. Lymph node cortical sinus organization and relationship to lymphocyte egress dynamics and antigen exposure. *Proceedings of the National Academy of Sciences of the United States of America*, 107(47):20447–20452, 2010.

Jenkins, M. K. and Moon, J. J. The role of naive T cell precursor frequency and recruitment in dictating immune response magnitude. *Journal of immunology (Baltimore, Md. : 1950)*, 188(9):4135–4140, 2012.

La Gruta, N. L., Rothwell, W. T., Cukalac, T., Swan, N. G., Valkenburg, S. A., Kedzierska, K., Thomas, P. G., Doherty, P. C. and Turner, S. J. Primary CTL response magnitude in mice is determined by the extent of naive T cell recruitment and subsequent clonal expansion. *The Journal of clinical investigation*, 120(6):1885–94, 2010.

Linderman, J. J., Riggs, T., Pande, M., Miller, M., Marino, S. and Kirschner, D. E. Characterizing the dynamics of CD4+ T cell priming within a lymph node. *Journal of immunology (Baltimore, Md. : 1950)*, 184(6):2873–2885, 2010.

Marino, S., Hogue, I. B., Ray, C. J. and Kirschner, D. E. A methodology for performing global uncertainty and sensitivity analysis in systems biology. *Journal of theoretical biology*, 254(1):178–196, 2008.

Miller, M. J., Hejazi, A. S., Wei, S. H., Cahalan, M. D. and Parker, I. T cell repertoire scanning is promoted by dynamic dendritic cell behavior and random T cell motility in the lymph node. *Proceedings of the National Academy of Sciences of the United States of America*, 101(4):998–1003, 2004a.

Miller, M. J., Safrina, O., Parker, I. and Cahalan, M. D. Imaging the single cell dynamics of CD4+ T cell activation by dendritic cells in lymph nodes. *The Journal of experimental medicine*, 200(7):847–856, 2004b.

Miller, M. J., Wei, S. H., Cahalan, M. D. and Parker, I. Autonomous T cell trafficking examined in vivo with intravital two-photon microscopy. *Proceedings of the National Academy of Sciences of the United States of America*, 100(5):2604–2609, 2003.

Miller, M. J., Wei, S. H., Parker, I. and Cahalan, M. D. Two-photon imaging of lymphocyte motility and antigen response in intact lymph node. *Science*, 296(5574):1869–1873, 2002.

Mirsky, H. P., Miller, M. J., Linderman, J. J. and Kirschner, D. E. Systems biology approaches for understanding cellular mechanisms of immunity in lymph nodes during infection. *Journal of theoretical biology*, 287:160–70, 2011.

Moon, J. J., Chu, H. H., Pepper, M., McSorley, S. J., Jameson, S. C., Kedl, R. M. and Jenkins, M. K. Naive CD4(+) T cell frequency varies for different epitopes and predicts repertoire diversity and response magnitude. *Immunity*, 27(2):203–213, 2007.

Obar, J. J., Khanna, K. M. and Lefrançois, L. Endogenous naive CD8+ T cell precursor frequency regulates primary and memory responses to infection. *Immunity*, 28(6):859–869, 2008.

Riggs, T., Walts, A., Perry, N., Bickle, L., Lynch, J. N., Myers, A., Flynn, J., Linderman, J. J., Miller, M. J. and Kirschner, D. E. A comparison of random vs. chemotaxis-driven contacts of T cells with dendritic cells during repertoire scanning. *Journal of theoretical biology*, 250(4):732–51, 2008.

Ruckwardt, T. J., Malloy, A. M. W., Gostick, E., Price, D. A., Dash, P., McClaren, J. L., Thomas, P. G. and Graham, B. S. Neonatal CD8 T-cell hierarchy is distinct from adults and is influenced

by intrinsic T cell properties in respiratory syncytial virus infected mice. *PLoS pathogens*, 7(12):e1002377, 2011.

Saltelli, A. and Bolado, R. An alternative way to compute Fourier amplitude sensitivity test (FAST). *Computational Statistics & Data Analysis*, 26(4):445–460, 1998.

Saltelli, A., Tarantola, S., Campolongo, F. and Ratto, M. *Sensitivity analysis in practice: a guide to assessing scientific models*. John Wiley & Sons, 2004.

Saltelli, A., Tarantola, S. and Chan, K. P.-S. A Quantitative Model-Independent Method for Global Sensitivity Analysis of Model Output. *Technometrics*, 41(1):39–56, 2012.

Shiow, L. R., Rosen, D. B., Brdicková, N., Xu, Y., An, J., Lanier, L. L., Cyster, J. G. and Matloubian, M. CD69 acts downstream of interferon-alpha/beta to inhibit S1P1 and lymphocyte egress from lymphoid organs. *Nature*, 440(7083):540–544, 2006.

Smith, C. M., Wilson, N. S., Waithman, J., Villadangos, J. A., Carbone, F. R., Heath, W. R. and Belz, G. T. Cognate CD4(+) T cell licensing of dendritic cells in CD8(+) T cell immunity. *Nature immunology*, 5(11):1143–1148, 2004.

Sprent, J. and Tough, D. F. T cell death and memory. *Science*, 293(5528):245–248, 2001.

Zehn, D., Cohen, C. J., Reiter, Y. and Walden, P. Extended presentation of specific MHC-peptide complexes by mature dendritic cells compared to other types of antigen-presenting cells. *European journal of immunology*, 34(6):1551–1560, 2004.

Zheng, H., Jin, B., Henrickson, S. E., Perelson, A. S., von Andrian, U. H. and Chakraborty, A. K. How antigen quantity and quality determine T-cell decisions in lymphoid tissue. *Molecular and cellular biology*, 28(12):4040–4051, 2008.

CHAPTER III

Re-evaluation of T cell motility in LNs: random vs. directed?

3.1 Introduction

Lymphocytes respond to foreign antigen during an adaptive immune response when the innate immune response fails to complete the task of protecting a host from infection. Lymphocytes recognize specific patterns of antigenic peptides presented via major histocompatibility complexes (MHC) on the surface of antigen presenting cells (APCs). T cell receptors expressed on lymphocyte cell surfaces bind specific peptide-MHC complexes (pMHCs) and must be activated by APCs to exert their full potential. Lymph nodes (LN) are secondary lymphatic organs that serve as the venue for these processes. In particular, nave T lymphocytes (or T cells) circulate between blood and lymphatics, and when they travel through a T-cell zone of a LN, they search for dendritic cells (DCs, a type of APC) that present antigens specific to their T cell receptors (TCR). The frequency of T cells expressing each type of TCR is extremely low (can be 10^{-5} to 10^{-6}) (Casrouge et al., 2000; Blattman et al., 2002; Jenkins and Moon, 2012). To facilitate this key interaction between T cells and DCs it is vital to have an efficient searching mechanism such that rare encounters can happen with a high enough probability to allow the chance the host to respond quickly to infection.

Studies have been done examining how T cells migrate into LNs and find their specific Ag-presenting DCs (Miller et al., 2003; Bajénoff et al., 2006; Gérard et al., 2014). However, this

The work in Chapter III is done in collaboration with Dr. Mark Miller. Manuscript is in preparation.

process is incompletely understood. The fibroblastic reticular cell (FRC) network is a network formed by one type of stromal cell in the T cell zone of LNs, and is thought to be essential to their structure and function. Purported functions of the FRC network include creating a scaffold in the paracortex for the support of T cell migration, releasing small molecules cytokines/chemokines that facilitate interactions between cells, and transporting small antigens via the conduits (Malhotra et al., 2013). Using intravital imaging techniques, some find the pattern of T cell motion in the LN is mainly an autonomous random walk (Miller et al., 2003). Others suggest that the motion of T cells is guided by and constrained to the FRC network (Bajénoff et al., 2006). In addition to FRC, there are studies suggesting that T cell motion in the LN is not random but rather directed by chemokines that are secreted by DCs to draw T cells to them which could enhance the efficiency of the searching (Lanzavecchia and Sallusto, 2000). A recent study examined the molecular basis of the T cell movement process, finding that even though the motion might be partially directed by environmental cues, a random strategy is important for searching efficiency (Gérard et al., 2014).

Modeling efforts have been made to help understand the roles of FRC constraint and chemotaxis and their involvement in T cell movement (Beauchemin et al., 2007; Beltman et al., 2007; Riggs et al., 2008); however there is not yet a consensus as to the true behaviors occurring as T cells search for antigen bearing DCs (ag-DC). In some more recent models, FRC networks are generated virtually to help simulate and analyze T cell migration (Graw and Regoes, 2012; Donovan and Lythe, 2012). However, these reconstructions of FRC network are not calibrated using FRC network structures retrieved from experimental data. One concern is that conclusions drawn from the particular network topologies chosen in these studies may not be applicable to a realistic FRC network. When such data are available, proper metrics need to be defined so that the randomly generated virtual FRC networks can be compared with experimental results before further analyses are made.

In this study, my goal is to use computational modeling to assess the roles of FRC constraint and

DC-induced chemotaxis of T cells in influencing T cell motility in LNs during adaptive immunity. Also, we study how those influences affect the efficiency of the DC-T cell searching process and T cell expansion. As discussed in Chapter II, we previously developed a 3 dimensional agent-based model, *LymphSim*, to study the dynamics of T cells in the LN by assuming T cell movement follows a persistent random walk (Gong et al., 2013; 2014). Using these models, we can track the movement and state changes of each single immune cell in our simulation and also make both qualitative and quantitative predictions for the system. In this work, we implement both an FRC network that can be calibrated against metrics from intravital microscopy, as well as chemokine secretion-diffusion from DCs as an attractant for T cells. Using this updated version of *LymphSim* and based on FRC networks generated by our algorithm, we predict how the presence of an FRC constraint and/or chemotaxis to DCs can influence T cell-DC searching efficiency and the number of effector and memory T cells that are produced in an LN during simulated immune responses.

3.2 Methods

3.2.1 Lymph node model

To assess the potential influence of FRC constraint and chemotaxis of T cells to DCs, we extend our existing agent-based model, *LymphSim*, that captures 3-dimensional dynamics of a LN (Gong et al., 2013). This model simulates the motility and dynamics of T cells and DCs within the T cell zone of a LN. *LymphSim* is a hybrid 2-compartment model that includes a 3-dimensional ABM LN compartment and an ODE blood compartment. The complete details of this model implementation are given in Gong et al. (2013) and in Chapter refcahp:ln, but we briefly summarize. The LN sub-model is developed with geometry emulating a section of a typical non-human primate (NHP) LN, with a cone-plug shape and T cell entry and exit ports distributed following patterns shown when fluorescent imaging was performed on NHP LNs. The cone-plug grid has a radius of 175 microns at the top, 81.7 microns at the bottom and a height of 800 microns. Each cell compartment is a cube

of 5 microns in all three dimensions (roughly the size of a T cell). T cells are recruited from blood and enter the LN via high-endothelial venules (HEVs), and exit via efferent lymphatics (ELs) to the blood circulation. When a T cell travels through the LN, it searches for and bind to DCs presenting specific antigens, accumulates stimulation signals, gets activated, divides and differentiates into effector and memory cells. We further implemented algorithms to (1) generate an FRC network, (2) handle chemokine secretion and diffusion, and (3) rules for T cells to sense these environmental factors and adjust their motility accordingly. Using an ABM framework, we can control the extent of influences from each of these directional signals while tracking how motion of T cells in LNs and corresponding generation of immune responses are affected.

3.2.2 Including Potential factors influencing T cell movement direction

Multiple mechanisms are thought to influence T cell directional movement. In different random search strategies proposed, T cell motion may be subject to an intrinsic persistent random walk (Miller et al., 2003), or be constrained to the directions of FRC network (Bajenoff et al., 2008); note that in the latter case the movement of T cells still appears to be random at a coarse-grain level. Some suggest that the search is directional rather than random as DCs create a gradient cue to attract T cells (Castellino et al., 2006). It is also argued that chemokines are released by DCs that are attached to FRC network, and together these two properties provide directional cues for T cells (Bajénoff et al., 2007). If all the sources of influence coexist, they may send conflicting directional signals to the T cell at any given time, making experimental analysis difficult.

To approach this problem, we utilized our 3D agent-based model of the LN T cell zone where the multiple choices of T cell movement (i.e. towards each of the 26 directions in the Moore neighborhood or staying in the current location) is probabilistic. We assume that probabilities of movement are composed of three parts: persistence, chemotaxis, and level of FRC constraint. The weight of each components is set by three factors, f_p, f_c, and f_F, where:

$$f_p + f_c + f_F = 1 \tag{3.1}$$

f_c (chemotaxis factor) and f_F (FRC constraint factor) are specified in the parameter file, and f_p is set to $1-(f_c+f_F)$. The values of these weights are unknown in reality. By varying these factors as parameters in the model, we can study the impact of each mechanism on various LN outputs. The probability to move to direction i is:

$$P_i = P_{p,i}f_p + P_{c,i}f_c + P_{F,i}f_F \tag{3.2}$$

Every time a T cell moves, one open destination is chosen based on this set of probabilities calculated at its current location. Note if space is not available, the T cell remains in place for that time step.

3.2.3 FRC constraint

Algorithm to generate FRC network

In this study, we create an algorithm to generate an FRC network so that the structure of the FRC network can be calibrated against experimental measurements. FRC network vertices are generated in the following manner: first, preliminary locations in the model grid are chosen in a face-centered cubic arrangement, so that vertices are almost evenly spaced. The size of a unit cell is parameterized (frcPackRadius). Around each preliminary location, one FRC network vertex is generated with coordinates following a multivariate Gaussian distribution in each direction of the three axes. After the FRC vertices are generated, each pair, with a distance smaller than a given threshold (edgeLengthLimit), are linked together, creating one edge of the FRC network. Grid compartments within certain distance to each edge (edgeRadius) are defined as FRC cells. An example of the FRC network generated using our algorithm is shown in Figure 3.1A.

Metrics of FRC structure

FRC network structure is compared with experimental data using the following 4 criteria: vertex degree distribution, edge length distribution, transitivity and percolation threshold (defined below). The degree of a vertex is defined as the number of edges connected to this vertex. Vertex degree distribution summarizes the degrees of all vertices, while edge length distribution summarizes the lengths of all edges of the FRC network.

In the context of graph theory, a local clustering coefficient of a vertex captures the probability that two neighbors of that vertex are immediately connected. So as not to confuse with a similar term already used in immunology, we will call this transitivity. We use the average of the transitivity of all vertices in this graph theoretical framework context to evaluate how likely that each vertex and its neighbors form a clique, or complete sub-graph. If T cells follow edges of a network and make turns at vertices randomly, having higher "cliqueness" value means the time expected for T cells to stay in confined clusters increases. Thus, this property of the FRC network may affect the efficiency of cells to explore a wider space of the LN following FRC.

Another metric we used to assess the topology of the FRC network is a percolation threshold. Percolation threshold can be used to describe long-range connectivity of a random graph. For a given graph, if we remove all edges and add each edge back at an occupation probability p, for p above certain threshold pc a giant connected component will appear. The value of pc is called the (bond) percolation threshold. Because of the high density of T cells in T cell zone of the LN (Gong et al., 2013), the surface of an FRC network available for T cells access is necessarily limited at any given time. In this situation, a high percolation threshold indicates that it is difficult for a T cell to traverse a LN, assuming its movement follows the network.

We estimate the percolation threshold of a simulated FRC network using the following algorithm adapted from Callaway et al. (2000). For a FRC network with N edges, we permute the order of the list of all edges and obtain M sequences (M=1000). With each sequence, we add

back the edges one by one, and check if any of the vertices at the top 25 microns in the LN is connected through the added edges to any of the vertices at the bottom 25 microns in a LN. If they are connected after the kth edge is added, c_i is set to c_i+1 for all $k \leq i \leq N$. After M sequences, percolation probabilities P corresponding to each edge occupation probability pe = i/N is estimated as c_i/M. The bond percolation threshold is set to $pc = min\{p_e; P(p_e) \geq 0.5\}$.

To account for the stochastic variability of the FRC network structure, we generate 10 replications generating potentially different networks for a given parameter set. The number of edges differs between each replication, so for each replication we calculated the relationship between percolation probability P and a series of chosen occupation probabilities q using convolution with a binomial distribution (Newman and Ziff, 2000):

$$P(q) = \sum_{i=0}^{N} \binom{N}{i} q^i (1-q)^{N-i} P(\frac{i}{N}) \tag{3.3}$$

Rules for FRC network constraint of T cell movement

For each FRC network edge, the compartments in the vicinity (Moore Neighborhood) are assessed for two criteria: first, the distance between the compartment and the edge is smaller than certain threshold (constraintRadius) and larger than the radius of the edge (edgeRadius); second, the perpendicular foot is between the two ends of the edge. If both criteria are met, this edge is considered to affect the compartment assessed (Figure 3.1B). Each grid compartment may be affected by multiple FRC edges. After all edges are processed, every grid compartment is examined for directional guidance/constraint imposed by all FRC edges that influence it. For every FRC edge affecting this compartment, the direction of the edge is compared with every movement directions from this compartment. The movement directions with an angle smaller than 30 degrees from any FRC edge influencing this compartment is considered as the guided directions. In addition, staying in the same location is also considered a guided direction. If in total n movement directions are

FRC guided, the probability of moving to different directions are:

$$P_{F,i} = \begin{cases} \frac{1}{n}, & \text{if i is a constrained direction.} \\ 0, & \text{otherwise.} \end{cases} \tag{3.4}$$

3.2.4 Chemotaxis

Diffusion

Chemokines are signaling molecules that direct the movement of cells. Once released from the cells where they are produced (DCs in this case), these molecules diffuse within their environment and form a gradient, which can be sensed by other cell types (T cells) that express corresponding receptors on their surfaces. We used the Alternative Direction Explicit (ADE) algorithm to solve the PDE describing diffusion, as described in (Barakat and Clark, 1966). This algorithm is unconditionally stable, but the time step for diffusion should still be chosen according to diffusivity for better accuracy. We choose a no-flux boundary condition, as laterally the cone-plug LN section is surrounded by other units of the same shape, and this compensates for the molecules diffusing out of our grid space. The top and bottom of the cone are assumed impermeable. For verification, the simulation result of our algorithm is compared with results generated using Comsol Multiphysics (http://www.comsol.com/comsol-multiphysics)

Secretion and degradation

We apply Strang splitting (Strang, 1968) to the secretion operator as discussed in Cilfone et al. (2014). Multiple diffusion steps happen within one agent time step, and the amount of chemokine secreted during one diffusion time step is further divided into two equal chunks, added to the grid before and after diffusion, respectively. Because we assume cells produce chemokine at a constant rate during a given agent time step, instead of iterating through the grid for every secretion-diffusion step, a map is created to indicate the concentration and locations to add chemokine before

the secretion-diffusion procedure starts. Degradation is solved analytically based on a linear degradation ODE for each diffusion time step.

Rule for T cell sensing the chemokine gradient

Together, secretion, diffusion and degradation of chemokine shape a chemokine gradient around DCs in a LN (Figure 3.1C). To determine the influence of this gradient on T cell movement, a chemokine concentration in a given grid compartment and neighbor compartments are assessed at time t (Figure 3.1D). For time step t+1, if the local concentration is above a certain level (chemGradientMax), cells are considered unable to sense gradient, thus all directions are set as chemotactic directions. Otherwise, the compartment with the highest chemokine concentration is set as chemotactic directions. However, if some other directions have chemokine concentrations high enough so that the differences from the highest are within a threshold (chemGradientMin), these directions are also considered chemotactic directions. In Figure 3.1D, C_j has the highest chemokine concentration among all the locations in the Moore neighborhood (26 nearest neighbors of the grid square) of C_0. However, C_i and C_k are close enough so that the cells cannot sense the difference. In this case, all three directions (C_i, C_j, C_k) are considered chemotactic directions. If the number of chemotactic directions is n, the probability of choosing each direction is:

$$P_{c,i} = \begin{cases} \frac{1}{n}, & \text{if i is a chemotactic direction.} \\ 0, & \text{otherwise.} \end{cases} \tag{3.5}$$

3.2.5 Computational implementation and mode simulations

The computational model is implemented with the C++ programming language. Documentation is available on our website (http://malthus.micro.med.umich.edu/lab/movies/3dLN/). The timestep for cell movement/state change is 25 seconds, and the timestep for diffusion is 1 second. A simulation of 10 days with the diffusion algorithm option takes approximately 15 hours of com-

putational time running on Linux using one core of a dual 6 core Intel Xeon 2.4 GHz processor. Five replications are simulated for each parameter combination to account for stochastic impact.

3.3 Results

3.3.1 FRC network structure

A set of parameters will determine the topology of the FRC network. These parameters are subject to calibration when we obtain experimental results from our collaborator. As an example of how the FRC network structure generator varies as parameters are varied, we show below how changing one FRC parameter value (edgeLengthLimit) affects metrics that we generate from the FRC network. We generated two sets of FRC networks (FRC1 and FRC2), using the same parameter set except for one: edgeLengthLimit, which sets the upper bound for the length of an edge in the FRC network. 10 replications are simulated for each parameter set to account for the stochastic variability. As shown in Figure 3.2, when the limit is set lower, the vertex degree distribution shifts to the left. Edges longer than the limit no longer form, resulting in the change in the distribution of the edge length. Percolation probability curve also shifts to the left. As summarized in Table 3.1, with these changes to the edgeLengthLimit, we obtain an FRC network with smaller average degrees, slightly smaller average edges lengths, smaller average transitivity and much higher percolation threshold. In the following sections, we use FRC1 as the network structure for our simulations. The results and implications may be limited to the scenario with this specific FRC network structure; however, we will calibrate the structure according to experimental measurements in a future step of the study.

3.3.2 Cells appear to follow FRC regardless of existence of FRC constraint

We first explore the impact of forcing FRC-constraint as a key directive. We track all movement of T cells in a LN to quantify what percent of the movement follows the direction of FRC, using different values for the FRC constraint factor, f_F, (weight of FRC constraint in the overall

direction-decision mechanism $f_p + f_c + f_F = 1$). The FRC network is generated using the same parameter set as FRC1. The FRC constraint factor is varied from 0 (no constraint at all) to 1.0 (the movement direction is solely determined by FRC constrained directions). No Ag-DCs are added to the LN to control for their influence. The results are shown in Figure 3.3. Our model predicts that the time (or distance, as we assume a constant velocity when they move) T cells travel in a LN following FRC guided directions remains the same across all values of FRC constraint factor tested. However, the time they travel in directions not constrained to FRC decrease as the constraint factor increases. These results indicate that observations of T cell-FRC association happens regardless of whether there is strict constraint to FRC of T cell movements in LNs, as we can see from Figure 3.3 a fraction of T cells apparently moves along the direction of FRC network edges regardless of lacking constraint to those directions. Even though the fraction of distance that T cells move along with FRC over the entire distance they travel increases with the constraint factor, this is a due to reduced motility in other directions.

3.3.3 DC-T cell scanning is more efficient without FRC constraint or Chemotaxis

To study how DC-T cell searching is affected by FRC constraint and chemotaxis, we performed a series of simulations with different combinations of both factors in the range of [0, 0.45] with step of 0.05, and compared four readouts: the search time required for these T cell to find a cognate matched Ag-DC while traveling through a LN; the percentage scanned T cells that were scanned at least once before exiting a LN; and the scanning rate of T cells by DCs with or without counting repeated scans. We reduce the number of DCs to 18, which is much smaller than numbers used in a simulated immune response as shown in Chapter II. This is to make sure that T cell access to DCs is limiting, resembling scenarios when Ag-DC is rare, such as in Mtb infection. Figure 3.4A shows model predictions that search time is insensitive to FRC constraint, but it increases from 2.5-3 hours to 4.5 as the DC chemotaxis factor increases. Results in Figure 3.4B indicate that

a higher FRC constraint factor reduces the chance of T cells to find a matching DC. Figure 3.4C and 3.4D show that numbers of T cells scanned by each DC is negatively affected by both FRC constraint and chemotaxis, and the influence is more significant if we count only unique scanning events (3-fold difference between bottom-left and top-right corner in Figure 3.4C vs. 2-folds in Figure 3.4D). Together, these results suggest that T cell searching of DCs is most efficient when neither FRC constraint nor DC chemotaxis is involved in the decisions driving T cell movement, at least for the FRC networks tested here.

3.4 Discussion

If FRC constraint plays an important role in deciding T cell movement directions when they transit through the LN, the topology of the FRC network will be key to determining patterns of T cell movement and thus influence DC-T cell searching and T cell expansion. We need to calibrate our FRC network to actual network topology carefully, using multiple metrics. In this chapter, I implemented algorithms to generate FRC networks in the *LymphSim*, which can be calibrated using a series of metrics including the distributions of node degree and edge length, as well as transitivity and percolation threshold. T measures the "cliqueness" of a graph. If the network possesses a lot of small very well connected subcomponents, when T cells undergo a random walk following the edges of the network, it may inhibit a T cell to quickly explore a wide range of locations. This is not optimal for searches between Ag-DC and T cells, especially when antigens are rare and only a small number of Ag-DCs are present. Percolation threshold gives a metric to evaluate connectivity of distant locations in a LN when the model grid is packed with cells and a large proportion of the network is not accessible. If the percolation threshold is high, a T cell will need a sparsely occupied FRC network to traverse the LN efficiently constrained the FRC, which is a very unlikely scenario. We performed a preliminary analysis based on a simulated FRC network without thorough calibration. When rigorously calibrated with data from our experimentalist collaborator,

we will be able to address those questions more definitively.

The observation that T cells appear to follow the FRC without actual influence from a constraining mechanism may indicate that there may not be such a mechanism at work. Based on the observed surface area of the FRC, the available space may be too limited to support all of the cell-cell interactions, with or without having an explicit constraining mechanism. In fact, the effect of having an FRC constraint imposed on T cell movement is that T cells lose motility while the amount of movement along FRC does not increase. This could be counter-productive for the DC-T cell searching, slowing or halting it completely. Interestingly, a random, persistent search strategy has been shown to be efficient in the foraging behavior of animals such as birds and insects (Viswanathan et al., 2001; Reynolds and Rhodes, 2009). Recently, a new study found that migrating birds also benefit energetically from an orographic lift by following the terrain instead of maintaining the same altitude (Bishop et al., 2015). Continuing the analogy, when searching for DCs in lymph nodes, T cells require a search strategy that is able to cover a large region in short time, and also a surface on which it can move efficiently. The FRC network could be playing the latter role by providing T cells a foothold, while T cells carry out their random search.

The prediction that when DCs use chemotaxic mechanisms to attract T cells it results in longer search times is counter-intuitive at first glance, but it can be explained as a result of crowding: if a chemokine gradient exists around DCs, T cells around DC will form a dynamic shell encapsulating the DC and prevent new T cells from accessing the vicinity of an Ag-DC. Similar results have been previously shown with 2D lymph node models (Riggs et al., 2008). Although this effect can potentially be neutralized by allowing T cells to desensitize quickly to a chemokine after certain amount of exposure (Iijima et al., 2002; DeFea, 2007), a cell will have to be able to rapidly go through multiple cycles of desensitization and re-sensitization in order to probe a sizable region with in the LN involving a complex chemokine gradient landscape created by multiple Ag-DCs. This will require significant energy and does not appear to be , economically efficient, especially

when the same DC scanning rates reported from literature (Miller et al., 2004) can be reached with a random search strategy.

In addition to the influences from chemotaxis, the probability od a T cel finding its matching Ag-DC can be further reduced in the presence of FRC constraint. This can be explained by a reduction of motility (Figure 3.3). Even though some T cells are still able to find DCs quickly if they are constrained to move along the edges of FRC network (Figure 3.4A), the number of T cells that are able to find one Ag-DC before exiting the LN is lower than when T cells are not constrained to FRCs. This could be explained by reduced motility as shown in Figure 3.3, which results in a limited exploration of the LN.

As shown by our preliminary results, both FRC directed movement and DC chemotaxis together significantly reduce T cell scanning efficiency by an Ag-DC, especially for T cells that have not been previously scanned by DCs. Reduced unique scanning does not only influence the immune response by limiting the number of cognate T cells to be scanned by DC in a given time and increasing the chance for some cognate cells to miss the target, it also affects cognate T cells that are able to bind a DC. Increasing the time period of direct DC-T cell binding or keeping the T cells in the vicinity of DC will alter the activation signal a T cell receives during priming, which will affect the ensuing proliferation and differentiation phases. If such mechanisms do play a role in the DC-T cell searching, quantifying their impact is key for understanding the search as well as for capturing events afterwards and predicting the overall outcome of an immune response.

Figures

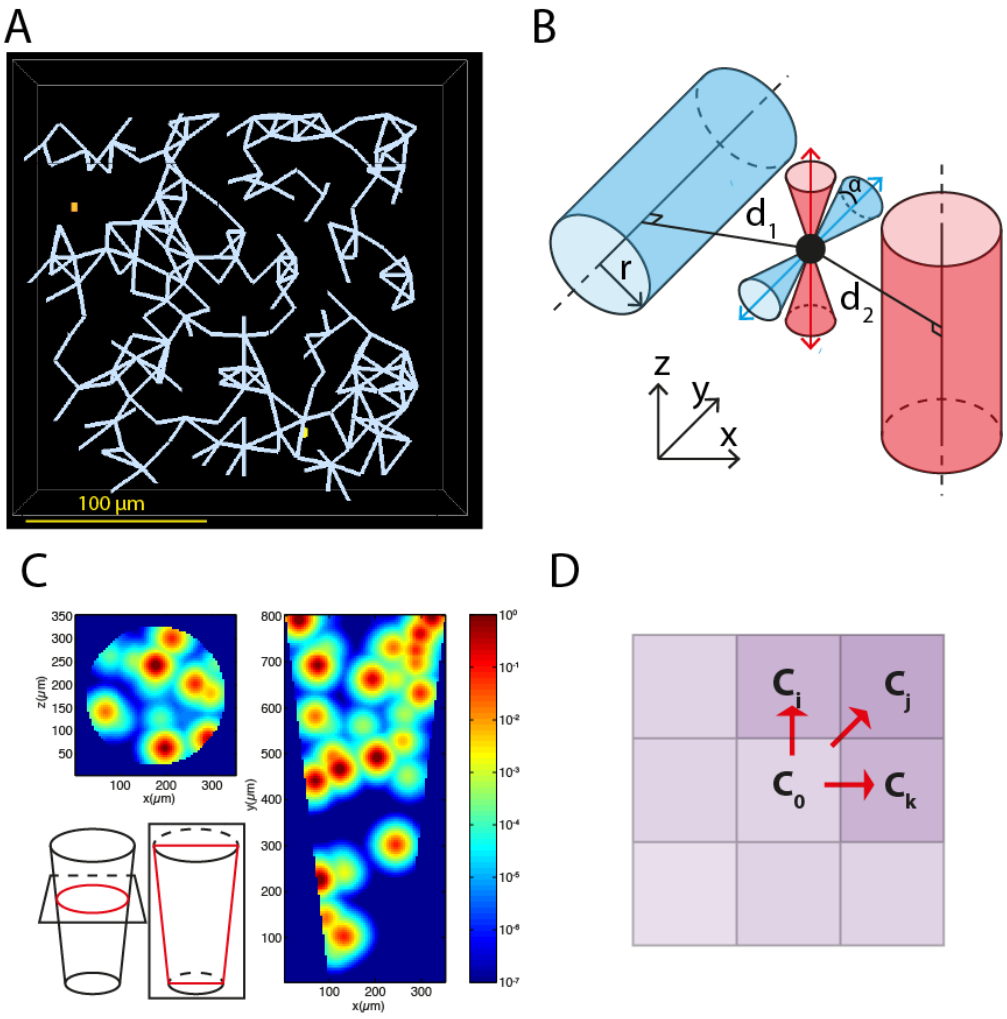

Figure 3.1: Algorithms for FRC network constraint and molecule diffusion. A. FRC network visualized in our model with parameters from Table 1. A 250x250x40 μm slice of a simulated LN is shown. B. FRC constraint. Blue and red cylinders are two FRC segments. Cell (black circle) is guided in two sets of directions: directions in the blue cones are guided by the blue FRC edge, and directions in the red cones are guided by the red FRC edge. r defines the radius of the FRC edge. Here d1 and d2 are within the constraint radius of the two edges respectively. C. Chemokine gradient created by DCs color indicate chemokine concentration with Ag-DC in the center. D. Chemotaxis rules with color indicating chemokine concentration (darker is higher concentration).

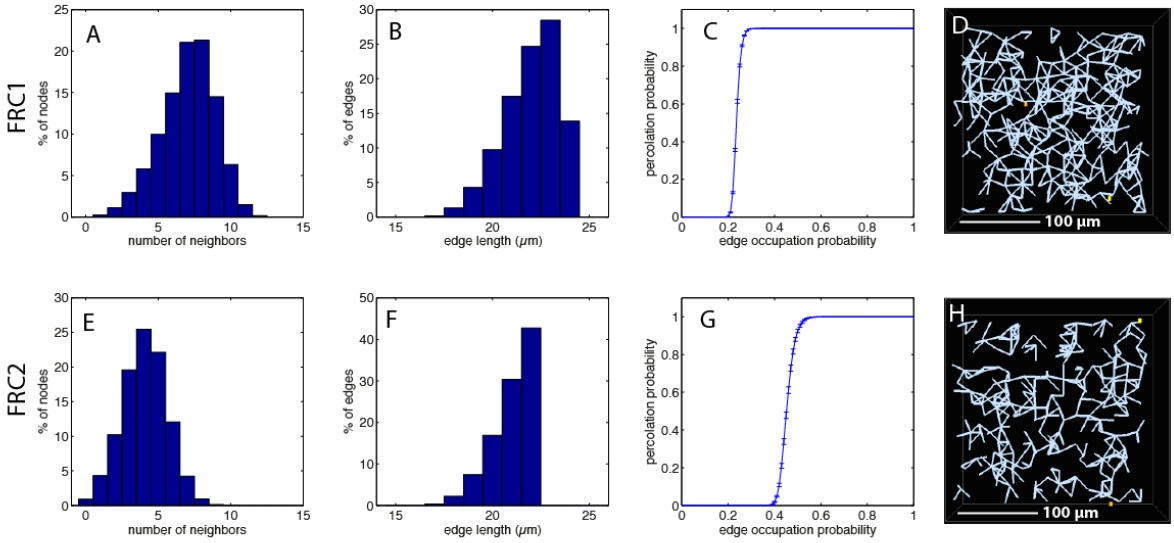

Figure 3.2: Metrics from model generated FRC networks. A-D: FRC1. A. Vertex degree distribution. B. Edge length distribution. C. Percolation probability vs. edge occupation probability. D. Snapshot of computer-generated FRC network. E-G: FRC2. E. Degree distribution. F. Edge length distribution. G. Percolation probability vs. edge occupation probability. H. Snapshot of computer-generated FRC network. See text for definitions.

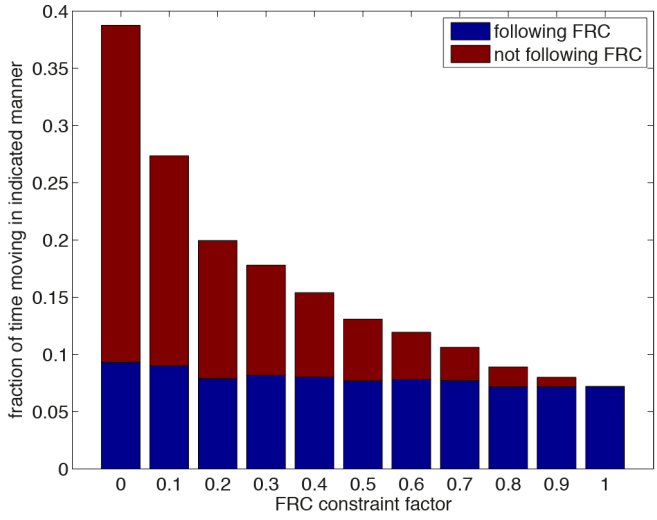

Figure 3.3: Apparent FRC constraint vs. FRC constraint factor. Fraction of time that T cells are moving in the FRC directions, regardless of constraint strengths. X-axis shows FRC constraint factor, from 0 to 1.0.

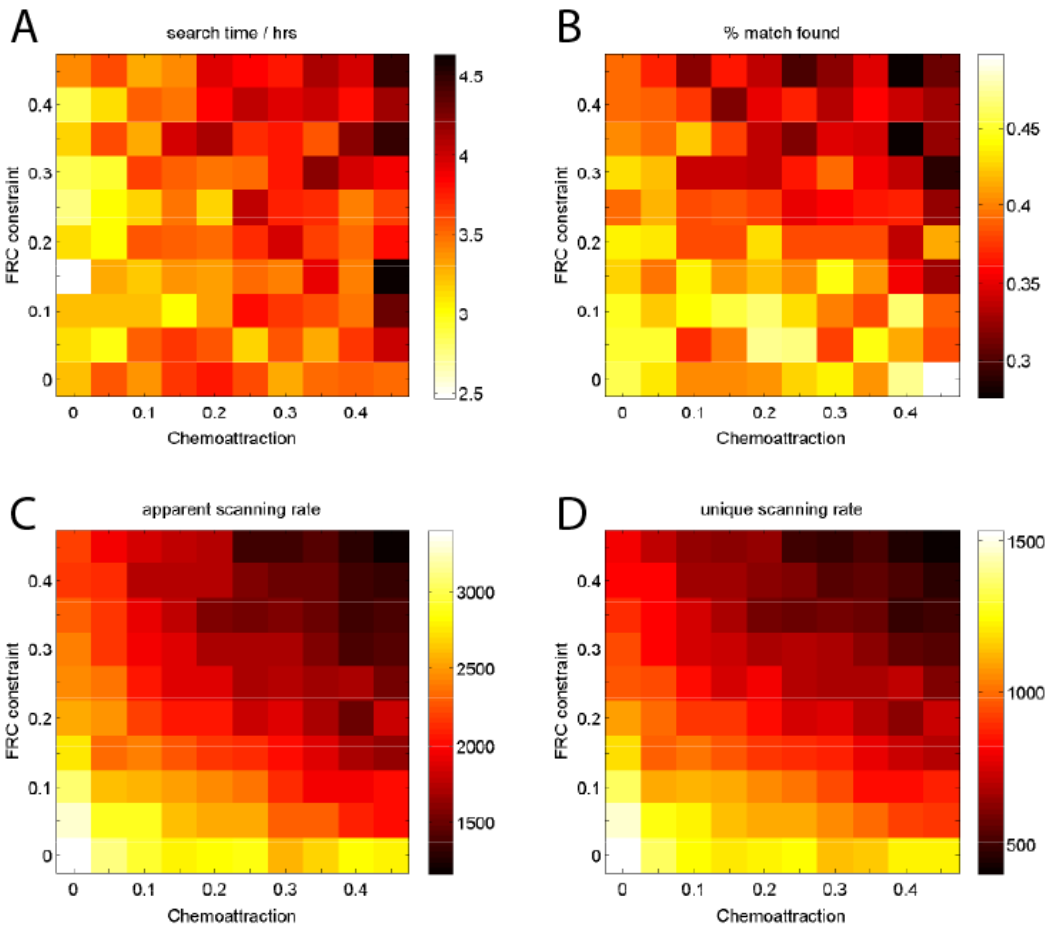

Figure 3.4: Influence of FRC constraint and DC chemotaxis on T cell-DC searching factors. Chemoattraction and FRC constraint correspond to f_c and f_F in Equation 3.2. A. Average time for T cells to find matching Ag-DC after entering a LN. B. Proportion of T cells having found at least one matching Ag-DC before exiting a LN. C. DC apparent scanning rate, per DC per hour. D. DC unique scanning rate. This measure only considers T cells that have not been previously scanned by the same DC, Per DC per hour.

Tables

Table 3.1: FRC network topology metrics

FRC group	FRC1	FRC2
parameters:		
edgeLengthLimit (μm)	24	22.5
metrics:		
average degree	7	4.1
average length (μm)	22	21.07
transitivity	0.3245	0.2848
percolation threshold	0.2353	0.4518

Bibliography

Bajénoff, M., Egen, J. G., Koo, L. Y., Laugier, J. P., Brau, F., Glaichenhaus, N. and Germain, R. N. Stromal cell networks regulate lymphocyte entry, migration, and territoriality in lymph nodes. *Immunity*, 25(6):989–1001, 2006.

Bajénoff, M., Egen, J. G., Qi, H., Huang, A. Y. C., Castellino, F. and Germain, R. N. Highways, byways and breadcrumbs: directing lymphocyte traffic in the lymph node. *Trends in immunology*, 28(8):346–52, 2007.

Bajenoff, M., Glaichenhaus, N. and Germain, R. N. Fibroblastic Reticular Cells Guide T Lymphocyte Entry into and Migration within the Splenic T Cell Zone. *The Journal of Immunology*, 181(6):3947–3954, 2008.

Barakat, H. Z. and Clark, J. A. On the Solution of the Diffusion Equations by Numerical Methods. *Journal of Heat Transfer*, 88(4):421, 1966.

Beauchemin, C., Dixit, N. M. and Perelson, A. S. Characterizing T Cell Movement within Lymph Nodes in the Absence of Antigen. *The Journal of Immunology*, 178(9):5505–5512, 2007.

Beltman, J. B., Maree, A. F., Lynch, J. N., Miller, M. J. and de Boer, R. J. Lymph node topology dictates T cell migration behavior. *Journal of Experimental Medicine*, 204(4):771–780, 2007.

Bishop, C. M., Spivey, R. J., Hawkes, L. A., Batbayar, N., Chua, B., Frappell, P. B., Milsom, W. K., Natsagdorj, T., Newman, S. H., Scott, G. R., Takekawa, J. Y., Wikelski, M. and Butler, P. J. The roller coaster flight strategy of bar-headed geese conserves energy during Himalayan migrations. *Science (New York, N.Y.)*, 347(6219):250–4, 2015.

Blattman, J. N., Antia, R., Sourdive, D. J. D., Wang, X., Kaech, S. M., Murali-Krishna, K., Altman,

J. D. and Ahmed, R. Estimating the precursor frequency of naive antigen-specific CD8 T cells. *The Journal of experimental medicine*, 195(5):657–664, 2002.

Callaway, D. S., Newman, M. E. J., Strogatz, S. H. and Watts, D. J. Network Robustness and Fragility: Percolation on Random Graphs. *Physical Review Letters*, 85(25):5468–5471, 2000.

Casrouge, A., Beaudoing, E., Dalle, S., Pannetier, C., Kanellopoulos, J. and Kourilsky, P. Size estimate of the alpha beta TCR repertoire of naive mouse splenocytes. *Journal of immunology (Baltimore, Md. : 1950)*, 164(11):5782–5787, 2000.

Castellino, F., Huang, A. Y., Altan-Bonnet, G., Stoll, S., Scheinecker, C. and Germain, R. N. Chemokines enhance immunity by guiding naive CD8+ T cells to sites of CD4+ T cell-dendritic cell interaction. *Nature*, 440(7086):890–5, 2006.

Cilfone, N. A., Kirschner, D. E. and Linderman, J. J. Strategies for Efficient Numerical Implementation of Hybrid Multi-scale Agent-Based Models to Describe Biological Systems. *Cellular and Molecular Bioengineering*, 8(1):119–136, 2014.

DeFea, K. A. Stop that cell! Beta-arrestin-dependent chemotaxis: a tale of localized actin assembly and receptor desensitization. *Annual review of physiology*, 69:535–60, 2007.

Donovan, G. M. and Lythe, G. T-cell movement on the reticular network. *Journal of theoretical biology*, 295:59–67, 2012.

Gérard, A., Patino-Lopez, G., Beemiller, P., Nambiar, R., Ben-Aissa, K., Liu, Y., Totah, F. J., Tyska, M. J., Shaw, S. and Krummel, M. F. Detection of rare antigen-presenting cells through T cell-intrinsic meandering motility, mediated by Myo1g. *Cell*, 158(3):492–505, 2014.

Gong, C., Linderman, J. J. and Kirschner, D. Harnessing the heterogeneity of T cell differentiation

fate to fine-tune generation of effector and memory T cells. *Frontiers in immunology*, 5:57, 2014.

Gong, C., Mattila, J. T., Miller, M., Flynn, J. L., Linderman, J. J. and Kirschner, D. Predicting lymph node output efficiency using systems biology. *Journal of theoretical biology*, 335:169–184, 2013.

Graw, F. and Regoes, R. R. Influence of the Fibroblastic Reticular Network on Cell-Cell Interactions in Lymphoid Organs. *PLoS Computational Biology*, 8(3):e1002436, 2012.

Iijima, M., Huang, Y. E. and Devreotes, P. Temporal and Spatial Regulation of Chemotaxis. *Developmental Cell*, 3(4):469–478, 2002.

Jenkins, M. K. and Moon, J. J. The role of naive T cell precursor frequency and recruitment in dictating immune response magnitude. *Journal of immunology (Baltimore, Md. : 1950)*, 188(9):4135–4140, 2012.

Lanzavecchia, A. and Sallusto, F. Dynamics of T lymphocyte responses: intermediates, effectors, and memory cells. *Science*, 290(5489):92–97, 2000.

Malhotra, D., Fletcher, A. L. and Turley, S. J. Stromal and hematopoietic cells in secondary lymphoid organs: partners in immunity. *Immunological reviews*, 251(1):160–76, 2013.

Miller, M. J., Hejazi, A. S., Wei, S. H., Cahalan, M. D. and Parker, I. T cell repertoire scanning is promoted by dynamic dendritic cell behavior and random T cell motility in the lymph node. *Proceedings of the National Academy of Sciences of the United States of America*, 101(4):998–1003, 2004.

Miller, M. J., Wei, S. H., Cahalan, M. D. and Parker, I. Autonomous T cell trafficking examined in

vivo with intravital two-photon microscopy. *Proceedings of the National Academy of Sciences of the United States of America*, 100(5):2604–2609, 2003.

Newman, M. E. J. and Ziff, R. M. Efficient Monte Carlo Algorithm and High-Precision Results for Percolation. *Physical Review Letters*, 85(19):4104–4107, 2000.

Reynolds, A. M. and Rhodes, C. J. The Lévy flight paradigm: random search patterns and mechanisms. *Ecology*, 90(4):877–887, 2009.

Riggs, T., Walts, A., Perry, N., Bickle, L., Lynch, J. N., Myers, A., Flynn, J., Linderman, J. J., Miller, M. J. and Kirschner, D. E. A comparison of random vs. chemotaxis-driven contacts of T cells with dendritic cells during repertoire scanning. *Journal of theoretical biology*, 250(4):732–51, 2008.

Strang, G. On the Construction and Comparison of Difference Schemes. *SIAM Journal on Numerical Analysis*, 5(3):506, 1968.

Viswanathan, G., Afanasyev, V., Buldyrev, S. V., Havlin, S., da Luz, M., Raposo, E. and Stanley, H. Lévy flights search patterns of biological organisms. *Physica A: Statistical Mechanics and its Applications*, 295(1-2):85–88, 2001.

CHAPTER IV

Harnessing the heterogeneity of T cell differentiation fate to fine-tune generation of effector and memory T cells

4.1 Introduction

Antigen-presenting cells (APC), especially dendritic cells (DCs), process antigens and carry information from sites of infection to secondary lymphoid organs, such as lymph nodes (LNs)(Randolph et al., 2005). T cells are produced in the thymus and are deployed into blood circulation to recognize millions of different epitopes from pathogenic organisms; each T cell is hardwired to have one type of T cell receptor (TCR) that recognizes a single pattern (i.e. "cognate" with respect to a specific antigen)(Arstila et al., 1999). The frequency of particular cognate T cells is as low as 10^{-5} to 10^{-6} (Casrouge et al., 2000; Blattman et al., 2002). Through high endothelial venules (HEVs), T cells are recruited to LNs, where they are exposed to antigenic peptides presented by MHC molecules expressed on DCs - this initiates the adaptive immune response (Chicz et al., 1992; Butcher and Picker, 1996; Banchereau and Steinman, 1998; Girard et al., 2012; Masopust and Schenkel, 2013). LNs are organized such that when T cells travel through they can be efficiently scanned by DCs to identify that rare cognate encounter (Bajenoff et al., 2003; Mempel et al., 2004; Grigorova et al., 2010). Such encounters result in binding of cognate T cells to DCs

The work in Chapter IV is pubished as Gong, Chang, Jennifer J Linderman, and Denise Kirschner. 2014. *"Harnessing the Heterogeneity of T Cell Differentiation Fate to Fine-Tune Generation of Effector and Memory T Cells."* Frontiers in Immunology 5 (January): 57. doi:10.3389/fimmu.2014.00057.

and subsequent activation and proliferation of the T cells. The expanded T cell population differentiates into two classes: effector cells, which perform immediate killing and cytokine secretion functions, and memory cells, which are reserved for long-term protection (Ahmed and Gray, 1996; Sallusto et al., 1999). These cells move out of LNs via efferent lymphatics (ELs) into blood circulation (Cyster, 2005). Through the blood, effector T cells reach sites of infection while memory T cells continue to recirculate and await a potential secondary infection for which they will wage a faster and stronger recall response (Mackay, 1993; Dutton et al., 1998). A snapshot of the trafficking of these cells is shown in Figure 4.1. The immune system responds differently to different antigenic materials; however, the same set of machinery is engaged to face each challenge. Thus, there should be a general program adaptively guiding the behavior of this system. In this study, we focus on cellular-mediated events shared among immune responses during the initiation of adaptive immunity and generation of immune memory.

Differentiation of T cells during generation of adaptive and memory responses is highly heterogeneous, and this heterogeneity is may be dependent on the environmental context that each cell experiences(Buchholz et al., 2013; Gerlach et al., 2013). However, the cause of such heterogeneity is poorly understood. If mechanisms other than mere stochasticity contribute to heterogeneity, it could be possible to more precisely direct the differentiation to favor the production of the desired output from an immune response (e.g. effectors in an immune therapy or memory cells in vaccination) by manipulating mechanisms involved. We are interested in which mechanisms could provide handles for such manipulation. Since T cell priming occurs in LNs, and blood circulation conveys effector and memory T cells to locations where they perform their specific functions, mechanisms in these two organs could be responsible for the heterogeneous differentiation. The dynamics of T cells in these compartments will also reflect progression of infection or effectiveness of vaccinations. Thus, understanding how different LN and blood mechanisms affect the dynamics of infection and treatment could help guide immunotherapy and vaccine design.

Computational and mathematical models are widely used in biological systems to assess hypotheses and generate predictions for experimental validation. Deterministic equation-based models have been developed to understand the dynamics of T cells responding to immunogenic antigens, and these models helped with estimating parameters, determining alternative hypothesis, and predicting outcomes of immune responses (Antia et al., 2005; De Boer and Perelson, 2013). Agent-based models (ABMs) have proven convenient in assessing roles of cellular and molecular level interactions during infection (Beltman et al., 2007; Riggs et al., 2008; Bogle and Dunbar, 2010). However, because of the extremely low cognate frequency that exists in primates, these models usually require large numbers of cells to be simulated and thus are very computationally intensive. In order to capture both heterogeneous stimuli-sensitive short-term activation events as well as average long-term dynamics, a model needs to be capable of adapting itself to both situations.

In this study, we present a hybrid computational model that uses an agent-based modeling to capture events occurring in a LN and a non-linear ordinary differential equation model (ODE) to capture events occurring in the well-mixed compartment of blood. This model allows us to track a highly stochastic immune response operating during the first few weeks of an immune response (with time resolution around seconds), as well as long-term dynamics afterwards (at a time scale of months to years). Using this model, we assess which mechanisms in both LN and blood compartments control the differentiation and clonal expansion processes of T cells and also direct the immune response toward potent effector T cell output and/or robust memory generation. These findings could bring insights to vaccine design strategies.

4.2 Method

4.2.1 LN ABM model

ABMs are computational models in which individual agents are represented on an explicitly formulated grid and they interact with each other according to a defined set of rules implemented in

discrete time steps. As these types of models can account for spatial- sensitive interactions between DC and cognate T cells, they are ideal for studying heterogeneous priming and differentiation of T cells in LNs (Riggs et al., 2008; Linderman et al., 2010; Mirsky et al., 2011; Kirschner and Linderman, 2009; Bogle and Dunbar, 2010).

We previously developed *LymphSim*, a three-dimensional (3D) LN computational model capturing dynamics of CD4+ T cells, CD8+ T cells and DCs during both steady state and infection(Gong et al., 2013). Briefly, cells move on a 3D grid that is shaped like a truncated cone and represents approx. 1/200 of a primate LN. T cells enter the LN via HEVs, search for DCs, activate and proliferate to generate effector cells that exit via efferent lymphatics. In *LymphSim*, cell motility and steady state values in a LN are calibrated to experimental data with model antigens such as OVA (Miller et al., 2002), and the dynamics during an immune response are not quantitatively fit to any specific infection. For simplicity, we only include one type of cognate T cell each for CD4+ and CD8+ T cells in current model, and DCs present the corresponding antigens on pMHC-II and pMHC-I for both primary and secondary infections. The model can be adapted to account for multiple sub-antigens. For the work herein, this single antigen study is sufficient to address the key questions under study. A complete list of rules can be found at: `http://malthus.micro.med.umich.edu/lab/movies/3dLN/`.

4.2.2 Effector and memory T cell differentiation rules

In the present study, we modified *LymphSim* to include two additional T cell differentiation states: central memory (CM) and effector memory (EM), for both CD4+ and CD8+ T cells. We also added rules that govern generation of these memory cells, and their interaction with other cells (Figure 4.2).

We based the cell differentiation process on a version of a "signal-strength model", in which the overall strength of signal received by a naive T cell during DC contact will determine the fate

of cell differentiation (Figure 4.3) (Constant et al., 1995; Lanzavecchia and Sallusto, 2000; Gett and Hodgkin, 2000; Kaech and Cui, 2012). A definitive differentiation scheme after T cell priming occurs has not been determined by experimentation. Previous modeling studies based on experimental data reject memory to effector differentiation in favor of effector to memory differentiation (Antia et al., 2005); however, more recent work showed that differentiation has as its backbone differentiation from naive to CM precursor to EM precursor to effector (Buchholz et al., 2013). The scheme we use in this study considers effector to EM differentiation, but is still topologically similar to the scheme from (Buchholz et al., 2013), with precursors of both EM and effectors differentiating into these two subtypes (Figure 4.3). The difference between the two schemes is that "effectors" in our model are cells that have differentiated toward effector phenotype sufficiently so as not to enter into the CM population, nor have they entered into the EM pool. They are allowed to exit the LN due to the loss of early activation markers (CD69), even though these cells do not perform effector functions until they would reach sites of infection, which is not studied in this current work.

In our model, a series of probabilistic checkpoints are established to determine to which state a cell will proceed (Viola and Lanzavecchia, 1996; Itoh and Germain, 1997; Iezzi et al., 1998; Lanzavecchia and Sallusto, 2002). When a cognate T cell finds an Ag-bearing DC (Ag-DC) or licensed DC (LDC) in its binding area, the corresponding pMHC value of the DC is checked to see if a successful binding can be established. If bound, a T cell continuously accumulates signals from the DC (Gett and Hodgkin, 2000), represented by pMHC levels at each time point. Here pMHC level is used as a proxy for the strength of antigenic stimulation from the DC or LDC. When a T cell unbinds from a DC or LDC, the accumulated signal value is used to determine whether a T cell proceeds to an activated state, or returns to a resting state (naive). Activated cells go through a set number of rounds of divisions, after which the accumulated signal level is checked again to decide if the cell can further differentiate into an effector state. Effector cells will divide a few

more rounds. With given probabilities, the cells with intermediate

differentiation status do not proceed to effector status, but become CM cells, while those effector cells with sufficient signals will become EM cells (Jacob and Baltimore, 1999; Opferman et al., 1999; Pepper and Jenkins, 2011). The probability of effector cell converting to EM is estimated between 0.1 and 0.4. CM T cells can be recruited to LNs from HEVs. These cells act similarly to cognate naive T cells. When they detect Ag-DCs or LDCs, CMs will bind to DC and accumulate signal more efficiently in comparison with naive cells (Byrne et al., 1988; Bachmann et al., 1999). The rules above apply to both CD4+ and CD8+ T cells. Because we developed some of these rules based on LCMV studies, one difference we captured between these two cell types is that CD8+ T cells can bind only to LDCs to generate functional memory cells in the primary response, whereas CD4+ T cells do not have this restriction and can generate memory cells after binding to both Ag-DCs and LDCs (Wiesel and Oxenius, 2012).

Other models of T cell differentiation exist, and some of these models are not mutually exclusive. We also integrated features from these models into our rule set, and excluded those that are inconsistent with current findings or are not applicable to our model at this stage. A single naive T cell can produce both effector and memory progenies (Stemberger et al., 2007; Gerlach et al., 2013), so we excluded the possibility that effector and memory arise from separate precursors. In the decreasing-potential model (Ahmed and Gray, 1996), the stimulation that T cells receive during infection drives greater clonal expansion but reduces their potential to differentiate into memory cells. Some studies show T cells are committed to massive proliferation after initial encounters with APCs, and can differentiate into both memory and effector subsets even if adoptively transferred into hosts absent of antigen (Kaech and Ahmed, 2001). Thus, we limited the signal accumulation stage to the period of time when a T cell is bound to a DC before its first division, similar to findings made in B cell expansion (Hawkins et al., 2009). In the asymmetric cell fate model (Chang et al., 2007), heterogeneity arises from unequal distribution of differentiation

factors into daughter cells during division. We will further study this hypothesis as we incorporate dynamics at molecular level, but currently account for these asymmetries using phenomenological probabilities.

4.2.3 Blood compartment sub-model: ODE and parameter estimation

We developed a blood compartment model by assuming the blood is a well-mixed, homogenous compartment. We use a system of non-linear ODEs to capture the dynamics of T cells therein. Equations for CD4+ T cells are:

$$\frac{dN_4}{dt} = s_{N4}(t) - \delta_{N4}N_4 + e^{LN}_{N4} \tag{4.1}$$

$$\frac{dE_4}{dt} = -\delta_{E4}E_4 - \xi_{E4}E_4 + e^{LN}_{E4} \tag{4.2}$$

$$\frac{dCM_4}{dt} = -\delta_{CM4}CM_4 + \alpha_{EM4}EM_4 + e^{LN}_{CM4} \tag{4.3}$$

$$\frac{dEM_4}{dt} = -\delta_{EM4}EM_4 - \xi_{E4}E_4 - \alpha_{EM4}EM_4 + e^{LN}_{E4} \tag{4.4}$$

N_4,E_4, CM_4 and EM_4 represent the blood concentrations of naive, effector, CM and EM CD4+ T cells, respectively. s_{N4}(t) is the time-dependent thymus output of naive CD4+ T cells (Bajaria et al., 2002). The initial output is estimated from healthy 30-year-old individuals, and declines by 5% per year (Steinmann et al., 1985). δ_{N4} is the overall death rate constant for naive cells, including homeostatic proliferation and death. We estimated this parameter by assuming a quasi-equalibrium between thymus output and peripheral loss. δ_{E4},δ_{CM4} and δ_{EM4} are the death rate constants for effector, CM and EM CD4+ T cells, respectively. δ_{E4} and δ_{EM4} account for the death of circulating effector and EM cells, excluding those recruited to sites of infection (Homann et al., 2001). δ_{CM4} reflects the overall loss of CM cells, including self-renewal and death (Homann et al., 2001). ξ_4 and ξ_{M4} are the rate constants for recruitment of CD4+ effectors and EM cells from blood to sites of infection. As the dynamics at a site of infection are not considered in this study,

these recruitment terms serve as a sink for the corresponding cell species in the blood compartment. α_{EM4} is the rate constant for EM cell differentiation into CM cells (Wherry et al., 2003). The terms e_{N4}^{LN}, e_{E4}^{LN}, e_{CM4}^{LN} and e_{EM4}^{LN} represent rates of LN net output of corresponding cells. These terms are converted to the changes in concentration in the blood per time step. For naive and CM cells, this is calcuated as the difference between the number of exited and recruited cells. For effector and EM cells, this calculated as the number of exited cells. These four terms are not solved directly in the ODE system but rather are added as an initial condition before each blood time step is processed in the computational model. We show them in the equations for completeness. Similar equations and paramter estimates are written for CD8+ T cells (see Appendix B). Because the CM CD8+ T cells population is maintained for life, we assume a very small value for the loss rate constant δ_{CM8}, corresponding to half-life of 20 years (Homann et al., 2001). See Appendix B Table B.1 for a complete list of parameters, definitions, values, units and source references.

4.2.4 Two-compartment hybrid model

Our goal is to develop a 2-compartment computational model that combines *LymphSim* and the blood ODE model described above. Recently, we published other models linking ODEs and ABMs (Fallahi-Sichani et al., 2011; Marino et al., 2011; Fallahi-Sichani et al., 2012). For this study, we use the implementation method we employed successfully to link a LN compartment with a lung (Marino et al., 2011). The LN and blood compartment models are processed sequentially during each time step of simulation (Figure 4.4). During the T cell recruitment subroutine of the LN ABM model, the probability of recruiting T cells of each type/state is calculated based on their blood concentration levels. At the end of LN compartment simulation time step, the LN net output is calculated as the difference between exited and recruited number of each cell type and is multiplied by a factor that accounts for physiological compartment-size scaling from 0.5% back to the entire paracortex and unit conversion from cell number to blood concentration. This

net output is then added to the corresponding variables in blood compartment ODEs. We have made a few assumptions regarding how we capture the LN to blood dynamics. First, we are only modeling dynamics of T cells and DCs within a single LN. There are approximately 700 LNs in the human body and they are connected via an intricate lymphoreticular network. T cells travel between multiple LNs via these lymphatics and eventually enter the blood via the superior vena cava. We assume that cells exit the LN and enter the blood compartment immediately, coarse-graining the time spent in the lymphatic system. However, our cells travel through the LN and blood in time frames consistent with experimental data (less than 24 hours; (Sprent and Tough, 2001)), accounting for the delay.

For computational efficiency, we use a method we term tunable resolution (TR) (Kirschner et al., 2014). One of the goals of TR is to develop multi-scale models with sub-models of different resolutions, so that models can be run with coarse- or fine-grained alternative versions of sub-models during simulation to save resources without sacrificing accuracy. Here, for each physiological compartment (blood or LN), there is a computational switch that allows the model in an automated fashion to bypass simulation of a given compartment. In this two-compartment model, we do not have an alternate version of each compartment per se; instead, each compartment can be suspended when specific criteria are met. For example, during the pre-simulation, the blood compartment is turned off, and the LN is simulated until a baseline steady state is reached. When an immune response is occurring, LN and blood compartments are both running to simulate the immune response in fine-grained, spatially explicit detail for a time scale of a few weeks. When an active immune response finishes and there are no Ag-DCs, LDCs, bound, active, effector or EM cells in the LN compartment, the LN compartment is suspended to allow rapid simulation of the blood compartment at longer time scales (months to years). When a secondary infection begins, the LN compartment is switched on again (Figure 4.4).

4.2.5 Model calibration

The hybrid model contains 103 parameters that govern mechanisms occurring in both physiological compartments and the interactions between them (See Appendix B,Table B.1 for a complete list of the parameters). For the LN compartment model, parameters governing T cell motility and trafficking are calibrated to data as described previously (Gong et al., 2013). Parameter estimates for the ODE model in the blood compartment are discussed in section 4.2.3 and Appendix B.

To use our model for memory T cell differentiation dynamics, we estimated parameters in our model using the limited data available in the literature for memory cell generation in LNs. We estimated parameters governing total production of expanded cognate CD8+ cells generated in the LN model (Appendix B,Table B.1, parameters marked with) to data from T cell clonal expansion studies in mice using OVA as a stimulating antigen (Prlic et al., 2006). In that study, DCs are ablated at different time points to show that the duration of antigen-presentation correlates with magnitude of T cell expansion, but a short exposure is sufficient to program CD8+ T cells to differentiate into both effector and memory subsets (Prlic et al., 2006). We adapted our model to reflect experimental methods used in these studies. DCs are removed from the LN grid at indicated time points after recruitment during primary challenge (Fig. 5A), as was done experimentally by injecting diptheria toxin (DT) (Prlic et al., 2006). Unlike rules for LCMV as previously discussed, CD8+ naive T cells are allowed to bind to both Ag-DC and LDC to be primed and enter memory state. This is because in these experiments, DCs are activated from LPS pulsing or Listeria monocytogenes-OVA. From our *in silico* experiments terminating antigen presentation from DCs at various time points after Ag-DC recruitment, we predict that the magnitude of the primary response is dependent of the duration of DC presence (Figure 4.5B). However, a very short period of stimulation is capable of generating memory cells, as we see a potent production of antigen specific CD8+ T cells after a secondary challenge (Figure 4.5C). Moreover, it takes only 3 days for the recall response to exceed the magnitude of primary response on day 5, indicating a faster reaction to previously experienced

antigens, as observed *in vivo*. Our simulation results are comparable to data from the Prlic study (Prlic et al., 2006). The parameter set we obtained is used as our baseline for simulating infection scenarios (See below and Appendix B, Table B.1).

4.2.6 Simulated infection and model validation

We next validated our model with data sets from experimental studies using LCMV or OVA as stimulating antigens. For each simulated infection, a three-day pre-simulation of the ABM LN sub-model precedes the actual experiment to allow cells to reach a steady state in terms of quantity and spatial distribution. During this period, the blood sub-model is suspended, with the naive CD4+ and CD8+ T cells concentrations fixed at 450 and 320/mm3, respectively (Roederer et al., 1995; Bajaria et al., 2002). Then Ag-DCs are introduced to stimulate the T cell response. We represent this by introducing antigen-bearing DCs in such a way as to mimic an acute infection (Riggs et al., 2008; Linderman et al., 2010; Gong et al., 2013). Ag-DCs carry and present a unique antigen and are recruited to the LN compartment for 2 days. These DCs will prime cognate T cells (cognate frequency is set to 10^{-4}) for about 5 days before they die, mimicking a hypothetical acute infection. To mimic a hypothetical secondary infection, Ag-DCs are recruited to the LN again from day 600 to day 602. Each experiment is simulated five times to reduce aleatory uncertainty.

To confirm that our model produces reasonable dynamics in the blood compartment, we qualitatively compare the time course of blood antigen-specific cells to data sets from LCMV studies, where the measurements are performed in spleen (De Boer et al., 2001; Antia et al., 2003; De Boer et al., 2003).

For lineage tracing simulations (see Section 4.3.4), every cognate naive T cell recruited to the LN is assigned a unique serial number. This number is passed to the daughter cells when these labeled T cells proliferate and differentiate, so T cells sharing the same serial number belong to the same single-cell derived progeny. When each differentiated cell exits the LN, its serial

number is recorded. For each individual cognate precursor, the number of descendant cells and their differentiation states are calculated. Cell progenies are ranked by the abundance of their progenies, from largest to smallest. Five replications are performed for this simulation.

We calculate the Index of disparity D between the expanded populations of different single-cell derived progenies (Gerlach et al., 2013), which is the inverse Simpson diversity index mapped to a 0 to 1 interval:

$$D = \frac{N - \frac{1}{\sum_{i=1}^{N} f_i^2}}{N - 1}, \tag{4.5}$$

where N is the number of progenies and f is the frequency of each single-cell derived progeny in the total population.

4.2.7 Uncertainty and sensitivity analysis

In this study, our goal is to reproduce patterns of generalized immune responses. In addition to using parameters estimated from previous work (See above and Table B.1) and experimental data, we use global uncertainty and sensitivity analysis (U/SA) to study how particular biological mechanisms affect simulation outputs (Marino et al., 2008).

For each set of sensitivity analysis, a list of parameters is chosen, and for each parameter of interest, a range is specified. Latin hypercube sampling (LHS) is applied to generate the matrix of parameter values, where each experiment represents one combination of sampled parameter values. LHS is a stratified sampling method that requires fewer samples compared with random sampling method but achieves the same accuracy (Mckay et al., 1979). This technique is particularly helpful for our ABM model where parameter values need to be estimated from a high-dimensional space (Marino et al., 2008). The parameter space is sampled completely and accurately, with a large sampling size. Each experiment is replicated five times to reduce aleatory uncertainty from inherent stochastic variations (Marino et al., 2008). After the simulation, model readouts are chosen and

partial rank correlation coefficients (PRCCs) are calculated between each readout-parameter pair to assess global sensitivity and detect monotonic relationship between mechanisms and output of interests.

To study how various mechanisms affect the generation of memory from within each compartment (blood and LN) as well as how they influence the other compartment (LN and blood, respectively), we performed intra- and inter-compartment sensitivity analysis (Marino et al., 2008). We choose two sets of parameters governing mechanisms in each sub-model and estimated a range for each parameter (See Table B.1). We use LHS to sample the parameter space and generate 100 or 408 experiments for blood and LN experiments, respectively. Here we performed 2540 simulations, which provides ample coverage of the space. Sensitivities of outputs to mechanisms are assessed with PRCCs.

4.2.8 Computational simulations and implementation

Our hybrid model is implemented in C++ and runs on Linux/MacOS/windows. Documentation and pseudo code are available in the online Supplement. A Forward Euler method is used to solve the ODEs. Each time step of the ABM simulation is further divided into 100 pieces (step size of 0.25 s) to reduce error. Each simulation of 350 days (LN sub-model is active for approximately 40 days) takes 30 to 40 hours to run.

4.3 Results

4.3.1 Healthy uninfected baseline dynamics of T cells are reached without simulated antigen presentation

Without Ag-DC introduced to the LN, all T cells remain naive. The cell dynamics in LN in the absence of any infection present show that over a short time scale (days to weeks), cells remain at the steady state of approximately 170 thousand, or $4.0 \times 10^6 cells/mm^3$. There is an equal input/output flow of about 1000 cells per million cells per minute, and an average transit time of

16 hours, which is consistent with previous data (Gong et al., 2013). The population of both CD4+ and CD8+ T cells in the blood declines long-term (20 years). By the end of year 20, the blood concentration of naive CD4+ T cells drops to 210 mm^{-3}, and that of naive CD8+ T cell drops to 170 mm^{-3}. Such long-term decline of naive T cell number is comparable to clinical observations (Erkeller-Yuksel et al., 1992; Douek et al., 1998).

4.3.2 Effector and memory T cell populations are generated in a simulated acute infection

We simulated immune responses to a hypothetical acute infection by introducing Ag-DCs into the LN compartment to activate cognate T cells as shown in Figure 4.6A. The cognate frequency is set to 10^{-4}. Figure 4.6B-E shows simulated immune cell dynamics in the LN and blood compartments.

In the LN compartment, the Ag-DC population increases first. These DCs scan surrounding CD4+ and CD8+ T cells and bind to their cognate matches. After this binding event, CD4+ and CD8+ T cells begin to proliferate and differentiate into active and effector T cells. After day 2, the influx of Ag-DCs to LN stops, and the number of Ag-DCs begins to decline (Figure 4.6A). At the same time, differentiated effector CD4+ T cells license Ag-DCs, further increasing their surface pMHC levels and stimulation strength, enabling them to allow CD8+ T cell memory potential. Because we assume that CD8+ T cell memory establishment requires LDCs, the appearance of CM and EM CD8+ T cells is delayed as compared with corresponding CD4+ T cells. After differentiation from the active state, effector, CM and EM cells can exit the LN from ELs, resulting in the decline of these populations within the LN. The system eventually returns to baseline, but CMs can still recirculate through LN (Figure 4.6, panels B and C).

In the blood compartment, the concentrations of effector, CM and EM cell populations increase as they exit the LN (Figure 4.6D, E). The total concentration of both CD4+ and CD8+ Ag-specific T cell (effector, EM and CM) peaks at about day 6 and day 8, respectively (0.91 mm^{-3} for CD4+

T cells and 2.49 mm^{-3} for CD8+ T cells). The lifespans of effector cells are relatively short. These cells either die, or are recruited to sites of infection, bringing about a contraction phase characterized by a decline of total blood Ag-specific T cells. However, about 5% of the peak level is maintained in the memory cell class, especially CM cells in the long-term as their lifespan is longer than EM cells. In the blood, some of the EM cells convert to CM cells, while others are recruited away to sites of infection (Figure 4.6D, E). While there are no data from primates on these dynamics, our results are qualitatively in accordance with experimental data from mouse LCMV studies(De Boer et al., 2001; Antia et al., 2003; De Boer et al., 2003).

4.3.3 Immune cells reach higher levels during a recall response as compared to a primary response

To understand the dynamics of a recall response, we simulated a scenario where Ag-DCs are introduced from day 0 to day 2 in an initial round of infection (the same as that of Section 4.3.2). Once that infection dampens and immune cells return to a resting state, we introduce a second round of challenge by recruiting Ag-DCs from day 600 to day 602. We challenge with the same antigen and use the same cognate frequency for naive cells, but CM populations are maintained in the blood after the primary response. The resulting dynamics of Ag-specific T cells occurring in blood are shown in Figure 4.6.

As above, the primary response is initiated after the first round of Ag-DC input. Blood Ag-specific T cell numbers rise as the response continues and peak at day 6 and day 8. After the peak, effector and EM T cells decline while the CM cell population is maintained. On day 600, the blood concentration of CM CD4+ T cells has dropped from 0.059 to 0.023 mm^{-3}, while the CM CD8+ T cell population remains at 0.16 mm-3. The stable maintenance of CD8+ memory and decline of CD4+ memory is in agreement with mouse LCMV infection data (Homann et al., 2001). During the recall response, because of a memory cell population generated during the primary response that can faster and more strongly respond to the same antigen, both CD4+ and CD8+ T cells in the

blood exceed peak levels of their primary response, peaking at 1.07 mm^{-3} for CD4+ and 6.05 mm-3 for CD8+ T cells. The recall response is more than twice as large as primary response for CD8+ T cells, but only marginally increased (18%) for CD4+ T cells. Such differences in CD4+ and CD8+ recall responses have been observed in LCMV experiments as well (Ravkov and Williams, 2009). After the recall response, higher levels of CM cells are maintained as compared to following the primary response (Figure 4.7). After the recall response ceases, the blood concentrations of CM cells are 0.094 and 0.84 mm^{-3} for CD4+ and CD8+ T cells, respectively. These results indicate that the antigen specific immune memory is reinforced after the second round of challenge, as the central memory population formed in the primary challenge gets further expanded during the second round of challenge.

4.3.4 Cognate naive cells undergo heterogeneous expansion

Recent lineage tracing studies showed that CD8+ T cells have a heterogeneous differentiation pattern (Buchholz et al., 2013; Gerlach et al., 2013). Because the LN compartment of our model is agent-based, it is possible to track the fate of each individual cell during a simulated infection. We take advantage of this feature to validate our model using data from these recent studies.

Figure 4.8 shows our lineage tracing analysis for the primary response. The fraction of each single-cell derived progeny in the total population is shown in Figure 4.8A for CD8+ and Figure 4.8E for CD4+ T cells. For both CD4+ and CD8+ T cells, a small number of progenies have a large expanded population. The average size of the largest population is about 2000 for CD4+ T cells and about 8000 for CD8+ T cells. However, the majority of derived progenies have intermediate to small population sizes, with about 50 for CD4+ T cells and 200 for CD8+ T cells. The maximum population size of CD8+ T cell is 50-fold larger than the median. The index of disparity in our simulations is 0.81 for CD8+ T cells, close to the range of 0.85 - 0.95 shown in (Gerlach et al., 2013). These results indicate our model matches well with the heterogeneous differentiation ex-

perimental observations. While these experimental studies were performed only for CD8+ T cells, we are able to use our model to simulate the dynamics of CD4+T cells as well. Our model predicts less heterogeneity for CD4+ T cells, with an index of disparity of 0.82 and a 50-fold difference between largest and median progenies (Figure 4.8F).

We also assessed the composition of these sub-populations. In Figure 4.8C and 8G, the proportion of CM cells of each single-cell derived progeny is plotted against the population size. These results suggest that progenies with a higher proportion of CM cells tend to have a smaller expanded population during the primary response. We calculated the Spearman correlation coefficients between each subtype and the total number of expanded cells (Figure 4.8D, 8H). The correlation is strong between effectors and overall total population size, but weak between CM and the overall population size. This is comparable to the results from (Buchholz et al., 2013). Thus, in addition to our other findings, these results confirm those previously identified (Buchholz et al., 2013; Gerlach et al., 2013) that the magnitude of the primary response for single-cell derived progenies might not be the sole predictor of immune memory. We next study which mechanisms influence the heterogeneous differentiation and clonal expansion processes of T cells.

4.3.5 Antigen presentation by DCs influences outcome of an immune response

It is no surprise that antigen stimulation plays a crucial role in T cell activation and differentiation Kaech and Cui (2012); Zehn et al. (2012). However, it is difficult to conduct experiments that quantitatively determine the mechanism of dependency. Here we varied the number of Ag-DCs recruited to LN in a range of 50 to 300 and the levels of pMHC molecules on the surface Ag-DCs from 100 to 300, and analyzed how they influence production of effector and central memory cells. Model pMHC levels are used as a proxy for DC stimulation strength. Results are shown in Figure 4.9.

Increasing the number of Ag-DC recruitment promote the output of both effector and memory

T cells from the LN. The number of Ag-DC has a larger impact when the pMHC molecule levels are low. This result indicates that more Ag-DCs are beneficial for production of higher levels of effector and memory cells, but this benefit is diminished when pMHC molecule levels are high.

Interestingly, for each subset of cells, the effects of increased pMHC molecule levels are different. pMHC levels are always negatively correlated with CM output of CD4+ T cells (Figure 4.9A). However, the highest numbers of effector CD4+ T cell output is reached at intermediate levels of pMHC (Figure 4.9C). CD8+ T cells are affected in a different pattern. Intermediate levels of pMHC are required for higher CM production (Figure 4.9B). Our explanation for this difference is that we defined our rules based on LCMV experiments and other studies suggesting that CD8+ T cell memory establishment is dependent on DC licensing by effector CD4+ T cells, and intermediate levels of pMHC are required so that LDC numbers will not be the bottleneck for memory CD8+ T cell production. Also different than CD4+ T cells, effector CD8+ T cell output first increases with pMHC levels on DCs and then remains relatively stable (Figure 4.9D). The fraction of CM among total expanded population is shown in Figure 4.9E and 9F.

In general, our simulations suggest that in order to obtain high CD4+ T CM cell production, DCs with lower pMHC levels should be provided. However, DCs with high pMHC levels maximize CD8+ effector output. CD4+ effectors and CD8+ CM T cells require intermediate pMHC levels. Increased recruitment of Ag-DC boosts all four subsets to different extents.

4.3.6 Sensitivity analysis detects mechanisms correlated with strength of recall responses

We also studied how other mechanisms, such as thresholds of different checkpoints in the LN, conversion rates of EM to CM and recruitment rate to sites of infection from the blood, shape model outputs (see Table B.1 for parameters varied. The mechanisms they control are explained in the column “description”). We performed intra- and inter- compartment sensitivity analysis (see methods), and PRCCs were calculated to assess the monotonic correlation between values

of the parameters governing these mechanisms, and outputs including: LN production and blood concentration of effector and central memory cells in both primary and recall responses (Table 4.1 to 4.3).

We found that production of effector cells in primary responses is most sensitive to the following mechanisms: binding time (negatively correlated, Table 4.1, 4.2), the probability of effectors differentiating into effector memory (negatively correlated, Table 1, 2) and extra recruitment in inflammation (positively correlated, Table 4.1, 4.2). In addition, CD4+ T cell effector output negatively correlates with the stimulation threshold for priming but positively correlates with the threshold for differentiation into effectors (Table 4.1, 4.2); CD8+ T cell effector cell output negatively correlates with extra recruitment of CD4+ T cells (Table 4.1, 4.2). Generation of central memory cells during a primary response is sensitive to a similar set of mechanisms, along with some additional ones: CD4+ T cell CM output is negatively affected by efficiency of CM cells to accumulate stimulation signal; CD8+ T cell CM output is positively correlated with threshold to become effectors (Table 4.1, 4.2). Interestingly, in the recall response, the mechanisms to which effector cell production is sensitive are consistent with that of those affecting effector cells and CM cells during primary responses. For instance, the LN output of effectors in the recall response has a more significant negative correlation with EM differentiation probability than in the primary response, blood CM concentration. This is in accordance with the intuition that a strong recall response requires both memory generation during a primary response and priming efficiency during secondary challenge.

We then perform an inter-compartment sensitivity analysis by comparing how the readouts for the same cell types from both LN and blood are affected by corresponding LN and blood mechanisms. LN mechanisms affect both LN and blood outputs in similar ways, but only blood outputs are sensitive to blood mechanisms (Table 4.3). The recruitment rates of effector cells to sites of infection reduce blood effector levels. Conversion rates from EM to CM induce both

blood CD4+ and CD8+ T cell CM levels. Dynamics occurring in blood do not significantly affect dynamics occurring in LNs during both primary or recall responses, as no significant correlation is detected.

4.4 Discussion

Single cognate naive T cells have been known to be able to generate both memory and effector progenies. Moreover, recent studies further demonstrated that the fate of identical naive cells is heterogeneous. By understanding which mechanisms contribute to this heterogeneity and in which way they are contributing, it is possible to manipulate the priming environment so that differentiation of activated precursor cells can be routed to favor generation of a desired population towards specific needs. For example, in the context of vaccination, establishing a significant antigen-specific central memory population has a high priority. On the other hand, massive production of effector cells could be the key issue considered when using immunotherapies against active diseases. Our new findings suggest that pMHC number provides such a handle; and using our model we can enhance the production of specific T cell types (CD4+/CD8+, effector/memory) in different ideal ranges. By fitting our model to data collected from experiments designed for a specific antigen, we will be capable of making quantitative predictions of DC stimulation levels that maximize the generation of particular subsets of T cells which are most relevant to the circumstances.

In order to study how mechanisms in LN and blood influence the generation of effector and memory T cells, we developed a hybrid model with both LN and blood compartments to simulate immune responses in both primary and recall challenges. Using this model, we generated T cell dynamics in blood and LN during infections that are similar to murine models (De Boer et al., 2001; Antia et al., 2003; De Boer et al., 2003) and also can capture heterogeneous differentiation observations of individual cognate naive T cells (Buchholz et al., 2013; Gerlach et al., 2013).

Furthermore, our model predicts that the outputs of different subsets of T cells that arise during immune responses, including effector and memory, CD4+ and CD8+ T cells, respond differently to the amount of stimulation they receive from antigen-bearing DCs during priming. Simulations showed that CD4+ central memory T cell generation is maximized at low pMHC-II stimulation, and intermediate levels of stimulation result in the highest number of effector CD4+ T cell generation. However, further increases in pMHC-II levels reduce generation of both effector and central memory CD4+ T cells. On the other hand, intermediate pMHC-I stimulation is required to generate the highest levels of CD8+ central memory cells, and high pMHC-I level favors CD8+ T effector cell generation.

Results from our previous study using a 2D model showed pMHC levels always compensate for DC numbers to induce effector T cell production (Linderman et al., 2010) in a trade-off fashion. We find a similar trend herein for CD8+ T cells, and for CD4+ T cells, when DC numbers are small. But when DC numbers are large, high pMHC levels are playing an opposite (for CD4+ T cell) or insignificant (for CD8+ T cell) role. This can be explained by the findings from our 3D LN model (Gong et al., 2013), that DC searching time for T cells is far more efficient in a 3D model environment than 2D. Thus, even for high total DC numbers in the 2D study, there are likely insufficient DCs, suggesting what we observed in the 2D model represents only the case with relatively low DC numbers in 3D.

While our model is able to make some important predictions, further development to include more detail regarding events during antigen presentation is called for. First, DCs are known to be a heterogeneous population, with subsets of cells diversified in origin and function. Different DC subsets are differentially involved in T cell priming. For example, lymphoid organ-resident DCs are specialized for cross-presentation, while inflammatory DCs stimulate TH17 polarization (Segura et al., 2013b;a). Furthermore, the stimulation that T cells receive from DCs are also combinations of multiple signals, including TCR avidity, co-stimulation regulation and environmental,

such as inflammatory cytokine profiles. Reducing these signals to a general stimulation signal package represented with pMHC levels as done here helps conceptualize the question and generate theoretical insights; nonetheless, adding these details will confer power for predicting more precise manipulations of the immune response. Harnessing the power of both mathematical and computational modeling and wet-lab investigation, our systems biology approach can eventually provide guidance for clinical practices in an era of personalized medicine.

Figures

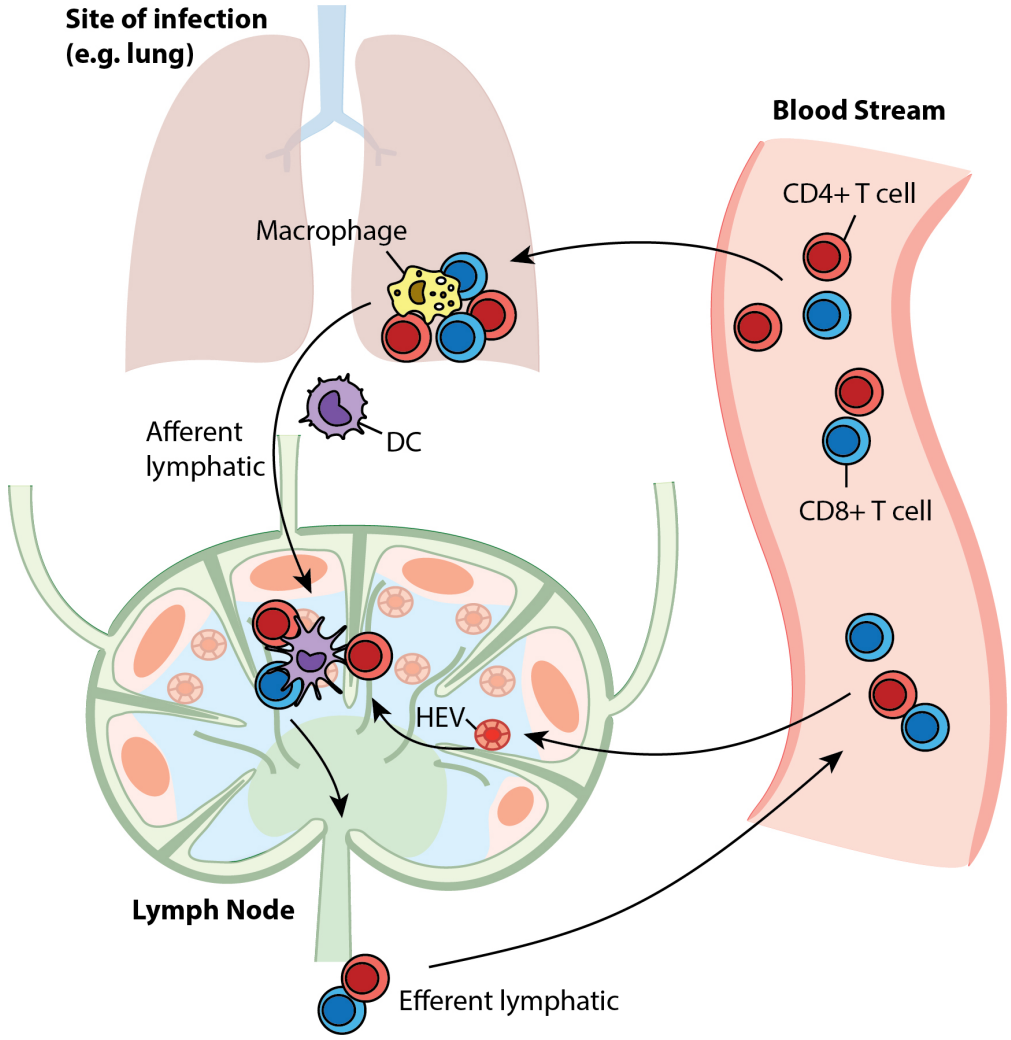

Figure 4.1: T cell trafficking between compartments. Naive T cells circulate between LNs and blood. Upon infection, APCs presents antigen to cognate T cells in LNs to initiate their proliferation and differentiation to generate effector and memory cells. After entering the blood, effector cells are recruited to sites to fight ongoing infection, while memory cells recirculate, awaiting secondary infections.

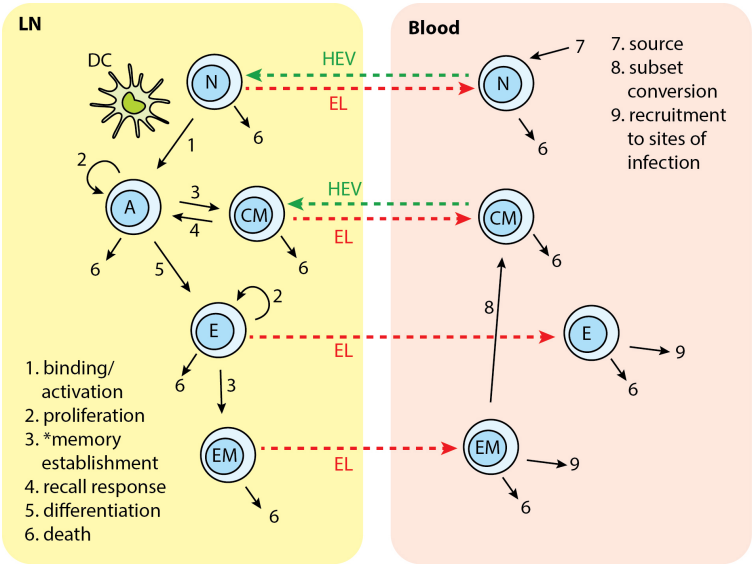

Figure 4.2: T cell subsets in two compartments of LNs and blood. N: naive; A: activated; CM: central memory; E: effector; EM: effector memory. Each number indicates a collection of processes occurring in that step and in different cell types. Naive T cells are recruited to LN from blood. In the LN, cognate T cells bind with Ag-DCs and get activated. Activated T cells proliferate and differentiate into central memory (CM) and effector cells. CM in the LN can bind to DC and be activated again. Effector T cells can further differentiate to effector memory (EM) cells. Naive, effector, CM and EM exit LN from EL. Naive and CM cells recirculate between LN and blood. Effector and EM are recruited to sites of infection. EM can covert to CMs. *memory establishment for CD8+ T cells requires LDCs.

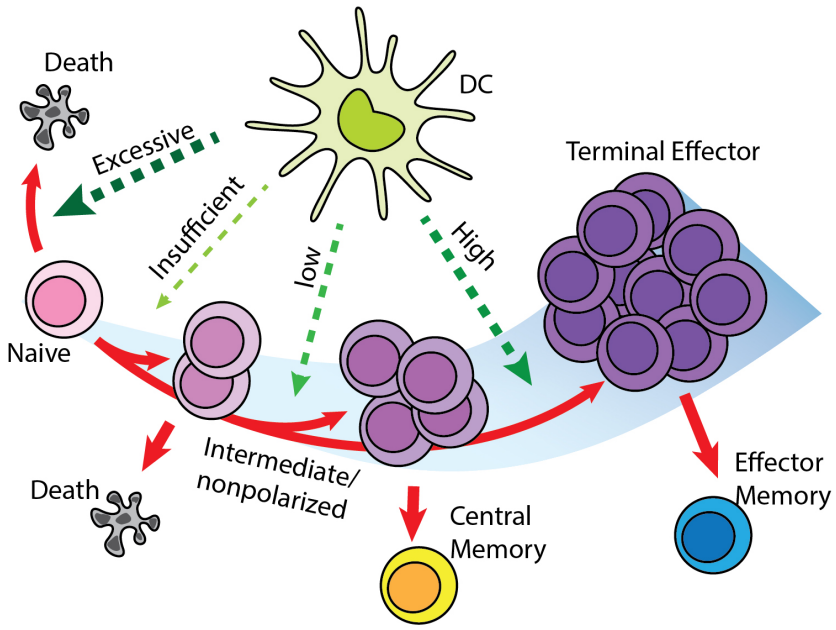

Figure 4.3: Signal-strength model of T cell differentiation. Combination of three (antigenic, co-stimulatory and inflammatory) signals a T cell received from DC during priming determines the fate of its clonal expansion and differentiation. Greater proliferation correlates with stronger signal. However, insufficient stimulation results in death by neglect, while excessive stimulation causes activation induced cell death. Stronger stimulation also drives T cells towards terminal differentiation and reduces their memory-forming potential. Please see text Section 4.2.2 for a description of differentiation models and how this was selected.

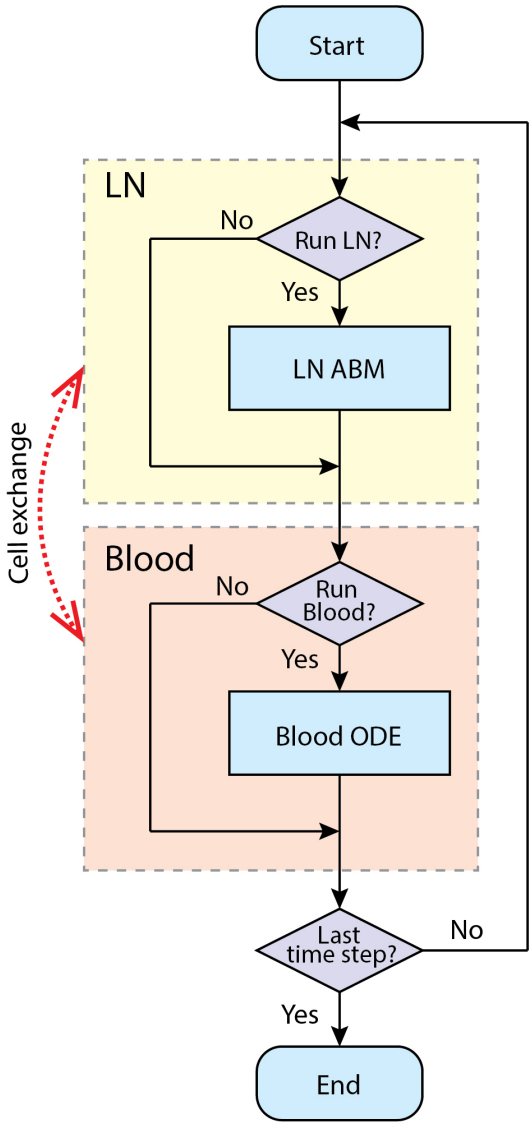

Figure 4.4: Simulation procedure using tunable resolution. LN and blood compartment are processed sequentially in each time step. LN recruit cells from blood and put exiting cells into it. The recruitment probabilities are modified by blood concentration of corresponding cell types. Each compartment has a switch to determine whether this compartment is processed in current time step, or will it be bypassed.

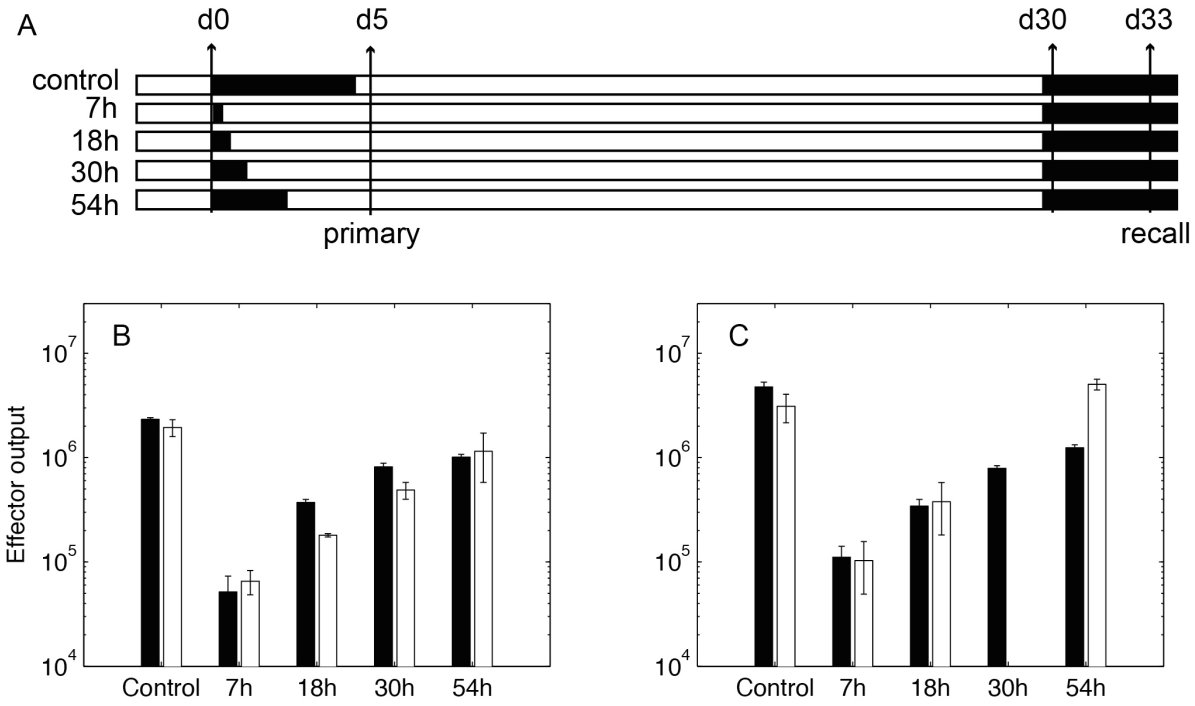

Figure 4.5: Expansion of CD8+ T cells in simulation. (A): *In silico* experimental schemes. Black bars show the duration of Ag-DC presence. In primary challenge, DC antigen-presentation is terminated at time points indicated on the left. "Control" indicates no termination and DC are allowed to live their natural lifespan. Recall challenge is given from day 30. Measurements are taken on day 5 for primary response and day 33 for recall response, respectively. (B, C): CD8+ T cell population in simulated responses (black bars) and experimental data (white bars) (Prlic et al., 2006). (B): size of expanded CD8+ T cell population in primary response. Values are measured from day 5 after Ag-DC are recruited to the LN. (C): size of expanded CD8+ T cell population during recall response on day 33. X-axis value indicates antigen-presentation times in the primary challenge.

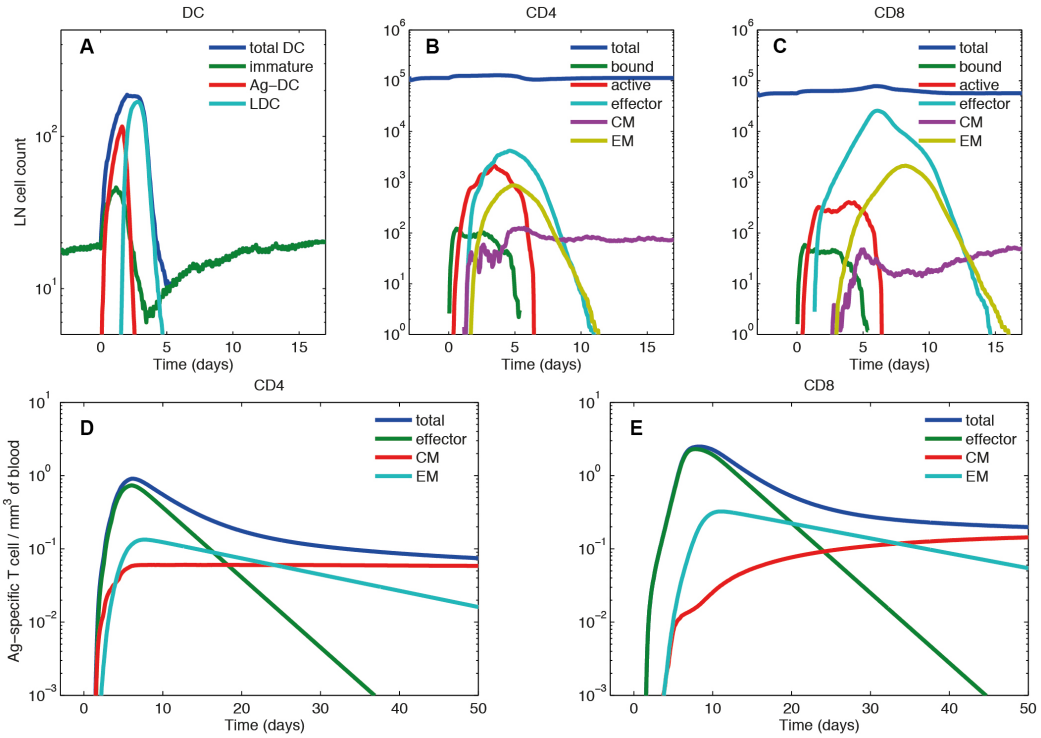

Figure 4.6: Primary response dynamics of immune cells in LN and blood during a hypothetical acute infection (log scale). (A-C): number of Dendritic cells, CD4+ and CD8+ T cells of different subsets in the LN compartment. (D, E): concentration of CD4+ and CD8+ T cells of different subsets in the blood compartment. Panel (A) is the model input of DCs representing a hypothetical acute infection, such as LCMV. Panels (B-E) are the output.

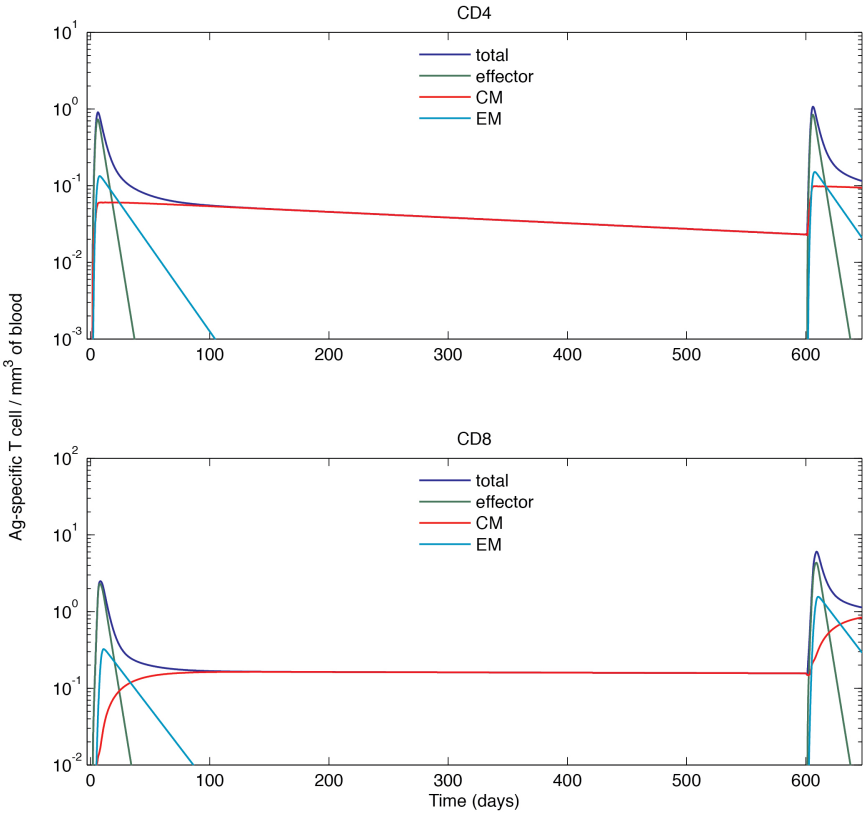

Figure 4.7: Simulated cell dynamics in the blood compartment during a primary and recall response to a hypothetical acute infection (log scale). (A): concentration of CD4+ T cells of different subsets in the blood. (B): concentration of CD8+ T cells of different subsets in the blood. The left parts of the graphs are identical to those of Figure 4.6.

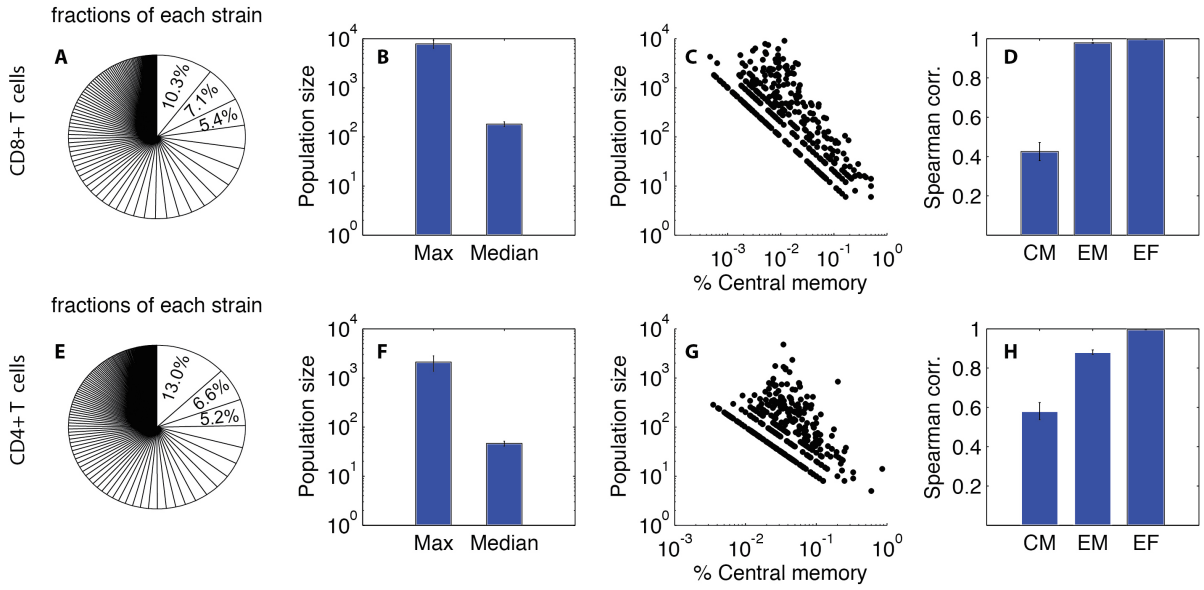

Figure 4.8: Heterogeneity of expanded T cell families. Upper panel: CD8+ T cells. (A): Sizes of expanded CD4+ T cell population from each single-cell derived progeny (strain), represented as fraction of total expanded population as done in Buchholz et al., 2013 and Gerlach et al., 2013. (B): Maximum and median size of CD4+ T cell progenies. (C): Correlation between population size and the percentage of central memory cells. Each dot represents progeny of a single-cell derived progeny. (D): Spearman correlation of CM, EM, and effector CD4+ T cell number versus total expanded population. Lower panel: prediction of CD4+ T cell heterogeneity in clonal expansion. (EH) Prediction of CD4+ T cell heterogeneity in clonal expansion. The four panels correspond to the same readouts as for panels AD.

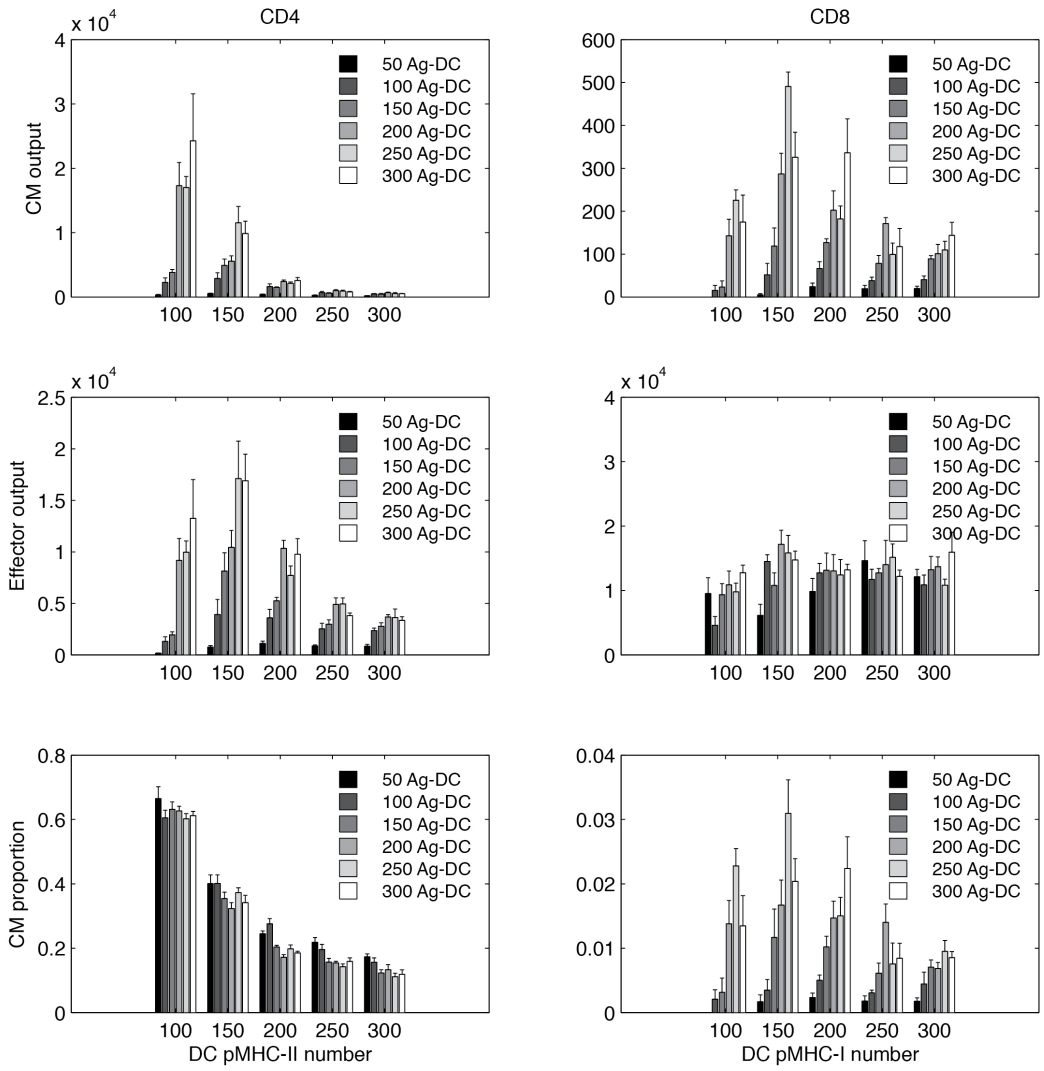

Figure 4.9: Simulated T cell differentiation is influenced by number of DCs and number of pMHC molecules displayed. X-axis: number of pMHC molecules on an Ag-DC. Bar color: Number of Ag-DCs recruited to the grid. (A, B): Number of central memory (CM) cells produced. (C, D): Number of effector cells produced. (E, F): Fraction of CM cells in the expanded population.

Tables

Table 4.1: PRCC results: tracking sensitivity of outputs of LN cells to LN mechanisms.

Primary			Recall		
mechanism	PRCC	Sign.	mechanism	PRCC	Sign.
CD4+ effector exit					
bind time	-0.9	−−−	bind time	-0.82	−−−
probability EM	-0.73	−−−	probability EM	-0.64	−−−
priming checkpoint threshold	-0.42	−−−	priming checkpoint threshold	-0.4	−−−
CM bind time	-0.29	−−	CM bind time	-0.37	−−−
DC licensing probability	-0.26	−−	DC licensing probability	-0.29	−−
extra recruitment	0.38	+++	efficiency CM	-0.27	−−
effector checkpoint threshold	0.67	+++	extra recruitment	0.35	+++
			effector checkpoint threshold	0.61	+++
CD4+ CM exit					
bind time	-0.88	−−−	bind time	-0.62	−−−
priming checkpoint threshold	-0.7	−−−	priming checkpoint threshold	-0.48	−−−
efficiency CM	-0.29	−−	CM bind time	-0.44	−−−
CM bind time	-0.26	−−	efficiency CM	-0.33	−−−
extra recruitment	0.33	+++	extra recruitment	0.26	++
effector checkpoint threshold	0.81	+++	effector checkpoint threshold	0.61	+++
CD8+ effector exit					
extra recruitment (CD4+)	-0.56	−−−	probability EM	-0.74	−−−
bind time	-0.41	−−−	extra recruitment (CD4+)	-0.56	−−−
DC licensing prob.	-0.25	−−	bind time (CD8+)	-0.37	−−−
probability EM	-0.25	−−	DC licensing probability	-0.21	−−
CD8+ CM exit					
bind time	-0.71	−−−	efficiency CM	-0.42	−−−
priming checkpoint threshold	-0.71	−−−	CM bind time	-0.35	−−−
CM bind time	-0.19	−	priming checkpoint threshold	-0.22	−
extra recruitment	0.3	++	bind time	-0.18	−
effector checkpoint threshold	0.77	+++	prob. EM	0.33	+++
			effector checkpoint threshold	0.35	+++

Significance:
−/+: p ¡ 0.001, with negative or positive correlation.
−−/++: p ¡ 10^{-6}, with negative or positive correlation.
−−−/+++: p ¡ $^{-9}$, with negative or positive correlation.

Table 4.2: PRCC results: tracking sensitivity of concentrations of cells in Blood to LN mechanisms.

Primary			Recall		
mechanism	PRCC	Sign.	mechanism	PRCC	Sign.
CD4+ effector concentration					
bind time	-0.83	−−−	bind time	-0.71	−−−
probability EM	-0.74	−−−	probability EM	-0.67	−−−
priming checkpoint threshold	-0.42	−−−	DC licensing probability	-0.39	−−−
DC licensing probability	-0.41	−−−	CM bind time	-0.38	−−−
CM bind time	-0.29	−−	priming checkpoint threshold	-0.35	−−−
extra recruitment	0.32	+++	efficiency CM	-0.25	−−
effector checkpoint threshold	0.64	+++	extra recruitment	0.27	++
			effector checkpoint threshold	0.53	+++
CD4+ CM concentration					
bind time	-0.89	−−−	bind time	-0.7	−−−
priming checkpoint threshold	-0.71	−−−	priming checkpoint threshold	-0.53	−−−
efficiency CM	-0.3	−−	CM bind time	-0.43	−−−
CM bind time	-0.26	−−	efficiency CM	-0.33	−−−
extra recruitment	0.33	+++	extra recruitment	0.26	++
effector checkpoint threshold	0.81	+++	effector checkpoint threshold	0.66	+++
CD8+ effector concentration					
extra recruitment(CD4+)	-0.57	−−−	probability EM	-0.72	−−−
bind time	-0.31	−−−	extra recruitment(CD4+)	-0.55	−−−
DC licensing probability	-0.28	−−	bind time (CD8+)	-0.28	−−
probability EM	-0.27	−−	DC licensing probability	-0.23	−
			bind time (CD4+)	0.18	+
CD8+ CM concentration					
probability EM	-0.78	−−−	probability EM	-0.82	−−−
bind time	-0.53	−−−	extra recruitment(CD4+)	-0.42	−−−
priming checkpoint threshold	-0.39	−−−	bind time	-0.38	−−−
extra recruitment(CD4+)	-0.37	−−−	efficiency CM	-0.3	−−
effector checkpoint threshold	0.52	+++	CM bind time	-0.27	−−
			priming checkpoint threshold	-0.25	−−
			effector checkpoint threshold	0.39	+++

Significance:
−/+: p ¡ 0.001, with negative or positive correlation.
−−/++: p ¡ 10^{-6}, with negative or positive correlation.
−−−/+++: p ¡ $^{-9}$, with negative or positive correlation.

Table 4.3: PRCC results: tracking sensitivity of concentrations of cells in blood to blood mechanisms.

Primary			Recall		
mechanism	PRCC	Sign.	mechanism	PRCC	Sign.
CD4+ effector concentration					
recruit to sites (ξ_{E4})	-0.79	−−−	recruit to sites (ξ_{E4})	-0.54	−−
CD4+ CM concentration					
recruit to sites (ξ_{EM4})	-0.39	−	probability EM	0.44	+
probability EM	-0.8	+++			
CD8+ effector concentration					
recruit to sites (ξ_{E8})	-0.39	−	recruit to sites (ξ_{E8})	-0.43	−
			recruit to sites (ξ_{EM8})	-0.36	−
			probability EM	0.72	+++
CD8+ CM concentration					
recruit to sites (ξ_{EM8})	-0.41	−	recruit to sites (ξ_{EM8})	-0.45	−
probability EM	0.93	+++	probability EM	0.83	+++

Significance:
−/+: p ¡ 0.001, with negative or positive correlation.
−−/++: p ¡ 10^{-6}, with negative or positive correlation.
−−−/+++: p ¡ $^{-9}$, with negative or positive correlation.

Bibliography

Ahmed, R. and Gray, D. Immunological memory and protective immunity: understanding their relation. *Science*, 272(5258):54–60, 1996.

Antia, R., Bergstrom, C. T., Pilyugin, S. S., Kaech, S. M. and Ahmed, R. Models of CD8+ responses: 1. What is the antigen-independent proliferation program. *Journal of theoretical biology*, 221(4):585–598, 2003.

Antia, R., Ganusov, V. V. and Ahmed, R. The role of models in understanding CD8+ T-cell memory. *Nature reviews. Immunology*, 5(2):101–111, 2005.

Arstila, T. P., Casrouge, A., Baron, V., Even, J., Kanellopoulos, J. and Kourilsky, P. A direct estimate of the human alphabeta T cell receptor diversity. *Science*, 286(5441):958–961, 1999.

Bachmann, M. F., Gallimore, A., Linkert, S., Cerundolo, V., Lanzavecchia, A., Kopf, M. and Viola, A. Developmental regulation of Lck targeting to the CD8 coreceptor controls signaling in naive and memory T cells. *The Journal of experimental medicine*, 189(10):1521–1530, 1999.

Bajaria, S. H., Webb, G., Cloyd, M. and Kirschner, D. Dynamics of naive and memory CD4+ T lymphocytes in HIV-1 disease progression. *Journal of acquired immune deficiency syndromes*, 30(1):41–58, 2002.

Bajenoff, M., Granjeaud, S., Guerder, S. and J. The strategy of T cell antigen-presenting cell encounter in antigen-draining lymph nodes revealed by imaging of initial T cell activation. *Med*, 198:715–724, 2003.

Banchereau, J. and Steinman, R. M. Dendritic cells and the control of immunity. *Nature*, 392(6673):245–252, 1998.

Beltman, J. B., Marée, A. F. M. and de Boer, R. J. Spatial modelling of brief and long interactions between T cells and dendritic cells. *Immunology and cell biology*, 85(4):306–314, 2007.

Blattman, J. N., Antia, R., Sourdive, D. J. D., Wang, X., Kaech, S. M., Murali-Krishna, K., Altman, J. D. and Ahmed, R. Estimating the precursor frequency of naive antigen-specific CD8 T cells. *The Journal of experimental medicine*, 195(5):657–664, 2002.

Bogle, G. and Dunbar, P. R. T cell responses in lymph nodes. *Wiley interdisciplinary reviews. Systems biology and medicine*, 2(1):107–116, 2010.

Buchholz, V. R., Flossdorf, M., Hensel, I., Kretschmer, L., Weissbrich, B., Gräf, P., Verschoor, A., Schiemann, M., Höfer, T. and Busch, D. H. Disparate individual fates compose robust CD8+ T cell immunity. *Science*, 340(6132):630–635, 2013.

Butcher, E. C. and Picker, L. J. Lymphocyte homing and homeostasis. *Science*, 272(5258):60–66, 1996.

Byrne, J. A., Butler, J. L. and Cooper, M. D. Differential activation requirements for virgin and memory T cells. *Journal of immunology (Baltimore, Md. : 1950)*, 141(10):3249–3257, 1988.

Casrouge, A., Beaudoing, E., Dalle, S., Pannetier, C., Kanellopoulos, J. and Kourilsky, P. Size estimate of the alpha beta TCR repertoire of naive mouse splenocytes. *Journal of immunology (Baltimore, Md. : 1950)*, 164(11):5782–5787, 2000.

Chang, J. T., Palanivel, V. R., Kinjyo, I., Schambach, F., Intlekofer, A. M., Banerjee, A., Longworth, S. A., Vinup, K. E., Mrass, P., Oliaro, J., Killeen, N., Orange, J. S., Russell, S. M., Weninger, W. and Reiner, S. L. Asymmetric T lymphocyte division in the initiation of adaptive immune responses. *Science*, 315(5819):1687–1691, 2007.

Chicz, R. M., Urban, R. G., Lane, W. S., Gorga, J. C., Stern, L. J., Vignali, D. A. and Strominger, J. L. Predominant naturally processed peptides bound to HLA-DR1 are derived from MHC-related molecules and are heterogeneous in size. *Nature*, 358(6389):764–768, 1992.

Constant, S., Pfeiffer, C., Woodard, A., Pasqualini, T. and Bottomly, K. Extent of T cell receptor ligation can determine the functional differentiation of naive CD4+ T cells. *The Journal of experimental medicine*, 182(5):1591–1596, 1995.

Cyster, J. G. Chemokines, sphingosine-1-phosphate, and cell migration in secondary lymphoid organs. *Annual review of immunology*, 23(1):127–159, 2005.

De Boer, R. J., Homann, D. and Perelson, A. S. Different dynamics of CD4+ and CD8+ T cell responses during and after acute lymphocytic choriomeningitis virus infection. *Journal of immunology*, 171(8):3928–3935, 2003.

De Boer, R. J., Oprea, M., Antia, R., Murali-Krishna, K., Ahmed, R. and Perelson, A. S. Recruitment times, proliferation, and apoptosis rates during the CD8(+) T-cell response to lymphocytic choriomeningitis virus. *Journal of virology*, 75(22):10663–10669, 2001.

De Boer, R. J. and Perelson, A. S. Quantifying T lymphocyte turnover. *Journal of theoretical biology*, 327:45–87, 2013.

Douek, D. C., McFarland, R. D., Keiser, P. H., Gage, E. A., Massey, J. M., Haynes, B. F., Polis, M. A., Haase, A. T., Feinberg, M. B., Sullivan, J. L., Jamieson, B. D., Zack, J. A., Picker, L. J. and Koup, R. A. Changes in thymic function with age and during the treatment of HIV infection. *Nature*, 396(6712):690–695, 1998.

Dutton, R. W., Bradley, L. M. and Swain, S. L. T cell memory. *Annual review of immunology*, 16:201–223, 1998.

Erkeller-Yuksel, F. M., Deneys, V., Yuksel, B., Hannet, I., Hulstaert, F., Hamilton, C., Mackinnon, H., Stokes, L. T., Munhyeshuli, V. and Vanlangendonck, F. Age-related changes in human blood lymphocyte subpopulations. *The Journal of pediatrics*, 120(2 Pt 1):216–222, 1992.

Fallahi-Sichani, M., El-Kebir, M., Marino, S., Kirschner, D. E. and Linderman, J. J. Multiscale computational modeling reveals a critical role for TNF-α receptor 1 dynamics in tuberculosis granuloma formation. *Journal of immunology*, 186(6):3472–3483, 2011.

Fallahi-Sichani, M., Kirschner, D. E. and Linderman, J. J. NF-κB Signaling Dynamics Play a Key Role in Infection Control in Tuberculosis. *Frontiers in physiology*, 3:170, 2012.

Gerlach, C., Rohr, J. C., Perié, L., van Rooij, N., van Heijst, J. W. J., Velds, A., Urbanus, J., Naik, S. H., Jacobs, H., Beltman, J. B., de Boer, R. J. and Schumacher, T. N. M. Heterogeneous differentiation patterns of individual CD8+ T cells. *Science*, 340(6132):635–639, 2013.

Gett, A. V. and Hodgkin, P. D. A cellular calculus for signal integration by T cells. *Nature immunology*, 1(3):239–244, 2000.

Girard, J.-P., Moussion, C. and Förster, R. HEVs, lymphatics and homeostatic immune cell trafficking in lymph nodes. *Nature reviews. Immunology*, 12(11):762–73, 2012.

Gong, C., Mattila, J. T., Miller, M., Flynn, J. L., Linderman, J. J. and Kirschner, D. Predicting lymph node output efficiency using systems biology. *Journal of theoretical biology*, 335:169–184, 2013.

Grigorova, I. L., Panteleev, M. and Cyster, J. G. Lymph node cortical sinus organization and relationship to lymphocyte egress dynamics and antigen exposure. *Proceedings of the National Academy of Sciences of the United States of America*, 107(47):20447–20452, 2010.

Hawkins, E. D., Markham, J. F., McGuinness, L. P. and Hodgkin, P. D. A single-cell pedigree analysis of alternative stochastic lymphocyte fates. *Proceedings of the National Academy of Sciences of the United States of America*, 106(32):13457–13462, 2009.

Homann, D., Teyton, L. and Oldstone, M. B. Differential regulation of antiviral T-cell immunity results in stable CD8+ but declining CD4+ T-cell memory. *Nature medicine*, 7(8):913–919, 2001.

Iezzi, G., Karjalainen, K. and Lanzavecchia, A. The duration of antigenic stimulation determines the fate of naive and effector T cells. *Immunity*, 8(1):89–95, 1998.

Itoh, Y. and Germain, R. N. Single cell analysis reveals regulated hierarchical T cell antigen receptor signaling thresholds and intraclonal heterogeneity for individual cytokine responses of CD4+ T cells. *The Journal of experimental medicine*, 186(5):757–766, 1997.

Jacob, J. and Baltimore, D. Modelling T-cell memory by genetic marking of memory T cells in vivo. *Nature*, 399(6736):593–597, 1999.

Kaech, S. M. and Ahmed, R. Memory CD8+ T cell differentiation: initial antigen encounter triggers a developmental program in naïve cells. *Nature immunology*, 2(5):415–422, 2001.

Kaech, S. M. and Cui, W. Transcriptional control of effector and memory CD8+ T cell differentiation. *Nature reviews. Immunology*, 12(11):749–761, 2012.

Kirschner, D. E., Hunt, C. A., Marino, S., Fallahi-Sichani, M. and Linderman, J. J. Tuneable resolution as a systems biology approach for multi-scale, multi-compartment computational models. *Wiley Interdisciplinary Reviews: Systems Biology and Medicine*, 6(4):289–309, 2014.

Kirschner, D. E. and Linderman, J. J. Mathematical and computational approaches can comple-

ment experimental studies of host-pathogen interactions. *Cellular microbiology*, 11(4):531–539, 2009.

Lanzavecchia, A. and Sallusto, F. Dynamics of T lymphocyte responses: intermediates, effectors, and memory cells. *Science*, 290(5489):92–97, 2000.

Lanzavecchia, A. and Sallusto, F. Progressive differentiation and selection of the fittest in the immune response. *Nature reviews. Immunology*, 2(12):982–987, 2002.

Linderman, J. J., Riggs, T., Pande, M., Miller, M., Marino, S. and Kirschner, D. E. Characterizing the dynamics of CD4+ T cell priming within a lymph node. *Journal of immunology (Baltimore, Md. : 1950)*, 184(6):2873–2885, 2010.

Mackay, C. R. Homing of naive, memory and effector lymphocytes. *Current opinion in immunology*, 5(3):423–427, 1993.

Marino, S., El-Kebir, M. and Kirschner, D. A hybrid multi-compartment model of granuloma formation and T cell priming in tuberculosis. *Journal of theoretical biology*, 280(1):50–62, 2011.

Marino, S., Hogue, I. B., Ray, C. J. and Kirschner, D. E. A methodology for performing global uncertainty and sensitivity analysis in systems biology. *Journal of theoretical biology*, 254(1):178–196, 2008.

Masopust, D. and Schenkel, J. M. The integration of T cell migration, differentiation and function. *Nature reviews. Immunology*, 13(5):309–320, 2013.

Mckay, M. D., Beckman, R. J. and Conover, W. J. Comparison of 3 Methods for Selecting Values of Input Variables in the Analysis of Output from a Computer Code. *Technometrics*, 21:239–245, 1979.

Mempel, T. R., Henrickson, S. E. and Von Andrian, U. H. T-cell priming by dendritic cells in lymph nodes occurs in three distinct phases. *Nature*, 427(6970):154–159, 2004.

Miller, M. J., Wei, S. H., Parker, I. and Cahalan, M. D. Two-photon imaging of lymphocyte motility and antigen response in intact lymph node. *Science*, 296(5574):1869–1873, 2002.

Mirsky, H. P., Miller, M. J., Linderman, J. J. and Kirschner, D. E. Systems biology approaches for understanding cellular mechanisms of immunity in lymph nodes during infection. *Journal of theoretical biology*, 287:160–70, 2011.

Opferman, J. T., Ober, B. T. and Ashton-Rickardt, P. G. Linear differentiation of cytotoxic effectors into memory T lymphocytes. *Science*, 283(5408):1745–1748, 1999.

Pepper, M. and Jenkins, M. K. Origins of CD4(+) effector and central memory T cells. *Nature immunology*, 12(6):467–471, 2011.

Prlic, M., Hernandez-Hoyos, G. and Bevan, M. J. Duration of the initial TCR stimulus controls the magnitude but not functionality of the CD8+ T cell response. *The Journal of experimental medicine*, 203(9):2135–2143, 2006.

Randolph, G. J., Angeli, V. and Swartz, M. A. Dendritic-cell trafficking to lymph nodes through lymphatic vessels. *Nature reviews. Immunology*, 5(8):617–28, 2005.

Ravkov, E. V. and Williams, M. A. The magnitude of CD4+ T cell recall responses is controlled by the duration of the secondary stimulus. *Journal of immunology (Baltimore, Md. : 1950)*, 183(4):2382–2389, 2009.

Riggs, T., Walts, A., Perry, N., Bickle, L., Lynch, J. N., Myers, A., Flynn, J., Linderman, J. J., Miller, M. J. and Kirschner, D. E. A comparison of random vs. chemotaxis-driven contacts of T

cells with dendritic cells during repertoire scanning. *Journal of theoretical biology*, 250(4):732–51, 2008.

Roederer, M., Dubs, J. G., Anderson, M. T., Raju, P. A. and Herzenberg, L. A. CD8 naive T cell counts decrease progressively in HIV-infected adults. *The Journal of clinical investigation*, 95(5):2061–2066, 1995.

Sallusto, F., Lenig, D., Förster, R., Lipp, M. and Lanzavecchia, A. Two subsets of memory T lymphocytes with distinct homing potentials and effector functions. *Nature*, 401(6754):708–712, 1999.

Segura, E., Durand, M. and Amigorena, S. Similar antigen cross-presentation capacity and phagocytic functions in all freshly isolated human lymphoid organ-resident dendritic cells. *The Journal of experimental medicine*, 210(5):1035–1047, 2013a.

Segura, E., Touzot, M., Bohineust, A., Cappuccio, A., Chiocchia, G., Hosmalin, A., Dalod, M., Soumelis, V. and Amigorena, S. Human inflammatory dendritic cells induce Th17 cell differentiation. *Immunity*, 38(2):336–348, 2013b.

Sprent, J. and Tough, D. F. T cell death and memory. *Science*, 293(5528):245–248, 2001.

Steinmann, G. G., Klaus, B. and Müller-Hermelink, H. K. The involution of the ageing human thymic epithelium is independent of puberty. A morphometric study. *Scandinavian journal of immunology*, 22(5):563–575, 1985.

Stemberger, C., Huster, K. M., Koffler, M., Anderl, F., Schiemann, M., Wagner, H. and Busch, D. H. A single naive CD8+ T cell precursor can develop into diverse effector and memory subsets. *Immunity*, 27(6):985–997, 2007.

Viola, A. and Lanzavecchia, A. T cell activation determined by T cell receptor number and tunable thresholds. *Science*, 273(5271):104–106, 1996.

Wherry, E. J., Teichgräber, V., Becker, T. C., Masopust, D., Kaech, S. M., Antia, R., von Andrian, U. H. and Ahmed, R. Lineage relationship and protective immunity of memory CD8 T cell subsets. *Nature immunology*, 4(3):225–234, 2003.

Wiesel, M. and Oxenius, A. From crucial to negligible: functional CD8 T-cell responses and their dependence on CD4 T-cell help. *European journal of immunology*, 42(5):1080–1088, 2012.

Zehn, D., King, C., Bevan, M. J. and Palmer, E. TCR signaling requirements for activating T cells and for generating memory. *Cellular and molecular life sciences*, 69(10):1565–1575, 2012.

CHAPTER V

Connecting adaptive immunity with TB granuloma development

5.1 Introduction

Tuberculosis (TB) is a potentially deadly infectious disease caused by *Mycobacteria tuberculosis* (Mtb). It is carried by one-third of the world's population, and caused 1.5 million deaths in 2013 (WHO, 2014). After primary infection, about 10% patients develop active tuberculosis (TB), while the rest 90% remain latently infected with 10% chance of future relapse in their lifetime, creating a reservoir at the population scale (Guzzetta and Kirschner, 2013; Lin and Flynn, 2010). Currently, we rely on lengthy treatment regimens with combinations of multiple antibiotics to control the global epidemic of TB (Blumberg et al., 2005). However, this ancient pathogen seems to be evolving fast to counter such efforts: multidrug-resistant (MDR) and extensively drug-resistant (XDR) Mtb strains emerge and spread, posing serious challenges to TB management in populations normally having access to the standard antibiotic treatment (Migliori et al., 2012). As the available antibiotics are about to become exhausted, other alternatives are of particular interest, including those utilizing the native defense mechanism of human immune system, such as vaccination.

Part of the work in Chapter V(Section 5.2.1 to 5.2.3) is pubished in Linderman, Jennifer J, Nicholas A Cilfone, Elsje Pienaar, Chang Gong, and Denise E Kirschner. 2015. *"A Multi-Scale Approach to Designing Therapeutics for Tuberculosis."* Integrative Biology 7 (5): 591609.

Part of the work in Chapter V(Section 5.2.4) is done in collaboration with Dr. Cordelia Ziraldo. Manuscript is in preparation.

Vaccines confer protection by stimulating the immune system to initiate an adaptive immune response and generate long-lived memory lymphocytes against specific antigens from a pathogen (See Chapter I). In the case of TB, Bacille Calmette-Guérin (BCG) can successfully prevent severe TB disease in children, but shows no efficacy against TB infection or reactivation after childhood. Currently, different groups are aiming to developing a TB vaccine (reviewed in Kaufmann et al. (2014), more information available at `http://www.aeras.org/`). However, no success has been reported to date. Presumably, combinations of different antigen-specific memory cell subsets would need to be involved to target antigens at various infection stages; however, what particular compositions correlate with efficacious immune protection are still unknown. Considering the high cost and length of time for performing animal testing, computational models developed using a systems biology approach can be an important supplement for hypothesis generation to aid TB vaccine design, especially in the early development stages. In this chapter, I will discuss a few pilot studies I conducted to this end, which laid groundwork to further investigate various aspects of this issue.

For a vaccine to be effective, the immune response needs to generate sufficient numbers and types of cells of each class to act quickly in a recall response to prevent the development of infection or control it immediately once infection starts. However, the relative abundance of each class of memory cell type that is required for successful protection is not clear. In order to design an efficacious vaccine against Mtb, we need to deepen our understanding regarding two related, but distinct, aspects of the events following vaccination. Firstly, we need to determine the characteristics of an immune response that correlates with successful protection against Mtb infection. Secondly, we need to investigate how the nature of vaccine influences the characteristic of the immune response it induces. This happens initially in lymph nodes (LNs). Combined knowledge of these two aspects will provide guidance to aid development of an effective TB vaccine.

Previously, our group developed a hybrid computational model (*GranSim*) to examine both the

dynamics of microbe and host immune cells in TB granulomas located inside the lung and immune generation in the lung-draining lymph node at the same time(Marino et al., 2011). Granuloma are ball-shaped collections of host immune cells and Mtb that are formed as a result as an on-going battle, while draining LNs accommodate antigen-presentation of Mtb by professional antigen-presenting cells (APC), in particular Dendritic cells (DCs), to T cells to induce adaptive cell-mediated immune responses. This model tracks granuloma formation by tracking the interaction between mycobacteria and host immune cells including macrophages and T cells with an agent-based model (ABM) and immune response induction with a set of ordinary differential equations (ODEs). However, this model is only intended to capture an on-going infection, and as a result, the mechanisms governing differentiation of activated T cells into memory cell subsets are by design missing from the tool.

Computational and mathematical models are also developed to characterize T cell memory generation in immune responses in forms of deterministic ODE systems or spatiotemporal explicit stochastic ABMs (Bajaria et al., 2002; Marino and Kirschner, 2004; Antia et al., 2005; Gong et al., 2013). In the model we developed and discussed in Chapter IV, primed T cells (e.g. CD4+ T helper cells and CD8+ cytotoxic T cells) give rise to not only immediately active effector cells but also various memory subtypes with differential longevity and recirculation patterns (Gong et al., 2014). However, this model is only limited to one "generic" antigen, and lacks the ability to accommodate multiple antigens from TB.

In this chapter, we show how we extend our current model of granuloma development (*GranSim*) and model of LN T cell priming dynamics *LymphSim* to meet the requirement described above. We also integrated the two models into one multi-compartment model with both LN and lung compartment implemented as ABMs. In the future, this model can help us test the predictions made with the two models in stand-alone fashions.

5.2 Methods

5.2.1 Granuloma formation captured in ABM GranSim

The computational model tracks cells and bacteria dynamics in three compartments: lung (granuloma site), blood and lymph node. A diagram of all 3 compartments is shown in Figure 1. Our *GranSim* ABM captures granuloma formation in the lung, while the lymph node and blood dynamics are captured by a system of ordinary differential equations (ODEs). The model used in this work is adapted from our previously published hybrid computational model (Marino et al., 2011) by including a blood compartment to track the recirculation of CD4+ and CD8+ T lymphocytes, and adding mechanism governing differentiation of activated T cells into memory cells.

The lung ABM is largely the same as the lung compartment in previously published version of hybrid model. Details of the lung compartment can be found in (Marino et al., 2011). The environment of the lung compartment ABM is implemented as a 2-dimensional (2D) grid, representing a 2x2 mm section of lung parenchyma tissue. Cell types tracked in the model include macrophages and T cells. Macrophages are in one the four different states: resting, activated, infected and chronically infected. T cells are categorized by function, namely Interferon-gamma (IFN-$gamma$) producing T cells (Tγ), cytotoxic T cells (T$_{cyt}$) and regulatory T cells (Treg). Their fu Tγ cells induce macrophage activation, inducing their ability to kill mycobacteria and produce tumor necrosis factor-α (TNF); T$_{cyt}$ targets infected macrophages and kill them in close contact; Treg negatively modulate the inflammation. On the molecular scale, we track TNF and interleukin 10 (IL-10). TNF induces apoptosis of infected cells, while IL-10 suppress immune cell activity. Two updates are made in the mechanisms included in *GranSim* version to adjust to the inclusion of a blood compartment and circulating memory cells: a T cell recruitment probability is made proportional to its blood concentration, and recruited T cells are allowed to proliferate at the site of infection.

5.2.2 T cell priming, differentiation and recirculation in LN and blood ODE systems

The blood-lymph node ODE model is illustrated in Figure 5.1, including all the different T cell subsets captured in the model and basic assumptions of T cell priming, differentiation and recirculation. T cells that are tracked in LNs include CD4+ and CD8+ T cells, and each of these can be further classified into N (Nave), CM (Central Memory), EM (Effector Memory), P(precursor cells), E (Effector). We assumed a constant cognate frequency of $1\times10^{-}5$ as the frequency of nave precursor T cells specific to Mtb antigens. Priming occurs in the LN compartmental model, driven by a proxy for antigen presenting cells (APCs), namely DCs, which is based on the number of new encounters between macrophages and Mtb in the lung compartment. Nave T cells first become early precursor cells, which then proliferate and further different into various effector and memory subsets. Except for early precursors which are not allowed to exit the LN, each subtype recirculate differently: nave and CMs recirculate between LN and blood, while effector and EM traffic via blood to the site of infection implemented as lung ABM. The terms of CD4+ and CD8+ T cell dynamics in the LN and their migration between compartments are kept the same. In addition to cognate cells, we track numbers of non-cognate cells (grey circles). These cells possess similarly migration patterns as their respective cognate counterparts, but lack the ability to respond to antigens being presented in the LN.

5.2.3 Simulating infection with pre-established memory populations

We set initial conditions such that the system starts with varying levels of central and effector memory, helper (CD4+) and cytotoxic (CD8+) T cells. The values are arbitrarily chosen, assuming we can generate any memory T cell compositions from a specifically designed vaccine. This is to mimic the scenario where a vaccine has been administrated and immune memory has been established. We simulate infection over a time span of 200 days, with rules and interactions solved on a 10-min time step. The cell and bacterial time courses and granuloma spatial outcomes in

the lung are tracked to assess the level of protection derived from the simulated vaccine. After simulating for 200 days, we evaluate the outcome of each granuloma by counting the number of cells and microbe. If we have more than 500 Macs and 10 replicating bugs, the granuloma is considered unresolved. 50 replications are done for each memory T cell initial condition, and clearance proportion under each condition is calculated from these replications.

5.2.4 Multiple types of antigen-specific T cells

In the basic version of LymphSim, T cells are divided into cognate and non-cognate categories. To expand this model to accommodate multiple antigens, we start simple with 5 antigens and thus 5 corresponding antigen specific T cell populations. Each T cell is assigned one Ag-specificity, indicating the antigen its TCR can recognize. Correspondingly, peptide-MHC complexes on each DC display different Ags in variable proportions. The model by default accommodates five antigen-specific populations for CD4+ and CD8+ T cells, but this number could easily be expanded. With multiple parallel yet independent binding populations, the binding affinities are parameterized independently. The amount of each antigen displayed on a DC is also controlled independently. Together, these parameters specify an antigen-specific binding probability for each cognate naive T cell (with Ag-specificity indicated with i) according to the following equation:

$$p_i = \frac{1}{1 + e^{-\frac{x_i - a_i}{b_i}}}, \tag{5.1}$$

where a_i and b_i determine the affinity of the TCR for the pMHC and x_i is the number of MHC complexes displaying antigen i, a quantity determined by the fraction of pMHC (p_i)that is specific to antigen i and the total amount of pMHC on the DC, Ptot ($i = 1to5$).

After a T cell binds to a DC, the amount of signal accumulated depends on binding time and the total pMHC on DC surface, which we assume can serve as a proxy for the aggregate of TCR, co-stimulatory and cytokines. The cell differentiation scheme that occurs after unbinding is the

same as in the single antigen version of the model (see Chapter IV). When cells reach the ELs, nave, effector, CM and EM leave the LN and enter the blood compartment, where T cells of each TCR type are then pooled and tracked with a set of ODEs to track each populations dynamics. The formulation is the same as described in Gong et al. (2014). The probability of recruitment of a T cell (either nave or CM) from the blood into a LN is based on the blood concentration of Nave and CM cells of each antigen-specific group.

5.2.5 Computationally Linking *GranSim* (lung granuloma ABM) with *LymphSim* (LN ABM).

As discussed in previous chapters, we develop an ABM capturing LN dynamics in a spatio-temporal explicit fashion (*LymphSim*). In order to gain higher resolution of the events in the LN compartment during priming, we developed a multi-compartment model with *LymphSim* serving as a sub-model by connecting it with GranSim (Figure 5.2). The connection is established with two additional compartments: blood and lymphatics. A blood compartment is implemented as an ODE system, same as described in Chapter IV but use multiple sets of them to capture each Ag-specific group. Blood also handles the LN traffic in the same way as well. Blood and provides effector and EMs to the site of infection in the lung in the same fashion as discussed in Section 2.2. APCs travel from the site of infection to LN via afferent lymphatics. We currently use a vector-based method to represent the afferent lymphatics, with each element in the vector representing one antigen-presenting cell with a timer tracking its time remaining time in this compartment. The mini ABM of lymphatics has elements that advance over time in a vector, reflecting their migration from site of infection to the lymph node in time and space. After the timer reaches zero, the APC enters a pool of arrived cells in a compartment resembling terminal afferent lymphatics and subcapsular sinus before these cells can be recruited to the LN.

One problem facing this model is that it is extremely computationally extensive and time consuming to simulate both ABMs in full. Immune responses in the LN usually last for a couple weeks

during an acute infection, and can be simulated within about 10 hours in real time using stand-alone LymphSim. However, TB infection lasts for years, making it unpractical to have *LymphSim* running during the entire time. To resolve this issue, the idea of "tuneable-resolution" (Kirschner et al., 2014) is incorporated into the computational design of this multi-compartment model. Because Mtb reside in the center of granuloma, their antigens are presumably less readily available to APCs trafficking to the LN. We take advantage of this and define algorithms in which at the beginning of each LN time step, the model examines whether or not there are any Antigen-bearing Dendritic cells (Ag-DCs) arriving at the end of afferent lymphatics and ready to be recruited to the LN. In addition, it also checks whether there are cells types that indicate an active immune response (including Ag-DCs, T cells that are bound, early precursors, effectors or EMs) within the LN. If neither is true, *LymphSim* can turn itself off in an automated fashion.

5.3 Results

5.3.1 Immune protection against TB from memory T cells is dependent on memory pool composition

We can compare "unvaccinated" with "vaccinated" cases to learn about the protection that memory cells can provide. For the unvaccinated case, infected macrophages, T cells and bacteria progress into a contained granuloma with a relatively stable structure over time (Figure 5.3, upper row), as seen with our earlier models. If sufficient numbers of memory cells are present from vaccination prior to the infection, the granuloma still undergo initial development, but resolves quickly after a short period of growth (Figure 5.3A, lower row).

The lung compartment is set up so that the initially infected Mac end up forming a contained granuloma without any preexisting antigen specific memory cells. To examine how levels of different types of memory cells affect protection, we varied the initial condition for the numbers of effector memory and central memory classes of both CD4+ and CD8+ T cells that are present in the blood compartment. Four groups of simulations are performed, each with a fixed low (20

μL^{-1}) or high (100 μL^{-1}) concentration of total CD4+ or CD8+ T memory cells. Within each group, the composition of memory cells are varied by setting the ratio of central memory (CM) to effector memory (EM) to 9:1, 1:1, or 1:9. We track how the presence of circulating memory cells affects granuloma outcomes. Each setup is replicated 50 times, and the probability that a granuloma clears its bacterial load is counted (Figure 5.3B). We see that increasing memory CD4+ T cells does not influence the outcome of a granuloma. However, the chance of sterilization (clearance) increases when more memory CD8+ T cells are present, especially when a high proportion of them are effector memory cells.

5.3.2 Antigen-specific T cell groups generate different memory cell populations during an immune response.

After implementing the model with multiple antigens and tracking corresponding T cell populations specific to these different antigens, simulations are performed to show that each of these T cell group can undergo differentiation and generate a different composition of memory cell classes (EM vs CM). The parameters used are shown in Table 1. In a simple example, we keep the cognate frequency constant at 10^{-4} across the 5 antigen specific groups. However, the affinity and abundance of each antigen are varied, with antigen 1 having highest affinity and largest amount presented, while antigen 5 has the lowest affinity, and smallest proportion of pMHC molecules on DC surface. Results are shown in Figure 5.4. These simulation results indicate that for both CD4+ and CD8+ T cells, each antigen specific population can be manipulated separately to generate different levels of CM vs EM which has important implications for vaccine design.

5.3.3 Pre-existing effector T cells affect successfulness of the immune system to control Mtb infection.

Effector T cells need to migrate to site of infection to further expand and exert their effector function. Upon arrival at the site of infection, these cells need to first cross barriers formed by vascular endothelium. This is achieved by adhesion molecules and chemokines induced lo-

cally by inflammation. When primed, T cells receive tissue-specific "imprinting" from APCs, and express receptors specific to the site of infection(Luster et al., 2005). However, such tissue-specificity is limited in that they do not discriminate between T cells the same way as TCRs' antigen-specificity, resulting in potential recruitment of Non-(antigen)-specific T cells (which can still be tissue-specific) to site of infection, reducing the chance to recruit antigen specific T cells.

UUsing the multi-compartment model with *LymphSim* capturing LN dynamics and *GranSim* capturing granuloma formation, we evaluated how preexisting non-specific effectors and EMs influences the outcome of a granuloma. Results are shown in Figure 5.5 and 5.6. In the case with non Mtb-specific effectors in circulation (Figure 5.5), Ag-DCs migrate to the LN and begin to prime cognate T cells. As effector cells are released to the blood (Figure 5.5B,C), they are recruited to the site of infection quickly (Figure 5.5H,I) and immediately activate macrophages to kill the pathogens (Figure 5.5E). The remaining inflammation continues to recruit macrophages to the granuloma (Figure 5.5G), but eventually resolves following the clearance of infection. When the non-specific effector and EM populations are set to$10mm^{-3}$, the recruitment of antigen specific T cells to site of infection is much delayed (Figure 5.6H,I), and clearance do not happen as in the clean-background scenario. This result indicate that the competition of non-specific T cells for molecular cues to enter the site of infection is partially responsible for the delayed arrival of antigen specific T cells and inability to successfully clear infection in the first place.

5.4 Discussion

In principle, a systems biology model for vaccine development assistance should incorporate both pathogen mechanisms to carry out the infection, and host mechanisms to generate immune memory. In this chapter, we discussed how we developed a prototype of framework in which we can study each aspect separately with fine-grain models of the compartment of interest, and then integrate them to test the predictions.

For the first aspect, we need to study how the composition of the immune cells generated from vaccination influence the course of Mtb infection. What is needed for this purpose are models incorporating multiple physiological compartments including the site of infection, which is the lung, and the LNs. Additionally, blood circulation is required to facilitate migration of effector cells from LNs to sites of infection, as well as to capture the recirculation of memory cells. To this end we built a 3-compartmental physiological model capturing relevant cells and molecules that participate in adaptive immune generation and responses during Mtb infection. Using this model, we were able to find memory types that are correlated with better protection. This means, in a translational perspective, given the levels of memory cells generated after vaccination, the results of such in-silico experiments provide a guideline to make predictions about the efficacy of a vaccine.

To understand the second aspect of the mechanism of a vaccine, we worked extensively to create models of dynamics of cells in LNs, as shown in Chapter IV. LNs are the site where adaptive immunity is generated, and thus including the priming and differentiation of immune cells is key to begin to explore vaccines. Proof-of-concept simulations showed that different properties among these antigens, such as affinity and abundance, can drive different CM vs EM outcomes within the same simulation.

As a higher resolution version of the ODE LN sub-model, the 3D *LymphSim* provides us with chances to investigate processes where space is an important factor, such as T cell-DC search during priming. Because ABM simulations are computationally intensive, often times we want to adjust the ODE version according to findings made in the ABM model, and run the ODE LN version instead of the full model. However, the ABM LN possesses another property in addition to the spatial explicity: it better captures the stochastic nature of T cell priming. As T cell precursor frequency is extremely low ($10^{-5} - 10^{-4}$), the rarity of DC flux to LNs may have a profound impact on the resulting immune response. Normally in an acute infection, abundant antigens are carried

to LNs by APC or lymphatics. In this situation, even though cognate T cells are of low frequency, they can still find matching APCs with high probability when migrating through the draining LN. On the other hand, when Ag-DC is also scarce in the LN, chances are the T cell may not be easily primed. This will result in different behaviors depending on the type of model. In deterministic continuous models such as an ODE system, the dynamics reflects a numerical average: low number of T cells and DCs produce a low, but constant level of effector cell output. However, in stochastic models such as ABM, cognate T cells may not get activated most of the time, but when they "get lucky" and are primed, the expanded population will produce a wave of effectors in greater numbers compared to the ODE solution. Such differences may have implications on the infection outcome through other mechanisms, such as the non-specific effectors shown in Section 3.3. For example, if non-specific effectors are limiting the access of specific effectors T cells to site of infection, temporarily reducing their numbers may create windows for specific T cells to better penetrate the granuloma. Such behavior can be captured in an ABM, but not an ODE, where the specific population is always constant but lukewarm. If such flash floods of antigen-specific effectors are induced, they can potentially turn the tide of the battle in a granuloma.

These finding provide insight into vaccine design, but the model at current status is not directly translatable to clinical development. To improve clinical relevance of our model, the next step is to include realistic TB antigens in both the lung and LN compartment that include abundance, affinities etc for each so the model can be calibrated. In the LN, a vaccine is administrated in a prime-boost series, with different antigenic combinations at each round. We can use this model to explore mechanisms that control the memory profile generated during an immune response involving multiple Mtb antigens. In the lung model, Mtb specific antigens are differentially expressed depending on the stage of infection. Our lab also developed a version of *GranSim* where Mtb is represented as discrete agents with their metabolism tracked explicitly (data not shown). This sub-model will allow us to track the spatio-temporal antigens distribution to immune cells in the site

of infection. If we couple these two models, we will be able to make predictions of what makes a good TB vaccine.

Figures

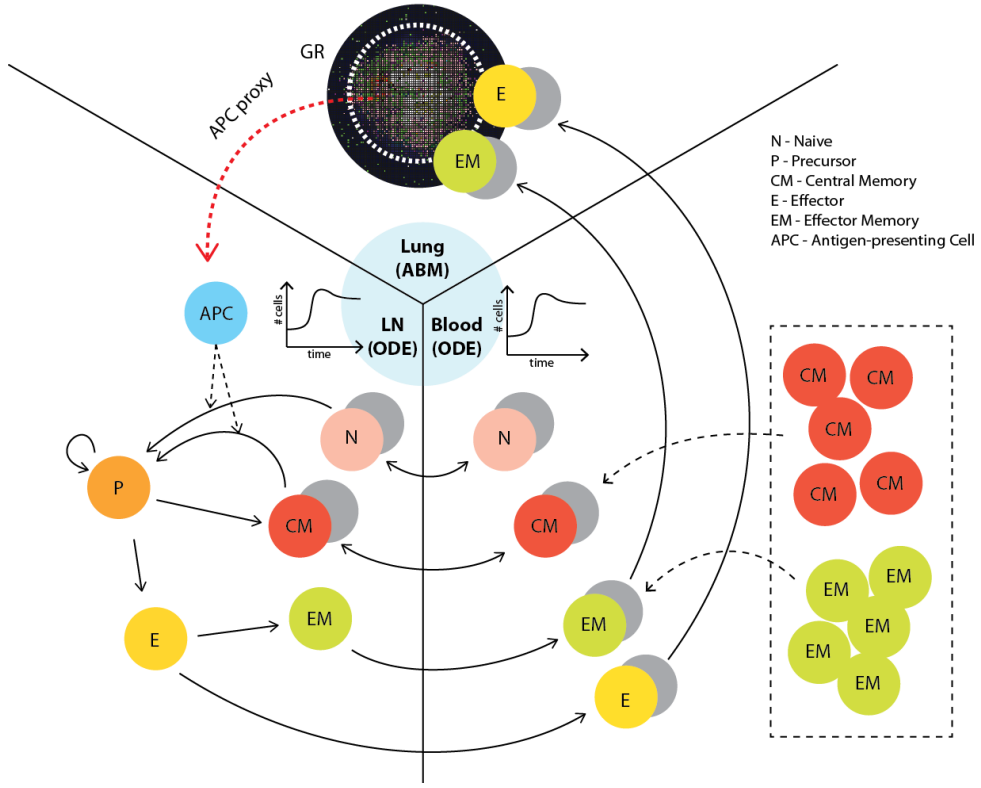

Figure 5.1: Three-compartment model: inter-compartmental dynamics of granuloma formation and immune function. ABM (*GranSim*) tracks movement and interaction of cells and pathogen at the site of infection (lung), while two ODE systems capture LN and blood dynamics. T cells that are tracked in LNs include CD4+ and CD8+ T cells. Each of the two can be further classified into nave (N), activated precursor (P), effector (E), central memory (CM), and effector memory (EM). APCs such as DCs migrate from the lung to the LN to prime the adaptive immune response. The N, E, CM, EM classes travel among LN, blood and site of infection as indicated by arrows. Only E and EM (total effector class) can travel to the site of infection. Both Mtb-specific and non-specific T cells (shown as grey shadows) are included. The initial conditions of species representing different memory classes in the blood are set to non-zero values, representing the memory cells that we assume have been generated after vaccination.

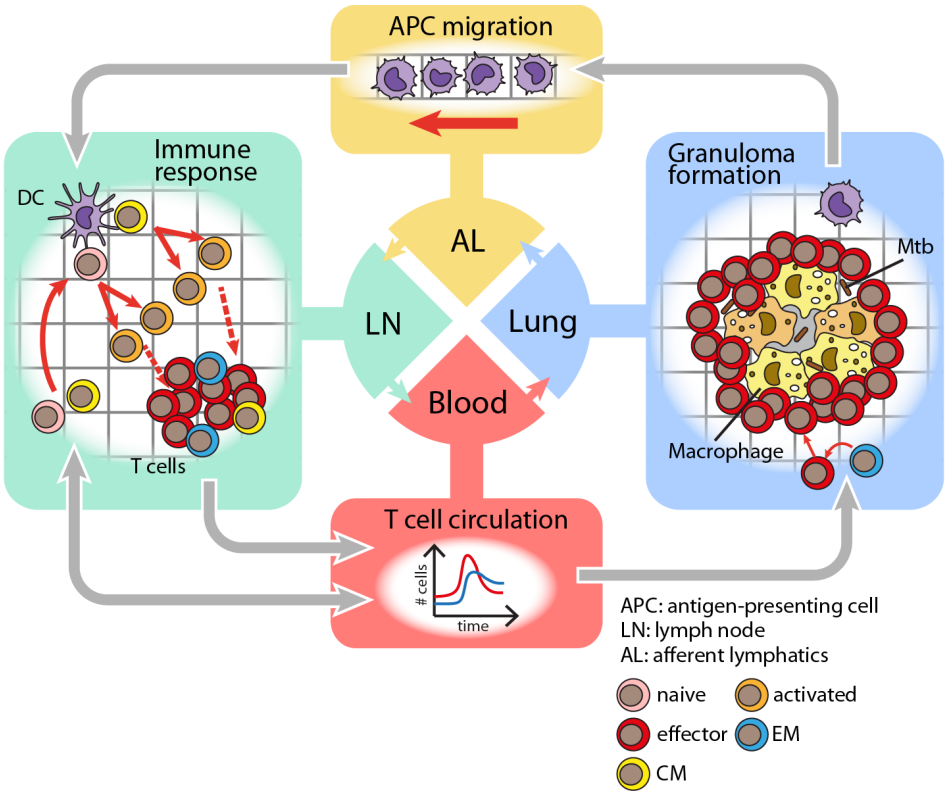

Figure 5.2: 4-Compartment model with both LN and Lung sub-model implemented as ABMs. APCs travel from lung to LN via afferent lymphatics. Here the lymphatics compartment is a simplistic ABM capturing the delay of APC during migration. Upon arrival in the LN, APC search and prime antigen-specific T cells. Primed T cell expand and differentiate into Effector, CM and EM. T cells either recirculate between blood and LN, or home to site of infection (Lung) via blood. The dynamics in the blood compartment is captured with an ODE system. Granuloma forms as a emergent behavior when T cells and macrophages recruited to the Lung interact with Mtb.

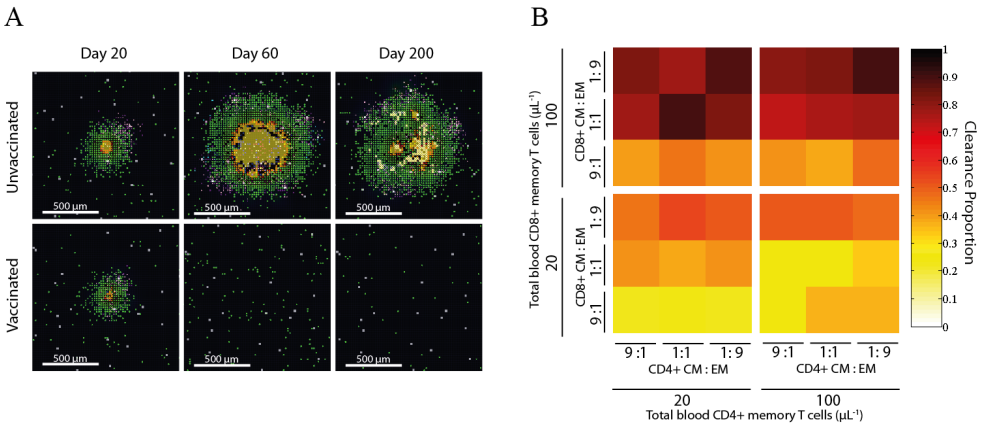

Figure 5.3: Effects of immune memory on granuloma formation. A: Snapshots of granuloma at day 20, 60 and 200 after infection, with or without memory cells generated from vaccination. When no memory cells are present at the beginning (top panel), the site of infection develops from an initially infected macrophage into a granuloma and maintains the structure through the 200 days of simulation. With pre-established memory cells (bottom row), a granuloma appears briefly but quickly resolves. B: Infection is simulated with different combinations of memory cell subtypes (CM, EM; CD4+ and CD8+ T cells). The colors indicate the how likely a granuloma resolves under each setup.

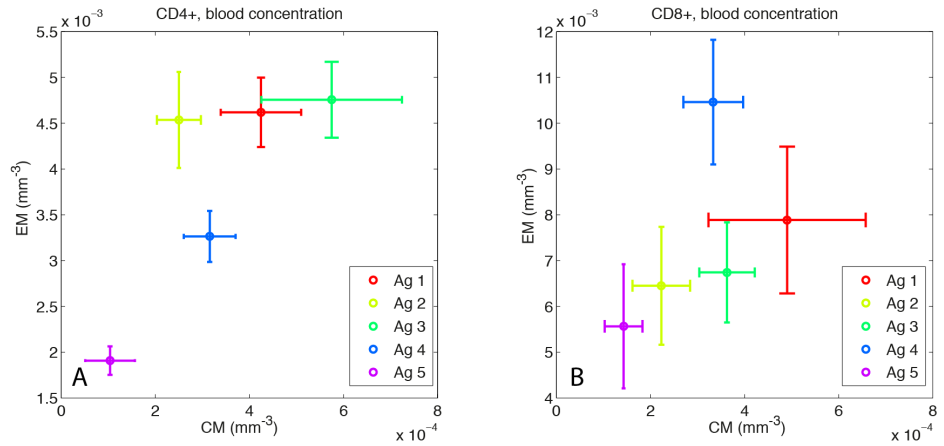

Figure 5.4: Memory cell composition of a multi-Ag simulation. Blood concentrations of central vs. effector memory T cells that are generated from different antigen types from the same set of simulations (N=10). A: CD4+ T cells; B: CD8+ T cells. Shown are mean and the SEM for each cell type tracked.

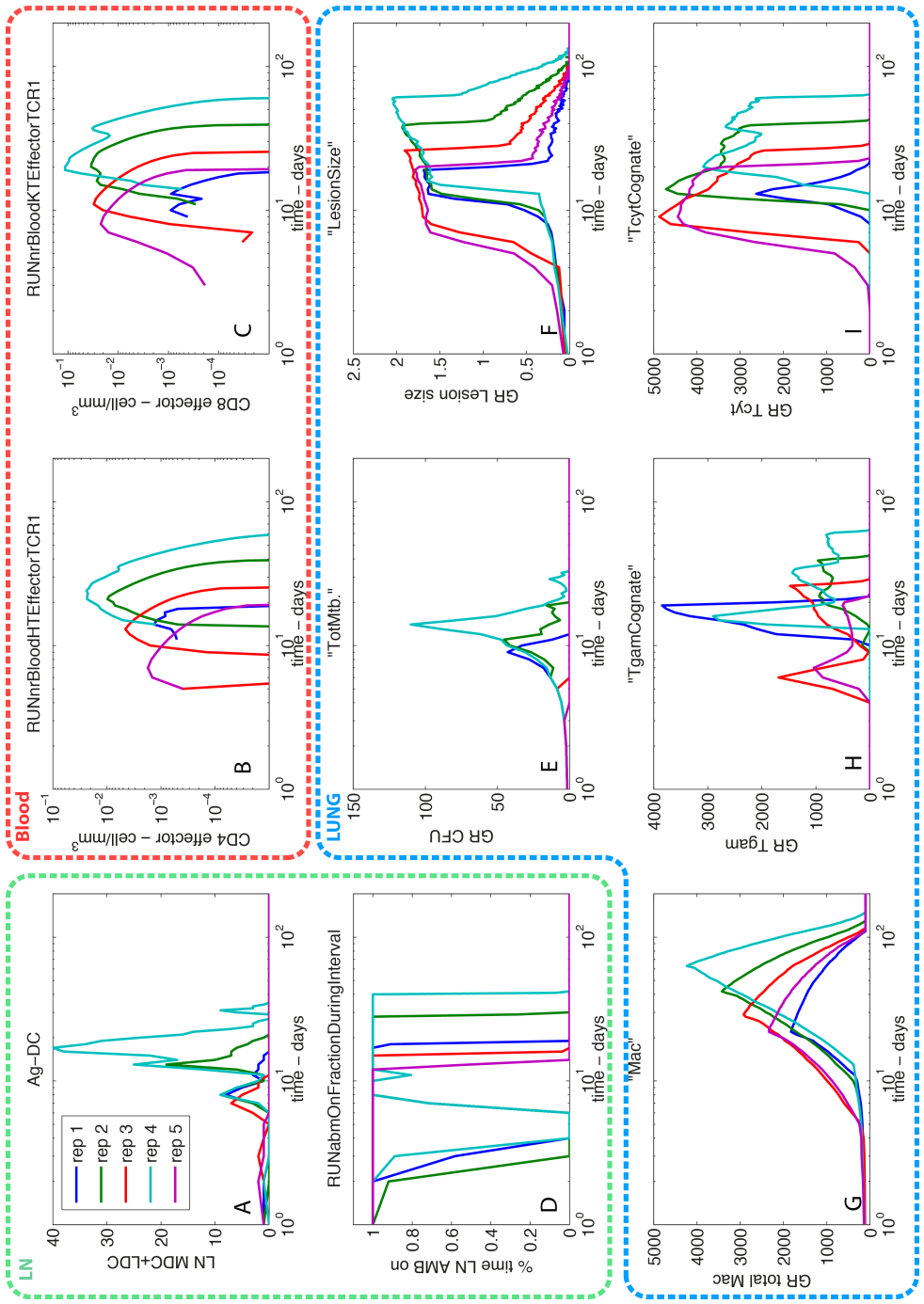

Figure 5.5: Dynamics of the LN-granuloma with no pre-existing non-specific effector/effector memory T cells. A: Number of antigen-bearing DCs in the LN ABM. B,C: Concentration of cells in blood ODE. B: Effector CD4+ T cells. C: Effector CD8+ T cells. D: % of time LN ABM is running during each day of simulation. E-I: Statistics taken from the Lung ABM. E: total bacteria count (CFU). F: Size of the granuloma. G: Total number of macrophages. H: Total number of T_{γ} cells. I: Total number of T_{cyt}.

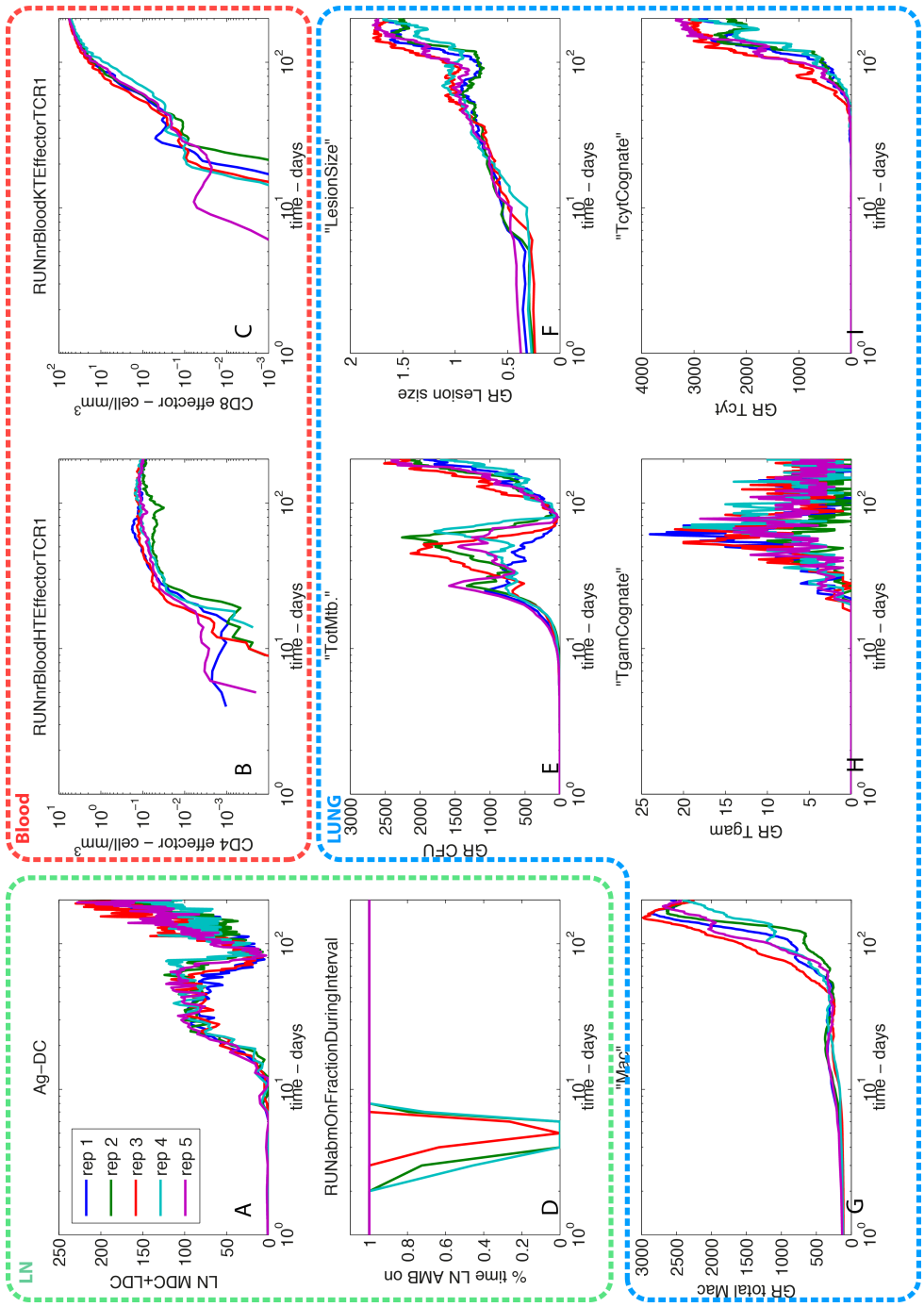

Figure 5.6: Dynamics of the LN-granuloma with pre-existing non-specific effector/effector memory T cells. A: Number of antigen-bearing DCs in the LN ABM. B,C: Concentration of cells in blood ODE. B: Effector CD4+ T cells. C: Effector CD8+ T cells. D: % of time LN ABM is running during each day of simulation. E-I: Statistics taken from the Lung ABM. E: total bacteria count (CFU). F: Size of the granuloma. G: Total number of macrophages. H: Total number of T_{γ} cells. I: Total number of T_{cyt}.

Tables

Table 5.1: Multiple-antigen on DC: peptide affinity and abundance

Ag specificity:	1	2	3	4	5
pMHC-I:					
a_i	100	200	300	400	500
p_i	0.3	0.25	0.2	0.15	0.1
pMHC-II:					
a_i	100	200	300	400	500
p_i	0.3	0.25	0.2	0.15	0.1

Bibliography

Antia, R., Ganusov, V. V. and Ahmed, R. The role of models in understanding CD8+ T-cell memory. *Nature reviews. Immunology*, 5(2):101–111, 2005.

Bajaria, S. H., Webb, G., Cloyd, M. and Kirschner, D. Dynamics of naive and memory CD4+ T lymphocytes in HIV-1 disease progression. *Journal of acquired immune deficiency syndromes*, 30(1):41–58, 2002.

Blumberg, H. M., Leonard, M. K. and Jasmer, R. M. Update on the treatment of tuberculosis and latent tuberculosis infection. *JAMA : the journal of the American Medical Association*, 293(22):2776–2784, 2005.

Gong, C., Linderman, J. J. and Kirschner, D. Harnessing the heterogeneity of T cell differentiation fate to fine-tune generation of effector and memory T cells. *Frontiers in immunology*, 5:57, 2014.

Gong, C., Mattila, J. T., Miller, M., Flynn, J. L., Linderman, J. J. and Kirschner, D. Predicting lymph node output efficiency using systems biology. *Journal of theoretical biology*, 335:169–184, 2013.

Guzzetta, G. and Kirschner, D. The Roles of Immune Memory and Aging in Protective Immunity and Endogenous Reactivation of Tuberculosis. *PLoS ONE*, 8(4), 2013.

Kaufmann, S. H. E., Lange, C., Rao, M., Balaji, K. N., Lotze, M., Schito, M., Zumla, A. I. and Maeurer, M. Progress in tuberculosis vaccine development and host-directed therapies-a state of the art review. 2014.

Kirschner, D. E., Hunt, C. A., Marino, S., Fallahi-Sichani, M. and Linderman, J. J. Tuneable reso-

lution as a systems biology approach for multi-scale, multi-compartment computational models. *Wiley Interdisciplinary Reviews: Systems Biology and Medicine*, 6(4):289–309, 2014.

Lin, P. L. and Flynn, J. L. Understanding latent tuberculosis: a moving target. *Journal of immunology (Baltimore, Md. : 1950)*, 185(1):15–22, 2010.

Luster, A. D., Alon, R. and von Andrian, U. H. Immune cell migration in inflammation: present and future therapeutic targets. *Nature immunology*, 6(12):1182–90, 2005.

Marino, S., El-Kebir, M. and Kirschner, D. A hybrid multi-compartment model of granuloma formation and T cell priming in tuberculosis. *Journal of theoretical biology*, 280(1):50–62, 2011.

Marino, S. and Kirschner, D. E. The human immune response to Mycobacterium tuberculosis in lung and lymph node. *Journal of theoretical biology*, 227(4):463–486, 2004.

Migliori, G. B., Sotgiu, G., D'Ambrosio, L., Centis, R., Lange, C., Bothamley, G., Cirillo, D. M., De Lorenzo, S., Guenther, G., Kliiman, K., Muetterlein, R., Spinu, V., Villar, M., Zellweger, J. P., Sandgren, A., Huitric, E. and Manissero, D. TB and MDR/XDR-TB in European Union and European Economic Area countries: Managed or mismanaged? *European Respiratory Journal*, 39(3):619–625, 2012.

WHO. *Global Tuberculosis Report 2014*. World Health Organization, 2014.

CHAPTER VI

A population model capturing dynamics of tuberculosis granulomas predicts host infection outcomes

6.1 Introduction

Tuberculosis (TB) is a disease caused by inhalation of Mycobacterium tuberculosis (Mtb). It mainly infects the lungs of adults, but other organs such as brain and kidneys can become infected as infection progresses, with bacteria disseminating via blood (extra-pulmonary TB). A third of the world population is estimated to be infected with Mtb(Organization, 2013). However, most people (about 80%) are able to control infection and are classified as having latent TB infection (or LTBI). Those with LTBI have a lifetime reactivate rate of 10%, which increases to a rate of 10% per year if individuals are co-infected with HIV-1 or other immunosuppressive scenarios (O'Garra et al., 2013; Corbett et al., 2003). Patients with LTBI cannot transmit the disease. The remaining 20% of individuals are not able to control infection and progress to active TB disease, which, if left untreated leads to death within a year or two. Treatment requires a long course of multiple antibiotics. What remains an open question in TB is why the course of infection differs from person to person leading to these different disease trajectories.

Mtb is an ancient pathogen (Egyptian mummies have been found that have TB granulomas

The work in Chapter VI is pubished as Gong, Chang, Jennifer J Linderman, and Denise Kirschner. 2015. *"A Population Model Capturing Dynamics of Tuberculosis Granulomas Predicts Host Infection Outcomes."* Mathematical Biosciences and Engineering: MBE 12 (3): 625642.

that have calcified) and has evolved unique ways to avoid being cleared by the host. Resident macrophages in the lungs take up inhaled particles via phagocytosis to keep lungs clear of foreign matter. However, Mtb grows inside macrophages; it is their cell of choice with optimal growth conditions (Rengarajan et al., 2005). During both latent and active Mtb infection, structures called granulomas form at sites of infection, primarily in lungs. A granuloma is a collection of host immune cells such as macrophages, T and B lymphocytes and neutrophils, as well as bacteria(Flynn and Chan, 2001). Granulomas are considered to be a protective structure that immunologically restrain and physically contain bacteria. Recently it has been suggested that bacteria might utilize this structure to avoid being cleared, promote proliferation, and even facilitate dissemination(Ramakrishnan, 2012). Therefore, the granuloma is a highly dynamic structure reflecting an on-going battle between host and pathogen.

A significant barrier to studying granulomas is that they are in lungs, and human lung tissue is not readily accessible. Recent findings have shown that in non-human primates (NHPs, the best animal model to study human TB), different granulomas, each seeded by a single mycobacterium, can have heterogeneous fates over time(Lin et al., 2014). For example, in one monkey with active disease there were 18 granulomas, 6 of which were completely sterile and 2 with over a million bacteria each. In another monkey with latent infection there were 5 granulomas, 3 of which were sterile and 2 with bacteria levels ranging from $10^3 - 10^5$(Lin et al., 2013). Granulomas do not form synchronously- after infection a few may form on the same time scale, but others get seeded later or are formed from disseminating granulomas that are present. These findings imply that infection outcome may be determined by the dynamics of the collection of granulomas within an individual. Granulomas are also found in lymph nodes (LN) in humans and NHPs(Chackerian et al., 2002; Lin et al., 2009). As LNs are the site where adaptive immune responses against Mtb are initiated, this could have important implications for the host-response and infection dynamics.

At present, there is no way to correlate counts of granulomas with infection status and disease

progression. We have published extensively using mathematical and computational models to understand the dynamics in-host of immune cells and bacteria interactions in TB. We have used ODE models to describe total populations in lungs over time(Wigginton and Kirschner, 2001; Marino and Kirschner, 2004), and developed agent-based models to capture spatio-temporal dynamics of individual granuloma formation and function(Segovia-Juarez et al., 2004; Fallahi-Sichani et al., 2010; Marino et al., 2011a;b; Fallahi-Sichani et al., 2012a;b; Cilfone et al., 2013). Others have studied this as well(Magombedze and Mulder, 2012; Magombedze et al., 2006; Cardona, 2007). However, these models do not bridge to the host scale as each captures only a portion of what occurs in the host that leads to an infection outcome. In addition to immune modeling, we and others have built models that track the dynamics of TB epidemics in many different populations and under various scenarios(Kirschner, 1999; Murphy et al., 2002; 2003; Singer and Kirschner, 2004; Young et al., 2008; Feng et al., 2000; Castillo-Chavez and Feng, 1997; Guzzetta et al., 2011; Castillo-Chávez and Aparicio, 2009; Blower et al., 1995; Dye et al., 1998; Milner et al., 2002).

Here we combine these approaches by using a standard SEIR population model to capture in-host features to track the "epidemic" evolving within an infected host. By adapting these epidemiological models to capture the dynamics of a "population" of granulomas in the entire body, we can bridge the two scales of lung granuloma and host to not only understand the role that lung and LN granulomas play in TB disease progression, but also to potentially foster a prediction tool for patient level disease trajectory. Such knowledge could guide development of advanced and personalized treatment strategies, and eventually help to control the global TB epidemic more effectively.

6.2 Methods

6.2.1 Granuloma in lung and LN

We constructed our mathematical model based on standard SEIR model formulations capturing a TB epidemic in human populations. In our model, granulomas form in two potential infection sites: the lung (species with subscript P, pulmonary) and LNs (species with subscript L) (Figure 6.1).

We treat the collection of granulomas of each state in both organs. Black arrows indicate transitions between states. In lung tissue, granuloma are in one of four states: Susceptible (S_P) represents healthy tissues that are potential sites for granulomas but are not yet seeded with bacteria; Exposed (E_P) represents granulomas that are able to contain or control bacteria growth and prevent dissemination of bacteria; Infected (I_P) represents granulomas that are unable to control bacteria proliferation and can disseminate and infect healthy tissue. Finally, a compartment called Dead (D_P) represents tissue that is cleared of bacteria but is unhealthy and damaged from the immune response and is unable to recover due to necrosis, caseation, fibrosis and/or calcification processes that occur naturally during infection. Because lung tissue regeneration in adult humans is minimal, we assume a fixed total number of sites in the lung(Petersen et al., 2010). Populations in the LNs are similar but not identical. LN tissues do regenerate, and dead tissue gets cleaned-up more effectively(Pabst et al., 1991). As a result, we introduce turnover to healthy sites (S_L) in LNs and do not track dead tissue; other conversions between states are similar for both compartments. Exposed sites (contained granulomas) can recover or progress and allow uncontrolled bacteria proliferation and are classified as infectious (I_P or I_L), disseminating to other susceptible sites in the lung (S_P) and LN (S_L).

6.2.2 Adaptive immunity

The adaptive immune system (f_I in Figure 6.1) is necessary for the body to clear or contain Mtb infection. To successfully generate a potent adaptive immune response, three factors are essential (dotted arrows): (1) antigen presentation events, (2) availability of Mtb-specific immune cells (e.g. naive T cells), and (3) an environment for immune cells to recognize the antigen and be primed (a healthy LN in this case). We combine these three components into a coarse-grained representation of an immune response. We use a simplified version of each based on our previous modeling studies that capture immune dynamics during Mtb infection(Kirschner et al., 2007; Ye and Kirschner, 2002; Gong et al., 2013; Linderman et al., 2010). Each is described in more details below.

Antigen presentation: Antigen is defined as a substance (usually as short proteins fragments called peptides) that the immune system recognizes as foreign. Mtb antigen must be "presented" by antigen presenting cells (APCs, such as macrophages and dendritic cells) to T cells to initiate and sustain a specific immune response to Mtb, i.e. the generation of cells that respond to the infection. Antigen presentation can be coarsely represented as a combination of numbers of contained and disseminating granulomas in lung and LNs, weighted by the accessibility (p and q) of antigenic materials from these granulomas to the APCs.

Immune cells: Mtb-specific immune cells, primarily T cells, are required for successful immune responses. Each T cell responds to one and only one antigen and there are a plethora of antigens that comprise Mtb; however, it remains unknown which key antigens that should be responded to in order to provide protection. We assume the initial maximum T cell response to be at its full potential (1.0 unit), and for long-term immune dynamics, we use a time-dependent decreasing function to capture the decline of immunity and available immune cells over the lifetime of the host(Ye and Kirschner, 2002). As TB is a disease that can last for decades, these two time-scales

are relevant and appropriate.

Lymph node environment: There are approximately 700 LNs in humans. Only a small fraction ($<$10) are lung-draining LNs that typically participate in infection dynamics. APCs from the lung migrate to one of the lung-draining LNs to initiative an adaptive response in that LN, but may also seed infection in the LN by trafficking Mtb. LNs provide an environment for immune cells to recognize Mtb antigen presented by APCs and be primed to return to the site of infection (lungs) to participate in the immune response, which for TB means granuloma formation and function. LN status will be evaluated by the fraction of LN sites not yet hosting granulomas, i.e. S_L/S_{L0}, where S_{L0} is the total number of LN uninfected sites available prior to infection.

This specific immune response influences granuloma development in multiple ways and at multiple stages. In the model, immunity affects the following processes (Figure 6.1, dashed arrows): (1) it can induce recovery of contained granulomas (E) to be resolved and return to a state of healthy tissue (S), (2) it reduces the cases of new infection (E and I from S) caused by disseminating granulomas, (3) it can inhibit contained granulomas from disseminating (E to I), and (4) it can aid elimination of disseminating granulomas (I to D) (Figure 6.1). These influences are captured as parameters that serve as multiplicative factors adjusting rates in the model (see below).

6.2.3 Model equations

Following typical SEIR dynamic modeling, the transitions between these states are represented by the following set of ODEs:

$$\dot{S_P} = -\frac{K_I}{K_I + f_I}(\beta_{PP}\frac{S_P I_P}{S_{P0}} + \beta_{PL}\frac{S_P I_L}{S_{P0}}) + f_I \delta_P E_P, \tag{6.1}$$

$$\dot{E_P} = \frac{\phi_P K_I}{K_I + f_I}(\beta_{PP}\frac{S_P I_P}{S_{P0}} + \beta_{PL}\frac{S_P I_L}{S_{P0}}) - f_I \delta_P E_P - (1 - f_I) k_P E_P - \mu_{EP} E_P, \tag{6.2}$$

$$\dot{I_P} = \frac{K_I(1 - \phi_P)}{K_I + f_I}(\beta_{PP}\frac{S_P I_P}{S_{P0}} + \beta_{PL}\frac{S_P I_L}{S_{P0}}) + (1 - f_I) k_P E_P - f_I \gamma_P I_P - \mu_{IP} I_P, \tag{6.3}$$

$$\dot{D_P} = f_I \gamma_1 I_P + \mu_{EP} E_P + \mu_{IP} I_P, \tag{6.4}$$

$$\dot{S_L} = \sigma_L - \frac{K_I}{K_I + f_I}(\beta_{LL}\frac{S_L I_L}{S_{L0}} + \beta_{LP}\frac{S_L I_P}{S_{L0}}) + f_I \delta_L E_L - \mu_{SL} S_L, \tag{6.5}$$

$$\dot{E_L} = \frac{\phi_L K_I}{K_I + f_I}(\beta_{LL}\frac{S_L I_L}{S_{L0}} + \beta_{LP}\frac{S_L I_P}{S_{L0}}) - f_I \delta_L E_L - (1 - f_I) k_L E_L - \mu_{EL} E_L \tag{6.6}$$

and

$$\dot{I_L} = \frac{K_I(1 - \phi_L)}{K_I + f_I}(\beta_{LL}\frac{S_L I_L}{S_{L0}} + \beta_{LP}\frac{S_L I_P}{S_{L0}}) + (1 - f_I) k_L E_L - f_I \gamma_L I_L - \mu_{IL} I_L, \tag{6.7}$$

where

$$\sigma_L = \mu_{SL} N_{L0}. \tag{6.8}$$

β_{PP} and β_{PL} are the rates of a healthy site in the lung infected with Mtb and forming a granuloma from a disseminating GR in lung or LN. β_{LP} and β_{LL} are the rates of a healthy site in LN being infected with Mtb and a granuloma forming from a disseminating GR in lung or LN. Infection is inhibited by adaptive immunity, as the rate is multiplied by a modifier term (K_I is a constant for dissemination inhibition):

$$\frac{K_I}{K_I + f_I}. \tag{6.9}$$

Newly infected sites will progress to either a contained (E) or disseminating (I) state, depending on various environmental factors, and we use a parameter ϕ to determine the probability of a GR site progressing to contained state as opposed to disseminating state upon new transmission. δ

is the rate that a contained GR heals via a functional immune response (f_I) and reverts to susceptible tissue again. k is the rate that contained (E) GR progress to a disseminating (I) GR without any immune response. γ is the rate of disseminating GRs being cleared by adaptive immunity. Contained and disseminating GRs might be cleared by mechanisms other than adaptive immunity, so we capture these mechanisms with a constant fractional rate μ_E or μ_I, which should be small compared with δ and γ. For δ, k, γ, μ_E and μ_I, subscript P or L indicate that the process happens in the lung or LN, respectively. S_{P0} and S_{L0} are the total number of initial susceptible sites in the lung and LN, respectively. Unlike in LNs where we explicitly capture the regeneration of healthy LN tissues, In the lung, the sum of sites of all four states is a constant:

$$N_P = S_P + E_P + I_P + D_P. \tag{6.10}$$

f_I is the overall adaptive immune response factor. It is the product of three factors: Antigen availability, time-dependent immunity potential, and the intactness of the LNs. It is calculated with Equation (6.11). The range for f_I is between 0 and 1:

$$f_I = \alpha(Ag)\tau(t)\frac{S_L}{S_{L0}}. \tag{6.11}$$

Ag represents the total amount of antigen available to the adaptive immune system. It is calculated by the sum of weighted numbers of contained and disseminating GRs in the lung and LN. p and q are larger than 1, assuming that antigens in a disseminating GR are more accessible than in a contained GR, and those in the LN are more accessible than in lung. The contribution of antigen to immunity follows a Michaelis-Menten function, where K_A is the amount of Ag required to achieve half maximum immune activity:

$$Ag = E_P + pI_P + q(E_L + pI_L), \tag{6.12}$$

$$\text{and } \alpha(Ag) = \frac{Ag}{Ag + K_A}. \tag{6.13}$$

$\tau(t)$ describes the fraction of optimal immune function in the body over time. In the long term, this function declines with age. It may also change in response to other events, such as HIV co-infection (which reduces the number of CD4+ T cells) or immunosuppressive therapies. Total numbers of naive T cells decline by 5% per year in humans(Ye and Kirschner, 2002), so we assume Mtb-specific T cells available in circulation decline at the same rate.

$$\tau(t) = e^{-\frac{0.05}{365}t}. \tag{6.14}$$

6.2.4 Uncertainty and sensitivity analysis

There are limited time course data on granulomas that could be used to calibrate model parameters. Thus, we estimated biologically reasonable ranges for each parameter by performing uncertainty analysis and examining the dynamics of different types of GRs to see if their numbers and trends are roughly within the range as observed in experiments(Lin et al., 2014; Coleman et al., 2014). We use Latin Hypercube Sampling (LHS) as it efficiently covers the high dimensional parameter space. Different regions of parameter space correspond to different dynamics, reflecting various disease trajectories in human. In our study, we define scenarios where the number of disseminating GR remains low ($<$0.1) as latency, and these where the disseminating GR quickly increase as reactivation. Among different possible combinations of parameters that produce latency dynamics, we picked a one as our baseline.

We also use sensitivity analysis to study how each model mechanism (via parameters) are correlated with different model outputs(Marino et al., 2008). The ranges used for each parameter

are shown in Table 6.3. 5000 parameter sets are generated, and we solve the model system numerically for each of the parameter sets using MATLAB (`http://www.mathworks.com/products/matlab/`). After simulations are performed, we calculate the Partial Rank Correlation Coefficients (PRCC) between model outputs of interest (e.g. number of disseminating GRs at time point 10 years in each compartment) and parameters that were varied. PRCCs are tested for significance with significance level of $\alpha = 1 \times 10^{-9}$.

6.3 Results

6.3.1 Basic reproduction number R_0

In epidemic modeling, R_0 is a metric calculated to determine the outcome of a disease at population level. It can be used as an indicator describing that when a few individuals in a susceptible population are infected with a disease, how likely the disease is going to spread in a population. If the value is smaller than 1, the disease will die out in the long term; however, if it's larger than 1 it will spread through the entire population. Similarly, we can calculate an R_0 for our system to see the potential of GR to spread in the lung and LNs.

When the system is at its disease-free equilibrium (S_{P0}, 0, 0, 0, S_{L0}, 0, 0), the Jacobian Matrix is calculated as:

$$J = \begin{bmatrix} \frac{\partial \dot{E_P}}{\partial E_P} & \frac{\partial \dot{E_P}}{\partial I_P} & \frac{\partial \dot{E_P}}{\partial E_L} & \frac{\partial \dot{E_P}}{\partial I_L} \\ \frac{\partial \dot{I_P}}{\partial E_P} & \frac{\partial \dot{I_P}}{\partial I_P} & \frac{\partial \dot{I_P}}{\partial E_L} & \frac{\partial \dot{I_P}}{\partial I_L} \\ \frac{\partial \dot{E_L}}{\partial E_P} & \frac{\partial \dot{E_L}}{\partial I_P} & \frac{\partial \dot{E_L}}{\partial E_L} & \frac{\partial \dot{E_L}}{\partial I_L} \\ \frac{\partial \dot{I_L}}{\partial E_P} & \frac{\partial \dot{I_L}}{\partial I_P} & \frac{\partial \dot{I_L}}{\partial E_L} & \frac{\partial \dot{I_L}}{\partial I_L} \end{bmatrix}$$

$$= \begin{bmatrix} -k_P - \mu_{EP} & \phi_P\beta_{PP} & 0 & \phi_P\beta_{PL} \\ k_P & (1-\phi_P)\beta_{PP} - \mu_{IP} & 0 & (1-\phi_P)\beta_{PL} \\ 0 & \phi_L\beta_{LP} & -k_L - \mu_{EL} & \phi_L\beta_{LL} \\ 0 & (1-\phi_L)\beta_{LP} & k_L & (1-\phi_L)\beta_{LL} - \mu_{IL} \end{bmatrix}. \tag{6.15}$$

After decomposition using a method introduced in(Diekmann et al., 2010), we get the transmission and transition matrices:

$$T = \begin{bmatrix} 0 & \phi_P\beta_{PP} & 0 & \phi_P\beta_{PL} \\ 0 & (1-\phi_P)\beta_{PP} & 0 & (1-\phi_P)\beta_{PL} \\ 0 & \phi_L\beta_{LP} & 0 & \phi_L\beta_{LL} \\ 0 & (1-\phi_L)\beta_{LP} & 0 & (1-\phi_L)\beta_{LL} \end{bmatrix} \tag{6.16}$$

$$= \begin{bmatrix} \phi_P\beta_{PP} & \phi_P\beta_{PL} \\ (1-\phi_P)\beta_{PP} & (1-\phi_P)\beta_{PL} \\ \phi_L\beta_{LP} & \phi_L\beta_{LL} \\ (1-\phi_L)\beta_{LP} & (1-\phi_L)\beta_{LL} \end{bmatrix} \begin{bmatrix} 0 & 0 \\ 0 & 1 \\ 0 & 0 \\ 1 & 0 \end{bmatrix}^T = CR \tag{6.17}$$

$$\text{and } \Sigma = \begin{bmatrix} -k_P - \mu_{EP} & 0 & 0 & 0 \\ k_P & -\mu_{IP} & 0 & 0 \\ 0 & 0 & -k_L - \mu_{EL} & 0 \\ 0 & 0 & k_L & -\mu_{IL} \end{bmatrix}. \tag{6.18}$$

From these results, we can calculate the next generation matrix (NGM) with small domain:

$$K_S = -R\Sigma^{-1}C = \begin{bmatrix} \frac{\beta_{PP}}{\mu_{IP}\xi_P} & \frac{\beta_{PL}}{\mu_{IP}\xi_P} \\ \frac{\beta_{LP}}{\mu_{IP}\xi_L} & \frac{\beta_{LL}}{\mu_{IP}\xi_L} \end{bmatrix}, \tag{6.19}$$

$$\text{where } \xi_P = 1 - \frac{\mu_{EP}}{k_P + \mu_{EP}}\phi_P, \quad \xi_L = 1 - \frac{\mu_{EL}}{k_L + \mu_{EL}}\phi_L. \tag{6.20}$$

The larger eigenvalue of K_S is:

$$R_0 = \frac{\beta_{PP}\xi_P}{2\mu_{IP}} + \frac{\beta_{LL}\xi_L}{2\mu_{IL}} + \frac{1}{2}\sqrt{(\frac{\beta_{PP}\xi_P}{\mu_{IP}} - \frac{\beta_{LL}\xi_L}{\mu_{IL}})^2 + \frac{4\beta_{PL}\beta_{LP}\xi_P\xi_L}{\mu_{IP}\mu_{IL}}}. \tag{6.21}$$

At the disease-free equilibrium, as the adaptive immune response has not yet been activated, the mechanism available to limit infection spread is solely innate immunity, which is represented by μ_E and μ_L in Equation (6.21). When adaptive immunity does not occur, TB infection always progresses to active disease. Such observation indicates that the R_0 for an in-host granuloma 'epidemic' is larger than 1.

6.3.2 Latency and reactivation

Although R_0 is larger than 1, the number of granulomas does not necessarily increase when the system is away from the disease-free equilibrium. This is because adaptive immunity is initiated upon antigen encounter. As a result of the model formulation, the system has only one equilibrium, which is the disease-free state. However, there could exist quasi-equilibria for E and I states, where the rates at which healthy sites become infected, and infected sites become damaged are both very slow. We found an example parameter set defined as the latent infection scenario (Table 6.1, "Latent"), and the dynamics are shown in Figure 6.2. The initial conditions are listed in Table 6.2 (the same initial conditions are applied to following simulations, with the initial E_P and I_P dependent on ϕ_P). In this simulation, we observe that after an initial decline, the number of contained GR increases very slowly. The percentage of disseminating GR is undetectable (below 0.1). In the model, this corresponds to a latently infected individual followed over a long period of time (more than 10 years).

By adjusting parameters, such as the sensitivity of adaptive immunity to antigen stimulation (K_A) (Table 6.1, "Reactivation"), we can simulate different disease outcomes at the 10-year time point, as shown in Figure 6.3. In this scenario, an individual remains latently infected for about 5 years, until the number of infectious GRs accumulates and the number of immune cell declines, together inducing a higher rate of dissemination. Then the number of both contained and disseminating GRs in the lung and LNs begin to increase rapidly, and we could classify the individual as having active TB (via reactivation). An individual who has active TB is infectious to others. Without treatment, the fraction of functional lung and LN tissue declines and eventually the host will succumb to disease.

6.3.3 Reinfection causes activation of latent disease

In areas with a high prevalence of active TB cases, patients with latent TB can experience reinfection when they contract bacteria from other infected hosts. To study the effects of such events, we tested how reinfection alters disease outcomes by initializing with the same parameter set as in the latent scenario, and then adding 20 new GRs to the system (lung and LN) each year. The result is shown in Figure 6.4. We can see that every time that a reinfection event occurs, the immune system attempts to control it. Such attempts are quite successful at first; however, we observe higher levels of disseminating GR levels after reinfection. After the fifth reinfection event, the system cannot bring the number of disseminating GRs back under control ($<$0.1). The dynamics then follow the pattern we see in the reactivation scenario.

6.3.4 Impaired immune function causes activation of latent disease

A host's immune system may not always remain at the same level. Aging can reduce the potential of the immune system, as the thymus shrinks and production of new T cells wanes. In patients with autoimmune diseases such as rheumatoid arthritis, treatment may involve immunosuppression. In South Africa, HIV co-infection with TB is seen in many cases, and the CD4+ T

cell population is severely reduced. We tested the impact of an impaired immune system on TB disease outcomes using the baseline parameter set for latent infection (Table 6.3). We assume that $\tau(t)$ (the fraction of T cells available) drops by half at time point 5 years. The result is shown in Figure 6.5. In this situation, the dynamics immediately switch to a reactivation pattern after the decline in immune function, indicating that latent infection progresses to active disease.

6.3.5 Role of lung granuloma formation

If contained GRs provide a place for bacteria to evade the immune system, exposing bacteria by expediting their transition to uncontained GRs might promote healing. To examine the role of contained GR in the lung, we modified the latent infection parameter set by increasing k_1 (the rate of GR reactivation) from 0.002 to 0.02 day^{-1}, so that GR stay in a contained state for a shorter period of time (Table 6.3). The simulation result is shown in Figure 6.6. In our simulation, even though the number of contained GRs drops to a slightly lower level initially at the one-year time point, the disease progresses to an active phase with a significantly shortened latent period. This result supports the hypothesis that contained GRs in lungs are favorable to the host by leading to a milder disease outcome rather than preventing the clearance of the bacteria.

6.3.6 Role of granuloma in LN

Granulomas are observed to develop in LNs of humans and NHP models of TB(Lin et al., 2009). On the one hand, granulomas present in LNs may provide continual antigen stimulation and facilitate development and maintenance of faster and stronger immune responses. On the other hand, infection within LNs will likely interrupt the immune response machinery by disrupting the physical structure as well as usurping immune cells headed for the lung and detaining them in LNs. We next examined the role of GRs disseminating to LNs. We altered the reactivation scenario parameter set by setting β_{LP} (dissemination from the lung to LNs) to 0 day^{-1}, so that lung GRs will not seed the LN. The result is shown in Figure 6.7. As expected, no infection occurs

in the LN compartment. The dynamics in lungs are different from what we see in a reactivation scenario (Figure 6.3). In the beginning, the immune system is not able to contain the infection as successfully as in the reactivation case. We see a larger number of contained GRs, and the number of disseminating GRs is larger than 0.1 from the beginning. However, the disease never progress to the catastrophic end stage as we see in the reactivation case. These results support a dual role of GRs in the LNs. By disseminating to the LN, the increased amount of bacteria material available to the immune system induces a more potent response and better controls infection; they also damage the LN structure and eventually cause the systemic collapse.

6.3.7 Sensitivity analysis

To identify mechanisms that contribute to differential host level disease outcomes, we varied the values of model parameters using uncertainty analysis and assessed the sensitivity of the model output to differences in model parameters. The mechanisms we included and the ranges of the parameter values examined are shown in Table 6.3 ("LHS"). We use the number of disseminating GRs as our model readout, as it is associated with uncontrolled growth of Mtb thus usually an indication of TB reactivation. We choose $\alpha = 1.0 \times 10^{-9}$ as the significance level, and the PRCC values are shown in Figure 6.8. Mechanisms corresponding to each of these parameters in the model can serve as possible therapeutic targets and should be explored.

We can see that γ_P (the rate of infected GRs turning into damaged tissues) has a high and negative correlation with disease, suggesting that one way to control infection is to tolerate a small level of tissue damage as a tradeoff for infection. Indeed, when antibiotics are given to TB patients, they induce fibrosis in the lung, a tissue damage that is irreversible(Cooper et al., 1986; Adamson, 1984; Daba et al., 2004).As long as the extent of damage is controlled, this option is viable. We can also see that other mechanisms, including β_{PP} (dissemination within the lung), β_{LP} (dissemination from the lung to LNs) and k_P (lung GR reactivation) are positively correlated with disease

progression. This suggests that efforts should focus on lung GRs, reducing their reactivation and dissemination as opposed to LN GRs. Furthermore, K_A, the sensitivity of adaptive immunity to antigen stimulation, is positively correlated with disease. This means that another potential method to containing infection is to reduce the amount of antigen required to mount an adaptive immune response by sensitizing the immune system.

6.4 Discussion

We constructed a deterministic model of a "within host" epidemic of TB infection based on dynamics of granulomas in lung and LNs. Granulomas are the key site of infection for Mtb infection, and many form in lungs and LNs in infected hosts over the time course of infection. Our model suggests that even though the R_0 is likely to be larger than 1, we can still achieve latent infection with almost constant levels of contained GRs. There is a new paradigm for TB that suggests that the infection outcomes are not a binary between latent and active TB individuals, but that hosts with latent TB really exist on a spectrum(Barry et al., 2009). On the reactivation side of the spectrum, one can more easily move to active disease, for example; however, one is less likely to develop active disease in their lifetime if they fall more to the other side(Via et al., 2013). Perturbations to the host (such as co-infections, aging, etc.) can move an infected individual along the spectrum during their lifetime increasing their risk of active infection. Our findings are consistent with this as they predict that latency is not truly an equilibrium state, but one in flux, even if that change happens over a very long timescale.

Latent infection is sensitive to the responsiveness of the adaptive immunity to antigen. The model shows that reinfection and decline of the immune system trigger reactivation of TB. We analyzed the differing roles of GR in both the lung and LNs. Results indicate that GRs in lungs have a protective function. However, the role of LN granuloma has two facets. On the one hand, they provide the immune system with more antigens, which helps to reduce the disseminating GRs

in the lung and prevent the host from becoming infectious. On the other hand, these GRs damage the LN structure and impair immune function, eventually resulting in severe tissue damage in both the lung and LN.

Our sensitivity analysis identified mechanisms that strongly correlate with better host-level outcomes. Figure 6.8 summarizes those findings, indicating mechanisms that could be potential targets for therapeutics. Healing of disseminating lung GRs induces tissue damage in the lung, as fibrotic lung tissue will not regain its normal function. However, one finding of the model is that by increasing the rate of this mechanism, we can induce low levels of lung tissue damage early on and avoid more severe infection outcomes long term. More obvious mechanisms include inhibition of bacteria dissemination within the lung. These predictions can aid researchers to focus design of possible targets for TB treatment.

The implication of our results is that by sensitizing a patient's immune system, we can lower the risk of the reactivation of TB significantly. Since the course of TB antibiotic treatment is long (over 6 months with multiple drugs), and the lack of treatment compliance is a major hurdle in TB treatment, it could be practical to stimulate patient immune systems even after diagnosis, if there is a suitable vaccine. By applying this method to the entire human population, we may keep more infected individuals in latency for a much longer period of time, in effect reducing the population level R_0.

Figures

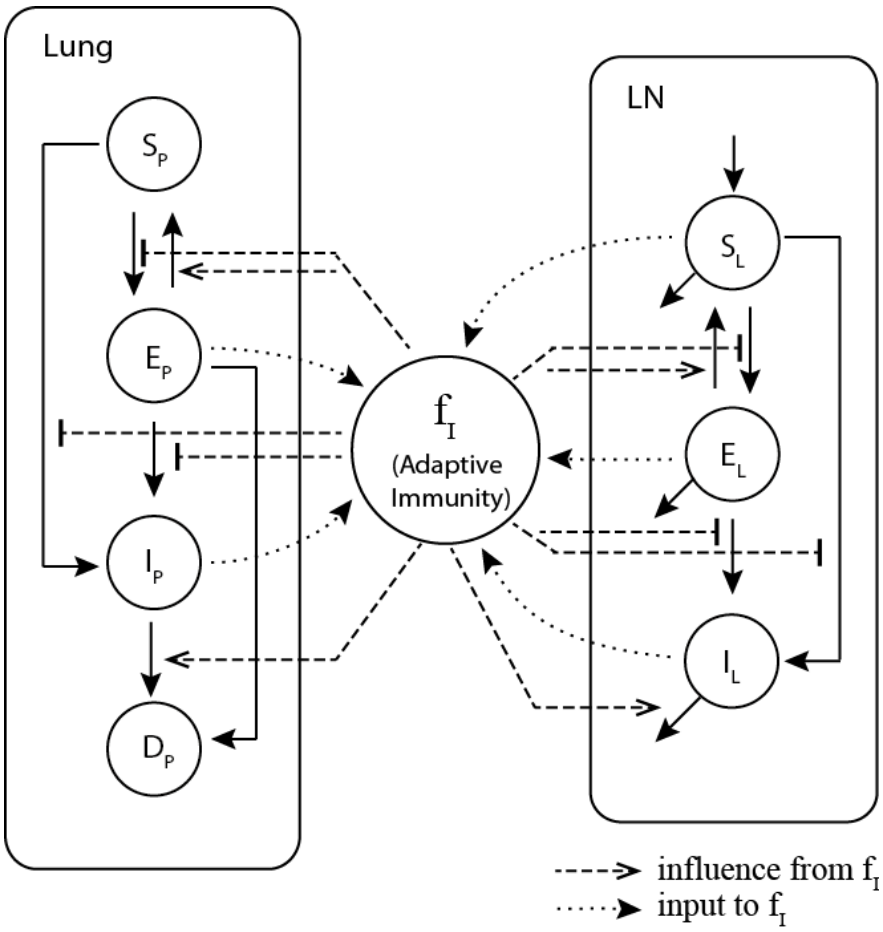

Figure 6.1: Schematic of granuloma population model. Granuloma sites in two compartments of lung and LN are tracked, with four different states (S, E, I, D) in the lung compartment and three different states (S, E, I) in the LN compartment. S represents susceptible, E-exposed, I-infected lung tissue and D is dead lung tissue. Solid arrows indicate transition between different states. Dotted arrows indicate input to the adaptive immunity. Dashed arrows indicate impact of adaptive immunity on granuloma state changes. f_I refers to the adaptive immune function that affects many processes in the model.

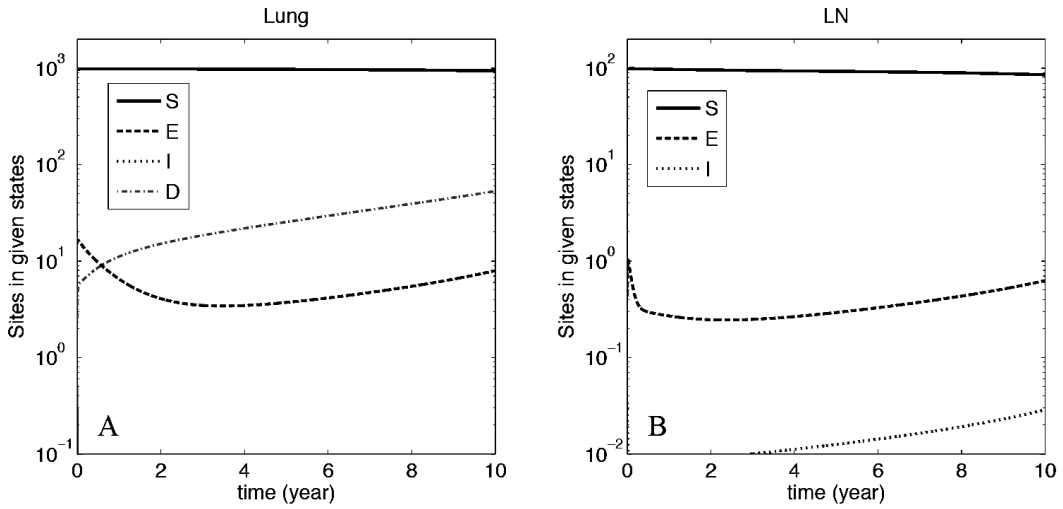

Figure 6.2: Quasi-steady state describing latent TB in an individual host. The numbers of susceptible, exposed, infected and dead sites in the lung (panel A) and LN (panel B) are plotted against time. After the initial drop, the number of contained granuloma stays relatively stable over the 10-year simulation period. Panel A (lung): S represents susceptible, E are exposed, I are infected lung tissue and D is dead lung tissue. Panel B (LN): S represents susceptible LN tissue, E are exposed and I are infected LN tissue. Parameters: Table 6.1, Latent.

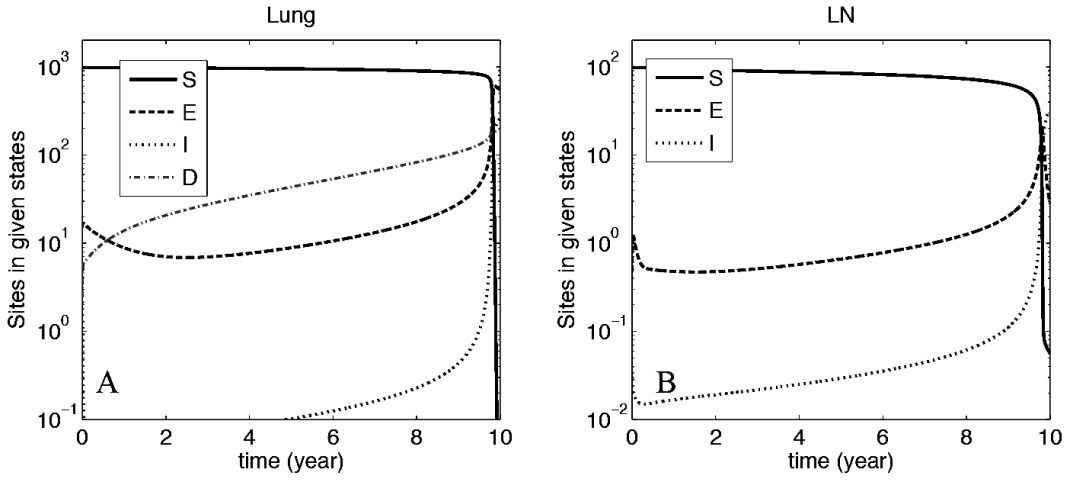

Figure 6.3: Dynamics of granulomas describing TB reactivation. For the first 8 years infection remains latent in a quasi-steady state. After that, disseminating GRs become detectable and the patient become infectious. Then levels of healthy lung (Panel A) and LN (Panel B) tissues drop sharply, leading to fatality if treatment is not applied. Panel A (lung): S represents susceptible, E are exposed, I are infected lung tissue and D is dead lung tissue. Panel B (LN): S represents susceptible LN tissue, E are exposed and I are infected LN tissue. Parameters: Table 6.1, Reactivation.

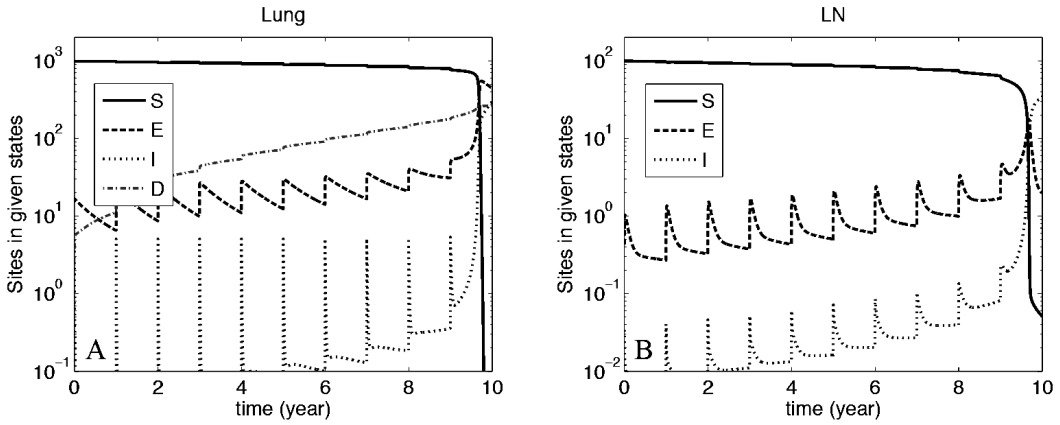

Figure 6.4: TB reactivation due to reinfection. Four rounds of reinfection occur at time points of 8 and 9 years after initial infection. Panel A shows dynamics in the lung and Panel B shows dynamics in the LN. Panel A (lung): S represents susceptible, E are exposed, I are infected lung tissue and D is dead lung tissue. Panel B (LN): S represents susceptible LN tissue, E are exposed and I are infected LN tissue. Parameters: 20 S sites (lung and LN together) are changed to E or I each year, otherwise the same as in Table 6.1, Latent.

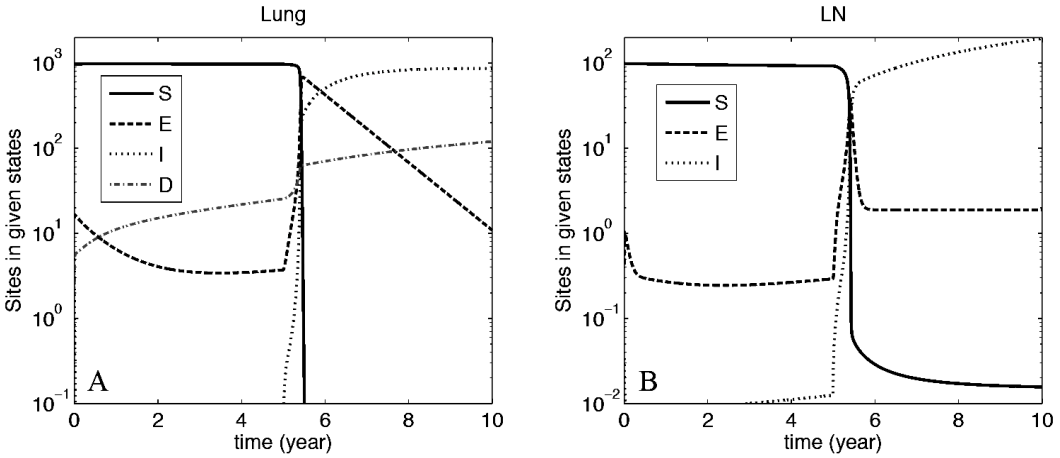

Figure 6.5: TB reactivation due to impaired immune function. Immune function potential is decreased by half at the 5-year time point. Panel A shows dynamics in the lung and Panel B shows dynamics in the LN. Panel A (lung): S represents susceptible, E are exposed, I are infected lung tissue and D is dead lung tissue. Panel B (LN): S represents susceptible LN tissue, E are exposed and I are infected LN tissue. Parameters: Table 6.1, Latent; $\tau(t)$ drops by half at 5 years.

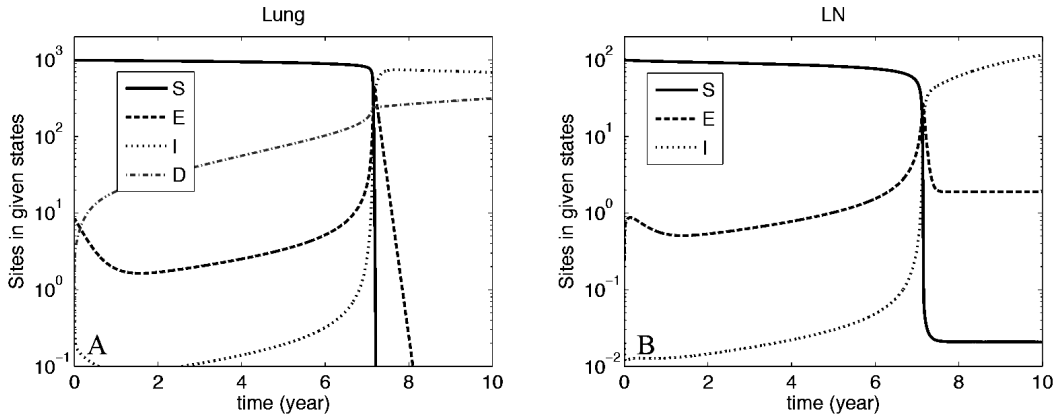

Figure 6.6: Active TB results when GR are not contained. The rate of contained granuloma progressing to dissemination is increased by 10-fold. Panel A shows dynamics in the lung and Panel B shows dynamics in the LN. Panel A (lung): S represents susceptible, E are exposed, I are infected lung tissue and D is dead lung tissue. Panel B (LN): S represents susceptible LN tissue, E are exposed and I are infected LN tissue. Parameters: Table 6.3, Lung GR role

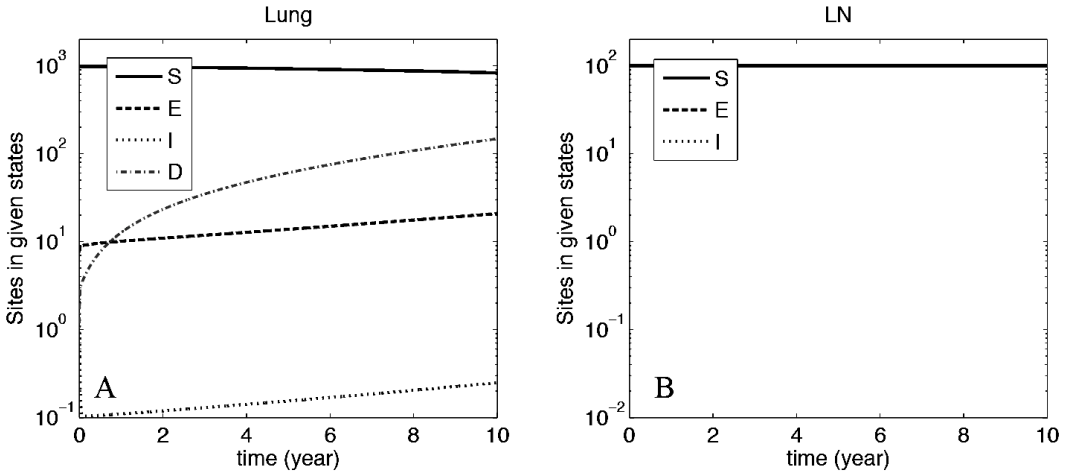

Figure 6.7: Infection dynamics without LN granuloma formation. Dissemination rate of TB from the lung to LN is set to 0. Panel A shows dynamics in the lung and Panel B shows dynamics in the LN. Panel A (lung): S represents susceptible, E are exposed, I are infected lung tissue and D is dead lung tissue. Panel B (LN): S represents susceptible LN tissue, E are exposed and I are infected LN tissue. Parameters: Table 6.3, LN GR role.

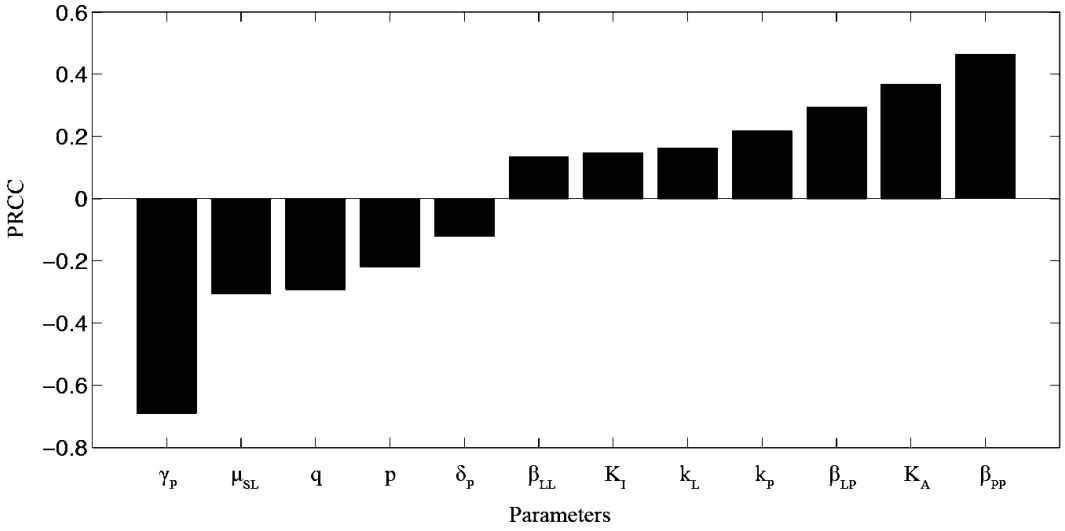

Figure 6.8: Sensitivity analysis results. All significant PRCC values for the outcome variable of disseminating GR in lung at the 10-year time point are shown. Significance level is chosen to be 1E-9. The mechanisms include: γ_P: healing of disseminating GRs; μ_{SL}: LN tissue turnover; q: fold of increase of antigen accessibility in LN GRs compared to lung GRs; p: fold of increase of antigen accessibility in disseminating GRs compared to contained GRs; δ_P: healing of contained GRs; β_{LL} : dissemination in LNs; K_I : adaptive immunity level required to reduce dissemination by half; k_L: GR reactivation in LNs; k_P: GR reactivation in the lung; β_{LP}: dissemination from the lung to LNs; K_A: sensitivity of the immune system to antigen; β_{PP}: dissemination in the lung. These processes are targets for therapeutics. Parameters: Table 6.3, LHS.

Tables

Table 6.1: Granuloma population model: parameter value for latent and reactivation.

Parameter	Latent	Reactivation	description
β_{PP} (day^{-1})	1.2	1.2	dissemination rate, lung to lung
β_{PL} (day^{-1})	6.0×10^{-3}	6.0×10^{-3}	dissemination rate, LN to lung
δ_P (day^{-1})	5.0×10^{-3}	5.0×10^{-3}	E_P resolution rate
k_P (day^{-1})	2.5×10^{-3}	2.5×10^{-3}	E_P progression rate
γ_P (day^{-1})	0.65	0.65	I_P fibrosis rate (induced)
μ_{EP} (day^{-1})	1.0×10^{-5}	1.0×10^{-5}	E_P fibrosis rate (base)
μ_{IP} (day^{-1})	1.0×10^{-5}	1.0×10^{-5}	I_P fibrosis rate (base)
μ_{SL} (day^{-1})	1.0×10^{-3}	1.0×10^{-3}	LN tissue renewal rate
β_{LL} (day^{-1})	0.6	0.6	dissemination rate, LN to LN
β_{LP} (day^{-1})	0.6	0.6	dissemination rate, lung to LN
δ_L (day^{-1})	1.5×10^{-2}	1.5×10^{-2}	E_L resolution rate
k_L (day^{-1})	4.5×10^{-2}	4.5×10^{-2}	E_L progression rate
γ_L (day^{-1})	2	2	I_L fibrosis rate (induced)
μ_{EL} (day^{-1})	2.0×10^{-5}	2.0×10^{-5}	E_L fibrosis rate (base)
μ_{IL} (day^{-1})	2.0×10^{-5}	2.0×10^{-5}	I_L fibrosis rate (base)
p	35	35	Infectious GR Ag factor
q	25	25	LN GR Ag factor
K_A	20	40	Ag amount for half max response
K_I	0.25	0.25	constant for dissemination inhibition
ϕ_P	0.75	0.75	fraction of contained new GR in lung
ϕ_L	0.85	0.85	fraction of contained new GR in LN

Table 6.2: Granuloma population model: initial conditions.

Species	Initial condition
S_{P0}	1000
E_{P0}	$20\times\phi_P$
I_{P0}	$20\times(1-\phi_P)$
D_{P0}	0
S_{L0}	100
E_{L0}	0
I_{L0}	0

Table 6.3: Granuloma population model: parameter values for other scenarios

Parameters	Lung GR role	LN GR role	LHS
β_{PP} (day^{-1})	1.2	1.2	0.2-5
β_{PL} (day^{-1})	6.0×10^{-3}	6.0×10^{-3}	$0.1\text{-}2.5\times10^{-2}$
δ_P (day^{-1})	5.0×10^{-3}	5.0×10^{-3}	$0.1\text{-}2.5\times10^{-2}$
k_P (day^{-1})	2.5×10^{-2}	2.5×10^{-3}	$0.1\text{-}2.5\times10^{-2}$
γ_P (day^{-1})	0.65	0.65	0.1-2.5
μ_{EP} (day^{-1})	1.0×10^{-5}	1.0×10^{-5}	$0.2\text{-}5\times10^{-5}$
μ_{IP} (day^{-1})	1.0×10^{-5}	1.0×10^{-5}	$0.2\text{-}5\times10^{-5}$
μ_{SL} (day^{-1})	1.0×10^{-3}	1.0×10^{-3}	$0.2\text{-}5\times10^{-3}$
β_{LL} (day^{-1})	0.6	0.6	0.1-2.5
β_{LP} (day^{-1})	0.6	0	0.1-2.5
δ_L (day^{-1})	1.5×10^{-2}	1.5×10^{-2}	$0.2\text{-}5\times10^{-2}$
k_L (day^{-1})	4.5×10^{-2}	4.5×10^{-2}	0.01-0.25
γ_L (day^{-1})	2	2	0.4-10
μ_{EL} (day^{-1})	2.0×10^{-5}	2.0×10^{-5}	$0.2\text{-}5\times10^{-2}$
μ_{IL} (day^{-1})	2.0×10^{-5}	2.0×10^{-5}	$0.2\text{-}5\times10^{-2}$
p	35	35	4-100
q	25	25	4-100
K_A	20	20	4-100
K_I	0.25	0.25	0.15-0.35
ϕ_P	0.75	0.75	0.72-0.96
ϕ_L	0.85	0.85	0.72-0.96

Bibliography

Adamson, I. Y. Drug-induced pulmonary fibrosis. *Environmental health perspectives*, 55:25–36, 1984.

Barry, C. E., Boshoff, H. I., Dartois, V., Dick, T., Ehrt, S., Flynn, J., Schnappinger, D., Wilkinson, R. J. and Young, D. The spectrum of latent tuberculosis: rethinking the biology and intervention strategies. *Nature reviews. Microbiology*, 7(12):845–55, 2009.

Blower, S. M., McLean, A. R., Porco, T. C., Small, P. M., Hopewell, P. C., Sanchez, M. A. and Moss, A. R. The intrinsic transmission dynamics of tuberculosis epidemics. *Nature Medicine*, 1(8):815–821, 1995.

Cardona, P.-J. New insights on the nature of latent tuberculosis infection and its treatment. *Inflammation & allergy drug targets*, 6(1):27–39, 2007.

Castillo-Chávez, C. and Aparicio, J. Mathematical modelling of tuberculosis epidemics. *Mathematical Biosciences and Engineering*, 6(2):209–237, 2009.

Castillo-Chavez, C. and Feng, Z. To treat or not to treat: the case of tuberculosis. *Journal of mathematical biology*, 35(6):629–656, 1997.

Chackerian, A. A., Alt, J. M., Perera, T. V., Dascher, C. C. and Behar, S. M. Dissemination of Mycobacterium tuberculosis Is Influenced by Host Factors and Precedes the Initiation of T-Cell Immunity. *Infection and Immunity*, 70(8):4501–4509, 2002.

Cilfone, N. A., Perry, C. R., Kirschner, D. E. and Linderman, J. J. Multi-scale modeling predicts a balance of tumor necrosis factor-α and interleukin-10 controls the granuloma environment during Mycobacterium tuberculosis infection. *PloS one*, 8(7):e68680, 2013.

Coleman, M. T., Chen, R. Y., Lee, M., Lin, P. L., Dodd, L. E., Maiello, P., Via, L. E., Kim, Y., Marriner, G., Dartois, V., Scanga, C., Janssen, C., Wang, J., Klein, E., Cho, S. N., Barry 3rd, C. E. and Flynn, J. L. PET/CT imaging reveals a therapeutic response to oxazolidinones in macaques and humans with tuberculosis. *Sci Transl Med*, 6(265):265ra167, 2014.

Cooper, J. A., White, D. A. and Matthay, R. A. Drug-induced pulmonary disease. Part 1: Cytotoxic drugs. *The American review of respiratory disease*, 133(2):321–40, 1986.

Corbett, E. L., Watt, C. J., Walker, N., Maher, D., Williams, B. G., Raviglione, M. C. and Dye, C. The growing burden of tuberculosis: global trends and interactions with the HIV epidemic. *Archives of internal medicine*, 163(9):1009–1021, 2003.

Daba, M. H., El-Tahir, K. E., Al-Arifi, M. N. and Gubara, O. A. Drug-induced pulmonary fibrosis. 2004.

Diekmann, O., Heesterbeek, J. A. P. and Roberts, M. G. The construction of next-generation matrices for compartmental epidemic models. *Journal of the Royal Society, Interface / the Royal Society*, 7(47):873–885, 2010.

Dye, C., Garnett, G. P., Sleeman, K. and Williams, B. G. Prospects for worldwide tuberculosis control under the WHO DOTS strategy. *The Lancet*, 352(9144):1886–1891, 1998.

Fallahi-Sichani, M., Flynn, J. L., Linderman, J. J. and Kirschner, D. E. Differential risk of tuberculosis reactivation among anti-TNF therapies is due to drug binding kinetics and permeability. *Journal of immunology (Baltimore, Md. : 1950)*, 188(7):3169–78, 2012a.

Fallahi-Sichani, M., Kirschner, D. E. and Linderman, J. J. NF-κB Signaling Dynamics Play a Key Role in Infection Control in Tuberculosis. *Frontiers in physiology*, 3:170, 2012b.

Fallahi-Sichani, M., Schaller, M. A., Kirschner, D. E., Kunkel, S. L. and Linderman, J. J. Identification of key processes that control tumor necrosis factor availability in a tuberculosis granuloma. *PLoS computational biology*, 6(5):e1000778, 2010.

Feng, Z., Castillo-Chavez, C. and Capurro, A. F. A model for tuberculosis with exogenous reinfection. *Theoretical population biology*, 57(3):235–247, 2000.

Flynn, J. L. and Chan, J. Immunology of tuberculosis. *Annual review of immunology*, 19:93–129, 2001.

Gong, C., Mattila, J. T., Miller, M., Flynn, J. L., Linderman, J. J. and Kirschner, D. Predicting lymph node output efficiency using systems biology. *Journal of theoretical biology*, 335:169–184, 2013.

Guzzetta, G., Ajelli, M., Yang, Z., Merler, S., Furlanello, C. and Kirschner, D. Modeling socio-demography to capture tuberculosis transmission dynamics in a low burden setting. *Journal of theoretical biology*, 289:197–205, 2011.

Kirschner, D. Dynamics of co-infection with M. Tuberculosis and HIV-1. *Theoretical population biology*, 55(1):94–109, 1999.

Kirschner, D. E., Chang, S. T., Riggs, T. W., Perry, N. and Linderman, J. J. Toward a multiscale model of antigen presentation in immunity. *Immunological reviews*, 216:93–118, 2007.

Lin, P. L., Coleman, T., Carney, J. P. J., Lopresti, B. J., Tomko, J., Fillmore, D., Dartois, V., Scanga, C., Frye, L. J., Janssen, C., Klein, E., Barry, C. E. and Flynn, J. L. Radiologic responses in cynomolgous macaques for assessing tuberculosis chemotherapy regimens. *Antimicrobial agents and chemotherapy*, 2013.

Lin, P. L., Ford, C. B., Coleman, M. T., Myers, A. J., Gawande, R., Ioerger, T., Sacchettini, J., Fortune, S. M. and Flynn, J. L. Sterilization of granulomas is common in active and latent tuberculosis despite within-host variability in bacterial killing. *Nature medicine*, 20(1):75–79, 2014.

Lin, P. L., Rodgers, M., Smith, L., Bigbee, M., Myers, A., Bigbee, C., Chiosea, I., Capuano, S. V., Fuhrman, C., Klein, E. and Flynn, J. L. Quantitative comparison of active and latent tuberculosis in the cynomolgus macaque model. *Infection and immunity*, 77(10):4631–4642, 2009.

Linderman, J. J., Riggs, T., Pande, M., Miller, M., Marino, S. and Kirschner, D. E. Characterizing the dynamics of CD4+ T cell priming within a lymph node. *Journal of immunology (Baltimore, Md. : 1950)*, 184(6):2873–2885, 2010.

Magombedze, G., Garira, W. and Mwenje, E. Modelling the human immune response mechanisms to mycobacterium tuberculosis infection in the lungs. *Mathematical biosciences and engineering : MBE*, 3(4):661–82, 2006.

Magombedze, G. and Mulder, N. A mathematical representation of the development of Mycobacterium tuberculosis active, latent and dormant stages. *Journal of theoretical biology*, 292:44–59, 2012.

Marino, S., El-Kebir, M. and Kirschner, D. A hybrid multi-compartment model of granuloma formation and T cell priming in tuberculosis. *Journal of theoretical biology*, 280(1):50–62, 2011a.

Marino, S., Hogue, I. B., Ray, C. J. and Kirschner, D. E. A methodology for performing global uncertainty and sensitivity analysis in systems biology. *Journal of theoretical biology*, 254(1):178–196, 2008.

Marino, S. and Kirschner, D. E. The human immune response to Mycobacterium tuberculosis in lung and lymph node. *Journal of theoretical biology*, 227(4):463–486, 2004.

Marino, S., Linderman, J. J. and Kirschner, D. E. A multifaceted approach to modeling the immune response in tuberculosis. *Wiley interdisciplinary reviews. Systems biology and medicine*, 3(4):479–89, 2011b.

Milner, F. A., Iannelli, M. and Feng, Z. A Two-Strain Tuberculosis Model with Age of Infection. *SIAM Journal on Applied Mathematics*, 62(5):1634–1656, 2002.

Murphy, B. M., Singer, B. H., Anderson, S. and Kirschner, D. Comparing epidemic tuberculosis in demographically distinct heterogeneous populations. *Mathematical Biosciences*, 180(1-2):161–185, 2002.

Murphy, B. M., Singer, B. H. and Kirschner, D. On treatment of tuberculosis in heterogeneous populations. *Journal of Theoretical Biology*, 223(4):391–404, 2003.

O'Garra, A., Redford, P. S., McNab, F. W., Bloom, C. I., Wilkinson, R. J. and Berry, M. P. R. The immune response in tuberculosis. *Annual review of immunology*, 31:475–527, 2013.

Organization, W. H. Global tuberculosis report 2013. 2013.

Pabst, R., Westermann, J. and Rothkotter, H. J. Immunoarchitecture of regenerated splenic and lymph node transplants. *Int Rev Cytol*, 128:215–260, 1991.

Petersen, T. H., Calle, E. A., Zhao, L., Lee, E. J., Gui, L., Raredon, M. B., Gavrilov, K., Yi, T., Zhuang, Z. W., Breuer, C., Herzog, E. and Niklason, L. E. Tissue-engineered lungs for in vivo implantation. *Science*, 329(5991):538–541, 2010.

Ramakrishnan, L. Revisiting the role of the granuloma in tuberculosis. *Nature reviews. Immunology*, 12(5):352–366, 2012.

Rengarajan, J., Bloom, B. R. and Rubin, E. J. Genome-wide requirements for Mycobacterium tuberculosis adaptation and survival in macrophages. *Proceedings of the National Academy of Sciences of the United States of America*, 102(23):8327–8332, 2005.

Segovia-Juarez, J. L., Ganguli, S. and Kirschner, D. Identifying control mechanisms of granuloma formation during M. tuberculosis infection using an agent-based model. *Journal of theoretical biology*, 231(3):357–76, 2004.

Singer, B. H. and Kirschner, D. E. Influence of backward bifurcation on interpretation of r(0) in a model of epidemic tuberculosis with reinfection. *Mathematical biosciences and engineering : MBE*, 1(1):81–93, 2004.

Via, L. E., Weiner, D. M., Schimel, D., Lin, P. L., Dayao, E., Tankersley, S. L., Cai, Y., Coleman, M. T., Tomko, J., Paripati, P., Orandle, M., Kastenmayer, R. J., Tartakovsky, M., Rosenthal, A., Portevin, D., Eum, S. Y., Lahouar, S., Gagneux, S., Young, D. B., Flynn, J. L. and Barry, C. E. Differential virulence and disease progression following Mycobacterium tuberculosis complex infection of the common marmoset (Callithrix jacchus). *Infection and immunity*, 81(8):2909–2919, 2013.

Wigginton, J. E. and Kirschner, D. A Model to Predict Cell-Mediated Immune Regulatory Mechanisms During Human Infection with Mycobacterium tuberculosis. *The Journal of Immunology*, 166(3):1951–1967, 2001.

Ye, P. and Kirschner, D. E. Reevaluation of T Cell Receptor Excision Circles as a Measure of Human Recent Thymic Emigrants. *The Journal of Immunology*, 168(10):4968–4979, 2002.

Young, D., Stark, J. and Kirschner, D. Systems biology of persistent infection: tuberculosis as a case study. *Nature reviews. Microbiology*, 6(7):520–528, 2008.

CHAPTER VII

Conclusions

7.1 Summary

The human body utilizes the immune system to deal with a huge variety of dangerous agents that we face constantly, including external pathogens. It is natural to wonder how one system is capable of being so versatile and yet precisely controlled to respond to such diverse contexts. A more fascinating question is, although it works effectively most of the time, why does the immune system fail in some situations, and in those situations what can be done to help? Tuberculosis (TB) is an infectious disease caused by *Mycobacteria tuberculosis*. The majority of individuals carrying Mtb have a latent infection, where bacteria are harbored inside granulomas typically in the lung. However, 5% - 10% of latently infected people develop active (and contagious) TB during their lifetime (WHO, 2014; Lin and Flynn, 2010). We have very limited knowledge of what induces these different disease outcomes. In addition, the lack of appropriate biomarkers to identify patients with latent infection is holding back efforts to control the worldwide prevalence of this disease.

In order to better understand adaptive immune responses and how it influences the course of TB disease, we focused our study on dynamics in three different physiological compartments: lungs, lymph nodes (LNs) and blood stream. When Mtb are inhaled into the lung, some of the bacteria will be picked up and processed by antigen presenting cells (APC) to be transported to LNs. In

LNs, precursor T cells make contact with APCs and initiate a program of T cell activation and proliferation. The activated T cells then travel back to the site of infection, where they interact with other immune cells and pathogen and develop into granulomas.

I worked with a multi-compartment model framework to begin to tackle this complex system. Each compartment can be instantiated in different levels of detail, depending on the level of resolution required to answer the questions of interest. For compartments that entail a great level of details, such as the LN, we use agent-based model (ABM) to simulate the dynamics of relevant immune cells: dendritic cells and T cells. The model is written in C++ programming language. In the LN model, we define an explicit 3-dimensional (3D) grid environment representing a LN structure and place elements onto this grid, including cells and ports where cells enter or exit the LN. We also define a set of rules regulating the movement and state change of agents, as well as their interactions. We implemented algorithms to solve molecular level events such as secretion-diffusion of cytokines and chemokines and ligand-receptor dynamics. Complying with these rules, every cell selects an action in a stochastic fashion from biologically grounded choices at each time step. When a granuloma is simulated, the lung compartment model is also instantiated as an ABM. When high resolution of a compartment is not necessary, we are able to substitute it with a low-resolution version implemented using ordinary differential equations (ODE) to increase computational efficiency. The blood compartment is always treated this way in this thesis. Using the framework described above, I conducted my thesis research to quantitatively study the dynamics of T cells in an immune response, and how these dynamics influences granuloma development and the course of TB infection. The key results are listed below and are organized according to my thesis Specific Aims.

7.1.1 T cell priming in the LN

Dendritic cells (DCs) capture pathogens and foreign antigen (Ag) in peripheral tissues and migrate to secondary lymphoid tissues, such as lymph nodes (LNs), where they present processed Ag as MHC-bound peptide (pMHC) to naive T cells. Interactions between DCs and T cells result, over periods of hours, in activation, clonal expansion and differentiation of antigen-specific T cells, leading to primed cells that can now participate in immune responses. Two-photon microscopy (2PM) has been widely adopted to analyze lymphocyte dynamics and can serve as a powerful in vivo assay for cell trafficking and activation over short length and time scales (Miller et al., 2003; 2004). Linking biological phenomena between vastly different spatiotemporal scales can be achieved using a systems biology approach.

In Chapter II, We developed a 3D agent-based model of a LN that allows for the simultaneous *in silico* simulation of T cell trafficking, activation and production of effector cells under different antigen (Ag) conditions. The model anatomy is based on in situ analysis of LN sections (from primates and mice) and cell dynamics based on quantitative measurements from 2PM imaging of mice. Our simulations make three important predictions. First, T cell encounters by DCs and T cell receptor (TCR) repertoire scanning are more efficient in a 3D model compared with 2D, suggesting that a 3D model is needed to analyze LN function. Second, LNs are able to produce primed CD4+ T cells at the same efficiency over broad ranges of cognate frequencies (from 10^{-5} to 10^{-2}). Third, reducing the time that naive T cells are required to bind DCs before becoming activated will increase the rate at which effector cells are produced. This 3D model provides a robust platform to study how T cell trafficking and activation dynamics relate to the efficiency of T cell priming and clonal expansion. We envision that this systems biology approach will provide novel insights for guiding vaccine development and understanding immune responses to infection.

Our findings with regard to the 2D/3D model comparison can potentially apply to other systems involving entities searching for each other. As discussed in Chapter II, in a 3D environment, targets

(DCs) spread out in the space with a smaller average distance between them. Also, the moving agents (T cells) cover a larger region with their searching path in 3D as opposed to 2D, because in 2D a random walk has a higher probability of repeated visits. However, when applying this result to other searching algorithms, generalization should be done with caution. For example, when the number of targets is extremely small, 2D space can guarantee agents finding each other given enough time, while in 3D this may never happen, as the returning probability in 3D is about 34%.

In Chapter III, I implemented algorithms to generate fibroblastic reticular cell (FRC) networks in LN with variable graph, and algorithms to solve diffusion-secretion of soluble molecules in this compartment. Using this model, I tested how the three factors affect the efficiency of DC-T cell searching: constraining the movement of T cells to FRC network, allowing chemotactic signals to facilitate T cell direction decision, base the movement of T cells on persistent random walks. My model predicted that the requirement of a FRC constraint reduces the fraction of T cells able to find their DCs before they exit from the LN, while chemotaxis towards DCs increases the time required before a T cell finds a DC. Together, these two mechanisms reduce the number of T cells that a DC scans per unit time, especially those that has not been previously scanned by the same DC.

7.1.2 T cell effector and memory differentiation

Wet lab studies showed that naive T cells bearing identical T cell receptors (TCR) experience heterogeneous differentiation and clonal expansion processes (Gerlach et al., 2013; Buchholz et al., 2013). The factors controlling this outcome are not well characterized, and their contributions to immune cell dynamics are similarly poorly understood. Understanding mechanisms controlling the differentiation of activated T cells will provide us with potential targets to manipulate the sizes of effector or memory cell populations generated during an immune response and optimize efficacies of clinical interventions.

In Chapter IV, we expanded the previous 3D LN ABM to elaborate mechanisms occurring within and between two important physiological compartments, lymph nodes and blood, to determine how immune cell dynamics, in particular, the generation of effector and memory T cells are controlled. Our multi-organ (multi-compartment) model integrates cellular and tissue level events and allows us to examine the heterogeneous differentiation of individual precursor cognate naive T cells to generate both effector and memory T lymphocytes. Using this model, we simulate a hypothetical immune response and reproduce both a primary and recall response to infection. The key prediction from this model is that increased numbers of antigen-bearing dendritic cells raise production of both effector and memory T cells, and distinct "sweet spots" of peptide-MHC (pMHC) levels on those dendritic cells exist that favor CD4+ or CD8+ T cell differentiation towards either effector or memory cell phenotypes. This has important implications for vaccine development and immunotherapy.

7.1.3 Connecting immune responses with dynamics at the site of infection

The next question I want to ask is how effector and memory T cells generated in an immune response interact with dynamics at the site of infection in the context of infectious diseases, e.g. TB. In particular, I am interested in using computational models to facilitate TB vaccine designs. This question can be addressed in two separate steps. First, we need to identify what composition(s) of memory T cell populations correlate with better immune protection against TB. Second, we need to know how we can stimulate the immune system so that it will generate such compositions of memory T cells.

In Chapter V, I made multiple modifications to our current model system to begin to address these questions, and performed proof-of-concept analysis with each implementation. First, the pathogen expresses a range of proteins that can serve as antigens, each of them having different properties, including unique affinities to bind MHC and frequencies of precursor T cells that can

recognize them when presented on an APC. I added the ability to track multiple antigens into the model, each of which can induce immune responses simultaneously, but with different outputs of specific T cells. I also developed a multi-compartment model by adding an existing agent-based lung granuloma model (previously developed in the lab) to study dynamics of cells in TB infection within all three physiological compartments involved (lung, LN, Blood). The model incorporates the idea of tunable resolution, allowing us to choose between ODE implementation of the LN dynamics or the full ABM. The key predictions of this model are as follows. First, different pre-existing memory T cell combinations exert different protection when Mtb infect the lung, with effector memory CD8+ T cells showing the strongest effects. Secondly, we predict that the population of non-specific effector T cells in circulation could compete with TB specific T cells at the site of infection and hinder an otherwise successful resolution of a granuloma.

7.1.4 Host-level outcomes: A population model of TB granuloma dynamics

Granulomas play a centric role in tuberculosis (TB) infection progression, but the outcomes of a single granuloma do not help predict the disease trajectories. Multiple granulomas usually develop within a single host (Lin et al., 2014; Coleman et al., 2014).These granulomas are not synchronized in size or bacteria load, and will follow different trajectories over time (Lin et al., 2014). How the fate of individual granulomas influence overall infection outcomes at host scale is not understood, although computational models have been developed to predict single granuloma behavior (Segovia-Juarez et al., 2004; Fallahi-Sichani et al., 2010; Marino et al., 2011; 2010; Fallahi-Sichani et al., 2012a;b; Cilfone et al., 2013).

In Chapter VI, I developed a within-host population model that tracks granulomas in two key organs during *Mycobacteria tuberculosis* (Mtb) infection: lung and lymph nodes (LN). I used a standard SIER model formulation in a unique way towards this end. The model captured various time courses of TB progression, including latency and reactivation. Using this very simple

model, we made novel predictions that the system is not in steady state; rather it is a continuous process of progressing to active disease over differing time periods. This prediction is consistent with recently posed ideas suggesting that latent TB exists as a spectrum of states and not a single state citepBarry2009, Lin2009. The model also predicts a novel dichotomous role for granuloma development in LNs during Mtb infection: in early phases of infection granulomas suppress infection by providing additional antigens to the site of immune priming; however, this induces more rapid reactivation at later stages by disrupting immune responses. We identify mechanisms that strongly correlate with better host-level outcomes, including elimination of uncontained lung granulomas by a non-intuitive idea of inducing low levels of lung tissue damage and inhibition of bacteria dissemination within the lung. These predictions are unexpected and non-intutitive, but can potentially be further tested through laboratory investigations.

7.2 Future direction: molecular scale details on control of proliferation and differentiation

In our current model, the outcomes of T cell priming are mechanistic in that they involves T cells binding with DCs via pMHC-I and pMHC-II molecules and accumulating stimulation signals to decide whether they get activated and how likely they can differentiate to various effector or memory subtypes. However, details of regulation at the molecular scale are not explicitly implemented. By introducing more mechanistic control of T cell proliferation and differentiation, we will be able to better recover the plasticity of immune responses, and identify more specific handles for interventions.

7.2.1 IL-2 driven T cell proliferation and Treg suppression

In steady state, naive and memory T cells undergo homeostatic proliferation in response to IL-7 and IL-15 (Sprent et al., 2008). After activation, the proliferation of T cells to support clonal expansion is mainly driven by IL-2 (Paliard et al., 1988). Down stream of TCR and co-stimulation

receptor CD28 signalling, IL-2 expression is activated after priming, while TCR also promotes expression of high affinity IL-2 receptors (Malek, 2008). This results in a self-sustaining proliferation program, which is captured in our current model by setting a minimum number of cell divisions (Gong et al., 2013). However, during the immune response, T cells are also exposed to environmental IL-2 produced by other activated T cells and mature APCs (Granucci et al., 2001) even after they down regulate their own IL-2 production. In our current *LymphSim* ABM, T cells can continue to divide before they exit the LN (Gong et al., 2014), but in reality the IL-2 distribution should follow a spatial distribution and is thus subject to competition. With IL-2 dynamics explicitly modeled, we can better capture the proliferation of T cells after priming. We already developed algorithms in Chapter III to simulate chemokine secretion-diffusion, which can also be used in this study. However, the activation of IL-2 and high affinity IL-2R should be implemented at sub-cellular scale.

Currently in the model, the immune response dampens as recruitment of APCs ceases. This is not the whole picture of negative regulation of T cell expansion. In reality, regulatory T cells are employed to suppress inflammation. Two subsets of Tregs are involved in this process: naturally occurring nTreg and inducible iTreg (Piccirillo and Shevach, 2004). They come from different sources: nTregs arise in the thymus and can recognize a wide range of self-antigens, while iTregs differentiates from normal naive CD4+ T cells and are specific to foreign antigens Hsieh et al. (2006); Curotto de Lafaille and Lafaille (2009). When activated, they expand in the presence of IL-2 produced by other cells and play immunosuppressive roles with similar mechanisms. iTregs employ contact-dependent mechanisms to suppress T cell activation (Strauss et al., 2009), and also release cytokines such as IL-10 and TGF-β to modulate the immune response and soluble IL-2 receptors to neutralize environmental IL-2 (Jonuleit et al., 2002; Pandiyan et al., 2007). With these details, we can more precisely capture the negative modulations involved in T cell proliferation and differentiation. The mechanisms involving IL-2 and Treg are summarized in Figure 7.1.

7.2.2 Signal transduction and differentiation

Although it's been verified that a single naive T cell can derive a heterogeneous progeny with effector and memory T cells (Gerlach et al., 2013; Buchholz et al., 2013), the process in which the decision is made and in which order each subtype arise are not known. In the current model, we use the product of the amount of specific pMHC on a DC and total binding time as a proxy to represent the overall stimulation that a T cell receives during the priming process, and employ a "signal-strength" model to determine its subsequent differentiation (similar to a signal accumulation idea). However, the signal a T cell receives is composed of three parts: TCR signal, co-stimulation and cytokine instruction. The three signals are all influenced by the activation status of DCs and are somewhat correlated, but still possess certain levels of independence. Furthermore, cytokines produced by other nearby cells also feed into the instructions for differentiation, and the influence continues as T cells proliferate after priming ends. Recently, progresses have been made to identify pathways that regulate T cell effector/memory fate decision (Kaech and Cui, 2012; Chang et al., 2014). The integration of signals from TCR, co-stimulation and cytokine initiate this process, inducing changes at metabolic and epigenetic level; however, no single "master regulator" associated with a memory differentiation state is found, and regulation is speculated to be carried out and maintained as a compound state of a network of transcription factors. The reasonable next step to explore the memory differentiation is to build a molecular systems biology model of this network to study its behaviors, and plug it into each individual model T cell. If we can successfully identify rules of thumb of how extracellular signals can control the meta-states of this network, a coarse-grain version of such model will then be plausible.

7.3 Future direction: immune model guided vaccine design: TB vaccine

As described in Chapter V, we started working towards a computational model that can facilitate TB vaccine design, with capabilities of testing its efficacy with *in silico* infection scenarios.

Our pilot study showed promising results, but additional work needs to be done before this model can have appropriate clinical relevance. First, we need to have a granuloma model that captures the process in which macrophages process and display Mtb antigens (i.e. have DCs explicitly represented) With this model, we can then track the spatio-temporal distribution of antigen-presentation profile at the site of infection, which would allow us to investigate what combination of antigen-specific T cells can effectively act in response. Secondly, we need a model to study mechanisms controlling the immunodominance hierarchy of T cell subsets generated as a result of multiple Mtb antigens.

7.3.1 TB antigen processing and presentation

Mtb express a range of immunogenic proteins, of which the composition varies during their lifecycle. One question we can address is which of these are suitable targets for adaptive immune cells at each stage of granuloma development. Previously, our group published works on interaction between Mtb and macrophage to study factors regulating Mtb antigen presentation, including host mechanisms to process antigen bacterial mechanisms to evade detection (Chang et al., 2005; Kirschner et al., 2007). In those studies, Mtb inhibition of antigen presentation is incorporated as proportional to the initial load of mycobacteria, which is essentially a fixed number. As we made significant progress over the years modeling granulomas, we are capable of not only measuring intracellular Mtb levels in each infected macrophage as a variable dependent on each granuloma trajectory, but also track the metabolic states of these microbes as discrete agents themselves (manuscript by P in preperation). It is time that we can revisit this issue and make more precise predictions of Mtb antigen presentation over time and in explicit spatial distributions, which will allow accurate prediction of amount and types of T cells needed to clear the infection.

7.3.2 Prime-boost series of simulated vaccination

When multiple antigens are involved in antigen presentation, the magnitude of each antigen specific T cell population arising from the resulting immune response is not proportional to the amount of input antigen, but can be poised to only a few or even only one particular antigen. This phenomenon is called immunodominance (Yewdell and Bennink, 1999). However, this hierarchy can be perturbed by a series of subsequent stimulations called "boosts" as opposed to the initial "prime" step (McShane and Hill, 2005). This technique is applied to the design of various vaccines used in practice (e.g. MMR vaccines are given 3 boosts as well as tetanus every 10 years). In addition to the current multiple antigen version of *LymphSim*, we need to obtain information about Mtb antigens with regard to their kinetics for forming complexes with MHC on DC and TCR on T cells. This will help design prime-boost series of proper combination of antigens to generate a mixture of memory T cells in correct numbers and phenotypes as predicted to be necessary in the previous section. Implementation of molecular scale details as described in Section 7.2 will further increase the accuracy of such prediction.

7.4 Future direction: host scale disease dynamics

The model of granuloma development by our group provides valuable insights into mechanisms governing host's control of the pathogen at tissue level. However, accumulating evidences indicate the disease outcome of an individual is the collective result of multiple granulomas through their interaction with the host immune system. We are working on methodologies to scale granuloma level outcomes to predict host level disease trajectories. In this process, employing a fine-grain LN sub-model to capture detailed events during the adaptive immune response can be helpful in multiple fronts.

7.4.1 Biomarker identification

One important property of TB is the majority of those infected with the pathogen are in a latent state without symptoms, and this population can reactivate with about 10% chance in their lifetime and thus serves as a reservoir of the disease (Lin and Flynn, 2010). The corresponding issue facing the management of this global TB epidemic is a lack of good biomarkers to help diagnose disease and predict its future development (Walzl et al., 2011). Our host scale multi-compartment model usually contains blood circulation as a separate compartment, which is perfect for biomarker discovery because it can be conveniently sampled in patients, and is a systemic reflection of the status of multiple granulomas as well as the activity of the immune system. In particular, the amount of information we preserve in the model system is largely determined by the complexity of LN ABM. If we model T cell differentiation as driven by explicit molecular scale events as discussed in Section 7.2, we can expect to recover memory subtype compositions, functional polarization and cytokine production profiles of Mtb specific T cells in the blood. If we include multiple Mtb antigens and their processing in APCs as discussed in Section 7.3, we can recover the natural immunodominance hierarchy of different antigen specificity in the immune response. Individually or in combinations, these statistics reflect the collective status of an infected host at the individual level. We can employ machine-learning techniques to find patterns in host datasets that can reveal current disease status and predict future development.

7.4.2 Granuloma development in ABM LN

Granulomas are observed to develop not only in the lung, but also in lung draining LNs as well (Chackerian et al., 2002; Lin et al., 2009), as shown in Figure 7.2. As described in Chapter VI, such phenomenon may have both potentially beneficial and harmful implications to the disease outlook of a host. Thus, exploring granuloma dynamics in LNs could be essential for predicting disease trajectories at a host scale. Even though our population model predicts practices that could promote

better disease outcomes, these suggestions are hardly directly translational in a quantitative sense due to the lack of mechanistic representation of events occurring on a fine-grain scale. To resolve this discrepancy, we can modify the current version of *LymphSim* to accommodate granuloma development occurring in LNs, and simulate LN infection dynamics. To this end, we need to first implement the same set of rules regarding Mtb-host cell interactions into *LymphSim*. Also, we need to look into which subsets of macrophages/DCs in the LN are susceptible to Mtb infection and are involved in granuloma development. Finally, we might need to connect the *LymphSim* ABM to one or more *GranSim* ABMs. This is because even though each granuloma is seeded by separate bacteria, they do not develop entirely independent of each other. The immune response generated by one granuloma will create a T cell population that can be recruited by all granulomas, so the fate of different granulomas are interconnected. With this model, we will be able to better understand the role of LN granuloma development and predict more specific targets for potential interventions.

Figures

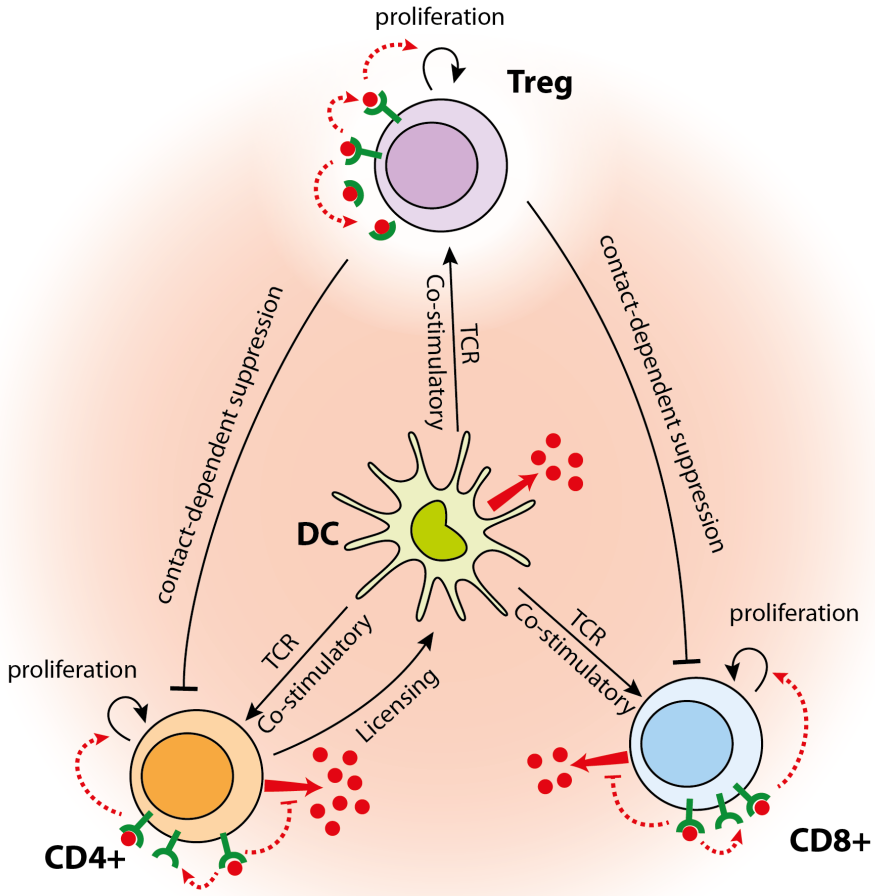

Figure 7.1: IL-2 and Treg are involved in CD4+ and CD8+ T cell proliferation after priming. Ab-DC is an antigen bearing DC that is presenting Ag to T cells.

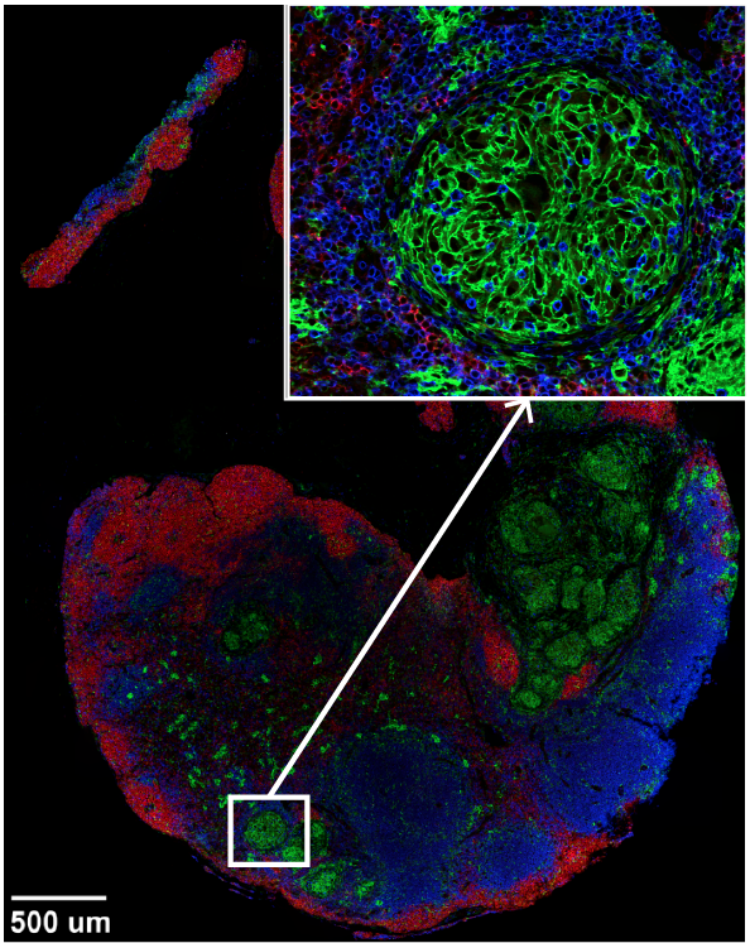

Figure 7.2: Granuloma in lymph nodes of non-human primates (courtesy of Flynn Lab). Stained for CD3 (blue; T cells), CD11c (green; DCs) and CD20 (red; B cells). On the insert panel, this is an enlargement of a granuloma.

Bibliography

Buchholz, V. R., Flossdorf, M., Hensel, I., Kretschmer, L., Weissbrich, B., Gräf, P., Verschoor, A., Schiemann, M., Höfer, T. and Busch, D. H. Disparate individual fates compose robust CD8+ T cell immunity. *Science*, 340(6132):630–635, 2013.

Chackerian, A. A., Alt, J. M., Perera, T. V., Dascher, C. C. and Behar, S. M. Dissemination of Mycobacterium tuberculosis Is Influenced by Host Factors and Precedes the Initiation of T-Cell Immunity. *Infection and Immunity*, 70(8):4501–4509, 2002.

Chang, J. T., Wherry, E. J. and Goldrath, A. W. Molecular regulation of effector and memory T cell differentiation. *Nature Immunology*, 15(12):1104–1115, 2014.

Chang, S. T., Linderman, J. J. and Kirschner, D. E. Multiple mechanisms allow Mycobacterium tuberculosis to continuously inhibit MHC class II-mediated antigen presentation by macrophages. *Proceedings of the National Academy of Sciences of the United States of America*, 102(12):4530–4535, 2005.

Cilfone, N. A., Perry, C. R., Kirschner, D. E. and Linderman, J. J. Multi-scale modeling predicts a balance of tumor necrosis factor-α and interleukin-10 controls the granuloma environment during Mycobacterium tuberculosis infection. *PloS one*, 8(7):e68680, 2013.

Coleman, M. T., Chen, R. Y., Lee, M., Lin, P. L., Dodd, L. E., Maiello, P., Via, L. E., Kim, Y., Marriner, G., Dartois, V., Scanga, C., Janssen, C., Wang, J., Klein, E., Cho, S. N., Barry 3rd, C. E. and Flynn, J. L. PET/CT imaging reveals a therapeutic response to oxazolidinones in macaques and humans with tuberculosis. *Sci Transl Med*, 6(265):265ra167, 2014.

Curotto de Lafaille, M. A. and Lafaille, J. J. Natural and adaptive foxp3+ regulatory T cells: more of the same or a division of labor? *Immunity*, 30(5):626–35, 2009.

Fallahi-Sichani, M., Flynn, J. L., Linderman, J. J. and Kirschner, D. E. Differential risk of tuberculosis reactivation among anti-TNF therapies is due to drug binding kinetics and permeability. *Journal of immunology (Baltimore, Md. : 1950)*, 188(7):3169–78, 2012a.

Fallahi-Sichani, M., Kirschner, D. E. and Linderman, J. J. NF-κB Signaling Dynamics Play a Key Role in Infection Control in Tuberculosis. *Frontiers in physiology*, 3:170, 2012b.

Fallahi-Sichani, M., Schaller, M. A., Kirschner, D. E., Kunkel, S. L. and Linderman, J. J. Identification of key processes that control tumor necrosis factor availability in a tuberculosis granuloma. *PLoS computational biology*, 6(5):e1000778, 2010.

Gerlach, C., Rohr, J. C., Perié, L., van Rooij, N., van Heijst, J. W. J., Velds, A., Urbanus, J., Naik, S. H., Jacobs, H., Beltman, J. B., de Boer, R. J. and Schumacher, T. N. M. Heterogeneous differentiation patterns of individual CD8+ T cells. *Science*, 340(6132):635–639, 2013.

Gong, C., Linderman, J. J. and Kirschner, D. Harnessing the heterogeneity of T cell differentiation fate to fine-tune generation of effector and memory T cells. *Frontiers in immunology*, 5:57, 2014.

Gong, C., Mattila, J. T., Miller, M., Flynn, J. L., Linderman, J. J. and Kirschner, D. Predicting lymph node output efficiency using systems biology. *Journal of theoretical biology*, 335:169–184, 2013.

Granucci, F., Vizzardelli, C., Pavelka, N., Feau, S., Persico, M., Virzi, E., Rescigno, M., Moro, G. and Ricciardi-Castagnoli, P. Inducible IL-2 production by dendritic cells revealed by global gene expression analysis. *Nature immunology*, 2(9):882–888, 2001.

Hsieh, C.-S., Zheng, Y., Liang, Y., Fontenot, J. D. and Rudensky, A. Y. An intersection between the self-reactive regulatory and nonregulatory T cell receptor repertoires. *Nature immunology*, 7(4):401–410, 2006.

Jonuleit, H., Schmitt, E., Kakirman, H., Stassen, M., Knop, J. and Enk, A. H. Infectious Tolerance: Human CD25+ Regulatory T Cells Convey Suppressor Activity to Conventional CD4+ T Helper Cells. 2002.

Kaech, S. M. and Cui, W. Transcriptional control of effector and memory CD8+ T cell differentiation. *Nature reviews. Immunology*, 12(11):749–761, 2012.

Kirschner, D. E., Chang, S. T., Riggs, T. W., Perry, N. and Linderman, J. J. Toward a multiscale model of antigen presentation in immunity. *Immunological Reviews*, 216(1):93–118, 2007.

Lin, P. L. and Flynn, J. L. Understanding latent tuberculosis: a moving target. *Journal of immunology (Baltimore, Md. : 1950)*, 185(1):15–22, 2010.

Lin, P. L., Ford, C. B., Coleman, M. T., Myers, A. J., Gawande, R., Ioerger, T., Sacchettini, J., Fortune, S. M. and Flynn, J. L. Sterilization of granulomas is common in active and latent tuberculosis despite within-host variability in bacterial killing. *Nature medicine*, 20(1):75–79, 2014.

Lin, P. L., Rodgers, M., Smith, L., Bigbee, M., Myers, A., Bigbee, C., Chiosea, I., Capuano, S. V., Fuhrman, C., Klein, E. and Flynn, J. L. Quantitative comparison of active and latent tuberculosis in the cynomolgus macaque model. *Infection and immunity*, 77(10):4631–4642, 2009.

Malek, T. R. The biology of interleukin-2. *Annu Rev Immunol*, 26:453–79, 2008.

Marino, S., El-Kebir, M. and Kirschner, D. A hybrid multi-compartment model of granuloma formation and T cell priming in tuberculosis. *Journal of theoretical biology*, 280(1):50–62, 2011.

Marino, S., Linderman, J. J. and Kirschner, D. E. A multifaceted approach to modeling the im-

mune response in tuberculosis. *Wiley interdisciplinary reviews. Systems biology and medicine*, 3(4):479–89, 2010.

McShane, H. and Hill, A. Prime-boost immunisation strategies for tuberculosis. 2005.

Miller, M. J., Safrina, O., Parker, I. and Cahalan, M. D. Imaging the single cell dynamics of CD4+ T cell activation by dendritic cells in lymph nodes. *The Journal of experimental medicine*, 200(7):847–856, 2004.

Miller, M. J., Wei, S. H., Cahalan, M. D. and Parker, I. Autonomous T cell trafficking examined in vivo with intravital two-photon microscopy. *Proceedings of the National Academy of Sciences of the United States of America*, 100(5):2604–2609, 2003.

Paliard, X., de Waal Malefijt, R., Yssel, H., Blanchard, D., Chrétien, I., Abrams, J., de Vries, J. and Spits, H. Simultaneous production of IL-2, IL-4, and IFN-gamma by activated human CD4+ and CD8+ T cell clones. *Journal of immunology (Baltimore, Md. : 1950)*, 141(3):849–855, 1988.

Pandiyan, P., Zheng, L., Ishihara, S., Reed, J. and Lenardo, M. J. CD4+CD25+Foxp3+ regulatory T cells induce cytokine deprivation-mediated apoptosis of effector CD4+ T cells. *Nature immunology*, 8(12):1353–1362, 2007.

Piccirillo, C. A. and Shevach, E. M. Naturally-occurring CD4+CD25+ immunoregulatory T cells: central players in the arena of peripheral tolerance. *Seminars in Immunology*, 16(2):81–88, 2004.

Segovia-Juarez, J. L., Ganguli, S. and Kirschner, D. Identifying control mechanisms of granuloma formation during M. tuberculosis infection using an agent-based model. *Journal of theoretical biology*, 231(3):357–76, 2004.

Sprent, J., Cho, J.-H., Boyman, O. and Surh, C. D. T cell homeostasis. *Immunology and cell biology*, 86(4):312–9, 2008.

Strauss, L., Bergmann, C. and Whiteside, T. L. Human circulating CD4+CD25highFoxp3+ regulatory T cells kill autologous CD8+ but not CD4+ responder cells by Fas-mediated apoptosis. *Journal of immunology (Baltimore, Md. : 1950)*, 182(3):1469–1480, 2009.

Walzl, G., Ronacher, K., Hanekom, W., Scriba, T. J. and Zumla, A. Immunological biomarkers of tuberculosis. *Nature reviews. Immunology*, 11(5):343–354, 2011.

WHO. *Global Tuberculosis Report 2014*. World Health Organization, 2014.

Yewdell, J. W. and Bennink, J. R. Immunodominance in major histocompatibility complex class I-restricted T lymphocyte responses. *Annual review of immunology*, 17:51–88, 1999.

APPENDIX A

Supplemental material for Chapter II

A.1 LNSim parameter values

Table A.1: Parameter values of LNSim

	Parameter	Baseline LHS	Priming LHS	Description
	General			
§	probMovePreferredDir	0.6 0.9	0.8	Probability of moving into preferred directions
§	probMoveNonOppositeDir	0.95 0.99	0.95	Probability not moving into opposite directions
§	probMovePreferredDirBlock	0.5 0.8	0.6	Probability of moving into preferred directions after being blocked
§	probMoveNonOppositeDirBlock	0.9 0.95	0.92	Probability not moving into opposite directions after being blocked
	ratio CD8+ to CD4+	NA	0.5 (Latif et al., 2001)	Ratio of the number of CD4+ T cells to that of CD8+ T cells
	binding radius	2 (Miller et al., 2004a)	2	T cells within this range can bind to DCs
	CD4+ T cell			
	min age	165 (McCune et al., 2000)	165	Minimum age of naive CD4+ T cell when recruited (days)
	max age	365 (McCune et al., 2000)	365	Maximum age of naive CD4+ T cell (days)
	max age stdev	15	15	Standard deviation of max age (days)
+	binding threshold	150 (Demotz et al., 1990)	100 300	pMHC-II level corresponding to 50% CD4+ T cell binding probability
+	binding shape	15	10 50	Shape parameter for CD4+ T cell binding probability curve
+	max bind time	16	5 20	Max time CD4+ T cell bind to DCs (hrs)
	max bind time stdev	4	4	Standard deviation of max bind time (hrs)

Table A.1 Continued

	Parameter	Baseline LHS	Priming LHS	Description
+	priming threshold	2000	1000 3000	pMHC-II level corresponding to 50% CD4+ T cell priming probability (hrs)
+	priming shape	200	100 300	Shape parameter for CD4+ T cell priming probability curve (hrs)
	max time active	96	96	Maximum lifetime of active CD4+ T cells (hrs)
	max time active stdev	4	4	Standard deviation of max time active (hrs)
	Number of division	4 (Miller et al., 2004b; Foulds et al., 2002)	4	Number divisions CD4+ T cells are allowed before exiting the LN
	double time	8 (Linderman et al., 2010)	8	Time it takes to divide (hrs)
	max time effector	60 (Sprent and Tough, 2001)	60	Maximum lifetime of effector CD4+ T cells (hrs)
	max time effector stdev	1	1	Standard deviation of max time effector (hrs)
§	recruitment prob.	0.15 0.4	0.26	Probability of naive CD4+ T cell recruitment each time step
	initializing prob.	0.422*	0.422	Probability that an empty grid compartment is initialized as naive CD4+ T cell
	cognate frequency	$3.3. \times 10^{-3}$	1.0×10^{-4} (Casrouge et al., 2000; Blattman et al., 2002)	Frequency of cognate CD4+ T cells
	CD8+ T cell			
	min age	165 (McCune et al., 2000)	165	Minimum age of naive CD8+ T cell when recruited (days)
	max age	365 (McCune et al., 2000)	365	Maximum age of naive CD8+ T cell (days)
	max age stdev	15	15	Standard deviation of max age (days)
+	binding threshold	150 (Henrickson et al., 2008)	100 300	pMHC-I level corresponding to 50% CD8+ T cell binding probability
+	binding shape	15	10 50	Shape parameter for CD8+ T cell binding probability curve
+	max bind time	16	5 20	Max time CD8+ T cell bind to DCs (hrs)
	max bind time stdev	4	4	Standard deviation of max bind time (hrs)
+	priming threshold	2000	1000 3000	pMHC-I level corresponding to 50% CD8+ T cell priming probability (hrs)
+	priming shape	200	100 300	Shape parameter for CD8+ T cell priming probability curve (hrs)
	max time active	96	96	Maximum lifetime of active CD8+ T cells (hrs)
	max time active stdev	4	4	Standard deviation of max time active (hrs)

Table A.1 Continued

	Parameter	Baseline LHS	Priming LHS	Description
	max division	8 (Miller et al., 2004a)	8	Number divisions CD8+ T cells are allowed before exiting the LN
	double time	8 (Linderman et al., 2010)	8	Time it takes to divide (hrs)
	max time effector	60 (Sprent and Tough, 2001)	60	Maximum lifetime of effector CD8+ T cells (hrs)
	max time effector stdev	1	1	Standard deviation of max time effector (hrs)
§	recruitment prob.	0.075 0.2	0.13	Probability of naive CD8+ T cell recruitment each time step
	initializing prob.	0.211*	0.211	Probability that an empty grid compartment is initialized as naive CD8+ T cell
	cognate frequency	$3.3. \times 10^{-3}$	1.0×10^{-4} (Casrouge et al., 2000; Blattman et al., 2002)	Frequency of cognate CD8+ T cells
DC				
	min age	1 (Kamath et al., 2002)	1	Minimum age of IDC when recruited (days)
	max age	11 (Kamath et al., 2002)	11	Maximum age of IDC (days)
	max age stdev	2	2	Standard deviation of max age (days)
+	IDC mature pMHC increment	50	50 200	Increment of pMHC when an IDC is activated
	IDC MDC threshold	50 (Linderman et al., 2010)	50	Boundary of pMHC-II level below which a DC is IDC
+	pMHC-I half life	25 (Cella et al., 1997)	10 100	Half life of pMHC-I (hrs)
+	pMHC-II half life	100 (Cella et al., 1997)	20 200	Half life of pMHC-II (hrs)
+	unbinding threshold	100	75 150	pMHC-I/II level below which a CD8+/CD4+ T cell unbind the DC
	mature ave age entry	20	20	Average age of Ag-DC when recruited
	max time mature	60 (Kamath et al., 2002)	60	Maximum age of Ag-DC (hrs)
	max time mature stdev	5	5	Standard deviation of max time mature (hrs)
+	licensing prob.	0.005	0.001 0.1	Probability that an effector CD4+ T cell licenses Ag-DC
	max time licensed	36 (Lanzavecchia and Sallusto, 2004; Lindquist et al., 2004)	36	Maximum age of LDC (hrs)
	max time licensed stdev	4	4	Standard deviation of LDC (hrs)
	recruitment prob.	1	0.06	Probability that an DC is recruited each time step
	initialization prob.	0.00115	0.00115	Probability that an empty grid compartment is initialized as IDC

Table A.1 Continued

	Parameter	Baseline LHS	Priming LHS	Description
+	IDC activation prob.	0.01	0.001 0.1	Probability that an Ag-DC or LDC activates IDC
	movement interval	4 (Miller et al., 2004b)	4	Number of time steps between each DC movement
	Ag-DC recruit start	NA	5	The day when Ag-DC begins to be recruited
	Ag-DC recruit end	NA	10 (acute) / 0 (chronic)	The day when Ag-DC stops being recruited
	recruit interval	35	1	Time step interval to recruit DCs
	recruit top slice	159	159	Top grid slice that DC is recruited
	recruit bottom slice	85	85	Bottom grid slice that DC is recruited
	recruit count	2	1	Number of DCs recruited each time
	size	2	2	Size of DC in each dimension
	max number DC	400	400	DC recruitment pauses when DC number exceeds this point
	number DC resting	40	40	Expected number of IDC at resting stage
	Ports			
§	HEV count	100 300	180	Number of HEV port
	HEV top	157*	157	Top slice allowed to generate HEV ports
	HEV bottom	50*	50	Bottom slice allowed to generate HEV ports
§	EL count	100 300	300	Number of exit ports
§	EL top	50 100	77	Top slice allowed to generate exit ports

§Varied in baseline LHS; + Varied in priming focused LHS; * Estimated from data

Bibliography

Blattman, J. N., Antia, R., Sourdive, D. J. D., Wang, X., Kaech, S. M., Murali-Krishna, K., Altman, J. D. and Ahmed, R. Estimating the precursor frequency of naive antigen-specific CD8 T cells. *The Journal of experimental medicine*, 195(5):657–664, 2002.

Casrouge, A., Beaudoing, E., Dalle, S., Pannetier, C., Kanellopoulos, J. and Kourilsky, P. Size estimate of the alpha beta TCR repertoire of naive mouse splenocytes. *Journal of immunology (Baltimore, Md. : 1950)*, 164(11):5782–5787, 2000.

Cella, M., Engering, A., Pinet, V., Pieters, J. and Lanzavecchia, A. Inflammatory stimuli induce accumulation of MHC class II complexes on dendritic cells. *Nature*, 388(6644):782–787, 1997.

Demotz, S., Grey, H. and Sette, A. The minimal number of class II MHC-antigen complexes needed for T cell activation. *Science*, 249(4972):1028–1030, 1990.

Foulds, K. E., Zenewicz, L. A., Shedlock, D. J., Jiang, J., Troy, A. E. and Shen, H. Cutting edge: CD4 and CD8 T cells are intrinsically different in their proliferative responses. *Journal of immunology (Baltimore, Md. : 1950)*, 168(4):1528–1532, 2002.

Henrickson, S. E., Mempel, T. R., Mazo, I. B., Liu, B., Artyomov, M. N., Zheng, H., Peixoto, A., Flynn, M. P., Senman, B., Junt, T., Wong, H. C., Chakraborty, A. K. and von Andrian, U. H. T cell sensing of antigen dose governs interactive behavior with dendritic cells and sets a threshold for T cell activation. *Nature immunology*, 9(3):282–291, 2008.

Kamath, A. T., Henri, S., Battye, F., Tough, D. F. and Shortman, K. Developmental kinetics and lifespan of dendritic cells in mouse lymphoid organs. *Blood*, 100(5):1734–1741, 2002.

Lanzavecchia, A. and Sallusto, F. Lead and follow: the dance of the dendritic cell and T cell. *Nature immunology*, 5(12):1201–1202, 2004.

Latif, R., de Rosbo, N., Amarant, T., Rappuoli, R., Sappler, G. and Ben-Nun, A. Reversal of the CD4(+)/CD8(+) T-cell ratio in lymph node cells upon in vitro mitogenic stimulation by highly purified, water-soluble S3-S4 dimer of pertussis toxin. *Infection and immunity*, 69(5):3073–3081, 2001.

Linderman, J. J., Riggs, T., Pande, M., Miller, M., Marino, S. and Kirschner, D. E. Characterizing the dynamics of CD4+ T cell priming within a lymph node. *Journal of immunology (Baltimore, Md. : 1950)*, 184(6):2873–2885, 2010.

Lindquist, R. L., Shakhar, G., Dudziak, D., Wardemann, H., Eisenreich, T., Dustin, M. L. and Nussenzweig, M. C. Visualizing dendritic cell networks in vivo. *Nature immunology*, 5(12):1243–1250, 2004.

McCune, J. M., Hanley, M. B., Cesar, D., Halvorsen, R., Hoh, R., Schmidt, D., Wieder, E., Deeks, S., Siler, S., Neese, R. and Hellerstein, M. Factors influencing T-cell turnover in HIV-1-seropositive patients. *The Journal of clinical investigation*, 105(5):R1–8, 2000.

Miller, M. J., Hejazi, A. S., Wei, S. H., Cahalan, M. D. and Parker, I. T cell repertoire scanning is promoted by dynamic dendritic cell behavior and random T cell motility in the lymph node. *Proceedings of the National Academy of Sciences of the United States of America*, 101(4):998–1003, 2004a.

Miller, M. J., Safrina, O., Parker, I. and Cahalan, M. D. Imaging the single cell dynamics of CD4+ T cell activation by dendritic cells in lymph nodes. *The Journal of experimental medicine*, 200(7):847–856, 2004b.

Sprent, J. and Tough, D. F. T cell death and memory. *Science*, 293(5528):245–248, 2001.

APPENDIX B

Supplemental material for Chapter I

B.1 ODE blood sub-model: equations

Dynamics of naive, effector, central memory and effector memory CD4+ T cells:

$$\frac{dN_4}{dt} = s_{N4}(t) - \delta_{N4}N_4 + e^{LN}_{N4} \tag{B.1}$$

$$\frac{dE_4}{dt} = -\delta_{E4}E_4 - \xi_{E4}E_4 + e^{LN}_{E4} \tag{B.2}$$

$$\frac{dCM_4}{dt} = -\delta_{CM4}CM_4 + \alpha_{EM4}EM_4 + e^{LN}_{CM4} \tag{B.3}$$

$$\frac{dEM_4}{dt} = -\delta_{EM4}EM_4 - \xi_{E4}E_4 - \alpha_{EM4}EM_4 + e^{LN}_{E4} \tag{B.4}$$

Dynamics of naive, effector, central memory and effector memory CD8+ T cells:

$$\frac{dN_8}{dt} = s_{N8}(t) - \delta_{N8}N_8 + e^{LN}_{N8} \tag{B.5}$$

$$\frac{dE_8}{dt} = -\delta_{E8}E_8 - \xi_{E8}E_8 + e^{LN}_{E8} \tag{B.6}$$

$$\frac{dCM_8}{dt} = -\delta_{CM8}CM_8 + \alpha_{EM8}EM_8 + e^{LN}_{CM8} \tag{B.7}$$

$$\frac{dEM_8}{dt} = -\delta_{EM8}EM_8 - \xi_{E8}E_8 - \alpha_{EM8}EM_8 + e^{LN}_{E8} \tag{B.8}$$

For Equation B.1 and B.5 respectively (t is time in day): e_{N4}^{LN}, e_{E4}^{LN}, e_{CM4}^{LN}, e_{EM4}^{LN}, e_{N8}^{Ln}, e_{E8}^{LN}, e_{CM8}^{LN}, e_{EM8}^{LN} are the blood concentration changes converted from LN net output of corresponding cells. For naive and CM cells, this is the difference between the number of exited and recruited cell, per time step. For effector and EM cells, this is the number of exited cells per time step. These eight terms are not solved in the ODE system but rather are added as an initial condition before each blood time step is processed in the computational model.

B.2 LNSim-blood parameter values and initial conditions

This table lists all parameter values in the models. Listed first are parameters governing T cell motility and trafficking within a LN (marked with⊥); these include number and location of LN entrance and exit ports (HEVs and ELs). These values were determined in our previous study (Gong et al., 2013). In this work, we added memory cells of different classes. To estimate parameters related to CD8+T cell proliferation and both CD4+ and CD8+ T cell memory differentiation (marked with ♮) we varied them to fit the model to experimental data (See Section 4.2.5 in the paper). The parameter set obtained from these different sources was then used as our infection baseline (Baseline Values column in the table below). All other parameters were fixed at their values in the previous study (Gong et al., 2013). In addition to parameter estimation, we perform sensitivity analyses to explore different model features. To this end, we chose two unique sets of parameters to be studied in intra- and inter- compartment sensitivity analyses (i.e. LN and blood related sensitivity analyses, marked with + and §, respectively). The range of the parameters varied in these analyses are shown in the Value or Range in Sensitivity Analysis column of Table B.1.

Table B.1: Parameter values of LNSim-blood

Parameter	Baseline Value	Value or Range in Sensitivity Analysis	Description
Parameter General			
⊥ probMovePreferredDir	0.85	0.85	Probability of moving into preferred directions

Table B.1 Continued

Parameter		Baseline Value	Value or Range in Sensitivity Analysis	Description
⊥	probMoveNonOppositeDir	0.95	0.95	Probability of not moving into opposite directions
⊥	probMovePreferredDirBlock	0.6	0.6	Probability of moving into preferred directions after being blocked
⊥	probMoveNonOppositeDirBlock	0.92	0.92	Probability of not moving into opposite directions after being blocked
	binding radius	2 (Miller et al., 2004a)	2	T cells within this range can bind to DCs
CD4+ T cell				
	average life naive (day)	365 (McCune et al., 2000)	365 (McCune et al., 2000)	Average lifetime of naive CD4+ T cell
+	binding checkpoint threshold	150 (Demotz et al., 1990)	100 200	pMHC-II level corresponding to 50% CD4+ T cell binding probability
	binding checkpoint shape	15	15	Shape of curve parameter for CD4+ T cell binding probability curve
+/♮	max bind time (hour)	12	6 20	Time CD4+ T cell bind to DCs
	max bind time stdev (hour)	4	4	Standard deviation of binding time
+	max CM bind time (min)	30	20 60	Time CM CD4+ T cell bind to DCs
	max CM bind time stdev (min)	10	10	Standard deviation of CM binding time
+/♮	priming checkpoint threshold (hour)	1000	500 - 2000	pMHC-II level corresponding to 50% CD4+ T cell priming probability
♮	priming checkpoint shape (hour)	100	150	Shape of curve parameter for CD4+ T cell priming probability curve
	average time active (hour)	96	96	Average lifetime of active CD4+ T cells
	minimum number of divisions	4 (Miller et al., 2004b; Foulds et al., 2002)	4	Number divisions CD4+ T cells are allowed before differentiating into effector T cells
	maximum number of divisions	20	8	Maximum number of divisions allowed by CD4 T cells
	double time (hour)	6 (Linderman et al., 2010)	8	Time interval between two divisions
+/♮	effector checkpoint threshold (hour)	2000	2000 4000	pMHC-II level corresponding to 50% probability CD4+ T cell entering effector state
♮	effector checkpoint shape (hour)	500	300	Shape of curve parameter for CD4+ T cell (probability curve of entering effector state)
	average time effector (hour)	60 (Sprent and Tough, 2001)	60	Average lifetime of effector CD4+ T cells
	cognate frequency	1.0×10^{-4} (Casrouge et al., 2000; Blattman et al., 2002)	1.0×10^{-4}	Frequency of cognate CD4+ T cells
+	extra recruitment	1.25	1 1.5	Extra recruitment during an immune response

Table B.1 Continued

	Parameter	Baseline Value	Value or Range in Sensitivity Analysis	Description
+/♮	efficiency CM	6	5 20	Efficiency of CM to accumulate DC signals
+/♮	probability EM	0.1	0.025 0.4	Probability of daughter cells differentiating into EM after effector T cell division
CD8+ T cell				
	average life naive (day)	365 (McCune et al., 2000)	365	Average lifetime of naive CD8+ T cell
+	binding checkpoint threshold	150 (Henrickson et al., 2008)	100 200	pMHC-I level corresponding to 50% CD8+ T cell binding probability
	binding checkpoint shape	15	15	Shape parameter for CD8+ T cell binding probability curve
+/♮	max bind time (hour)	12	6 20	Time CD8+ T cell bind to DCs
	max bind time stdev (hour)	4	4	Standard deviation of binding time
+	max CM bind time (min)	30	20 60	Time CM CD8+ T cell bind to DCs
	max CM bind time stdev (min)	10	10	Standard deviation of CM binding time
+/♮	priming checkpoint threshold (hour)	1000	500 - 2000	pMHC-I level corresponding to 50% CD8+ T cell priming probability
♮	priming checkpoint shape (hour)	100	150	Shape parameter for CD8+ T cell priming probability curve
	average time active (hour)	96	96	Average lifetime of active CD8+ T cells
♮	minimum number of divisions	4 (Miller et al., 2004a)	4	Number divisions CD8+ T cells are allowed before advancing to effectors
♮	maximum number of divisions	20	20	Maximum number of divisions allowed
♮	double time (hour)	6 (Linderman et al., 2010)	6	Time interval between two divisions
+/♮	effector checkpoint threshold (hour)	2000	1500 - 3000	pMHC-I level corresponding to 50% probability CD8+ T cell entering effector state
♮	effector checkpoint shape (hour)	500	500	Shape parameter for CD8+ T cell probability curve of differentiating into effector state
	average time effector (hour)	60 (Sprent and Tough, 2001)	60	Average lifetime of effector CD8+ T cells
	cognate frequency	1.0×10^{-4} (Casrouge et al., 2000; Blattman et al., 2002)	1.0×10^{-4}	Frequency of cognate CD8+ T cells
+	extra recruitment	1.25	1 1.5	Extra recruitment during an immune response
+/♮	efficiency CM	6	5 20	Efficiency of CM to accumulate DC signals
+/♮	probability EM	0.1	0.025 - 0.4	Probability of daughter cells differentiating into EM after effector T cell division
DC				

Table B.1 Continued

	Parameter	Baseline Value	Value or Range in Sensitivity Analysis	Description
	min life immature (day)	60 (Kamath et al., 2002)	5	Average lifetime of IDC
	IDC mature pMHC increment	150	150	Increment of pMHC when an IDC is activated
	IDC MDC threshold	50 (Linderman et al., 2010)	50	Boundary of pMHC-II level below which a DC is IDC
+	pMHC-I half life (hour)	25 (Cella et al., 1997)	10 - 100	Half life of pMHC-I
+	pMHC-II half life (hour)	100 (Cella et al., 1997)	20 - 200	Half life of pMHC-II
	unbinding threshold	100	100	pMHC-I/II level below which a CD8/CD4+ T cell unbind the DC
	mature ave age entry (hour)	20	20	Average age of Ag-DC when recruited
	max time mature (hour)	60 (Kamath et al., 2002)	60	Maximum age of Ag-DC
	max time mature stdev (hour)	5	5	Standard deviation of max time mature
+	licensing prob.	0.005	0.001 - 0.1	Probability that an effector CD4+ T cell licenses Ag-DC
	max time licensed (hour)	36 (Lanzavecchia and Sallusto, 2004; Lindquist et al., 2004)	36	Maximum age of LDC
	max time licensed stdev (hour)	4	4	Standard deviation of LDC
	recruitment prob.	0.03	0.03	Probability that an DC is recruited each time step
+	IDC activation prob.	0.01	0.001 - 0.2	Probability that an Ag-DC or LDC activates IDC
	movement interval	4 (Miller et al., 2004b)	4	Number of time steps between each DC movement
	Ag-DC recruit start (day)	3	3	Ag-DC recruitment starting time
	Ag-DC recruit end (day)	5	5	Ag-DC recruitment ending time
	recall response Ag-DC start (day)	603	303	Recall response Ag-DC recruitment starting time
	recall response Ag-DC start (day)	605	305	Recall response Ag- DC recruitment ending time
⊥	recruit top slice	159	159	Top grid slice that DC is recruited
⊥	recruit bottom slice	85	85	Bottom grid slice that DC is recruited
	size	2	2	Size of DC in each dimension
	max number DC	200	200	DC recruitment pauses when DC number exceeds this point
	number DC resting	20	20	Expected number of IDC at resting stage
	Ports			
⊥	HEV count	100 300	180	Number of HEV port
⊥	HEV top	154	154	Top slice allowed to generate HEV ports

Table B.1 Continued

	Parameter	Baseline Value	Value or Range in Sensitivity Analysis	Description
⊥	HEV bottom	50	50	Bottom slice allowed to generate HEV ports
⊥	EL count	300	300	Number of exit ports
⊥	EL top	77	77	Top slice allowed to generate exit ports
	Blood Initial Conditions			
	$N_4(0)$ $(cell \cdot mm^{-3})$	(Bajaria et al., 2002)	450	Initial concentration of naive CD4+ T cells
	$E_4(0)$ $(cell \cdot mm^{-3})$	0	0	Initial concentration of effector CD4+ T cells
	$CM_4(0)$ $(cell \cdot mm^{-3})$	0	0	Initial concentration of CM CD4+ T cells
	$EM_4(0)$ $(cell \cdot mm^{-3})$	0	0	Initial concentration of EM CD4+ T cells
	$N_8(0)$ $(cell \cdot mm^{-3})$	(Roederer et al., 1995)	320	Initial concentration of naive CD8+ T cells
	$E_8(0)$ $(cell \cdot mm^{-3})$	0	0	Initial concentration of effector CD8+ T cells
	$CM_8(0)$ $(cell \cdot mm^{-3})$	0	0	Initial concentration of CM CD8+ T cells
	$EM_8(0)$ $(cell \cdot mm^{-3})$	0	0	Initial concentration of EM CD8+ T cells
	s_{N4} $(cell \cdot mm^{-3} day^{-1})$	0.272 (Bains et al., 2009)	0.272	Initial thymus output of CD4
	s_{N8} $(cell \cdot mm^{-3} day^{-1})$	0.128 (Clark et al., 1999; Jamieson et al., 1999)	0.128	Initial thymus output of CD8
	Blood			
⊥	Naive CD4+ recruit prob. (mm^3)	0.00058	0.00058	Recruitment probability of naive CD4
♮	CM CD4+ recruit prob. (mm^3)	0.0029	0.0029	Recruitment probability of CM CD4
⊥	Naive CD8+ recruit prob. (mm^3)	0.000408	0.000408	Recruitment probability of naive CD8
♮	CM CD8+ recruit prob. (mm^3)	0.00204	0.00204	Recruitment probability of CM CD8
	δ_{N4} (day^{-1})	0.0006	0.0006	Naive CD4+ death rate
	δ_{E4} (day^{-1})	0.2	0.2	Effector CD4+ death rate
	δ_{CM4} (day^{-1})	0.0017 (Homann et al., 2001)	0.0017	CM CD4+ death rate
	δ_{EM4} (day^{-1})	0.04 (Homann et al., 2001)	0.04	EM CD4+ death rate
	δ_{N8} (day^{-1})	0.0004	0.0004	Naive CD8+ death rate
	δ_{E8} (day^{-1})	0.2	0.2	Effector CD8+ death rate
	δ_{CM8} (day^{-1})	0.0001	0.0001	CM CD8+ death rate
	δ_{EM8} (day^{-1})	0.0188 (Ely et al., 2003)	0.018	EM CD8+ death rate
§	ξ_{E4} (day^{-1})	0.02	0.1 - 0.4	Recruitment rate of effector CD4+ to sites of infection
§	ξ_{EM4} (day^{-1})	0.01	0.05 - 0.2	Recruitment rate of EM CD4+ to sites of infection

Table B.1 Continued

	Parameter	Baseline Value	Value or Range in Sensitivity Analysis	Description
§	ξ_{E8} (day^{-1})	0.02	0.1 - 0.4	Recruitment rate of effector CD8+ to sites of infection
§	ξ_{EM8} (day^{-1})	0.01	0.05 - 0.2	Recruitment rate of EM CD8+ to sites of infection
§	α_{EM4} (day^{-1})	0.001	0.001 - 0.1	EM to CM conversion rate of CD4
§	α_{EM8} (day^{-1})	0.0188 (Wherry et al., 2003)	0.005 - 0.1	EM to CM conversion rate of CD8
	e_{N4}^{LN} $(cell \cdot mm^{-3} timestep^{-1})$	Calculated during simulation		Net LN naive CD4+ output converted to change in blood concentration per time step
	e_{E4}^{LN} $(cell \cdot mm^{-3} timestep^{-1})$	Calculated during simulation		Net LN effector CD4+ output converted to change in blood concentration per time step
	e_{CM4}^{LN} $(cell \cdot mm^{-3} timestep^{-1})$	Calculated during simulation		Net LN CM CD4+ output converted to change in blood concentration per time step
	e_{EM4}^{LN} $(cell \cdot mm^{-3} timestep^{-1})$	Calculated during simulation		Net LN EM CD4+ output converted to change in blood concentration per time step
	e_{N8}^{LN} $(cell \cdot mm^{-3} timestep^{-1})$	Calculated during simulation		Net LN naive CD8+ output converted to change in blood concentration per time step
	e_{E8}^{LN} $(cell \cdot mm^{-3} timestep^{-1})$	Calculated during simulation		Net LN effector CD8+ output converted to change in blood concentration per time step
	e_{CM8}^{LN} $(cell \cdot mm^{-3} timestep^{-1})$	Calculated during simulation		Net LN CM CD8+ output converted to change in blood concentration per time step
	e_{EM8}^{LN} $(cell \cdot mm^{-3} timestep^{-1})$	Calculated during simulation		Net LN EM CD8+ output converted to change in blood concentration per time step
	LN to blood factor	200	200	Scaling factor from model section to one LN

+Varied in LN related sensitivity analysis; §varied in blood related sensitivity analysis.

Bibliography

Bains, I., Antia, R., Callard, R. and Yates, A. J. Quantifying the development of the peripheral naive CD4+ T-cell pool in humans. *Blood*, 113(22):5480–5487, 2009.

Bajaria, S. H., Webb, G., Cloyd, M. and Kirschner, D. Dynamics of naive and memory CD4+ T lymphocytes in HIV-1 disease progression. *Journal of acquired immune deficiency syndromes*, 30(1):41–58, 2002.

Blattman, J. N., Antia, R., Sourdive, D. J. D., Wang, X., Kaech, S. M., Murali-Krishna, K., Altman, J. D. and Ahmed, R. Estimating the precursor frequency of naive antigen-specific CD8 T cells. *The Journal of experimental medicine*, 195(5):657–664, 2002.

Casrouge, A., Beaudoing, E., Dalle, S., Pannetier, C., Kanellopoulos, J. and Kourilsky, P. Size estimate of the alpha beta TCR repertoire of naive mouse splenocytes. *Journal of immunology (Baltimore, Md. : 1950)*, 164(11):5782–5787, 2000.

Cella, M., Engering, A., Pinet, V., Pieters, J. and Lanzavecchia, A. Inflammatory stimuli induce accumulation of MHC class II complexes on dendritic cells. *Nature*, 388(6644):782–787, 1997.

Clark, D., de Boer, R. J., Wolthers, K. and Miedema, F. T cell dynamics in HIV-1 infection. *advances in immunology*, 73:301–327, 1999.

Demotz, S., Grey, H. and Sette, A. The minimal number of class II MHC-antigen complexes needed for T cell activation. *Science*, 249(4972):1028–1030, 1990.

Ely, K. H., Roberts, A. D. and Woodland, D. L. Cutting edge: effector memory CD8+ T cells in the lung airways retain the potential to mediate recall responses. *Journal of immunology (Baltimore, Md. : 1950)*, 171(7):3338–3342, 2003.

Foulds, K. E., Zenewicz, L. A., Shedlock, D. J., Jiang, J., Troy, A. E. and Shen, H. Cutting edge: CD4 and CD8 T cells are intrinsically different in their proliferative responses. *Journal of immunology (Baltimore, Md. : 1950)*, 168(4):1528–1532, 2002.

Gong, C., Mattila, J. T., Miller, M., Flynn, J. L., Linderman, J. J. and Kirschner, D. Predicting lymph node output efficiency using systems biology. *Journal of theoretical biology*, 335:169–184, 2013.

Henrickson, S. E., Mempel, T. R., Mazo, I. B., Liu, B., Artyomov, M. N., Zheng, H., Peixoto, A., Flynn, M. P., Senman, B., Junt, T., Wong, H. C., Chakraborty, A. K. and von Andrian, U. H. T cell sensing of antigen dose governs interactive behavior with dendritic cells and sets a threshold for T cell activation. *Nature immunology*, 9(3):282–291, 2008.

Homann, D., Teyton, L. and Oldstone, M. B. Differential regulation of antiviral T-cell immunity results in stable CD8+ but declining CD4+ T-cell memory. *Nature medicine*, 7(8):913–919, 2001.

Jamieson, B. D., Douek, D. C., Killian, S., Hultin, L. E., Scripture-Adams, D. D., Giorgi, J. V., Marelli, D., Koup, R. A. and Zack, J. A. Generation of functional thymocytes in the human adult. *Immunity*, 10(5):569–575, 1999.

Kamath, A. T., Henri, S., Battye, F., Tough, D. F. and Shortman, K. Developmental kinetics and lifespan of dendritic cells in mouse lymphoid organs. *Blood*, 100(5):1734–1741, 2002.

Lanzavecchia, A. and Sallusto, F. Lead and follow: the dance of the dendritic cell and T cell. *Nature immunology*, 5(12):1201–1202, 2004.

Linderman, J. J., Riggs, T., Pande, M., Miller, M., Marino, S. and Kirschner, D. E. Characterizing the dynamics of CD4+ T cell priming within a lymph node. *Journal of immunology (Baltimore, Md. : 1950)*, 184(6):2873–2885, 2010.

Lindquist, R. L., Shakhar, G., Dudziak, D., Wardemann, H., Eisenreich, T., Dustin, M. L. and Nussenzweig, M. C. Visualizing dendritic cell networks in vivo. *Nature immunology*, 5(12):1243–1250, 2004.

McCune, J. M., Hanley, M. B., Cesar, D., Halvorsen, R., Hoh, R., Schmidt, D., Wieder, E., Decks, S., Siler, S., Neese, R., Hellerstein, M., Deeks, S., Siler, S., Neese, R. and Hellerstein, M. Factors influencing T-cell turnover in HIV-1-seropositive patients. *The Journal of clinical investigation*, 105(5):R1–8, 2000.

Miller, M. J., Hejazi, A. S., Wei, S. H., Cahalan, M. D. and Parker, I. T cell repertoire scanning is promoted by dynamic dendritic cell behavior and random T cell motility in the lymph node. *Proceedings of the National Academy of Sciences of the United States of America*, 101(4):998–1003, 2004a.

Miller, M. J., Safrina, O., Parker, I. and Cahalan, M. D. Imaging the single cell dynamics of CD4+ T cell activation by dendritic cells in lymph nodes. *The Journal of experimental medicine*, 200(7):847–856, 2004b.

Roederer, M., Dubs, J. G., Anderson, M. T., Raju, P. A. and Herzenberg, L. A. CD8 naive T cell counts decrease progressively in HIV-infected adults. *The Journal of clinical investigation*, 95(5):2061–2066, 1995.

Sprent, J. and Tough, D. F. T cell death and memory. *Science*, 293(5528):245–248, 2001.

Wherry, E. J., Teichgräber, V., Becker, T. C., Masopust, D., Kaech, S. M., Antia, R., von Andrian, U. H. and Ahmed, R. Lineage relationship and protective immunity of memory CD8 T cell subsets. *Nature immunology*, 4(3):225–234, 2003.